

APPENDICES

NCHRP 12-101

App. A – Literature Review

App. B – Survey of State Departments of Transportation

App. C – Synthesis of Literature

App. D – Novel Column and Construction Concepts

App. E – Demonstration of Evaluation Guidelines

App. F – Detailed Design Examples for Three Novel Columns

App. G – Benefits and Economic Impact of Novel Columns

App. H – Relationship between Drift Ratio and Displacement Ductility

App. I – Modeling Methods and Validation for Novel Columns

TABLE OF CONTENTS

APPENDICES	I
TABLE OF CONTENTS.....	II
APPENDIX A.....	A-1
A.1 Introduction.....	A-2
A.2 Ultra-High Performance Concrete (UHPC).....	A-2
A.2.1 Mechanical Properties of UHPC	A-2
A.2.2 Applications and Design Specifications	A-4
A.3 Engineered Cementitious Composite (ECC)	A-7
A.3.1 Mechanical Properties of ECC	A-7
A.3.2 Applications and Design Specifications	A-8
A.4 Shape Memory Alloy (SMA).....	A-11
A.4.1 Mechanical Properties of SMA	A-11
A.4.2 Applications and Design Specifications	A-12
A.5 Fiber Reinforced Polymer (FRP).....	A-14
A.5.1 Mechanical Properties of FRP.....	A-14
A.5.2 Applications and Design Specifications	A-15
A.6 Rubber.....	A-16
A.6.1 Mechanical Properties of Rubber	A-17
A.6.2 Applications and Design Specifications	A-17
A.7 References.....	A-18

APPENDIX A

Literature Review

Conduct a literature review of relevant domestic and international guidelines and manuals. The review should include research conducted through the NCHRP; Strategic Highway Research Program 2 (SHRP 2); FHWA; and other national, international, state, and pooled-fund sponsored research. The review should cover research findings and owner and industry experiences.

A.1 Introduction

Engineered materials such as concrete and steel have been used for more than a century. Even though concrete has negligible tensile strength and brittle behavior in compression, and steel is vulnerable to corrosion and fatigue, they are the most common construction materials and are utilized in almost all civil structures. For example, construction materials incorporated in new and replaced bridges in 2013 according to the Federal Highway Administration (FHWA) were 47% concrete, 43% steel, and 10% other materials such as wood or aluminum (FHWA Annual Material Report, 2013). New materials are emerging with superior properties than concrete and steel that can be incorporated in structural applications to enhance performance of structures under severe events or in harsh environments.

In this section, the existing literature on advanced materials that are good candidates to become the next generation of construction materials is reviewed. Ultra-high performance concrete (UHPC), engineered cementitious composite (ECC), shape memory alloy (SMA), fiber reinforced polymer (FRP), and rubber are covered. Mechanical properties, material model, national and international design specifications, and previous applications for each material type are presented. The focus of the review was on those properties that are relevant to civil engineering applications rather than the molecular characteristics of different materials.

In addition to review of past research on advanced materials, an online survey of state departments of transportation bridge engineers was conducted to determine any past and planned application of these materials and the views of bridge owners towards these materials. The blank survey form and the survey results are presented in App. B.

A.2 Ultra-High Performance Concrete (UHPC)

UHPC is a type of fiber-reinforced cementitious materials with a minimum specified compressive strength of 22000 *psi* (150 *MPa*) (ACI Committee 239, 2012). Durability, toughness, and corrosion resistance of UHPC are significantly better than those of conventional concrete. Superior properties of UHPC are attained by mixing very fine aggregates that are in the size of dust with usually 2% volumetric ratio high-strength steel fibers. Table A-1 presents a typical field-cast mix design for UHPC. The most common commercially available type of UHPC in the US and Canada is Ductal[®], which is a proprietary product. But other, non-proprietary materials with similar characteristics are emerging.

Table A-1. Typical field-cast UHPC mix design

Material	Weight, lbs/yd ³ (kg/m ³)	Percent by Weight
Portland Cement	1200 (712)	28.5
Fine Sand	1720 (1020)	40.8
Silica Fume	390 (231)	9.3
Ground Quartz	355 (211)	8.4
Superplasticizer	51 (30)	1.2
Steel Fibers ^(a)	263 (156)	6.2
Water	218 (130)	5.2

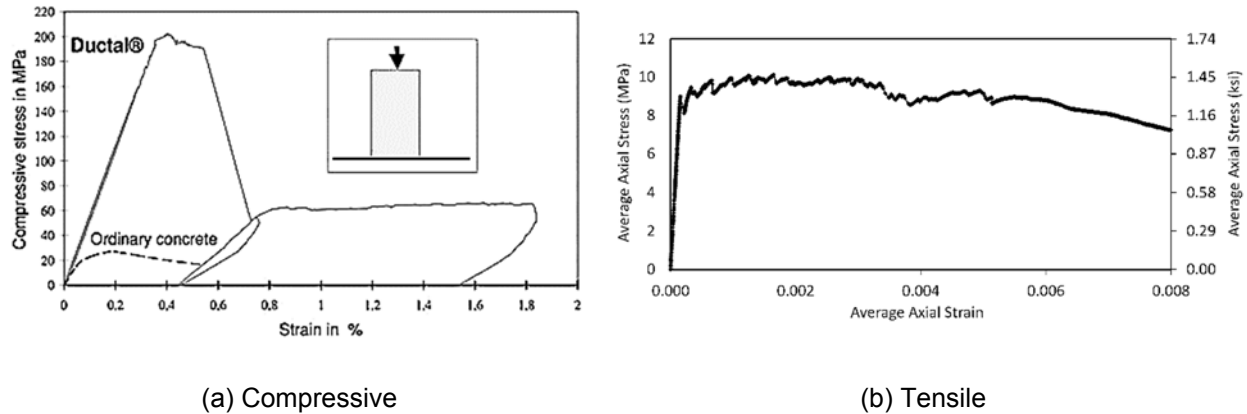
^(a) Usually 2% in volume high-strength steel fibers

Source: FHWA Publication No. FHWA-HRT-11-023 (Graybeal, 2010)

A.2.1 Mechanical Properties of UHPC

Figure A-1 shows the measured compressive and tensile stress-strain curves for UHPC. It can be seen that the compressive strength and ductility of UHPC are substantially higher than those of conventional

concrete (approximately four times). Furthermore, the tensile strain capacity of UHPC is 0.8%, which is significantly higher than the tensile strain capacity of conventional concrete. The tensile strength for the field-cast UHPC is approximately 900 *psi* (6.2 *MPa*) (Graybeal, 2006; Gowripalan and Gilbert, 2000).



Source: (a) www.Lafarge.com with permission, (b) FHWA Publication No. FHWA-HRT-13-060 (Russell and Graybeal, 2013) with permission

Figure A-1. Measured stress-strain of UHPC

Russell and Graybeal (2013) conducted a state-of-the-art literature review on the development, properties, and worldwide applications of UHPC. A range for each UHPC material property as well as design equations extracted from the report are presented in Table A-2. These properties are mainly for Ductal®. UHPC sections are usually smaller than concrete sections because of the higher strength of UHPC. As a result, dynamic properties of bridges supported on UHPC columns can be different. This variation should be considered in design.

Table A-2. UHPC mechanical properties

Properties	Range	Equation
Compressive Strength (f'_{UHPC})	20 to 30 <i>ksi</i> , (140 to 200 <i>MPa</i>)	A time-dependent equation for UHPC strength is available.
Tensile Cracking Strength ($f_{t,UHPC}$)	0.9 to 1.5 <i>ksi</i> , (6 to 10 <i>MPa</i>)	$f_{t,UHPC} = 6.7\sqrt{f'_{UHPC}}$ (<i>psi</i>)
Modulus of Elasticity (E_{UHPC})	6000 to 10000 <i>ksi</i> , (40 to 70 <i>GPa</i>)	$E_{UHPC} = 49000\sqrt{f'_{UHPC}}$ (<i>psi</i>)
Poisson's Ratio	0.2	
Coefficient of Thermal Expansion	(5.5 to 8.5) $\times 10^{-6}/^{\circ}F$, (10 to 15) $\times 10^{-6}/^{\circ}C$	
Creep Coefficient ^(a)	0.2 to 0.8	
Specific Creep ^(a)	(0.04 to 0.3) $\times 10^{-6}/psi$, (6 to 45) $\times 10^{-6}/MPa$	
Total Shrinkage ^(b)	up to 900×10^{-6}	

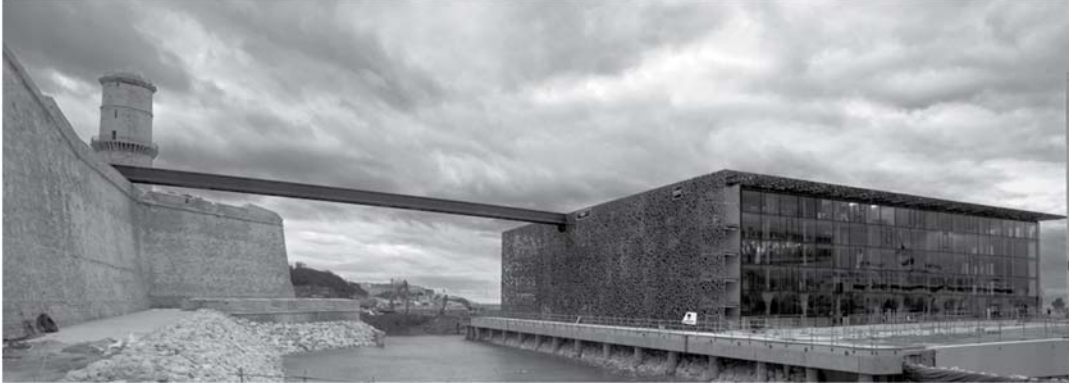
Note: ^(a) Depends on curing conditions and age of loading

^(b) Combination of drying shrinkage and autogenous shrinkage and depends on curing method

Source: FHWA Publication No. FHWA-HRT-13-060 (Russell and Graybeal, 2013)

A.2.2 Applications and Design Specifications

UHPC has been incorporated in many structures worldwide (Fig. A-2). UHPC in the commercial form has been available in the US since 2000. It has been incorporated in more than 50 bridges in the North America, mainly in bridge superstructure elements such as precast deck-to-deck connections.



(a) 250-ft (76-m) long pedestrian bridge, France



(b) Y-shape UHPC piers, Montpellier, France

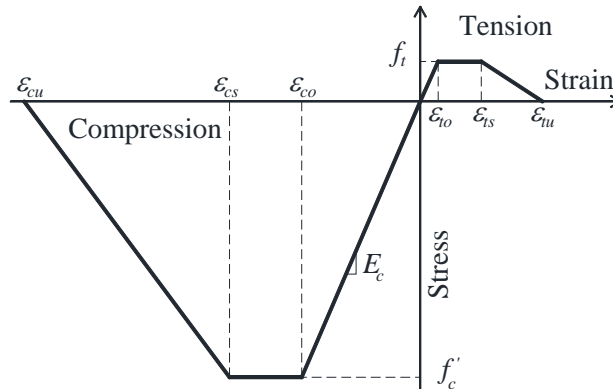


(c) Little Cedar Creek Bridge, Iowa, The first bridge in North America constructed with UHPC waffle deck, girders and joints

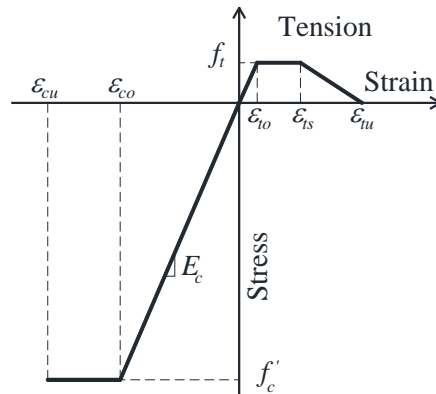
Source: www.Lafarge.com with permission

Figure A-2. UHPC worldwide applications

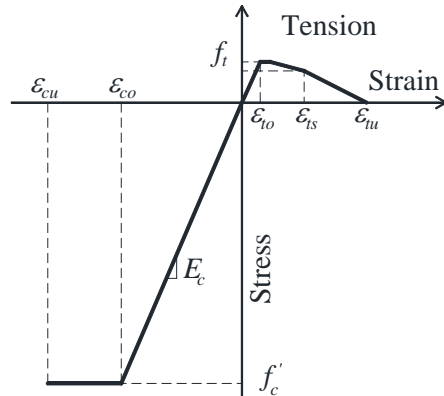
Three design guidelines and construction recommendations are available at the time of this writing for UHPC: (1) Proposed Design Guidelines for Ductal Prestressed Concrete Beams (Australia) (Gowripalan and Gilbert, 2000), (2) Recommendations for Design and Construction of Ultra High Strength Fiber Reinforced Concrete Structures by the Japan Society of Civil Engineers (Uchida et al., 2006), and (3) Ultra High Performance Fiber-Reinforced Concretes, Recommendations prepared by French Association of Civil Engineers (AFGC) (AFGC, 2013). Figure A-3 shows UHPC stress-strain models proposed in these specifications. Table A-3 presents the mechanical properties specified in each code. It is worth mentioning that these codes use different notations. However, a unified notation was used in this report for ease of comparison.



(a) Australian code (proposed)



(b) Japanese code (recommendations)



(c) French code (recommendations)

Figure A-3. UHPC material model for design

Table A-3. UHPC mechanical properties for design

Properties	Australian Guide	Japanese Code	French Code
Compressive Strength (f'_c)	$0.85f'_{UHPC}$	$0.85f'_{UHPC}/\gamma_{c1}$	$\alpha f'_{UHPC}/\gamma_{c2}$
Modulus of Elasticity (E_c)	7250 ksi, (50000 MPa)	7250 ksi, (50000 MPa)	7250 ksi, (50000 MPa)
ε_{co} (in./in. or m/m)	$0.85f'_{UHPC}/E_c$	$0.85f'_{UHPC}/\gamma_{c1}/E_c$	$\alpha f'_{UHPC}/\gamma_{c2}/E_c$
ε_{cs} (in./in. or m/m)	0.004	N/A	N/A
Ultimate Comp. Strain (ε_{cu})	0.007	0.0035	$[1 + \frac{14f_{ctfm}}{f_{cm}}]\varepsilon_{co}$ or 0.0027
Tensile Strength (f_t)	0.725 ksi (5 MPa)	$1.275/\gamma_{c1}$ ksi (8.8/ γ_{c1} MPa)	$1.3/(\gamma_{cf} \cdot K)$ ksi (9.0/ $(\gamma_{cf} \cdot K)$ MPa)
ε_{to} (in./in. or m/m)	0.0001	f_t/E_c	f_t/E_c
ε_{ts} (in./in. or m/m)	$\frac{0.16L_f}{1.2h} \leq 0.004$	$\varepsilon_{to} + \frac{w_{1k}}{L_{eq}}$	$\frac{f_t}{E_{c,eff}} + \frac{w_{1\%}}{l_c}$
Ultimate Tensile Strain (ε_{tu})	$\frac{L_f}{1.2h} \leq 0.01$	$\frac{w_{2k}}{L_{eq}}$	$\frac{L_f}{4l_c} \leq 0.025$

Note: Compressive material model is for unconfined UHPC. No model is available for steel confined UHPC.

f'_{UHPC} : Specified 28-day compressive strength of UHPC (usually 22 ksi [150 MPa]).

ε_{co} : Strain at start of plateau in compression.

ε_{cs} : Strain at end of plateau in compression.

L_f : Length of fibers (0.5 in. [12.7 mm] for Ductal®).

h : Overall depth of the member.

γ_{c1} : Concrete material factor presented in the Japan Standard Specifications for Concrete Structures is 1.3 and 1 for the ultimate and serviceability limit states, respectively.

w_{1k} = 0.0196 in. (0.5 mm), crack width at the end of tensile plateau.

w_{2k} = 0.1693 in. (4.3 mm), crack width at the ultimate tensile strain.

L_{eq} = $0.8h(1 - \frac{1}{[1.05 + \frac{6h}{l_{ch}}]^4})$, where l_{ch} is the characteristic length (417 in. [10.6 m]) and h is the height of section.

α = 0.85, long-term strength reduction factor.

γ_{c2} : Partial factor for concrete may be taken as 1.5 and 1.2 for "Persistent and Transient" and "Accidental" design situations, respectively. Design for Highway bridges is in "Persistent and Transient" category.

f_{ctfm} : The maximum mean post-cracking stress in tension.

f_{cm} : The maximum mean stress in compression.

γ_{cf} : 1.3 in the case of durable/transient situations and 1.05 in the case of accidental situations.

K = 1.25 and 1.75 when the global and local effects are considered, respectively.

$w_{1\%}$ = 0.01 h where h is the height of prism tested under flexure.

$E_{c,eff}$ = $E_c/(1 + \varphi)$, where φ is the creep coefficient. φ is 0.8 if there is no heat treatment, 0.4 when heat treatment applies during the first hours of curing, and 0.2 when heat treated after UHPC has hardened.

l_c = $2l_{cs}/3$, characteristic length, where l_{cs} = $\min\{S_{min}, y\}$, S_{min} is minimum distance between cracks, and y is the distance between the neutral axis and tensile side of the cross section.

It can be seen that the Japanese and French codes are more conservative since they are legal design specifications while the Australian document is a proposed guideline at this time. At the time of this writing, no steel confined UHPC material model was available.

A.3 Engineered Cementitious Composite (ECC)

ECC is in another class of fiber-reinforced cementitious materials with substantial tensile ductility. Compressive strength of ECC is usually higher than conventional concrete but it can be adjusted to be on the order of conventional concrete strength. Similar to UHPC, the size of aggregates is very small in the ECC mix. Polyvinyl alcohol (PVA) fibers with 2% volumetric ratio are usually used in ECC mix design. But other types of fibers may also be used such as polyethylene and polypropylene (Li, 2008; Kawashima et al., 2011; Kawashima et al., 2012). Table A-4 presents a typical mix design for ECC.

Table A-4. Typical ECC mix design

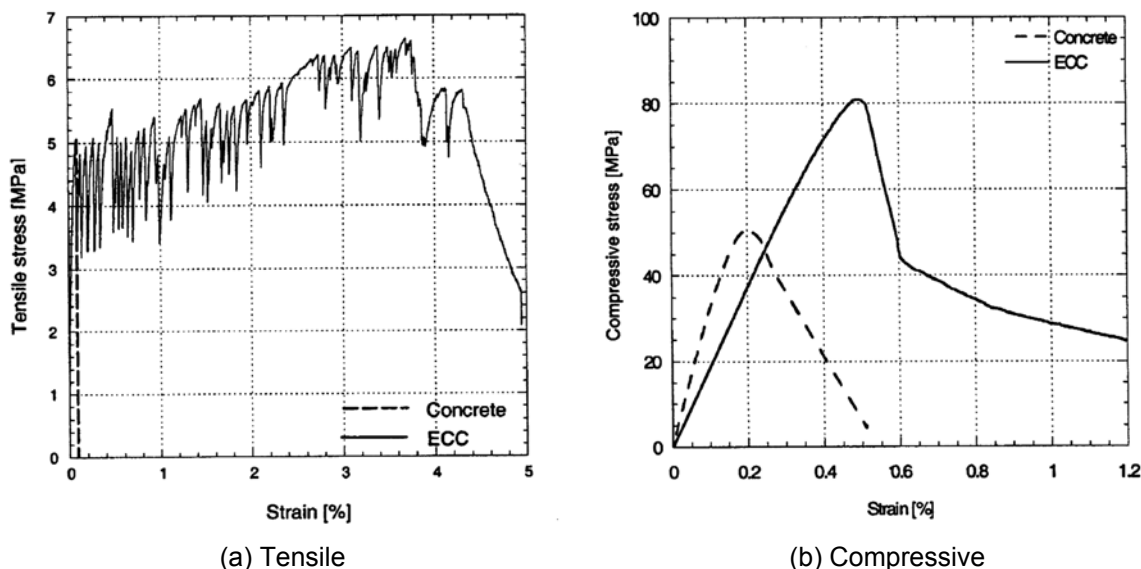
Material	Percent by Weight
Cement	37.0
Fly Ash	31.5
Sand	24.7
Silica Powder	5.4
PVA Fiber	1.4
Superplasticizer	---

Note: Water to Cement & Fly Ash ratio= 0.315; Fly Ash to Cement ratio= 0.85

What makes ECC different from UHPC is its fiber functionality and tensile ductility. Steel fibers are added to UHPC matrix to provide ductility for the densified matrix and increase both tensile and compressive strength, whereas the fibers in ECC are used to maximize the tensile ductility by developing multiple microcracks (Li, 2008). This is achieved by coating the fibers with a material that allows the fibers to slip partially when they are over loaded, thus preventing fiber fracture and leading to formation of multiple hairline cracks instead of a few wide cracks.

A.3.1 Mechanical Properties of ECC

Figure A-4 shows the measured stress-strain relationship of a typical PVA-ECC. It can be seen that the strain capacity of ECC is more than 4%, which provides significant ductility for members built with ECC compared to conventionally cast concrete members. Mechanical properties of ECC can vary substantially depending on mix design, fiber type, and fiber dosage as presented in Table A-5. Experiments have shown that due to superior properties of ECC, shear reinforcement may be reduced or eliminated in ECC members (Li, 2008). Under cyclic loading, ECC members generally provide higher ductility and wider hysteretic loops with no strength degradation compared to concrete members (Fischer and Li, 2003).



Source: Fischer and Li (2003) with permission
Figure A-4. Measured stress-strain of ECC

Table A-5. ECC major mechanical properties

Properties	Range
Compressive Strength	3 to 14 <i>ksi</i> (20 to 95 <i>MPa</i>)
First Crack Strength	0.4 to 1.0 <i>ksi</i> (3 to 7 <i>MPa</i>)
Ultimate Tensile Strength	0.6 to 1.7 <i>ksi</i> (4 to 12 <i>MPa</i>)
Ultimate Tensile Strain	1 to 8%
Modulus of Elasticity	2600 to 5000 <i>ksi</i> (18 to 34 <i>GPa</i>)
Flexural Strength	1.5 to 4.5 <i>ksi</i> (10 to 30 <i>MPa</i>)

Source: Li (2008)

A.3.2 Applications and Design Specifications

A summary of experimental studies investigating the seismic performance of ECC structural components is presented in Li (2008). Performance of ECC large-scale bridge columns was investigated in a few studies (Saiidi and Wang, 2006; Saiidi et al., 2009; Kawashima et al., 2011; Motaref et al., 2011; Kawashima et al., 2012; Cruz and Saiidi, 2012; Nakashoji and Saiidi, 2014; Varela and Saiidi, 2013; Mehrsoroush and Saiidi, 2014; Aviram et al., 2014; Panagiotou et al., 2014; Tazarv and Saiidi, 2014a). All studies showed low damage with minimal post-event repair need for ECC columns.

Even though ECC has been utilized in many experiments, field applications of ECC are scarce. ECC was incorporated in structural applications in Japan, Korea, Switzerland, Australia and the US. However, these applications were limited to concrete repair in bridge deck, dam, and retaining wall (Fig. A-5). The Washington Department of Transportation has designed and plans to construct the first SMA-ECC bridge in the world in Seattle at the time of this writing (SR99 SMA-ECC Bridge, 2014).



(a) Deck preparation



(b) After repair

Source: MDOT Research Report RC-1484 (Li et al., 2006)

Figure A-5. Bridge deck repair with ECC

Only one design specification is available for ECC, which was developed by the Japan Society of Civil Engineers (JSCE Concrete Library 127, 2008). Figure A-6 shows the design stress-strain model and Table A-6 presents the material model properties in detail. Even though models were provided for tension and compression, most of the parameters should be determined from appropriate tests that are specified in the code. Preliminary design parameters were extracted from different parts of the Japanese code and are listed in Table A-6.

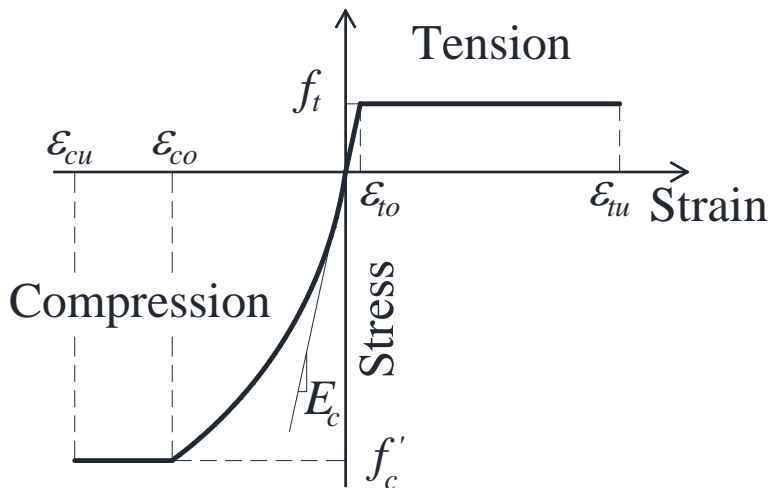


Figure A-6. ECC material model for design

Stress-strain relationship for the initial compressive zone is:

$$f_c = \frac{0.85f'_{ECC}}{\gamma_c} \cdot \frac{\epsilon_c}{\epsilon_{co}} \left(2 - \frac{\epsilon_c}{\epsilon_{co}} \right) \quad (2-1)$$

All parameters are defined in the footnote of Table A-6.

Table A-6. ECC mechanical properties for design

Properties	Japanese Code	Recommended for Preliminary Design ^(a)
Compressive Strength (f'_c)	$0.85f'_{ECC}/\gamma_c$	$f'_{ECC} = 4.35 \text{ ksi (30 MPa)}$
Modulus of Elasticity (E_c)	$17700 \sqrt{\frac{\gamma}{18.5}} \times \left(\frac{f'_{ECC}}{60}\right)^{1/3} \text{ (N-mm)}$	$2300 \text{ ksi (16000 MPa)}$
ε_{co} (in./in. or m/m)	by testing	0.004
Ultimate Comp. Strain (ε_{cu})	by testing	0.01
Tensile Strength (f_t)	$f_{t,ECC}/\gamma_c$	$f_{t,ECC} = 0.29 \text{ ksi (2 MPa)}$
ε_{to} (in./in. or m/m)	f_t/E_c	
Ultimate Tensile Strain (ε_{tu})	$\varepsilon_{tu,ECC}/\gamma_c$	$\varepsilon_{tu,ECC} = 0.008$

Note: Compressive material model is for unconfined ECC.

f'_{ECC} : Specified/measured 28-day compressive strength of ECC.

γ_c : Concrete material factor presented in the Japan Standard Specifications for Concrete Structures is 1.3 and 1 for the ultimate and serviceability limit states, respectively.

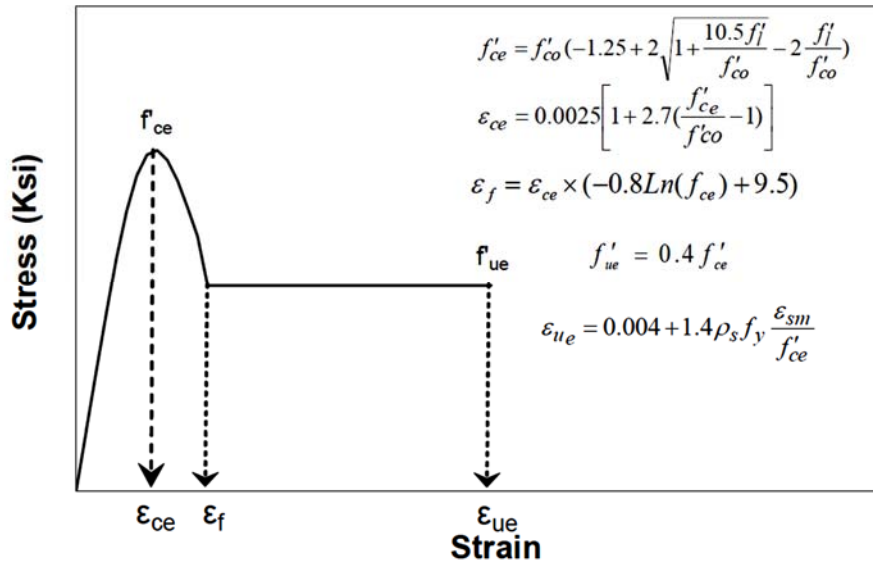
$f_{t,ECC}$: Characteristic tensile strength of ECC.

$\varepsilon_{tu,ECC}$: Characteristic tensile strain of ECC.

Poisson's Ratio may be taken as 0.23.

^(a) Appendix I-1 of JSCE Concrete Library 127 (2008)

Similar to the UHPC codes described in the previous section, the Japan ECC code does not provide confined properties of ECC. However, these properties are important for seismic design of ECC members. A steel confined material model for ECC was developed by Motaref et al. (2011) for seismic design and analysis (Fig. A-7).



Source: Motaref et al., 2011

Figure A-7. Steel confined material model for ECC

A.4 Shape Memory Alloy (SMA)

SMA refers to a class of metallic materials that may be used as reinforcement in concrete structures. SMA can recover its original shape upon heating (shape memory effect) or unloading (superelastic effect) (Otsuka and Wayman, 1998). From strength of material perspective, shape recovery means negligible permanent (or residual) strains in the stress-strain diagram under cyclic actions. The superelastic effect of SMA is desired as reinforcement in which the bars are usually trained to be straight thus axial, flexural, and torsional deformations are recovered when the load is released.

More than 10 alloys of SMA have been developed and new types are emerging. Among those, an alloy of nickel and titanium (commonly referred as NiTi or Nitinol) has gained more interest since NiTi SMA shows very high superelastic strain capacity, low- and high-cycle fatigue resistance, excellent corrosion resistance, and good energy dissipation (DesRoches and Delemont, 2002). An alloy of Cu-Al-Mn has been recently developed that exhibits reasonable mechanical properties, is relatively inexpensive, and has low toughness that facilitates machining (Araki et al., 2011; Shrestha et al., 2013; NSF-PFI Project, 2014).

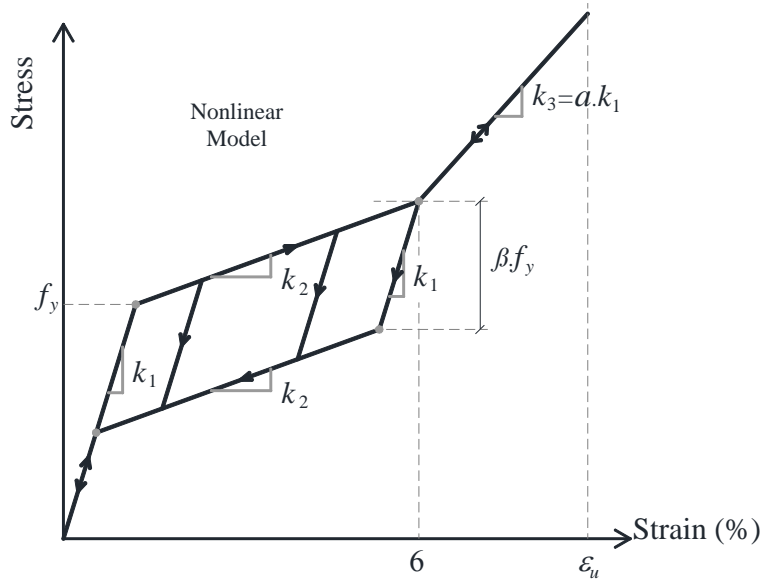
A.4.1 Mechanical Properties of SMA

Several stress-strain models have been developed for SMA at different austenite and martensite phases (Atanackovic and Achenbach, 1989; Graesser and Cozzarelli, 1991; Auricchio and Sacco, 1997). However, no systematic definition of SMA mechanical properties from structural engineering viewpoint has been devised in those studies. Tazarv and Saiidi (2014a and 2014b) defined key mechanical properties of SMA (Table A-7) for structural engineering application. A stress-strain model was specifically developed for NiTi superelastic SMA (Fig. A-8) but the model may be used for any SMA alloys with flag-shape hysteretic relationship.

Table A-7. Definition of SMA mechanical properties

Properties	Notation	Definition
Austenite modulus	k_1	the average slope between 15 to 70% of f_{y0}
Post-yield stiffness	k_2	the average slope of curve between 2.5% and 3.5% of strain on the upper plateau of the first cycle of loading to 6% strain
Observed yield strength	f_{y0}	the stress at the initiation of nonlinearity on the first cycle of loading to the upper plateau
Austenite yield strength	f_y	the stress at intersection of line passing through origin with slope of k_1 and line passing through stress at 3% strain with slope of k_2
Lower plateau inflection strength	f_i	the stress at the inflection point of lower plateau during unloading from the first cycle to 6% strain
Lower plateau stress factor	β	$1 - \frac{f_i}{f_y}$
Residual strain	ϵ_{res}	the tensile strain after one cycle to 6% and unloading to 1 ksi (7 MPa)
Recoverable superelastic strain	ϵ_r	The maximum strain with at least 90% strain recovery capacity
Martensite modulus	k_3	the slope of the curve between 8 to 9% strain after the first cycle of loading to failure
Secondary post-yield stiffness ratio	α	$\frac{k_3}{k_1}$
Ultimate strain	ϵ_u	the strain at failure

Source: Tazarv and Saiidi, 2014b



Source: Tazarv and Saiidi, 2014b

Figure A-8. Superelastic SMA material model

A.4.2 Applications and Design Specifications

SMA has been widely used in medical, aerospace, and industrial products and has been implemented in a few structural applications. Review of structural applications were presented in DesRoches and Smith (2003), Wilson and Wesolowsky (2005), Song et al. (2006), Alam et al. (2007), and Dong et al. (2011). SMA wires and rods were studied as restrainers to prevent bridge deck unseating. Shake table tests showed satisfactory performance with minimal residual deformations of the restraining device (Johnson et al., 2008). Andrawes et al. (2010) proposed using SMA as external active confinement for seismic retrofit of reinforced concrete columns. Concrete strength and strain capacity were increased by 15 and 310%, respectively. In another study, SMA was utilized as main fibers in a FRP matrix to provide energy dissipation capacity (Wierschem and Andrawes, 2010). SMA has been utilized in a few studies as longitudinal reinforcement in concrete members. The first of such studies was on beams by Ayoub et al. (2003) and later Saiidi et al. (2007). Saiidi and Wang (2006), Youssef et al. (2008), Saiidi et al. (2009), Cruz and Saiidi (2012), and Tazarv and Saiidi (2014a) subsequently showed that reinforcing SMA can substantially reduce residual displacements in other concrete member (mainly large-scale bridge columns) even after undergoing large deformations.

At the time of this writing, there is no field application of SMA as column reinforcement but, as mentioned before, the Washington Department of Transportation plans to construct the first SMA-ECC bridge in the world in Seattle (SR99 SMA-ECC Bridge, 2014) through funding by the FHWA Innovative Bridge Research and Deployment (IBRD) program. Figure A-9 shows the bridge architectural rendering and No. 10 ($\text{Ø}32 \text{ mm}$) SMA bars with headed reinforcement coupler that represent the longitudinal reinforcement that will be used in the bridge.



(a) Bridge sketch



(b) SMA bars connected to steel bars

Source: <http://wolfweb.unr.edu/homepage/saiidi/WashDOT/SR99/index.html>

Figure A-9. First SMA-reinforced ECC bridge in the world to be built in Seattle, USA

No national or international design specification is available for SMA. However, Tazarv and Saiidi (2014a and 2014b) recently proposed a design specification for reinforcing NiTi superelastic SMA. Table A-8 presents the minimum and expected mechanical properties of superelastic Nitinol. Other material properties such as specific weight, Poisson’s ratio, electrical resistivity, and weldability were discussed in Tazarv and Saiidi (2014a and 2014b).

Table A-8. Minimum and expected tensile NiTi Superelastic SMA mechanical properties

Parameter	Minimum ^(a)	Expected ^(b)
Austenite modulus, k_1	4500 ksi (31025 MPa)	5500 ksi (37900 MPa)
Post yield stiffness, k_2	--	250 ksi (1725 MPa)
Austenite yield strength, f_y	45 ksi (310 MPa)	55 ksi (380 MPa)
Lower plateau stress factor, β	0.45	0.65
Recoverable superelastic strain, ε_r	6%	6%
Secondary post-yield stiffness ratio, α	--	0.3
Ultimate strain, ε_u	10%	10%

Note: ^(a) to be used in material production

^(b) to be used in seismic design of SMA-reinforced concrete members

Source: Tazarv and Saiidi, 2014a & 2014b

It is well documented that the stress-strain of NiTi superelastic SMA is not symmetric, and SMA behavior is affected by temperature, loading type, strain rate, and cyclic loading. However, a simple symmetrical material model based on “expected tensile mechanical properties” (Table A-8) was proposed by the writers for design of SMA-reinforced members. This model led to successful simulations of global and local response of large-scale SMA-reinforced bridge column tests. The minimum values should be the baseline for reinforcing SMA production but the products with expected properties are desired for seismic applications.

A.5 Fiber Reinforced Polymer (FRP)

Fiber reinforced polymer (or fiber reinforced plastic) refers to a class of composite materials with linear-elastic behavior and superior strength (Gibson, 2011). Many types of FRP (S-glass, E-glass, Carbon, Aramid, Boron, and Silicon carbide) are available in many forms (bars, sheets, tubes, and structural sections) as shown in Fig. A-10. The fibers may be laid in single or more directions depending on the intended usage of FRP members or fabrics.



(a) Different forms of FRP



(b) FRP structural shapes

Source: (a) www.isiscanada.com, (b) www.nationalgrating.com

Figure A-10. FRP commercial forms

A.5.1 Mechanical Properties of FRP

Behavior of FRPs varies depending on the type of the fibers as shown in Fig. A-11. However, a linear-elastic stress-strain relationship with brittle fracture is common among all FRP types. Therefore, the tensile stress-strain behavior of FRP can be established by knowing the modulus of elasticity and the strength at the fracture. These properties are usually provided by FRP manufacturers. Compressive strength of FRP, however, is often neglected since FRP may fail by micro-buckling of fibers or shear failure when stressed under compressive actions (ACI 440.1R-06, 2006; ACI 440.2R-08, 2008).

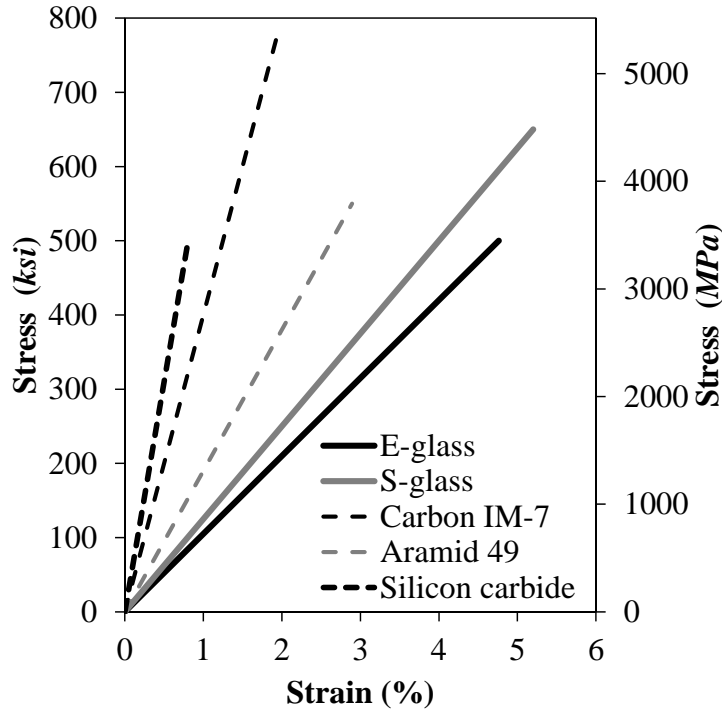


Figure A-11. FRP mechanical properties

A.5.2 Applications and Design Specifications

FRP is perhaps the most common type of advanced materials adopted in civil engineering. It has been incorporated in many structures worldwide (Bank, 2006) mostly for repair and retrofit. Carbon and glass FRP have routinely been used for column retrofit of bridges in seismic regions (Hollaway and Teng, 2008). More than 25 national and international design guidelines, codes, and specifications are available for FRP. NCHRP has published four reports regarding aspects of FRP application in bridges (Mertz et al., 2003; Mirmiran et al., 2004; Zureick et al., 2010; Belarbi et al., 2011). Externally bonded FRP systems for repair and retrofit of bridge components were studied in these reports. Design guidelines proposed by ACI for bonded FRP, reinforcing FRP bars, and FRP tendons are adopted in the present study:

- Guide for the Design and Construction of Structural Concrete Reinforced with FRP Bars (ACI 440.1R-06, 2006)
- Guide for the Design and Construction of Externally Bonded FRP Systems for Strengthening Concrete Structures (ACI 440.2R-08, 2008)
- Guide Test Methods for Fiber-Reinforced Polymer (FRP) Composites for Reinforcing or Strengthening Concrete and Masonry Structures (ACI 440.3R-12, 2012)
- Prestressing Concrete Structures with FRP Tendons (ACI 440.4R-04, 2004)
- Specification for Construction with Fiber-Reinforced Polymer Reinforcing Bars (ACI 440.5-08, 2008)

A range for each mechanical property of GFRP (glass FRP), CFRP (carbon FRP), and AFRP (aramid FRP) was proposed (Table A-9) by ACI440.1R-06 (2006). A guaranteed tensile strength (f_{fu}^*) and a guaranteed tensile strain (ϵ_{fu}^*) should be reported by manufacturers, which are defined as the average of a

sample of test data minus three standard deviations. The design tensile strength (f_{fu}) should be determined by

$$f_{fu} = C_E f_{fu}^* \quad (2-2)$$

where C_E is the environmental reduction factor ranging from 0.5 to 0.95 for different FRP types, FRP forms, and exposure conditions.

Table A-9. ACI proposed mechanical properties for FRP bars

Properties	GFRP	CFRP	AFRP
Tensile Strength, <i>ksi (MPa)</i>	70 to 230 (483 to 1600)	87 to 535 (600 to 3690)	250 to 368 (1720 to 2540)
Modulus of Elasticity, <i>ksi (GPa)</i>	5100 to 7400 (35 to 51)	15900 to 84000 (120 to 580)	6000 to 18200 (41 to 125)
Rupture Tensile Strain (%)	1.2 to 3.1	0.5 to 1.7	1.9 to 4.4

Note: Typical values for fiber volume fractions ranging from 0.5 to 0.7

Source: ACI 440.1R-06 (2006)

Despite conventional steel-reinforced concrete member design in which reinforcements must yield prior to concrete failure to provide sufficient ductility and warning, members reinforced with FRP are designed assuming either FRP fracture or concrete compressive failure.

Since there are many types of FRP with a wide range of properties, ACI guidelines allow any type of FRP with a guaranteed tensile strength between 60 *ksi* (414 *MPa*) to 300 *ksi* (2069 *MPa*). Strength grade F60 is designated to FRP with a guaranteed tensile strength between 60 *ksi* (414 *MPa*) to 70 *ksi* (483 *MPa*) and grade F290 is designated to FRP that has a guaranteed tensile strength between 290 *ksi* (1999 *MPa*) to 300 *ksi* (2069 *MPa*). A 10 *ksi* (69 *MPa*) increment is selected for strength grades. A bar identification method is also proposed to facilitate design and construction with FRP bars.

A.6 Rubber

Rubber is in a class of polymeric materials with elastomeric behavior. Natural and synthetic rubbers have been commercially available for more than a century. Elastomeric bearings have been utilized in bridges since 1950 and have shown remarkably good performance (Yura et al., 2001). Furthermore, rubber is the most important component of lead rubber isolators (Mayes et al., 1992; Kelly, 1993), which have been extensively utilized in bridges to elongate the natural period thus reducing force demand on protected members.

Even though rubber has been in use in bridges for many decades and its properties are specified in AASHTO, it is treated in the current project as an advanced material in the context of usage in column plastic hinge zones. Recent studies on plastic hinges that substitute rubber for concrete in plastic hinges have shown superior plastic hinges with minimal damage even under strong earthquakes (Kawashima and Nagai, 2002; Motaref et al., 2011; Cruz and Saiidi, 2012; Saiidi et al., 2014). The primary features of rubber used in plastic hinges is its ability to undergo large tensile and compressive strains and tendency to recover deformation without permanent damage making it a viable alternative to conventional concrete in plastic hinges. This application is in clear contrast to the past application of rubber in bridge bearings or isolation systems, in which rubber acts primarily in shear.

A.6.1 Mechanical Properties of Rubber

Figure A-12a shows a typical tensile stress-strain behavior of rubber. It can be seen that the tensile ductility of rubber is substantially higher than all previously described advanced materials (100 times higher). Similarly, rubber exhibits high compressive strain capacities compared to the previously discussed materials. Rubber is usually reinforced with steel shims to enhance its normal stiffness and horizontal flexibility (Kelly and Konstantinidis, 2011). Figure A-12b shows a typical reinforced rubber compressive behavior. In the initial phase of studies on use of rubber in plastic hinges, no shims were used and the column performance was found to be partially successful (Kawashima and Nagai, 2002). However, shimmed rubber was used in subsequent studies and satisfactory results were obtained. The overall seismic performance was improved because the shims further helped prevent buckling of the column longitudinal reinforcing bars in the plastic hinge.

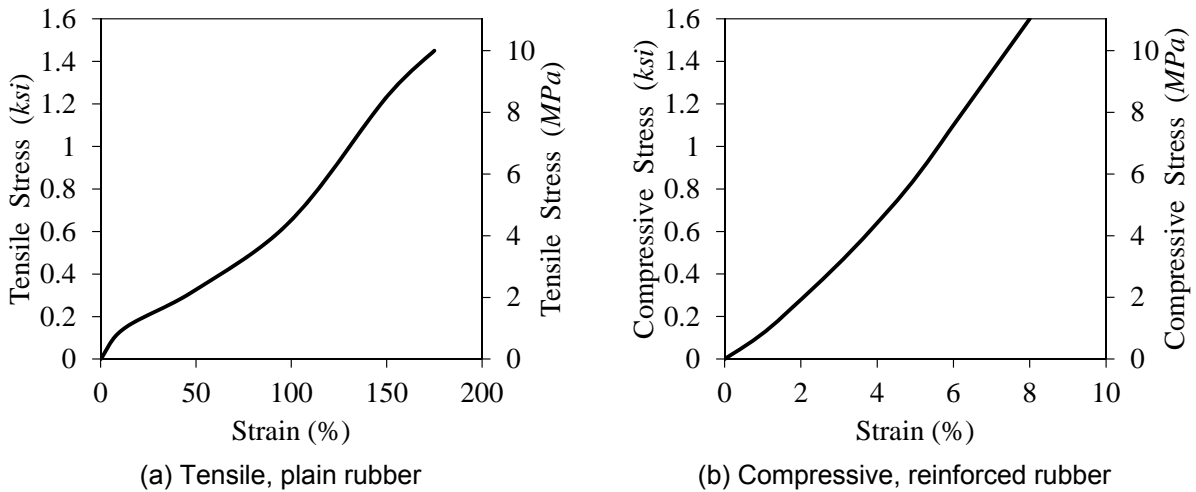


Figure A-12. Typical stress-strain relationship for rubber

A.6.2 Applications and Design Specifications

As indicated before, rubber has been incorporated in bridges either as bearings or seismic protection devices. Since both cases are fully regulated by AASHTO, only references to those publications are provided in this section. In the subsequent sections, however, an innovative application of the reinforced rubber as damage-free plastic hinge is discussed, which is not addressed in AASHTO.

- AASHTO LRFD Bridge Design Specifications (2014), Chapter 14
- Guide Specifications for Seismic Isolation Design (2010)

A.7 References

1. AASHTO. (2010). "Guide Specifications for Seismic Isolation Design," 3rd Edition. Washington, DC, American Association of State Highway and Transportation Officials.
2. AASHTO. (2013). "AASHTO LRFD Bridge Design Specification," Washington, DC, American Association of State Highway and Transportation Officials.
3. ACI 440.1R-06. (2006). "Guide for the Design and Construction of Structural Concrete Reinforced with FRP Bars," Reported by American Concrete Institute Committee 440, Farmington Hills, Mich., 44 pp.
4. ACI 440.2R-08. (2008). "Guide for the Design and Construction of Externally Bonded FRP Systems for Strengthening Concrete Structures," Reported by American Concrete Institute Committee 440, 80 pp.
5. ACI 440.3R-12. (2012). "Guide Test Methods for Fiber-Reinforced Polymer (FRP) Composites for Reinforcing or Strengthening Concrete and Masonry Structures," Reported by American Concrete Institute Committee 440, 23 pp.
6. ACI 440.4R-04. (2004). "Prestressing Concrete Structures with FRP Tendons," Reported by American Concrete Institute Committee 440, 35 pp.
7. ACI 440.5-08. (2008). "Specification for Construction with Fiber-Reinforced Polymer Reinforcing Bars," Reported by American Concrete Institute Committee 440, 5 pp.
8. ACI Committee 239. (2012). "Ultra-High Performance Concrete," ACI Fall Convention. Toronto, Ontario, Canada.
9. AFGC. (2013). "Ultra High Performance Fibre-Reinforced Concretes," Recommendations, French Association of Civil Engineers (AFGC), Paris, France, 358 pp.
10. Alam, M.S., Youssef, M.A. and Nehdi, M. (2007). "Utilizing Shape Memory Alloys to Enhance the Performance and Safety of Civil Infrastructures: a Review," *Canadian Journal of Civil Engineering*, Vol. 34, pp. 1075-1086.
11. Andrawes, B., Shin, M., and Wierschem, N. (2010). "Active Confinement of Reinforced Concrete Bridge Columns Using Shape Memory Alloys," *Journal of Bridge Engineering*, ASCE, Vol. 15, No. 1, pp. 81-89.
12. Araki, Y., Endo, T., Omori, T., Sutou, Y., Koetaka, Y., Kainuma, R., and Ishida, K. (2011). "Potential of Superelastic Cu-Al-Mn Alloy Bars for Seismic Applications," *Earthquake Engineering and Structural Dynamics*, Vol. 40, No. 1, pp. 107-115.
13. Atanackovic, T. and Achenbach, M. (1989). "Moment-Curvature Relations for a Pseudoelastic Beam," *Continuum Mechanics and Thermodynamics*, Vol. 1, pp. 73-80.
14. Auricchio, F. and Sacco, E. (1997). "A Superelastic Shape-Memory-Alloy Beam Model," *Journal of Intelligent Material Systems and Structures*, Vol. 8, pp. 489-501.
15. Aviram, A., Stojadinovic, B., and Parra-Montesinos, G.J. (2014). "High-Performance Fiber-Reinforced Concrete Bridge Columns under Bidirectional Cyclic Loading," *ACI Structural Journal*, Vol. 111, No. 2, pp. 303-312.
16. Ayoub, C., Saiidi, M.S., and Itani, A. (2003). "A Study of Shape-Memory Alloy-Reinforced Beams and Cubes," *Report No. CCEER-03-7*, Center for Civil Engineering Earthquake Research, Dept. of Civil Engineering, Univ. of Nevada, Reno, NV.
17. Bank, C. (2006). "Composites for Construction: Structural Design with FRP Materials," John Wiley & Sons, 551 pp.
18. Belarbi, A., Bae, S.W., Ayoub, A., Kuchma, D., Mirmiran, A., and Okeil, A. (2011). "Design of FRP Systems for Strengthening Concrete Girders in Shear," Washington, D.C., National Cooperative Highway Research Program (NCHRP) Report No. 678, 130 pp.
19. Cruz Noguez C.A. and Saiidi, M.S. (2012). "Shake Table Studies of a 4-Span Bridge Model with Advanced Materials," *Journal of Structural Engineering*, ASCE, Vol. 138, No. 2, pp. 183-192.

20. DesRoches, R. and Delemont, M. (2002). "Seismic Retrofit of Simply Supported Bridges Using Shape Memory Alloys," *Engineering Structures*, Vol. 24, pp. 325–332.
21. DesRoches, R. and Smith, B. (2003). "Shape Memory Alloys in Seismic Resistant Design and Retrofit: A Critical Review of their Potential and Limitations," *Journal of Earthquake Engineering*, Vol. 7, No. 3, pp. 1-15.
22. Dong, J., Cai, C.S. and Okeil, A.M. (2011). "Overview of Potential and Existing Applications of Shape Memory Alloys in Bridges," *Journal of Bridge Engineering*, Vol. 16, No. 2, pp. 305-315.
23. FHWA Annual Materials Report. (2013). Retrieved August 28, 2014, from <http://www.fhwa.dot.gov/bridge/britab.cfm>.
24. Fischer, G. and Li, V.C. (2003). "Deformation Behavior of Fiber-Reinforced Polymer Reinforced Engineered Cementitious Composite (ECC) Flexural Members under Reversed Cyclic Loading Conditions," *ACI Structural Journal*, Vol. 100, No. 1, pp. 25-35.
25. Gibson, R.F. (2011). "*Principles of Composite Material Mechanics*," Third Edition. Boca Raton, FL: CRC Press.
26. Gowripalan, N., and Gilbert, IR. (2000). "Design Guidelines for Ductal Prestressed Concrete Beams," School of Civil and Environmental Engineering, The University of New South Wales.
27. Graesser, E.J. and Cozzarelli, F.A. (1991). "Shape-Memory Alloys as New Materials for Aseismic Isolation," *Journal of Engineering Mechanics*, Vol. 117, No. 11, pp. 2590-608.
28. Graybeal, B. (2006). "Material Property Characterization of Ultra-High Performance Concrete," McLean, VA: FHWA, U.S. Department of Transportation, *Report No. FHWA-HRT-06-103*.
29. Graybeal, B. (2010). "Behavior of Field-Cast Ultra-High Performance Concrete Bridge Deck Connections under Cyclic and Static Structural Loading," Federal Highway Administration *Report No. FHWA-HRT-11-023*.
30. Holloway, L.C. and Teng, J.G. (2008). "Strengthening and Rehabilitation of Civil Infrastructures Using Fibre-Reinforced Polymer (FRP) Composites," *Woodhead Publishing Series in Civil and Structural Engineering*, 416 pp.
31. Johnson, R., Padgett, J.E., Maragakis, M.E., DesRoches, R., and Saiidi, M.S. (2008). "Large Scale Testing of Nitinol Shape Memory Alloy Devices for Retrofitting of Bridges," *Smart Materials and Structures*, Vol. 17, No. 3, 10 pp.
32. JSCE Concrete Library 127. (2008). "Recommendations for Design and Construction of High Performance Fiber Reinforced Cement Composites with Multiple Fine Cracks (HPFRCC)," Japan Society of Civil Engineers.
33. Kawashima, K., and Nagai, M. (2002). "Development of a Reinforced Concrete Pier with a Rubber Layer in the Plastic Hinge Region," *Structural Earthquake Engineering, JSCE*, Vol. 703, No. I-59, pp. 113-128.
34. Kawashima, K., Zafra, R.G., Sasaki, T., Kajiwara, K., and Nakayama, M. (2011). "Effect of Polypropylene Fiber Reinforced Cement Composite and Steel Fiber Reinforced Concrete for Enhancing the Seismic Performance of Bridge Columns," *Journal of Earthquake Engineering*, Vol. 15, No. 8, pp. 1194–1211.
35. Kawashima, K., Zafra, R.G., Sasaki, T., Kajiwara, K., Nakayama, M., Unjoh, S., Sakai, J., Kosa, K., Takahashi, Y., and Yabe, M. (2012). "Seismic Performance of a Full-Size Polypropylene Fiber-Reinforced Cement Composite Bridge Column Based on E-Defense Shake Table Experiments," *Journal of Earthquake Engineering*, Vol. 16, No. 4, pp. 463–495.
36. Kelly, J.M. (1993). "*Earthquake-Resistant Design with Rubber*," London, UK: Springer-Verlag, 134 pp.
37. Kelly, J.M. and Konstantinidis, D.A. (2001). "*Mechanics of Rubber Bearings for Seismic and Vibration Isolation*," United Kingdom, John Wiley & Sons, Ltd.

38. Li V.C., Li, M. and Lepech, M. (2006). "High Performance Material for Rapid Durable Repair of Bridges and Structures," Michigan Department of Transportation *Research Report RC-1484*, 142 pp.
39. Li, V.C. (2008). "*Engineered Cementitious Composites (ECC): Material, Structural, and Durability Performance*," in Concrete Construction Engineering Handbook, Chapter 24, Ed. E. Nawy: published by CRC Press.
40. Mayes, R.L., Buckle, I.G., Kelly, T.E., and Jones, L.R. (1992). "AASHTO Seismic Isolation Design Requirements for Highway Bridges," *Journal of Structural Engineering, ASCE*, Vol. 118, No. 1, pp. 284-304.
41. Mehrsoroush, A. and Saiidi, M.S. (2014). "Seismic Performance of Two-Column Bridge Piers with Innovative Precast Members and Pipe Pin Connections," 7th International Conference on Bridge Maintenance, Safety and Management (IABMAS). Shanghai, China.
42. Mertz, D.R., Chajes, M.J., Gillespie, J.W., Kukich, D.S., Sabol, S.A., Hawkins, N.M., Aquino, W., and Deen, T.B. (2003). "Application of Fiber Reinforced Polymer Composites to the Highway Infrastructure," Washington, D.C., National Cooperative Highway Research Program (NCHRP) Report No. 503, 87 pp.
43. Mirmiran, A., Shahawy, M., Nanni, A., and Karbhari, V. (2004). "Bonded Repair and Retrofit of Concrete Structures Using FRP Composites: Recommended, Construction, Specifications, and Process Control Manual," Washington, D.C., National Cooperative Highway Research Program (NCHRP) Report No. 514, 102 pp.
44. Motaref, S., Saiidi, M.S., and Sanders, D. (2011). "Seismic Response of Precast Bridge Columns with Energy Dissipating Joints," Center for Civil Engineering Earthquake Research, Department of Civil and Environmental Engineering, University of Nevada, Reno, *Report No. CCEER-11-01*.
45. Nakashoji, B. and Saiidi, M.S. (2014). "Seismic Performance of Square Nickel-Titanium Reinforced ECC Columns with Headed Couplers," Center For Civil Engineering Earthquake Research, Department Of Civil and Environmental Engineering, University of Nevada, Reno, Nevada, *Report No. CCEER-14-05*, 252 pp.
46. NSF-PFI Project. (2014). Retrieved July 09, 2014, from <http://wolfweb.unr.edu/homepage/saiidi/NSF-PFI/index.html>.
47. Otsuka, K., and Wayman, C. M. (1998). "*Mechanism of Shape Memory Effect and Superplasticity*," Cambridge University Press, Cambridge, U.K., pp. 27-48.
48. Panagiotou, M., Trono, W., Jen, G., Kumar, P., and Ostertag, C.P. (2014). "Experimental Seismic Response of Hybrid Fiber-Reinforced Concrete Bridge Columns with Novel Longitudinal Reinforcement Detailing," *Journal of Bridge Engineering, ASCE*, ISSN 1084-0702/04014090(12), 12 pp.
49. Russell, H.G. and Graybeal B.A. (2013). "Ultra-High Performance Concrete: A State-of-the-Art Report for the Bridge Community," Federal Highway Administration, *Report No. FHWA-HRT-13-060*, 171 pp.
50. Saiidi, M.S. and Wang H. (2006). "Exploratory Study of Seismic Response of Concrete Columns with Shape Memory Alloys Reinforcement," *ACI Structural Journal*, Vol. 103, No. 3, 436-443.
51. Saiidi, M.S., O'Brien, M. and Sadrossadat-Zadeh, M. (2009). "Cyclic Response of Concrete Bridge Columns Using Superelastic Nitinol and Bendable Concrete," *ACI Structural Journal*, Vol. 106, No. 1, pp. 69-77.
52. Saiidi, M.S., Sadrossadat-Zadeh, M., Ayoub, C., and Itani, A. (2007). "Pilot Study of Behavior of Concrete Beams Reinforced with Shape Memory Alloys," *Journal of Materials in Civil Engineering, ASCE*, Vol. 19, No. 6, pp. 454-461.
53. Saiidi, M.S., Tazarv, M., Nakashoji, B., Varela, S., and Kavianipour, F. (2014). "Resilient and Sustainable Bridges of the Future," (Keynote Paper), *Proceedings of 2nd International*

- Conference on bridges "Innovations on Bridges and Soil-Bridge Interaction"*, Athens, Greece, 12 pp.
54. Shrestha, K.C., Araki, Y., Nagae, T., Koetaka, Y., Suzuki, Y., Omori, T., Sutou, Y., Kainuma, R., and Ishida, k. (2013). "Feasibility of Cu-Al-Mn Superelastic Alloy Bars as Reinforcement Elements in Concrete Beams," *Smart Materials and Structures*, Vol. 22, No. 2, 15 pp.
 55. Song, G., Ma, N. and Li, H.N. (2006). "Applications of Shape Memory Alloys in Civil Structures," *Engineering Structures*, Vol. 28, pp. 1266-1274.
 56. SR99 SMA-ECC Bridge. (2014). Retrieved July 09, 2014, from <http://wolfweb.unr.edu/homepage/saiidi/WashDOT/SR99/index.html>.
 57. Tazarv, M. and Saiidi, M.S. (2014a). "Next Generation of Bridge Columns for Accelerated Bridge Construction in High Seismic Zones," Center For Civil Engineering Earthquake Research, Department of Civil and Environmental Engineering, University of Nevada, Reno, Nevada, *Report No. CCEER-14-06*, 400 pp.
 58. Tazarv, M. and Saiidi, M.S. (2014b). "Reinforcing NiTi Superelastic SMA for Concrete Structures," *Journal of Structural Engineering, ASCE*, DOI: 10.1061/(ASCE)ST.1943-541X.0001176, 10 pp.
 59. Uchida, Y., Niwa, J., Tanaka, Y., Katagiri, M. (2006). "Outlines of "Recommendations for Design and Construction of Ultra High Strength Fiber Reinforced Concrete Structures" By JSCE," International RILEM Workshop on High Performance Fiber Reinforced Cementitious Composites in Structural Applications (pp. 343-351). RILEM Publications SARL.
 60. Varela, S. and Saiidi, M.S. (2013). "Innovation in Sustainable Earthquake-Resistant Highway Bridges with Advanced Materials," NEES Annual Meeting, Quake Summit 2013, Session 13. Reno, Nevada.
 61. Wierschem, N. and Andrawes, B. (2010). "Superelastic SMA-FRP Composite Reinforcement for Concrete Structures," *Smart Materials and Structures*, Vol. 19, 13 pp.
 62. Wilson, J.C. and Wesolowsky, M.J. (2005). "Shape Memory Alloys for Seismic Response Modification: A State-of-the-Art Review," *Earthquake Spectra*, Vol. 21, No. 2, pp. 569–601.
 63. Youssef, M.A., Alam, M.S. and Nehdi, M. (2008). "Experimental Investigation on the Seismic Behavior of Beam-Column Joints Reinforced with Superelastic Shape Memory Alloys," *Journal of Earthquake Engineering*, Vol. 12, No. 7, pp. 1205-1222.
 64. Yura, J., Kumar, A., Yakut, A., Topkaya, C., Becker, E., and Collingwood, J. (2001). "Elastomeric Bridge Bearings-Recommended Test Methods," National Cooperative Highway Research Program (NCHRP) *Report No. 449*, 125 pp.
 65. Zureick, A.H., Ellingwood, B.R., Nowak, A.S., Mertz, D.R., and Triantafillou, T.C. (2010). "Recommended Guide Specification for the Design of Externally Bonded FRP Systems for Repair and Strengthening of Concrete Bridge Elements," Washington, D.C., National Cooperative Highway Research Program (NCHRP) *Report No. 655*, 118 pp.

APPENDICES

NCHRP 12-101

App. A – Literature Review

App. B – Survey of State Departments of Transportation

App. C – Synthesis of Literature

App. D – Novel Column and Construction Concepts

App. E – Demonstration of Evaluation Guidelines

App. F – Detailed Design Examples for Three Novel Columns

App. G – Benefits and Economic Impact of Novel Columns

App. H – Relationship between Drift Ratio and Displacement Ductility

App. I – Modeling Methods and Validation for Novel Columns

TABLE OF CONTENTS

APPENDICES	I
TABLE OF CONTENTS.....	II
APPENDIX B	B-1
B.1 Blank Survey Form	B-2
B.2 Survey Results.....	B-5
B.2.1 Familiarity with Advanced Materials	B-5
B.2.2 Application of Advanced Materials in New Bridges.....	B-7
B.2.3 Application of Advanced Materials in Bridge Repair	B-7
B.2.4 Future Application of Advanced Materials in New Bridges	B-8
B.2.5 Application of Rocking Systems	B-8
B.2.6 Other Advanced Materials	B-8
B.3 Conclusions	B-8

APPENDIX B

Survey of State Departments of Transportation on Familiarity and Implementation of Advanced Materials and Innovative Technologies in Seismic Design of Bridge Columns

An online survey of state DOT bridge/structures divisions was conducted from 09/17/2014 to 10/16/2014 to collect data on familiarity, past deployment, and potential future application of advanced materials (AMs) including SMA, ECC, UHPC, FRP, and built-in rubber pad in bridge columns under their jurisdiction. An email was sent to members of the AASHTO 2013 Subcommittee on Bridges and Structures. A total of 119 individuals were contacted, of whom 37 from 34 states responded. Both application in bridge repair and new bridge construction were included in the survey, even though the NCHRP 12-101 project is about new bridges. It was believed that past application could indicate the actual degree of receptiveness to AMs and any field experience that might be useful. The survey form and statistical analysis of the survey results are presented in this appendix.

B.1 Blank Survey Form

A study funded by NCHRP is underway to develop (1) proposed AASHTO guidelines for the evaluation of new techniques for the design and construction of bridge columns with energy dissipation mechanisms in order to minimize bridge damage and replacement after a seismic event; and (2) design and construction concepts based on new materials and techniques. New material includes, but not limited to: shape memory alloy (SMA), engineered cementitious composite (ECC), ultra-high performance concrete (UHPC), fiber reinforced polymer (FRP), and rubber. They are referred to as advanced materials since they exhibit improved performance over conventional concrete and steel such as higher strength, higher ductility, and excellent corrosion resistance. Proper combination of these materials in bridge components specifically columns may result in low-damage columns with improved energy dissipation mechanism.

The purpose of the survey is to explore the past, present, and planned future application of advanced materials in the US bridges, conduct a statistical analysis, and include the results in the NCHRP report. We very much appreciate your time and effort in providing the information.

1. Are you or other DOT staff in your state familiar with the following advanced materials within the context of bridge column design?

	0 (Not at all)	1	2	3	4	5 (Very familiar)
SMA	<input type="checkbox"/>					
ECC	<input type="checkbox"/>					
UHPC	<input type="checkbox"/>					
FRP	<input type="checkbox"/>					
Rubber (not as isolators or bearings)	<input type="checkbox"/>					

2. Do you or other DOT staff in your state know any other advanced materials within the context of bridge column design beside what was presented in Q1?

Yes No

Material 1

Material 2

Material 3

How familiar are you with the materials you listed?

	0 (Not at all)	1	2	3	4	5 (Very familiar)
Material 1	<input type="checkbox"/>					
Material 2	<input type="checkbox"/>					
Material 3	<input type="checkbox"/>					

3. Has your state DOT ever used advanced materials in new bridge construction?

Yes No

If yes, please select material(s):

SMA ECC UHPC FRP Rubber (not as isolators or bearings) Other
advanced materials

SMA: What bridge component?

ECC: What bridge component?

UHPC: What bridge component?

FRP: What bridge component?

Rubber: What bridge component?

Other: Name the material/What bridge component?

4. Has your state DOT ever used advanced materials in bridge repair?

Yes No

If yes, please select material(s):

SMA ECC UHPC FRP Rubber (not as isolators or bearings) Other
advanced materials

SMA: What bridge component?

ECC: What bridge component?

UHPC: What bridge component?

FRP: What bridge component?

Rubber: What bridge component?

Other: Name the material/What bridge component?

5. Does your state DOT plan to use advanced materials in the next three years for either repair or new construction?

Yes No

If yes, please select material(s):

SMA ECC UHPC FRP Rubber (not as isolators or bearings) Other
advanced materials

SMA: What bridge component?

ECC: What bridge component?

UHPC: What bridge component?

FRP: What bridge component?

Rubber: What bridge component?

Other -- Name the material and what bridge component

Rocking columns and rocking foundations showed promising seismic performance in experimental studies.

6. Has your state DOT ever used rocking systems?

Yes No

If yes, how many projects?

7. Does your state DOT plan to use rocking systems in the next three years?

Yes No

If yes, how many projects?

An emerging technology is application of post-tensioning tendons in bridge columns to increase self-centering tendency. Columns in this category are connected to adjoining members with moment-resisting detailing as well as post-tensioning tendons, which are referred to as hybrid systems.

8. Has your state DOT ever used hybrid systems?

Yes No

If yes, how many projects?

9. Does your state DOT plan to use hybrid systems in the next three years?

Yes No

If yes, how many projects?

Please provide your contact information.

Name

First Name

Last Name

Email

State

B.2 Survey Results

The survey was sent to members of the AASHTO 2013 Subcommittee on Bridges and Structures. Thirty seven members from 34 state DOTs participated in the survey. Summary of the collected data is presented in this section.

B.2.1 Familiarity with Advanced Materials

Bridge engineers were most familiar with FRP. UHPC was the second most known advanced material in the bridge engineering community and SMA, ECC, and built-in rubber pad were almost new to state DOTs. Figure B-1 shows familiarity of state DOTs with advance materials. The breakdowns are shown in Fig. B-2.

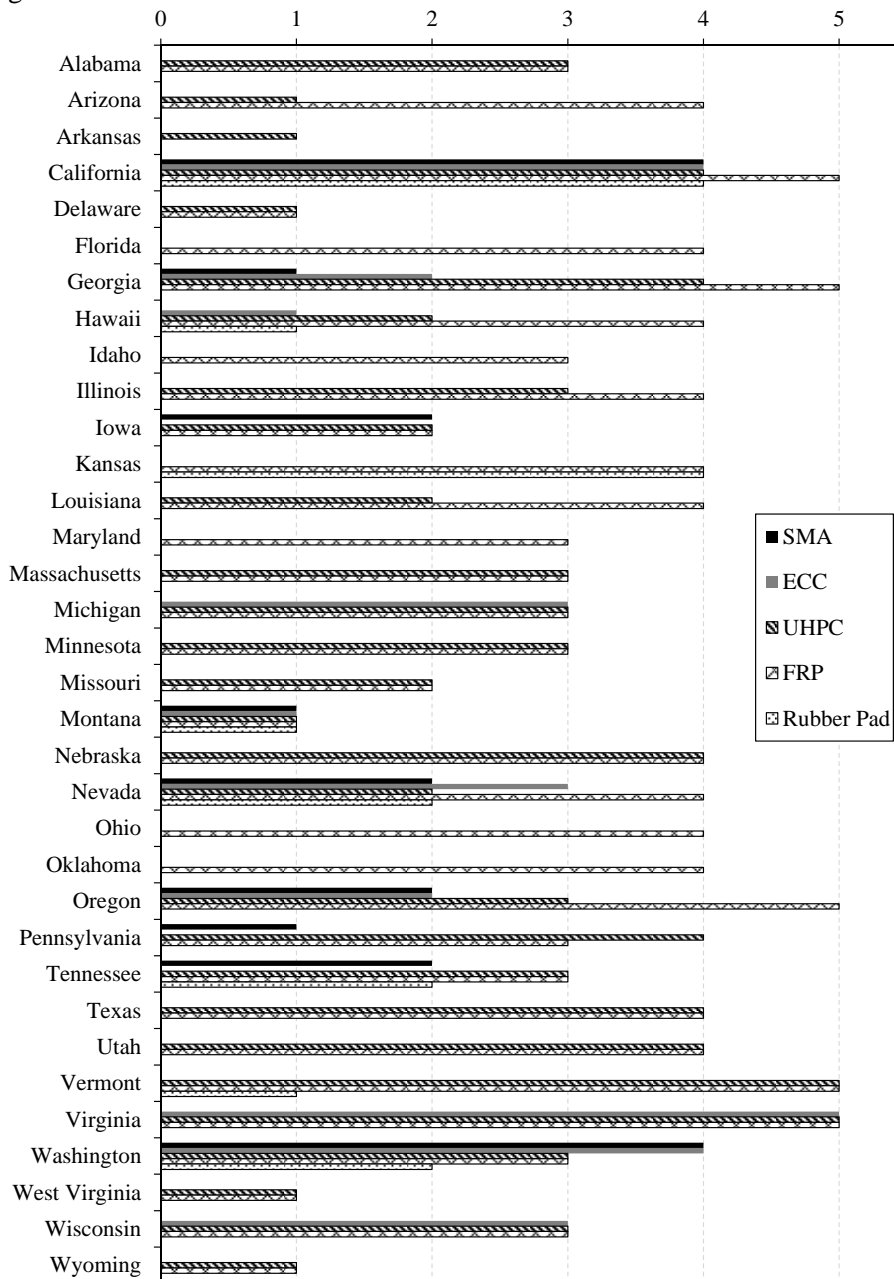


Figure B-1. Participated state DOT familiarity with advanced materials (0 is unfamiliar)

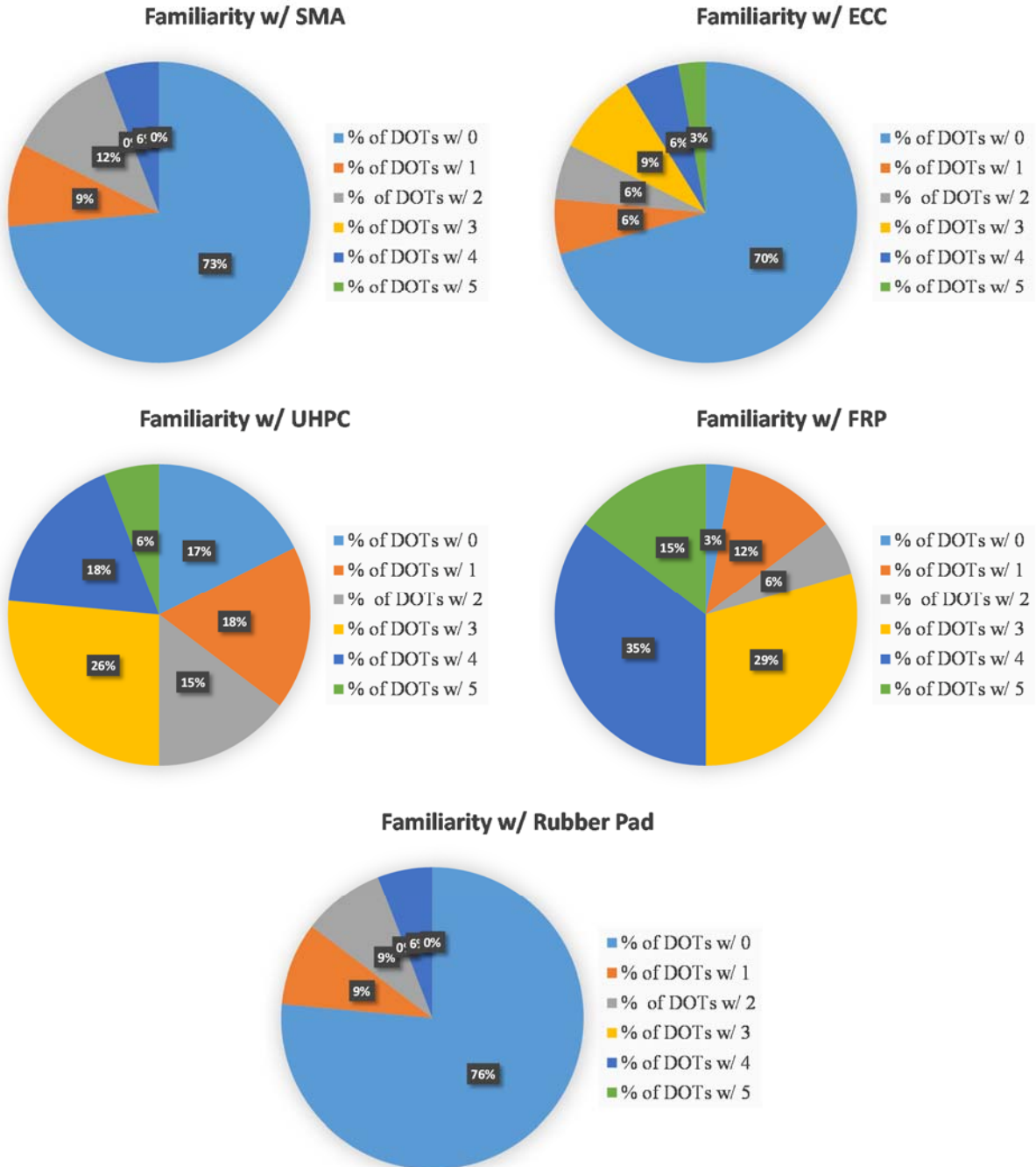


Figure B-2. Participated state DOT familiarity breakdown with advanced materials (0 is unfamiliar)

B.2.2 Application of Advanced Materials in New Bridges

It was found that 47% of participating state DOTs (16 DOTs) have incorporated one or more type of advanced material/s in new bridge construction (Fig. B-3). It can be seen that FRP and UHPC have been utilized more than other materials. FRP has been mainly used in superstructures such as deck and cap beams as reinforcement. UHPC has been only incorporated in deck connections. ECC has been utilized as grout between adjacent box beams in two states.

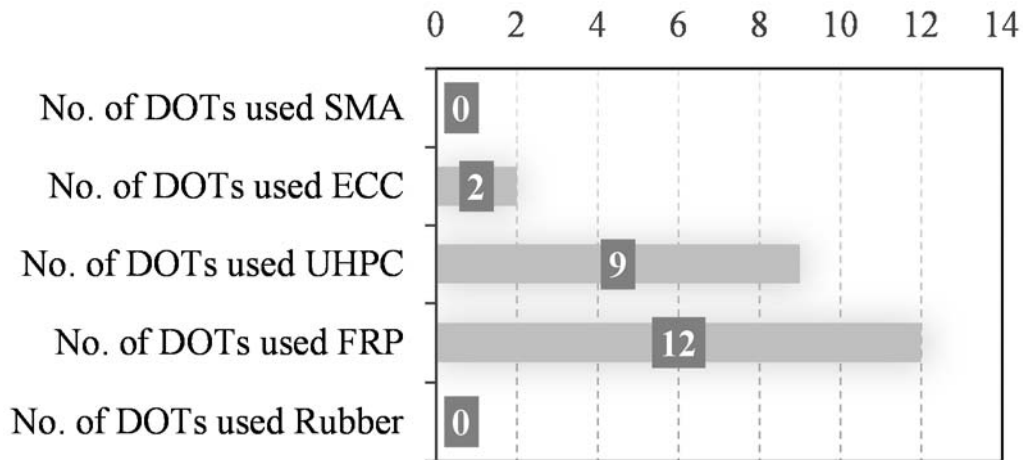


Figure B-3. Deployment of advanced materials in new bridge construction

B.2.3 Application of Advanced Materials in Bridge Repair

FRP has been extensively utilized by 82% of participated state DOTs (28 DOTs) as repair material (Fig. B-4). FRP wraps have been used in piles, columns, cap beams, and girders for seismic and non-seismic repair or retrofit. ECC and UHPC have been incorporated in closure pours of precast elements.

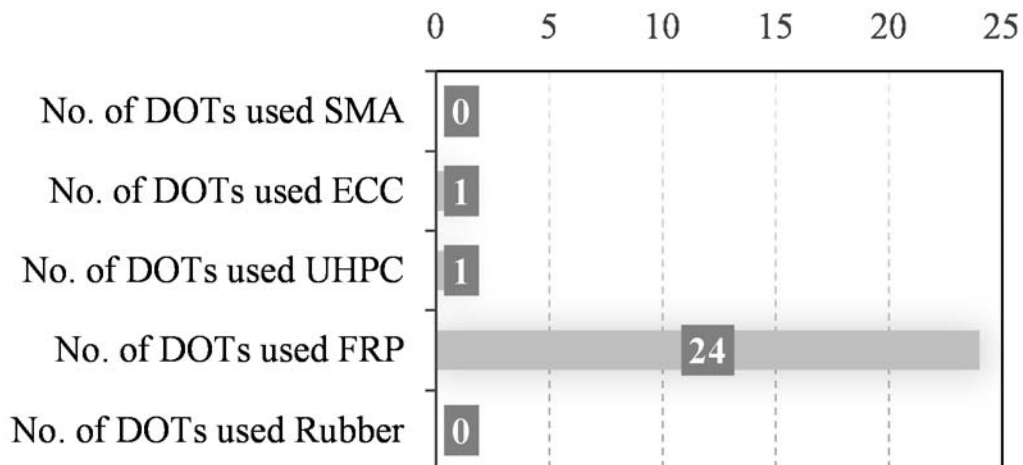


Figure B-4. Deployment of advanced materials in bridge repair

B.2.4 Future Application of Advanced Materials in New Bridges

Many state DOTs expressed interest in utilizing advanced materials in construction of new bridges, and 23 state DOTs (68% of participants) plan to deploy them in the next three years. Figure B-5 shows the number of state DOTs that will be using each advance material.

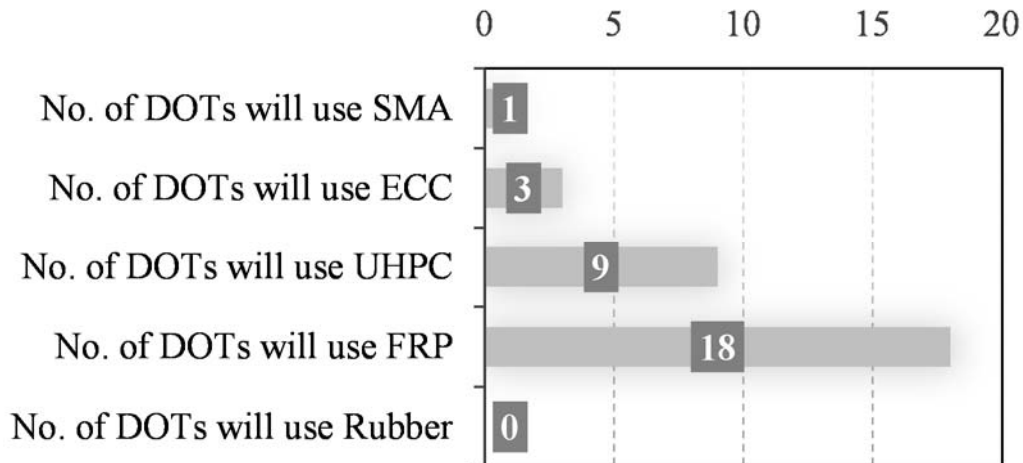


Figure B-5. Deployment of advanced materials in new bridge construction in next three years

B.2.5 Application of Rocking Systems

The survey results showed that five state DOTs have incorporated or plan to utilize rocking column systems (column rocking, footing rocking, or hybrid connection rocking) in the next three years: California, Massachusetts, Oregon, Utah, and Washington.

B.2.6 Other Advanced Materials

Carbon fiber strands were used by the Virginia DOT as prestressing tendons in piles and bulb T members.

B.3 Conclusions

There is a clear correlation between the familiarity of bridge engineers with advance materials (or innovative systems) and field applications. FRP has been utilized more than other advanced materials due to availability of guidelines and specifications. Tasks 1 through 3 of the NCHRP 12-101 (Appendix A) project revealed that the number of available codes/guidelines for FRP is five times those for all other materials, combined.

Novel bridge columns incorporating advanced materials or innovative systems can exhibit superior seismic performance compared to conventional reinforced concrete columns, eliminate or substantially minimize post-earthquake repair cost, and ensure serviceability of bridges after severe earthquakes. The main objectives of the current project are to develop design guidelines for novel columns, to show robustness of proposed columns, and pave the way for field deployments. The survey results were encouraging and demonstrate the receptiveness of the bridge engineering community to new concepts. Successful execution of project 12-101 is likely to enable and encourage more engineers to consider deploying new technologies to improve resiliency of bridges.

APPENDICES

NCHRP 12-101

App. A – Literature Review

App. B – Survey of State Departments of Transportation

App. C – Synthesis of Literature

App. D – Novel Column and Construction Concepts

App. E – Demonstration of Evaluation Guidelines

App. F – Detailed Design Examples for Three Novel Columns

App. G – Benefits and Economic Impact of Novel Columns

App. H – Relationship between Drift Ratio and Displacement Ductility

App. I – Modeling Methods and Validation for Novel Columns

TABLE OF CONTENTS

APPENDICES	I
TABLE OF CONTENTS.....	II
APPENDIX C	C-1
C.1 Introduction	C-2
C.2 Advanced Material Readiness for Design and Deployment	C-2

APPENDIX C

Synthesis of Literature

Synthesize the literature to identify knowledge gaps regarding advanced materials.

C.1 Introduction

Advanced materials were introduced in previous sections. A summary of readiness of advanced materials for field deployment is presented herein.

C.2 Advanced Material Readiness for Design and Deployment

A summary of advantages, commercial availability, knowledge gap, regulatory needs, and costs for each of the aforementioned advanced material is presented in Table C-2. Desired application of each advanced material as concrete or reinforcement was proposed. Commercial products that are available are presented. Then durability was evaluated based on performance data. All materials exhibit equal or better resistant to climatic effects than conventional materials. Limitations for regional usage (e.g. applicability in very cold or very hot regions) are suggested. SMA superelastic behavior is lost when ambient temperature is below the austenite finish temperature. Rubber becomes brittle under very low temperatures. Therefore, these two materials are not appropriate for cold regions such as Alaska unless proper insulation is provided. Issues regarding field application of each advanced material were identified. The need for post-earthquake inspection was also evaluated. Only the behavior of NiTi SMA is well known and other existing or emerging SMAs have yet to be studied. Areas of needed future studies before application of these materials in moderate and high seismic zones are identified in the section on knowledge gaps. Specifications should be prepared for design and field application of UHPC, ECC, and SMA. AASHTO design specifications for rubber may be modified to accommodate innovative application of rubber pad at plastic hinges. Unit cost for each material was collected from major manufacturers. They were asked to estimate the cost of their product in 2016, which is the end date of the NCHRP 12-101 project.

Table C-2. Advanced material readiness for design and deployment

Material	UHPC	ECC	SMA	FRP	Rubber
Application	in lieu of concrete	in lieu of concrete	as reinforcement	as reinforcement, jacket, tendon	in lieu of concrete
Commercial Availability	Avail., Premixed	Avail., Premixed	Avail., Bars & Wires	Avail., Sheets, Bars, Tendons	Avail., Unit Component
Durability	Excellent	Good	Excellent	Good	Good
Material Limitations	None	None	Shall not be used in very cold regions e.g. Alaska	Shall be protected against fire and solar radiation	Shall not be used in very cold regions e.g. Alaska
Constructability	Has its own batching procedure	Similar to concrete	SMA bars should not be dented and welded	Tendon anchorage still emerging	Avoid exposure to fire
Post-Earthquake Inspection	May not be needed	Needed	Not required	May not be needed	Not required
knowledge Gap	Confined properties are unknown	None	None for NiTi SMA	None	None
Specification & Guideline Gap	USA	N/A	N/A	Avail.	Avail.
	Int.	Avail.	Avail.	Avail.	--
	P.R.	--	--	Avail.	--
Unit Price	\$2,100/yd ³	\$250/yd ³	\$105/lb	\$10/ft ²	\$5,500/ft ³

Note: "Avail." is an abbreviation for "Available"; "N/A" denotes "Not Available"; "Int." is an abbreviation for "International"; "P.R." denotes "Proposed by Researchers". FRP unit price is for CFRP. Rubber unit price is for rubber pad reinforced with internal steel shims and vulcanized to two stainless steel plates at both ends of rubber. All prices in USD. 1 yd = 0.9144 m. 1 ft = 0.3048 m. 1 lb = 0.4536 kg.

APPENDICES

NCHRP 12-101

App. A – Literature Review

App. B – Survey of State Departments of Transportation

App. C – Synthesis of Literature

App. D – Novel Column and Construction Concepts

App. E – Demonstration of Evaluation Guidelines

App. F – Detailed Design Examples for Three Novel Columns

App. G – Benefits and Economic Impact of Novel Columns

App. H – Relationship between Drift Ratio and Displacement Ductility

App. I – Modeling Methods and Validation for Novel Columns

TABLE OF CONTENTS

APPENDICES	I
TABLE OF CONTENTS.....	II
APPENDIX D.....	D-1
D.1 Introduction.....	D-2
D.2 Novel Column Concepts	D-2
D.2.1 Column Type 1	D-2
D.2.2 Column Type 3	D-6
D.2.3 Column Type 7	D-6
D.2.4 Column Type 10	D-8
D.2.5 Column Type 14	D-9
D.2.6 Column Type 15	D-10
D.2.7 Column Type 20	D-10
D.2.8 Column Type 31	D-10
D.3 References.....	D-11

APPENDIX D

Novel Column and Construction Concepts

Synthesize the literature to identify novel columns. Develop new column concepts with improved seismic performance using the combination of advanced materials and new technology.

D.1 Introduction

Current design philosophy for standard bridges is to prevent collapse in the event of earthquakes by allowing plastic deformations of columns and other sacrificial components such as shear key. Severe column damage and potentially large permanent deformation of columns are expected using current bridge specifications. Novel columns are emerging to overcome these shortcomings while providing sufficient resiliency. Existing and potential novel columns are introduced in this section that may satisfy two or all of the following performance criteria: (1) large displacement or drift capacity, (2) minimal plastic hinge damage, and (3) negligible lateral residual deformations. Displacement or drift capacity is evaluated in this report instead of other common terms such as displacement ductility since novel column yield displacement may be higher than that of conventional columns, and using displacement ductility as the sole evaluation criterion may be misleading. For example, displacement capacity of a SMA-reinforced column may be twice a conventional reinforced concrete (RC) column capacity, but, because yield strain of SMA is greater than steel yield strain, the effective yield displacement of an SMA-reinforced column is relatively large and its “displacement ductility” may be lower than that of a conventional RC member.

Advanced materials were introduced in previous sections and their stress-strain behavior, advantages, and applicability were evaluated. Combination of these materials with conventional materials may lead to several feasible novel column concepts and configurations with the aforementioned performance objectives. These combinations are presented in this section.

D.2 Novel Column Concepts

Table D-1 presents existing and potential novel feasible column concepts made with combinations of advanced and conventional materials, and Fig. D-1 illustrates plastic hinges of these columns. It is useful to categorize column performance with respect to their role in improving resiliency of bridge columns as (a) large displacement (or drift) capacity (LDC), (b) minimizing damage mechanism (MDM), and (c) re-centering mechanism (RM). The expected seismic performance based on the type of advanced material/s incorporated in each column type is evaluated and discussed.

Of the 39 feasible combinations, the seismic performance of eight column types has been experimentally evaluated. The remaining combinations are “concept” columns in which the seismic performance and other aspects are yet to be explored. Review of previous studies on the performance of these eight column types and their suitability for moderate and high zones are presented in this section.

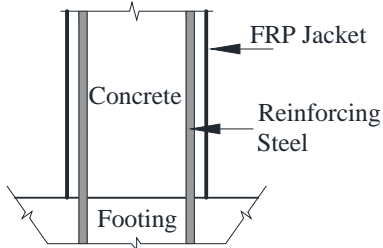
D.2.1 Column Type 1

Performance of concrete-filled FRP tube (CFFT) columns reinforced lightly with steel has been investigated in many studies. The concept was proposed by Mirmiran and Shahawy (1996). Confined concrete model and effect of different parameters were investigated by Samaan et al. (1998) and Mirmiran et al. (1998). Seismic performance of CFFT bridge columns or columns retrofitted with FRP jacket was studied by Seible et al. (1997), Shao and Mirmiran (2005), Zhu et al. (2006), Ozbakkaloglu and Saatcioglu (2006), Zoghi et al. (2012), and Kavianipour and Saiidi (2013). It was found that FRP tubes made with fibers aligned at ± 55 degree result in optimal performance. Plastic hinge damage was minimal in the tests, and more than 9% drift ratio capacity was observed in cyclic and dynamic tests. The displacement capacity and lateral force capacity of CFFT columns were higher than those of conventional columns. In summary, Column Type 1 (commonly referred as a CFFT column) satisfies LDC and MDM performance criteria but significant yielding of steel reinforcements is expected that leads to residual displacements. Nonetheless, the elastic response of the shell leads to smaller permanent displacements compared to that of conventional RC columns.

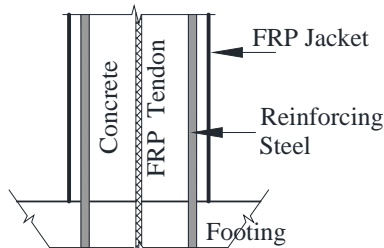
Table D-1. Novel column plastic hinges

Column Type	Material								Performance			Poof Test
	C	S	UHPC	ECC	SMA	FRP	Rub.	Tendon	LDC	MDM	RM	
1	X	X				J			X	X		X
2	X	X				J&T			X	X	X	
3	X	X				J		X	X	X	X	X
4	X	X				J&T	X		X	X	X	
5	X	X				J	X	X	X	X	X	
6	X	X				T	X		X	X	X	
7	X	X					X	X	X	X	X	X
8	X				X	J			X	X	X	
9	X					J&R			X	X		
10	X				X	J	X		X	X	X	X
11	X				X	J&T	X		X	X	X	
12	X					J,R,T	X		X	X	X	
13	X				X	J	X	X	X	X	X	
14		X	X							X		X
15		X	X			J				X	X	X
16		X	X			T			X	X	X	
17		X	X			T	X		X	X	X	
18		X	X					X	X	X	X	
19		X	X				X	X	X	X	X	
20		X		X					X	X		X
21		X		X		T			X	X	X	
22		X		X				X	X	X	X	
23			X		X				X	X	X	
24			X		X		X		X	X	X	
25			X		X	T	X		X	X	X	
26			X		X		X	X	X	X	X	
27			X			R&T	X		X	X	X	
28			X			R			X	X		
29			X			T			X	X	X	
30			X					X	X	X	X	
31				X	X				X	X	X	X
32				X	X		X		X	X	X	
33				X	X	T	X		X	X	X	
34				X	X		X	X	X	X	X	
35				X		R&T	X		X	X	X	
36				X		R			X	X		
37				X		R	X	X	X	X	X	
38				X		J&T			X	X	X	
39				X		J		X	X	X	X	

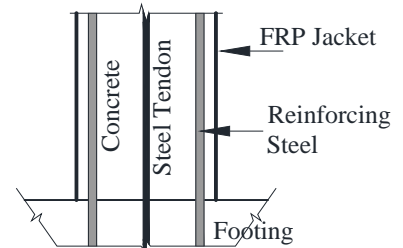
Note: "C" denotes "Conventional Concrete"; "S" refers to "Conventional Steel"; "Rub." denotes "Reinforced Rubber"; "J" denotes "FRP Jacket"; "R" denotes "FRP Reinforcement"; and "T" denotes "FRP Tendon"; "Tendon" denotes "Steel Tendon"; LDC is an acronym for Large Displacement (or Drift) Capacity, MDM is an acronym for Minimized Damage Mechanism, and RM is an acronym for Re-centering (or self-centering) Mechanism.



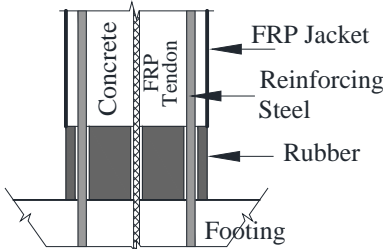
Column Type 1



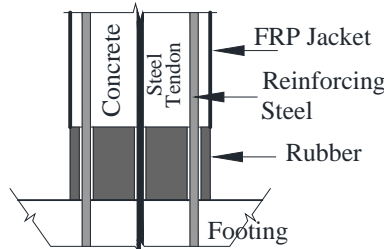
Column Type 2



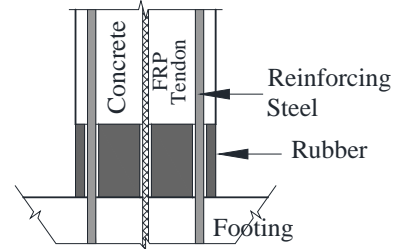
Column Type 3



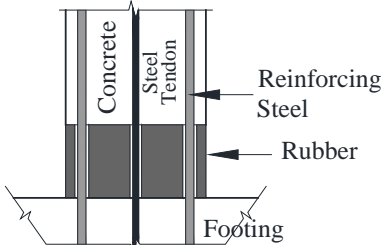
Column Type 4



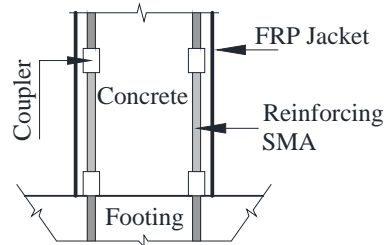
Column Type 5



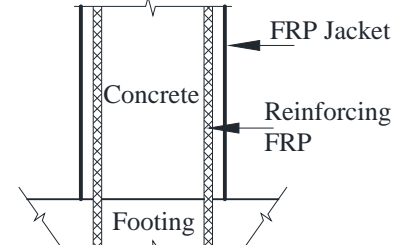
Column Type 6



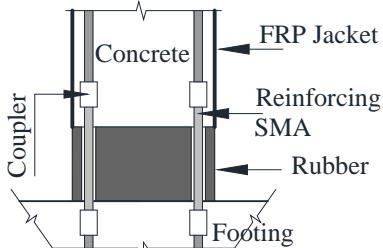
Column Type 7



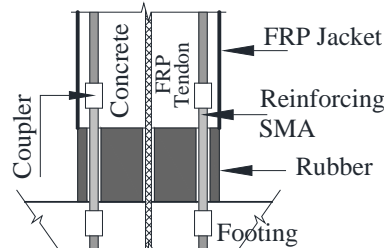
Column Type 8



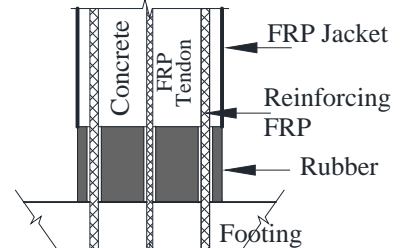
Column Type 9



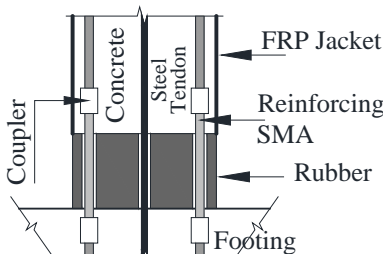
Column Type 10



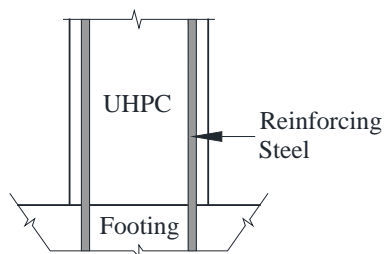
Column Type 11



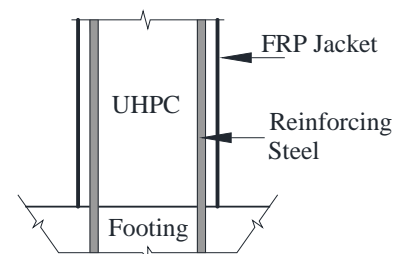
Column Type 12



Column Type 13



Column Type 14



Column Type 15

Figure D-1. Novel column plastic hinges

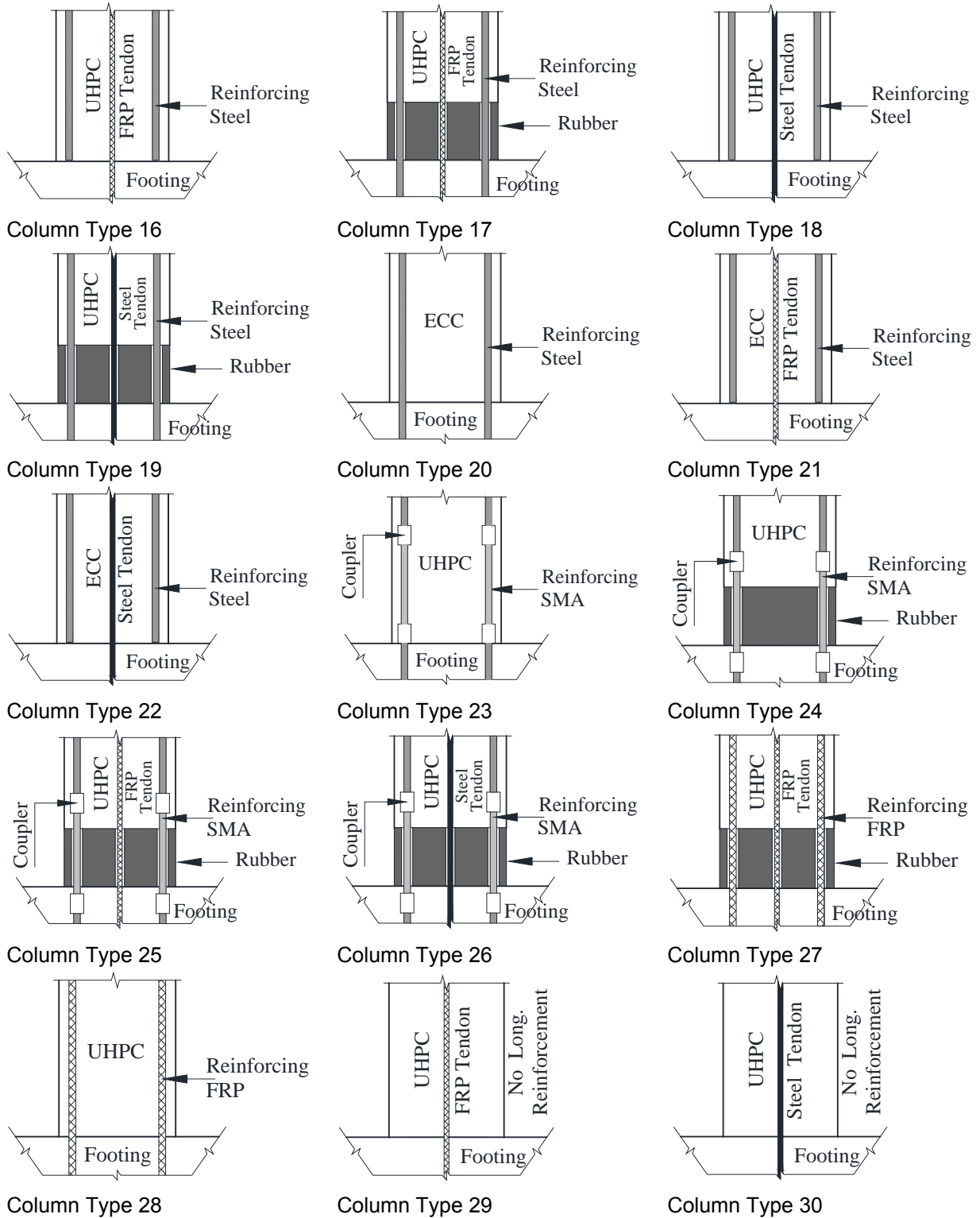


Figure D-1. Novel column plastic hinges (continued)

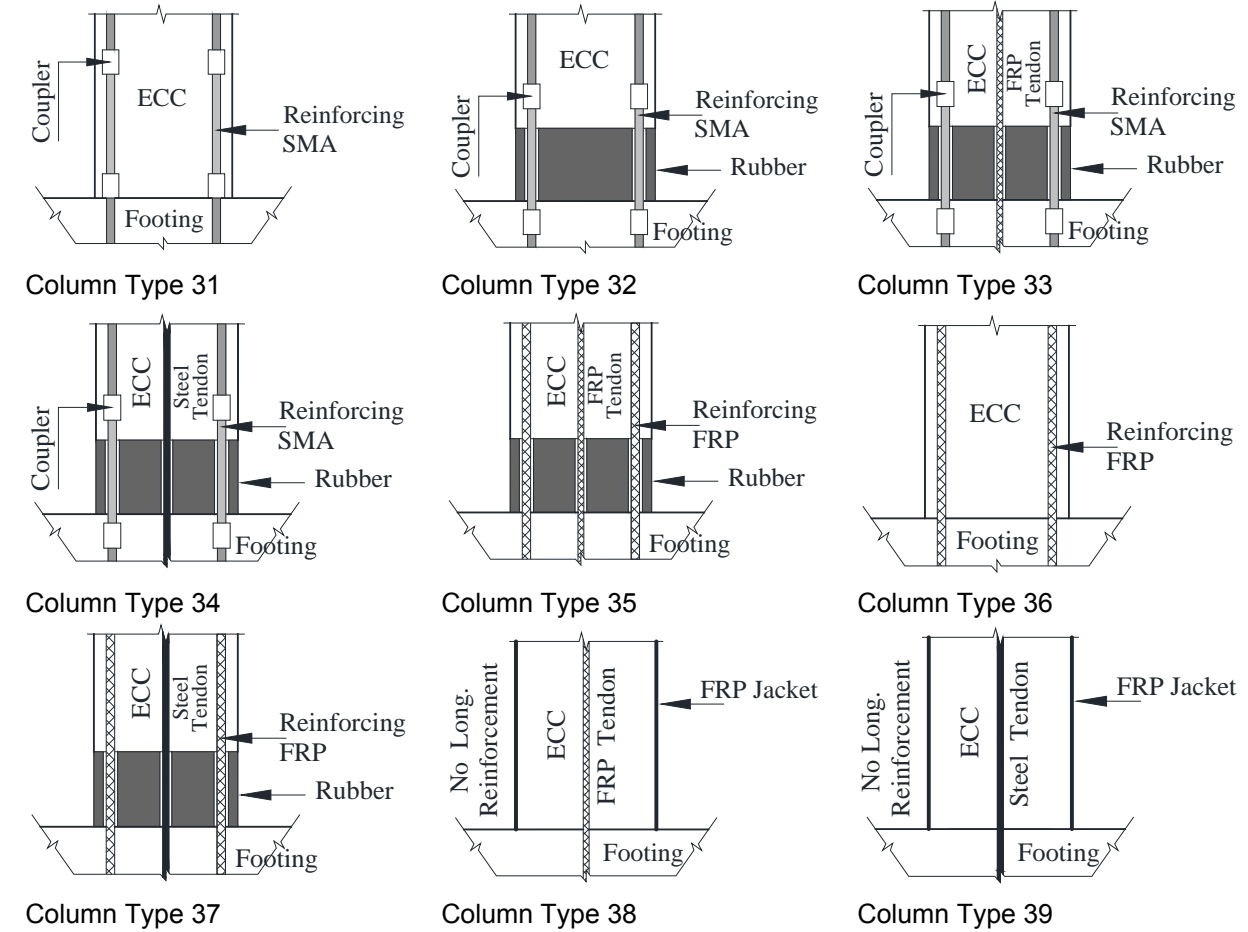


Figure D-1. Novel column plastic hinges (continued)

D.2.2 Column Type 3

Concrete filled FRP tube (CFFT) columns can be additionally reinforced with steel tendons to enhance the self-centering tendency. CFFT column longitudinal reinforcements may or may not be extended to adjoining member/s, but both columns are categorized in Column Type 3, which is commonly referred to as rocking system. Tendons are usually designed to remain elastic. Several analytical and experimental studies have investigated behavior and performance of rocking columns (Mander and Cheng, 1997; Garcia, 1998; Hewes and Priestley, 2002; Kwan and Billington, 2003a & b; Billington and Yoon, 2004; Chou and Chen, 2005; Palermo et al., 2005; Ou et al., 2007; Cheng, 2008; Jeong et al., 2008; Yamashita and Sanders, 2009; ElGawady et al., 2010; Lee and Billington, 2010; Barthès, 2012; Cruz and Saiidi, 2012; Schaefer, 2013; Stanton et al., 2014; Mantawy et al., 2014). Residual displacements of bridge columns in cyclic and dynamic tests were negligible in these studies. It was found that up to 6% drift ratio, there was no damage in rocking columns but minor concrete spalling was observed starting at 10% drift ratio. Overall, Column Type 3 satisfies LDC, MDM, and RM performance criteria. The RM feature exists in these columns despite the significant yielding of steel reinforcements because tendons help recover residual displacements.

D.2.3 Column Type 7

Most of bridge column damage is expected to be in the plastic hinge area during an earthquake, and it is this region that may need repair or total replacement due to severe damage. Reinforced rubber may be

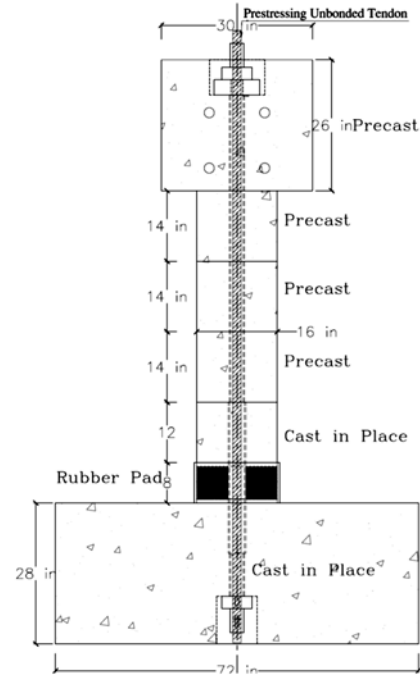
incorporated in lieu of concrete in the plastic hinge area to eliminate damage. In contrast to bearing pads and isolators, the function of rubber in plastic hinges is to deform in tension and compression due to flexure. The concept was first introduced and experimentally investigated by Kawashima and Nagai (2002). Four columns with different rubber pads, which had thicknesses of 1.18 *in.* [30 *mm*] and 2.36 *in.* [60 *mm*], and boundary steel plates (vulcanized or non-vulcanized) as well as one conventional column were tested. The ratio of the pad thicknesses to the column side dimension was 0.075 and 0.15. Minor damage was observed in columns with rubber pad. However, several longitudinal column bars passing through the rubber pad fractured under relatively low drift levels due to buckling of column longitudinal steel reinforcement within the rubber. For example, in one of the columns in which steel plates were installed at both ends of rubber and the column was partially post-tensioned with steel tendons in the plastic hinge area, the longitudinal reinforcement ruptured at 4.5% drift ratio while the first bar fracture in the conventional column was observed during 5.5% drift ratio cycles. Large permanent deformations were observed in both conventional and rubber pad columns despite partial prestressing of the model with rubber pad.

Rubber can be combined with other low-damage or self-centering materials to develop a column with no-damage, high drift capacity, and negligible residual displacements (Table D-1). One of these combinations in which the concept was experimentally evaluated is Column Type 7. Motaref et al. (2010 and 2011) developed a new rubber plastic hinge system for bridge columns that withstood large drift ratios with no-damage in the rubber pad and minor damage of concrete above the pad. Figure D-2 shows the rubber column details. Rubber pad was relatively thick compared to that used in the previous study (the ratio of the rubber pad thickness to the column diameter was 0.50), but was reinforced internally with steel shims, had vulcanized steel plates at both ends, had a center hole to allow the entire length of column to be post-tensioned with steel rods, and had steel pipes and shear studs to resist shear and prevent shear deformations. The single column bent was tested on a shake table. Rubber pads with similar components but different geometry were used in the bottom plastic hinges of a two-column bent of a four-span bridge tested on shake tables using biaxial ground motions (Cruz and Saiidi, 2012). Damage of rubber pad plastic hinges was minimal with negligible residual deformations of the bent after seven runs. It is worth mentioning that the single column bent discussed above was a segmental column but the two-column bent was cast monolithically. However, similar performance was observed in both systems incorporating built-in rubber pads.

In summary, Column Type 7 satisfies LDC, MDM, and RM performance criteria. Energy is dissipated through significant yielding of steel reinforcements, but residual displacements are small because of the re-centering effect of prestressing.



(a) Column base



(b) Column details

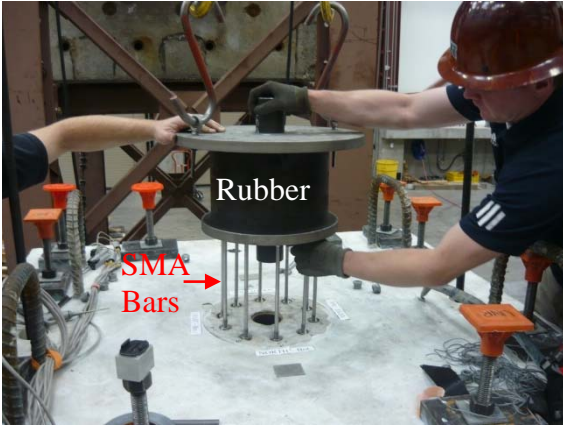
Source: Motaref et al. (2011)

Figure D-2. Rubber pad column details

D.2.4 Column Type 10

Rubber pad column performance may be enhanced by using low-damage systems above the rubber pad and different self-centering mechanisms. One alternative that was experimentally evaluated recently is Column Type 10 in which CFPT was used above the rubber pad and superelastic reinforcing SMA bars were incorporated in the plastic hinge in lieu of reinforcing steel. Since SMA has self-centering ability, steel tendons can be eliminated. An ongoing research project that is focused on deconstructible column plastic hinge elements has developed and utilized Column Type 10 details (NSF-PFI Project, 2014; Saiidi et al., 2014). Figure D-3 shows the plastic hinge assembly. Figure D-4 shows the plastic hinge damage after 250% design level earthquake. No damage was observed. The column was completely disassembled, reassembled, and re-tested. Similar to the initial testing, no damage was observed in the re-testing step. Residual displacements were insignificant in both test series.

In summary, Column Type 10 satisfies LDC, MDM, and RM performance criteria with no component damage.



(a) Rubber pad and SMA bars

(b) Column test setup

Source: <http://wolfweb.unr.edu/homepage/saiidi/NSF-PFI/index.html>

Figure D-3. Rubber/SMA column details and shake table setup



Source: <http://wolfweb.unr.edu/homepage/saiidi/NSF-PFI/index.html>

Figure D-4. Damage of Rubber/SMA column after 250% design earthquake

D.2.5 Column Type 14

UHPC may be used in plastic hinge of bridge columns to reduce damage. Cyclic performance of a quarter-scale steel-reinforced UHPC column was investigated by Zohrevand and Mirmiran (2012) in which UHPC was incorporated only at the column base over a height of two column diameters. Lower plastic hinge damage compared to a conventional reference column was reported. Geometry, confinement, and longitudinal steel arrangements of the two columns were the same. Even though the base shear capacity of steel-reinforced UHPC column was similar to that of the conventional column, 30% lower drift capacity and 30% lower displacement ductility capacity were observed compared to the conventional column. Residual displacements were significant in both columns. From this test data, it can be concluded that Column Type 14 satisfies only MDM performance criterion.

D.2.6 Column Type 15

This column concept is similar to CFFT columns but UHPC is used to fill the FRP tube instead of conventional concrete to reduce the damage. Stress-strain behavior of UHPC confined with FRP jacket was investigated by Zohrevand and Mirmiran (2011). It was found that ultimate stress and strain capacities of confined UHPC were significantly higher than those of unconfined UHPC. It was reported that confined material model developed by Lam and Teng (2003) resulted in a better agreement with measured test data. Cyclic performance of a quarter-scale UHPC filled FRP tube column was studied by Zohrevand and Mirmiran (2012) in which UHPC was utilized only at the base of FRP tube within a height of two column diameters, and column had no steel reinforcement. No visible damage was reported up to the fracture of FRP tube on the tension side. The lateral load capacity of UHPC filled FRP tube without steel reinforcements was comparable to that of a conventional concrete but 46% lower drift capacity was observed. Lower residual displacements compared to the conventional column was also reported. It can be concluded that Column Type 15 without steel reinforcements stratifies MDM and RM performance criteria.

D.2.7 Column Type 20

ECC may be incorporated in the plastic hinge area of bridge columns instead of conventional concrete to reduce post-earthquake damage. Performance of this column type was evaluated in experimental cyclic and dynamic tests in which lower plastic hinge damage was reported compared to conventional column plastic hinge damage (Kawashima et al., 2011; Motaref et al., 2011; Kawashima et al. 2012; Gencturk et al., 2013; Mehrsoroush and Saiidi, 2014; Panagiotou et al., 2014; Aviram et al., 2014). Since columns of this category had no self-centering mechanism, large permanent deformations were observed in the tests.

Overall, Column Type 20 is expected to exhibit LDC and MDM but extensive yielding of steel reinforcements is inevitable in this system and there is no mechanism to counteract the resulting residual displacements.

D.2.8 Column Type 31

Seismic performance of Column Type 20 can be enhanced if longitudinal reinforcing steel be replaced with superelastic reinforcing SMA to increase self-centering tendency. The seismic performance of Column Type 31 was investigated in a few studies (Saiidi and Wang, 2006; Saiidi et al., 2009; Cruz and Saiidi, 2012; Nakashoji and Saiidi, 2014; Tazarv and Saiidi, 2014; NSF-PFI Project, 2014). Minimal damage of plastic hinge with insignificant residual displacement of columns even after undergoing 10% maximum drift ratio or more was reported in all these studies. Even though SMA-reinforced conventional concrete column show satisfactory performance, combination of reinforcing SMA and ECC results in a better performance with minimal plastic hinge damage (Saiidi et al., 2009).

In summary, Column Type 31 satisfies LDC, MDM, and RM performance criteria with minimal damage ensuring post-earthquake functionality of bridges.

D.3 References

1. Aviram, A., Stojadinovic, B., and Parra-Montesinos, G.J. (2014). "High-Performance Fiber-Reinforced Concrete Bridge Columns under Bidirectional Cyclic Loading," *ACI Structural Journal*, Vol. 111, No. 2, pp. 303–312.
2. Barthès, C. (2012). "Design of Earthquake Resistant Bridges Using Rocking Columns," PhD Dissertation, Department of Civil and Environmental Engineering, University of California, Berkeley, 160 pp.
3. Billington, S.L., and Yoon, J.K. (2004). "Cyclic Response of Unbonded Posttensioned Precast Columns with Ductile Fiber-Reinforced Concrete," *Journal of Bridge Engineering, ASCE*, Vol. 9, No. 4, pp. 353-363.
4. Cheng, C. (2008). "Shaking Table Tests of a Self-Centering Designed Bridge Substructure," *Engineering Structures*, Vol. 30, pp. 3426-3433.
5. Chou, C.C., and Chen, Y.C. (2006). "Cyclic Tests of Post-Tensioned Precast CFT Segmental Bridge Columns with Unbonded Strands," *Earthquake Engineering and Structural Dynamics*, Vol. 35, pp. 159–175.
6. Cruz Noguez C.A. and Saiidi, M.S. (2012). "Shake Table Studies of a 4-Span Bridge Model with Advanced Materials," *Journal of Structural Engineering, ASCE*, Vol. 138, No. 2, pp. 183-192.
7. ElGawady, M., Booker, A.J., and Dawood, H.M. (2010). "Seismic Behavior of Posttensioned Concrete-Filled Fiber Tubes," *Journal of Composites for Construction, ACSE*, Vol. 14, No. 5, pp. 616–628.
8. Garcia, R. (1998). "Shaking Table Study of Rocking Column Bridge Based on Damage Avoidance Design," MS.c Thesis, Dept. of Civil, Structural and Environmental Engineering, SUNY at Buffalo.
9. Gencturk, B., Elnashai, A.S., Lepech, M.D., and Billington, S. (2013). "Behavior of Concrete and ECC Structures under Simulated Earthquake Motion," *Journal of Structural Engineering, ASCE*, Vol. 139, No. 3, pp. 389-399.
10. Hewes, J.T. and Priestley, M.J.N. (2002). "Seismic Design and Performance of Precast Concrete Segmental Bridge Columns," *Structural Systems Research Report SSRP-2001/25*, University of California at San Diego, 241 pp.
11. Jeong, H.I.L., Sakai, J., Mahin, S.A. (2008). "Shaking Table Tests and Numerical Investigation of Self-Centering Reinforced Concrete Bridge Columns," *PEER-2008/06*, Pacific Earthq. Engrg. Res. Center, Univ. of California at Berkeley, California, 399 pp.
12. Kaviani-pour, F. and Saiidi, M.S. (2013). "Experimental and Analytical Seismic Studies of a Four-span Bridge System with Composite Piers," Center for Civil Engineering Earthquake Research, Department of Civil and Environmental Engineering, University of Nevada, Reno, Nevada, *Report No. CCEER-13-17*.
13. Kawashima, K., and Nagai, M. (2002). "Development of a Reinforced Concrete Pier with a Rubber Layer in the Plastic Hinge Region," *Structural Earthquake Engineering, JSCE*, Vol. 703, No. I-59, pp. 113-128.
14. Kawashima, K., Zafra, R.G., Sasaki, T., Kajiwara, K., and Nakayama, M. (2011). "Effect of Polypropylene Fiber Reinforced Cement Composite and Steel Fiber Reinforced Concrete for Enhancing the Seismic Performance of Bridge Columns," *Journal of Earthquake Engineering*, Vol. 15, No. 8, pp. 1194–1211.
15. Kawashima, K., Zafra, R.G., Sasaki, T., Kajiwara, K., Nakayama, M., Unjoh, S., Sakai, J., Kosa, K., Takahashi, Y., and Yabe, M. (2012). "Seismic Performance of a Full-Size Polypropylene Fiber-Reinforced Cement Composite Bridge Column Based on E-Defense Shake Table Experiments," *Journal of Earthquake Engineering*, Vol. 16, No. 4, pp. 463–495.

16. Kwan, W.P., Billington, S.L. (2003a). “Unbonded Post-Tensioned Concrete Bridge Piers. I: Monotonic and Cyclic Analyses,” *Journal of Bridge Engineering, ASCE*, Vol. 8, No. 2, pp. 92-101.
17. Kwan, W.P., Billington, S.L. (2003b). “Unbonded Post-Tensioned Concrete Bridge Piers. II: Seismic Analyses,” *Journal of Bridge Engineering, ASCE*, Vol. 8, No. 2, pp. 102-111.
18. Lam, L., and Teng, J.G. (2003). “Design-Oriented Stress-Strain Model for FRP-Confined Concrete,” *Construction and Building Materials*, Vol. 17, No. 6-7, pp. 471-489.
19. Lee, W. K. and Billington S.L. (2010). “Modeling Residual Displacements of Concrete Bridge Columns under Earthquake Loads Using Fiber Elements,” *Journal of Bridge Engineering*, Vol. 15, No. 3, pp. 201-249.
20. Mander, J.B. and Cheng, C.T. (1997). “Seismic Resistance of Bridge Pier Based on Damage Avoidance Design,” *Tech. Rep. No. NCEER-97-0014*, National Center for Earthquake Engineering Research, Dept. of Civil, Structural and Environmental Engineering, State University of New York, Buffalo, NY, 130 pp.
21. Mantawy, I., Thonstand, T., Sanders, D.H., Stanton, J., and Eberhard, M. (2014). “Earthquake Shake Table Testing of Self-Centering ABC Bridge,” 2014 National Accelerated Bridge Construction Conference, Miami, Florida, 10 pp.
22. Mehrsoroush, A. and Saiidi, M.S. (2014). “Seismic Performance of Two-Column Bridge Piers with Innovative Precast Members and Pipe Pin Connections,” 7th International Conference on Bridge Maintenance, Safety and Management (IABMAS), Shanghai, China.
23. Mirmiran, A., and Shahawy, M. (1996). “A New Concrete-Filled Hollow FRP Composite Column,” *Composites Part B: Engineering*, Vol. 27, No. 3-4, pp. 263-268.
24. Mirmiran, A., Shahawy, M., Samaan, M., El-Echary, H., Mastrapa, J.C., and Pico, O. (1998). “Effect of Column Parameters on FRP-Confined Concrete,” *Journal of Composites for Construction, ASCE*, Vol. 2, No. 4, pp. 175-185.
25. Motaref, S., Saiidi, M.S. and Sanders, D. (2010). “Experimental Study of Precast Bridge Columns with Built-In Elastomer,” *Transportation Research Record: Journal of the Transportation Research Board, Bridge Engineering*, Vol. 3, pp. 109-116.
26. Motaref, S., Saiidi, M.S., and Sanders, D. (2011). “Seismic Response of Precast Bridge Columns with Energy Dissipating Joints,” Center for Civil Engineering Earthquake Research, Department of Civil and Environmental Engineering, University of Nevada, Reno, *Report No. CCEER-11-01*, 760 pp.
27. Nakashoji, B. and Saiidi, M.S. (2014). “Seismic Performance of Square Nickel-Titanium Reinforced ECC Columns with Headed Couplers,” Center For Civil Engineering Earthquake Research, Department Of Civil and Environmental Engineering, University of Nevada, Reno, Nevada, *Report No. CCEER-14-05*, 252 pp.
28. NSF-PFI Project. (2014). Retrieved July 09, 2014, from <http://wolfweb.unr.edu/homepage/saiidi/NSF-PFI/index.html>.
29. Ou, Y.C., Chiewanichakorn, M., Aref, A.J., and Lee, G.C. (2007). “Seismic Performance of Segmental Precast Unbonded Posttensioned Concrete Bridge Columns,” *Journal of Structural Engineering, ASCE*, Vol. 133, No. 11, pp. 1636–1647.
30. Palermo A., Pampanin S., and Calvi, G.M. (2005). “Concept and Development of Hybrid Solutions for Seismic Resistant Bridge Systems,” *Journal of Earthquake Engineering*, Vol. 9, No. 6, pp. 899-921.
31. Panagiotou, M., Trono, W., Jen, G., Kumar, P., and Ostertag, C.P. (2014). “Experimental Seismic Response of Hybrid Fiber-Reinforced Concrete Bridge Columns with Novel Longitudinal Reinforcement Detailing,” *Journal of Bridge Engineering, ASCE*, ISSN 1084-0702/04014090(12), 12 pp.

32. Saiidi, M.S. and Wang H. (2006). "Exploratory Study of Seismic Response of Concrete Columns with Shape Memory Alloys Reinforcement," *ACI Structural Journal*, Vol. 103, No. 3, pp. 436-443.
33. Saiidi, M.S., O'Brien, M. and Sadrossadat-Zadeh, M. (2009). "Cyclic Response of Concrete Bridge Columns Using Superelastic Nitinol and Bendable Concrete," *ACI Structural Journal*, Vol. 106, No. 1, pp. 69-77.
34. Saiidi, M.S., Tazarv, M., Nakashoji, B., Varela, S., and Kavianipour, F. (2014). "Resilient and Sustainable Bridges of the Future," (Keynote Paper), *Proceedings of 2nd International Conference on bridges "Innovations on Bridges and Soil-Bridge Interaction"*, Athens, Greece, 12 pp.
35. Samaan, M., Mirmiran, A., and Shahawy, M. (1998). "Model of Concrete Confined by Fiber Composites," *Journal of Structural Engineering, ASCE*, Vol. 124, No. 9, pp. 1025-1031.
36. Schaefer, J. (2013). "Unbonded Pre-tensioned Bridge Columns with Rocking Detail," MSc Thesis, Department of Civil and Environmental Engineering, University of Washington, Seattle, 154 pp.
37. Seible, F., Priestley, M., Hegemier, G., and Innamorato, D. (1997). "Seismic Retrofit of RC Columns with Continuous Carbon Fiber Jackets," *Journal of Composites for Construction, ASCE*, Vol. 1, No 2, pp. 52-62.
38. Shao, Y., and Mirmiran, A. (2005). "Experimental Investigation of Cyclic Behavior of Concrete-Filled Fiber Reinforced Polymer Tubes," *Journal of Composites for Construction, ASCE*, Vol. 9, No. 3, pp. 263-273.
39. Stanton, J., Eberhard, M., Sanders, D.H., Thonstad, T., Schaefer, J., Kennedy, B., Haraldsson, O., and Mantawy, I. (2014). "A Pre-Tensioned, Rocking Bridge Bent for ABC in Seismic Regions," *Proceedings of the 10th U.S. National Conference on Earthquake Engineering*, Anchorage, Alaska.
40. Tazarv, M. and Saiidi, M.S. (2014). "Next Generation of Bridge Columns for Accelerated Bridge Construction in High Seismic Zones," Center For Civil Engineering Earthquake Research, Department of Civil and Environmental Engineering, University of Nevada, Reno, Nevada, *Report No. CCEER-14-06*, 400 pp.
41. Yamashita, R., and Sanders, D.H. (2009). "Seismic Performance of Precast Unbonded Prestressed Concrete Columns," *ACI Structural Journal*, Vol. 106, No. 6, pp. 821-830.
42. Zaghi, A., Saiidi, M.S., and Mirmiran, A. (2012). "Shake Table Response of a Concrete-Filled FRP Tube Bridge Column," *Composite Structures*, Elsevier, Vol. 94, Issue 5, April 2012, pp 1564-1574.
43. Zhu, Z., Ahmad, I., and Mirmiran, A. (2006). "Seismic Performance of Concrete-Filled FRP Tube Columns for Bridge Substructure," *Journal of Bridge Engineering, ASCE*, Vol. 11, No. 3, pp. 359-370.
44. Zohrevand, P., and Mirmiran, A. (2011). "Behavior of Ultrahigh-Performance Concrete Confined by Fiber-Reinforced Polymers," *Journal of Materials in Civil Engineering, ASCE*, Vol. 23, No. 12, pp. 1727-1734.
45. Zohrevand, P., and Mirmiran, A. (2012). "Cyclic Behavior of Hybrid Columns Made of Ultra High Performance Concrete and Fiber Reinforced Polymers," *Journal of Composites for Construction, ASCE*, Vol. 16, No. 1, pp. 91-99.

APPENDICES

NCHRP 12-101

App. A – Literature Review

App. B – Survey of State Departments of Transportation

App. C – Synthesis of Literature

App. D – Novel Column and Construction Concepts

App. E – Demonstration of Evaluation Guidelines

App. F – Detailed Design Examples for Three Novel Columns

App. G – Benefits and Economic Impact of Novel Columns

App. H – Relationship between Drift Ratio and Displacement Ductility

App. I – Modeling Methods and Validation for Novel Columns

TABLE OF CONTENTS

APPENDICES	I
TABLE OF CONTENTS.....	II
APPENDIX E	E-1
E.1 Introduction	E-2
E.2 Demonstration of Pre-Design Evaluation.....	E-2
E.2.1 Plastic Hinge Damage.....	E-2
E.2.2 Displacement Capacity	E-2
E.2.3 Residual Displacements	E-3
E.2.4 Evaluation and Rating of 39 Novel Columns	E-3

APPENDIX E

Demonstration of Evaluation Guidelines

Demonstrate the use of the proposed evaluation guidelines for 39 novel columns as well as RC columns.

E.1 Introduction

The proposed evaluation guidelines (Ch. 2) may be utilized prior to the actual design or subsequent to design. Pre-design evaluation is important for selection of a few alternative novel columns that possibly meet the owner’s performance requirements. Subsequently, the feasible alternatives may be analyzed to obtain accurate and sufficient data for the owner to select the most appropriate novel column for field deployment. In this section, each of the previously discussed 39 novel columns (App. D) incorporating SMA, ECC, UHPC, FRP, and rubber as well as conventional columns is first categorized in terms of the plastic hinge damage, displacement capacity, and residual displacement. Subsequently these columns are quantitatively assessed based on the proposed evaluation guidelines.

E.2 Demonstration of Pre-Design Evaluation

E.2.1 Plastic Hinge Damage

Table E.2.1-1 presents plastic hinge damage categorization for the 39 novel columns listed in Table D-1 mainly based on their constituent material performance and their connections (e.g. rocking). The general trend is that combination of two advanced materials for reinforcement and cementitious material will minimize the plastic hinge damage. This table indicates the expected damage level for each novel column based on this trend. Nevertheless, the actual performance of each novel column must be proven through large-scale model testing under simulated earthquakes before field deployment. Furthermore, reliable analyses (e.g. pushover analyses using fiber models) must be performed by the designer to estimate the damage level by monitoring the material strain and stress demands (such as those shown in Appendices F and G). Material models for each advanced materials were presented in previous sections.

Table E.2.1-1. Novel column pre-design seismic damage categorization

Category	Plastic Hinge Material	Column Type ^(a)
Severe	Steel and conventional concrete	Conventional RC columns
Moderate	Use either ECC/UHPC to reduce concrete damage <u>or</u> SMA/FRP bars to eliminate yielding	6, 7, 14, 18, 20, 21, & 22
Low	Use ECC/UHPC to reduce concrete damage, <u>and</u> SMA/FRP bar to reduce permanent yielding. Use rubber or FRP jacket with steel bars	1, 2, 3, 4, 5, 7, 15, 16, 17, 19, 23, 28, 29, 30, 31, & 36
No	Use rubber/FRP jacket to eliminate concrete damage <u>and</u> SMA/FRP bars to reduce permanent yielding	8, 9, 10, 11, 12, 13, 24, 25, 26, 27, 32, 33, 34, 35, 37, 38, & 39

Note: ^(a) Refer to Table D-1 in Appendix D.

E.2.2 Displacement Capacity

The displacement capacity of 39 novel columns can be categorized based on their constituent materials (Table E.2.2-1). The general trend is that columns with linear elastic materials (e.g. FRP bars) are not expected to achieve large displacements while columns with SMA bars or debonded bars will show large displacement capacities. This table can be used in pre-design evaluation of the 39 novel columns.

Table E.2.2-1. Novel column pre-design displacement capacity categorization

Category	Displacement Ductility	Column Type ^(a)
Low	$\mu_c < 3$	9, 12, 14, 15, 27, 28, 35, 36, & 37
Normal	$3 \leq \mu_c < 5$	Conv. columns, 1, 2, 3, 16, 18, 20, 21, 22, 23, 29, 30, 38, & 39
High	$\mu_c \geq 5$	4, 5, 6, 7, 8, 10, 11, 13, 17, 19, 24, 25, 26, 31, 32, 33, & 34

Note: ^(a) Refer to Table D-1 in Appendix D.

E.2.3 Residual Displacements

Table E.2.3-1 presents the expected residual displacement level for each novel column to serve solely as a guide for designers. Similar to the previous measures, the residual displacement can be initially categorized based on the column constituent materials and connections. The general trend is that columns with post-tensioning tendons, reinforcing FRP bars, or reinforcing SMA bars will experience minimal residual displacements. The expected performance shown in the table must be first validated with experiments then the actual performance may be estimated using reliable analyses.

Table E.2.3-1. Novel column pre-design residual displacement categorization

Category	Residual Drift Limit	Column Type ^(a)
Low	$\delta_r > 1.5\%$	8, 9, 10, 11, 12, 13, 23, 24, 25, 26, 27, 28, 29, 30, 31, 32, 33, 34, 35, 36, 37, 38, & 39
Normal	$1.0\% < \delta_r \leq 1.5\%$	2, 3, 4, 5, 6, 7, 16, 17, 18, 19, 21, & 22
High	$\delta_r \leq 1.0\%$	Conv. Columns, 1, 14, 15, & 20

Note: ^(a) Refer to Table D-1 in Appendix D.

E.2.4 Evaluation and Rating of 39 Novel Columns

In this section, the conventional RC and the 39 novel columns that were discussed in previous sections are evaluated based on the pre-design guidelines (Table E.2.4-1). This table demonstrates the application of Table 2.8.1 (Ch. 2) to the 39 novel columns made with SMA, ECC, FRP, UHPC, and rubber and rocking connections. A score between 0.0 to 1.0 at increments of 0.25 was assigned to each parameter with unity meaning full readiness, desired performance, and substantial improvement compared to conventional columns. This table also presents conditions that lead to penalizing each parameter. Some of the parameters can only be accurately quantified after the design. Therefore, both pre- and post-design recommendations are presented for these parameters. Pre-design recommendations are to facilitate selection of columns that are likely to meet the owner's requirements.

A pre-design evaluation for all the 39 novel columns plus conventional columns was performed based on the proposed guideline to demonstrate how the ratings are determined and translated into a star-based system (Tables E.2.4-2 to E.2.4-4). The number of stars in the far right column is the same as the relative scores listed in the table.

Table E.2.4-1. Quantification of 39 novel column evaluation parameters

Parameter	Quantification (deduction ^(a) from unity unless stated otherwise)	Weight
Seismic Performance		
Plastic Hinge Damage	<p>Pre-Design Evaluation: -0.25 when reinforcing steel is used in plastic hinge, -0.50 when any unconfined concrete is used in plastic hinge, -0.25 when any unconfined concrete is used above rubber, -0.25 when any unconfined ECC is used in plastic hinge.</p> <p>Post-Design Evaluation: Based on demands on material and engineering judgement comment on the score as: 1.0 for no-damage, 0.75 for low damage 0.25 for moderate damage, 0.0 for severe damage.</p>	1.0
Large Displacement Capacity	<p>Pre-Design Evaluation: -0.25 when linear-elastic materials are used in plastic hinge, -0.25 to -0.75 when LDC was not satisfactory in concept test.</p> <p>Post Design Evaluation: 1.0 for high displacement capacity: $\mu_c \geq 5$ 0.5 for normal displacement capacity: $3 \leq \mu_c < 5$ 0.0 for low displacement capacity: $\mu_c < 3$</p>	1.0
Residual Displacement	<p>Pre-Design Evaluation: -0.25 when <u>only</u> tendon is used (rocking system), -0.25 when <u>only</u> reinforcing SMA is used, -0.75 for CFFT column with no tendon or SMA bars, -1.00 for others.</p> <p>Post-Design Evaluation: 1.0 for low residual displacement: $\delta_r \leq 1.0\%$ 0.5 for moderate residual displacement: $1.0\% < \delta_r \leq 1.5\%$ 0.0 for high residual displacement: $\delta_r > 1.5\%$</p>	1.0
Design Considerations		
Proof Test	1.0 when laboratory test data is available, 0.0 when there is no test data.	1.0
Analysis Tools	-0.25 when UHPC is confined by steel, -0.25 when rubber is used.	0.75
Guidelines Readiness	-0.25 when the concept was tested, but there are no guidelines -0.50 when there is no concept test and there are no guidelines	0.25
Field Application	1.0 when novel system has been used (or will be by 2016), 0.0 when there is no field application (by 2016).	0.25
Construction and other Considerations		
Initial Cost	<p>Pre-Design Evaluation: -0.25 when UHPC is used, -0.25 when rubber is used, -0.50 when reinforcing SMA is used.</p> <p>Post-Design Evaluation: Estimate the cost then the ratio of the RC column cost to the novel column cost will be the score.</p>	0.25
Material Limitation	None of following cases shall be allowed for field deployment: - SMA in very cold weather, see material section, - Rubber in very cold weather, see "AASHTO Guide Specifications for Seismic Isolation Design", - Bonded FRP in salt water, see "ACI Guides on FRP".	N/A
Constructability	-0.25 when rubber is used, -0.25 when coupler is used, -0.25 when post-tensioning is used.	1.0
Inspectability	-0.25 when rubber is used, -0.25 when exposed FRP is used, -0.50 when unbonded steel tendons are used.	0.75
Maintenance	-0.25 when either steel (bar or tendon) or unconfined conventional concrete is used in plastic hinge, -0.25 when either exposed FRP or rubber is used in plastic hinge.	0.75
System Performance	-0.25 when SMA bars or rubber pad is used, -0.5 when both SMA bars and rubber pad are used.	1.0

Note: (a) Deductions are additive for each parameter. Post-earthquake repair is needed when column is built with materials susceptible to damage. This parameter is implicit in the plastic hinge damage.

Table E.2.4-2. Novel column pre-design seismic performance evaluation

Column Type	Damage	Displacement Capacity	Residual Displacement	Weighted Score	Relative Score	Star Rating (Out of Five)
Conv. Col.	0	1	0	1	1.7	★☆☆☆☆
Col. 1	0.75	0.75	0.25	1.75	2.9	★★★★☆
Col. 2	0.75	0.75	0.75	2.25	3.8	★★★★☆
Col. 3	0.75	0.75	0.75	2.25	3.8	★★★★☆
Col. 4	0.75	1	0.75	2.5	4.2	★★★★☆
Col. 5	0.75	1	0.75	2.5	4.2	★★★★☆
Col. 6	0.5	1	0.75	2.25	3.8	★★★★☆
Col. 7	0.75	1	0.75	2.5	4.2	★★★★☆
Col. 8	1	0.75	0.75	2.5	4.2	★★★★☆
Col. 9	1	0.75	0.25	2	3.3	★★★★☆
Col. 10	1	1	0.75	2.75	4.6	★★★★☆
Col. 11	1	1	1	3	5.0	★★★★★
Col. 12	1	0.75	0.75	2.5	4.2	★★★★☆
Col. 13	1	1	1	3	5.0	★★★★★
Col. 14	0.75	0.5	0	1.25	2.1	★★★☆☆
Col. 15	0.75	0.25	0.25	1.25	2.1	★★★☆☆
Col. 16	0.75	1	0.75	2.5	4.2	★★★★☆
Col. 17	0.75	1	0.75	2.5	4.2	★★★★☆
Col. 18	1	1	0.75	2.75	4.6	★★★★☆
Col. 19	0.75	1	0.75	2.5	4.2	★★★★☆
Col. 20	0.5	1	0	1.5	2.5	★★★☆☆
Col. 21	0.5	1	0.75	2.25	3.8	★★★★☆
Col. 22	0.5	1	0.75	2.25	3.8	★★★★☆
Col. 23	1	0.75	0.75	2.5	4.2	★★★★☆
Col. 24	1	1	0.75	2.75	4.6	★★★★☆
Col. 25	1	1	1	3	5.0	★★★★★
Col. 26	1	1	1	3	5.0	★★★★★
Col. 27	1	0.75	0.75	2.5	4.2	★★★★☆
Col. 28	1	0.75	0	1.75	2.9	★★★★☆
Col. 29	0.75	1	0.75	2.5	4.2	★★★★☆
Col. 30	0.75	1	0.75	2.5	4.2	★★★★☆
Col. 31	0.75	1	0.75	2.5	4.2	★★★★☆
Col. 32	1	1	0.75	2.75	4.6	★★★★☆
Col. 33	1	1	1	3	5.0	★★★★★
Col. 34	1	1	1	3	5.0	★★★★★
Col. 35	1	0.75	0.75	2.5	4.2	★★★★☆
Col. 36	0.75	0.75	0	1.5	2.5	★★★☆☆
Col. 37	1	0.75	0.75	2.5	4.2	★★★★☆
Col. 38	1	1	0.75	2.75	4.6	★★★★☆
Col. 39	1	1	0.75	2.75	4.6	★★★★☆

Table E.2.4-3. Novel column design consideration evaluation

Column Type	Proof Test	Analysis Tools	Guideline	Field Application	Weighted Score	Relative Score	Star Rating (Out of Five)
Conv. Col.	1	1	1	1	2.25	5.0	★★★★★
Col. 1	1	1	0.75	1	2.19	4.9	★★★★★
Col. 2	0	1	0.5	0	0.88	1.9	★★☆☆☆
Col. 3	1	1	0.75	0	1.94	4.3	★★★★☆
Col. 4	0	0.75	0.5	0	0.69	1.5	★★☆☆☆
Col. 5	0	0.75	0.5	0	0.69	1.5	★★☆☆☆
Col. 6	0	0.75	0.5	0	0.69	1.5	★★☆☆☆
Col. 7	1	0.75	0.75	0	1.75	3.9	★★★★☆
Col. 8	0	1	0.5	0	0.88	1.9	★★☆☆☆
Col. 9	0	1	0.5	0	0.88	1.9	★★☆☆☆
Col. 10	1	0.75	0.75	0	1.75	3.9	★★★★☆
Col. 11	0	0.75	0.5	0	0.69	1.5	★★☆☆☆
Col. 12	0	0.75	0.5	0	0.69	1.5	★★☆☆☆
Col. 13	0	0.75	0.5	0	0.69	1.5	★★☆☆☆
Col. 14	1	0.75	0.75	0	1.75	3.9	★★★★☆
Col. 15	1	1	0.75	0	1.94	4.3	★★★★☆
Col. 16	0	0.75	0.5	0	0.69	1.5	★★☆☆☆
Col. 17	0	0.5	0.5	0	0.50	1.1	★☆☆☆☆
Col. 18	0	0.75	0.5	0	0.69	1.5	★★☆☆☆
Col. 19	0	0.5	0.5	0	0.50	1.1	★☆☆☆☆
Col. 20	1	1	0.75	0	1.94	4.3	★★★★☆
Col. 21	0	1	0.5	0	0.88	1.9	★★☆☆☆
Col. 22	0	1	0.5	0	0.88	1.9	★★☆☆☆
Col. 23	0	0.75	0.5	0	0.69	1.5	★★☆☆☆
Col. 24	0	0.75	0.5	0	0.69	1.5	★★☆☆☆
Col. 25	0	0.5	0.5	0	0.50	1.1	★☆☆☆☆
Col. 26	0	0.5	0.5	0	0.50	1.1	★☆☆☆☆
Col. 27	0	0.75	0.5	0	0.69	1.5	★★☆☆☆
Col. 28	0	0.75	0.5	0	0.69	1.5	★★☆☆☆
Col. 29	0	1	0.5	0	0.88	1.9	★★☆☆☆
Col. 30	0	1	0.5	0	0.88	1.9	★★☆☆☆
Col. 31	1	1	0.75	1	2.19	4.9	★★★★★
Col. 32	0	0.75	0.5	0	0.69	1.5	★★☆☆☆
Col. 33	0	0.75	0.5	0	0.69	1.5	★★☆☆☆
Col. 34	0	0.75	0.5	0	0.69	1.5	★★☆☆☆
Col. 35	0	0.75	0.5	0	0.69	1.5	★★☆☆☆
Col. 36	0	1	0.5	0	0.88	1.9	★★☆☆☆
Col. 37	0	0.75	0.5	0	0.69	1.5	★★☆☆☆
Col. 38	0	1	0.5	0	0.88	1.9	★★☆☆☆
Col. 39	0	1	0.5	0	0.88	1.9	★★☆☆☆

Table E.2.4-4. Novel column pre-design construction and other considerations evaluation

Column Type	Initial Cost	Material Limitation	Const.	Inspect.	Maint.	System Perf.	Weighted Score	Relative Score	Star Rating (Out of Five)
Conv. Col.	1	N/A	1	1	0.75	1	3.56	4.8	★★★★★
Col. 1	1	N/A	1	0.75	0.75	1	3.38	4.5	★★★★☆
Col. 2	1	N/A	0.75	0.75	0.5	1	2.94	3.9	★★★★☆
Col. 3	1	N/A	0.75	0.25	0.5	1	2.56	3.4	★★★★☆
Col. 4	0.75	N/A	0.5	0.5	0.5	0.75	2.19	2.9	★★★★☆
Col. 5	0.75	N/A	0.5	0	0.5	0.75	1.81	2.4	★★★☆☆
Col. 6	0.75	N/A	0.5	0.75	0.5	0.75	2.38	3.2	★★★★☆
Col. 7	0.75	N/A	0.5	0.25	0.75	0.75	2.19	2.9	★★★★☆
Col. 8	0.5	N/A	0.75	0.75	0.75	0.75	2.75	3.7	★★★★☆
Col. 9	1	N/A	1	0.75	0.75	1	3.38	4.5	★★★★☆
Col. 10	0.25	N/A	0.5	0.5	0.75	0.5	2.00	2.7	★★★★☆
Col. 11	0.25	N/A	0.25	0.5	0.75	0.5	1.75	2.3	★★★☆☆
Col. 12	0.75	N/A	0.5	0.5	0.75	0.75	2.38	3.2	★★★★☆
Col. 13	0.25	N/A	0.25	0.5	0.75	0.5	1.75	2.3	★★★☆☆
Col. 14	0.75	N/A	1	1	1	1	3.69	4.9	★★★★★
Col. 15	0.75	N/A	1	0.75	0.5	1	3.13	4.2	★★★★☆
Col. 16	0.75	N/A	0.75	1	1	1	3.44	4.6	★★★★☆
Col. 17	0.5	N/A	0.5	0.75	0.75	0.75	2.50	3.3	★★★★☆
Col. 18	0.75	N/A	0.75	0.5	0.75	1	2.88	3.8	★★★★☆
Col. 19	0.5	N/A	0.5	0.25	0.75	0.75	2.13	2.8	★★★★☆
Col. 20	1	N/A	1	1	0.75	1	3.56	4.8	★★★★★
Col. 21	1	N/A	0.75	1	0.75	1	3.31	4.4	★★★★☆
Col. 22	1	N/A	0.75	0.5	0.75	1	2.94	3.9	★★★★☆
Col. 23	0.25	N/A	0.75	1	1	0.75	3.06	4.1	★★★★☆
Col. 24	0	N/A	0.5	0.75	0.75	0.5	2.13	2.8	★★★★☆
Col. 25	0	N/A	0.25	0.75	0.75	0.5	1.88	2.5	★★★☆☆
Col. 26	0	N/A	0.25	0.25	0.75	0.5	1.50	2.0	★★★☆☆
Col. 27	0.75	N/A	0.5	0.75	0.75	0.75	2.56	3.4	★★★★☆
Col. 28	0.75	N/A	1	1	1	1	3.69	4.9	★★★★★
Col. 29	0.75	N/A	0.75	1	1	1	3.44	4.6	★★★★☆
Col. 30	0.75	N/A	0.75	0.5	0.75	1	2.88	3.8	★★★★☆
Col. 31	0.5	N/A	0.75	1	1	0.75	3.13	4.2	★★★★☆
Col. 32	0.25	N/A	0.5	0.75	0.75	0.5	2.19	2.9	★★★★☆
Col. 33	0.25	N/A	0.25	0.75	0.75	0.5	1.94	2.6	★★★☆☆
Col. 34	0.25	N/A	0.25	0.25	0.5	0.5	1.38	1.8	★★★☆☆
Col. 35	0.75	N/A	0.5	0.75	0.75	0.75	2.56	3.4	★★★★☆
Col. 36	1	N/A	1	1	1	1	3.75	5.0	★★★★★
Col. 37	0.75	N/A	0.5	0.25	0.75	0.75	2.19	2.9	★★★★☆
Col. 38	1	N/A	0.75	0.75	0.75	1	3.13	4.2	★★★★☆
Col. 39	1	N/A	0.75	0.25	0.5	1	2.56	3.4	★★★★☆

Note: "Conv." is an abbreviation for "Conventional"; "Const." is an abbreviation for "Constructability"; "Inspect" is an abbreviation for "Inspectability"; "Maint." is an abbreviation for "Maintenance"; "Perf." is an abbreviation for "Performance".

The individual and combined evaluation results for the aforementioned three categories for the novel columns described previously are what are expected to be reported to the bridge owner. Table E.2.4-5

presents the combined star ratings obtained by simple averaging of the results for the seismic performance, design consideration, and construction and other considerations.

Table E.2.4-5. Summary of pre-design evaluation for novel columns

Column Type	Seismic Performance	Design Considerations	Construction and other Considerations	Average Score	Star Rating (Out of Five)
Conv. Col.	1.7	5.0	4.8	3.8	★★★★☆
Col. 1	2.9	4.9	4.5	4.1	★★★★☆
Col. 2	3.8	1.9	3.9	3.2	★★★★☆
Col. 3	3.8	4.3	3.4	3.8	★★★★☆
Col. 4	4.2	1.5	2.9	2.9	★★★★☆
Col. 5	4.2	1.5	2.4	2.7	★★★★☆
Col. 6	3.8	1.5	3.2	2.8	★★★★☆
Col. 7	4.2	3.9	2.9	3.7	★★★★☆
Col. 8	4.2	1.9	3.7	3.3	★★★★☆
Col. 9	3.3	1.9	4.5	3.3	★★★★☆
Col. 10	4.6	3.9	2.7	3.7	★★★★☆
Col. 11	5.0	1.5	2.3	3.0	★★★★☆
Col. 12	4.2	1.5	3.2	3.0	★★★★☆
Col. 13	5.0	1.5	2.3	3.0	★★★★☆
Col. 14	2.1	3.9	4.9	3.6	★★★★☆
Col. 15	2.1	4.3	4.2	3.5	★★★★☆
Col. 16	4.2	1.5	4.6	3.4	★★★★☆
Col. 17	4.2	1.1	3.3	2.9	★★★★☆
Col. 18	4.6	1.5	3.8	3.3	★★★★☆
Col. 19	4.2	1.1	2.8	2.7	★★★★☆
Col. 20	2.5	4.3	4.8	3.9	★★★★☆
Col. 21	3.8	1.9	4.4	3.4	★★★★☆
Col. 22	3.8	1.9	3.9	3.2	★★★★☆
Col. 23	4.2	1.5	4.1	3.3	★★★★☆
Col. 24	4.6	1.5	2.8	3.0	★★★★☆
Col. 25	5.0	1.1	2.5	2.9	★★★★☆
Col. 26	5.0	1.1	2.0	2.7	★★★★☆
Col. 27	4.2	1.5	3.4	3.0	★★★★☆
Col. 28	2.9	1.5	4.9	3.1	★★★★☆
Col. 29	4.2	1.9	4.6	3.6	★★★★☆
Col. 30	4.2	1.9	3.8	3.3	★★★★☆
Col. 31	4.2	4.9	4.2	4.4	★★★★☆
Col. 32	4.6	1.5	2.9	3.0	★★★★☆
Col. 33	5.0	1.5	2.6	3.0	★★★★☆
Col. 34	5.0	1.5	1.8	2.8	★★★★☆
Col. 35	4.2	1.5	3.4	3.0	★★★★☆
Col. 36	2.5	1.9	5.0	3.1	★★★★☆
Col. 37	4.2	1.5	2.9	2.9	★★★★☆
Col. 38	4.6	1.9	4.2	3.6	★★★★☆
Col. 39	4.6	1.9	3.4	3.3	★★★★☆

APPENDIX F

Detailed Design Examples of Three Novel Columns

NATIONAL COOPERATIVE HIGHWAY
RESEARCH PROGRAM

Project 12-101

BergerABAM
24 February 2017

Iman Ghorbani
Stuart Bennion
Lee Marsh

TABLE OF CONTENTS	Page
F1 - PROJECT INFORMATION	
F1-1: Introduction	1-1
F1-2: Strength Limit State Load Combination Input	1-5
F2 - CONVENTIONAL REINFORCED CONCRETE COLUMN DESIGN	
F2-1: Strength Design of Conventional Column.....	2-1
F2-2: Seismic Design of Conventional Column.....	2-8
F3 - SMA-ECC COLUMN DESIGN	
F3-1: Strength Design of SMA-ECC Column.....	3-1
F3-2: Seismic Design of SMA-ECC Column	3-8
F4 - SMA-FRP CONFINED NOVEL COLUMN DESIGN	
F4-1: Strength Design of SMA-FRP Confined Column.....	4-1
F4-2: Seismic Design of SMA-FRP Confined Column.....	4-12
F5 - FRP CONFINED HYBRID ROCKING COLUMN DESIGN	
F5-1: Strength Design of FRP Confined Hybrid Rocking Column.....	5-1
F5-2: Seismic Design of FRP Confined Hybrid Rocking Column.....	5-9
F6 - REFERENCES	
F6-1: References	6-1

F1 - PROJECT INFORMATION

F1-1: Introduction

The following examples are generated to demonstrate the basis of seismic design for novel columns and compare them with a conventional cast-in-place reinforced concrete column designed with the current AASHTO Guide Specifications for LRFD Seismic Bridge Design (2011).

A simplified bridge was selected to minimize variables in the design process. There are several simplifications used herein that need to be evaluated in further detail for specific applications. These examples are to be used solely to understand the basics of the design process for each design example, and practicing engineers should validate the methodology for their specific application.

The bridge represents a ramp structure carrying a single lane collector distributor alignment to keep the elements slender and allow for a single column pier support for these design examples. The superstructure consists of precast concrete girders, a cast-in-place deck, and concrete barriers that are integral with the intermediate raised cross beam. Square spread footings are used at the intermediate piers so spring values can be determined easily. The end abutments are conventional and the supports are assumed to be roller bearings to eliminate resistance and spring values at the abutments. The footing size is assumed to be the same for each of the design examples. The abutment back wall location is considered far enough to accommodate the seismic motions of all the bridge design examples used herein.

The design process for each design example was performed as follows.

Step 1 Determine the Strengths I and III load combination forces acting on the column. The Service load combinations are assumed to be satisfied for all design examples. These novel columns may have service Limit State considerations that could change the design, but these are not addressed in these design examples as they are generally based on construction methods and local environmental conditions. The transverse loading is only considered for the Strength design, but not for Seismic, as discussed later on.

Step 2 Use moment magnification to amplify the strength Limit State moment. The methodology is simplified by ignoring the reinforcing effects of the Euler Buckling equations, and C_{sm} is assumed to be 1.0 for all cases.

Step 3 Determine the nominal P-M capacity of the column and design the amount of flexural reinforcing required to meet the Strength Limit State demands. Note that the shear design and capacity check for the Strength Limit State is not performed in this example, assuming the design is controlled by overstrength plastic shear demands.

Step 4 Determine appropriate material and seismic input, such as column stiffness, damping ratio, and others as appropriate, and develop a Response Spectral Analysis (RSA) model of the bridge to determine the displacement demands.

Step 5 Determine appropriate material properties, hinge length, and other input to develop and run a pushover analysis. Use the output of this analysis to verify that the displacement demand is less than the displacement capacity and that the ductility or drift ratio, for conventional or novel columns, respectively, are satisfied.

Step 6 Perform other design checks as specified in the Novel Column design guidelines. These design checks vary for each of the Novel Columns but are consistent in checking the shear capacity of the column against the overstrength plastic demands. Note that the design shows a single solution, when an iterative process is actually required to properly model the confinement of the column core with the final shear reinforcement design. Other aspects of this process also require iteration, but these are not shown in this design example.

The corresponding global and local axes of the bridge are oriented with the X-axis along the bridge from Pier 1 to Pier 3, the Y-axis transverse (out of the page), and the Z-axis vertical. The superstructure depth is 5 feet and the uncracked section properties of the superstructure used in these design examples are shown in Table 1-1. The cross beam for all the design examples is 5.5 feet deep and 2 feet wider than the column diameter. The jointed barriers were included as part of Dead Load only.

The demand on the column for the strength load combinations is checked against the factored axial-moment interaction of columns (P-M). The interaction curve and resistance factors are developed according to AASHTO (2014) using the nominal material properties; it was assumed that the highest compressive strain in concrete was limited to 0.003 as described in the code.

Seismic analysis of a bridge system to determine displacement demands and minimal lateral strength per AASHTO (2011) is generally modeled using Elastic Dynamic Analysis (EDA), though both lesser and more sophisticated methods are allowed in the specifications. This EDA method uses linear elastic multimodal spectral analysis with an appropriate response spectrum (i.e., generally 5 percent damping for conventional columns), energy dissipating systems (EDS), energy dissipating elements (EDE), foundation springs, and expected material properties and behavior to capture idealized displacements. These displacements occur in various directions to the structure and are combined into orthogonal seismic displacement demands. The specifications then allow you to verify the displacement demands and capacities (including drift in these design examples) along the local principle axis of the ductile member (or pier in these examples). To simplify these examples and show the unique qualities of the novel column material properties and behavior, the analysis has been simplified to only include the longitudinal (or lengthwise) direction of the bridge in demand and capacity.

Model boundary conditions can be modified to change the seismic behavior of a bridge. In these examples, inclusion of abutment restraints would have reduced the calculated damage in each case to a varying degree, but was not included in the models to create a simplified and similar comparison for each example. AASHTO (2011) provides recommendations for analysis methods, EDS, EDE, and boundary conditions. These recommendations should be considered in the complete analysis and design of novel columns to ensure adequate behavior and life-safety practices. The four girders were based on the Washington State Department of Transportation (WSDOT) 50-inch-deep girders. Reinforcement for the 7.5-inch thick deck and girders was assumed to meet the AASHTO (2014) design specifications.

The foundation design process for a bridge located in a high seismic region is critical to the design. The effort includes an iterative process with all the applicable load combinations, soil parameters to bracket the soil variations, and the soil-structure interaction. Engineers shall follow the design procedures outlined in AASHTO (2011). For the design examples presented in this document, the iteration and effort are simplified by using a 20-foot-square, 5-foot-deep spread footing that is assumed sufficient to resist all demands for the Service, Strength, and Extreme limit states. The soil is assumed to be dense glacial till with minimal settlement and adequate bearing capacity. Spring constants used were based on the assumed geometry, minimum embedment depth, Poisson's ratio, and shear modulus. These spring constants are used for all design limit states, including soft and stiff soil conditions for seismic loading of the Extreme limit state, without any significant change (see Table 1-2). Therefore, the iterative process was excluded in these design examples.

Graphs used in these design examples may show the inverse of the units of measure in order to produce a graph that is unitless.

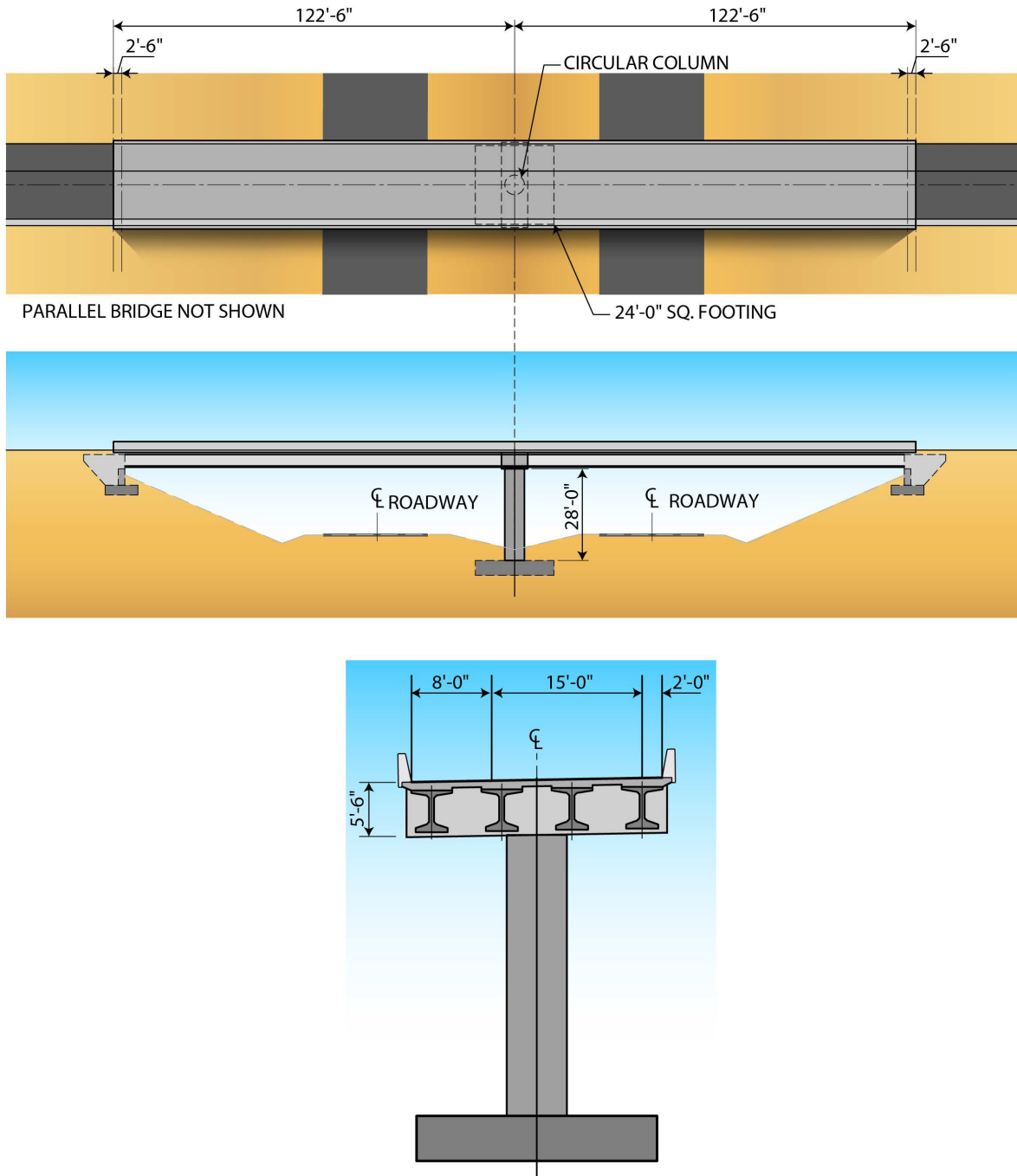
Data, specifications, suggested practices, and drawings presented herein are based on the best available information, are delineated in accordance with recognized professional engineering principles and practices, and are provided for general use only. State and local agencies may have prescriptive requirements and practices that go beyond or vary from those assumed and used herein. These design examples assume the reader has a basic understanding of seismic design principles. None of the procedures suggested or discussed should be used without first securing competent advice regarding their suitability for any given application as recommended in the guidelines.

Area	Moment of Inertia Longitudinal (I _x)	Moment of Inertia Transverse (I _y)	Torsional Constant (J)
ft ²	ft ⁴	ft ⁴	ft ⁴
35	113	2113	10

Table 1-1: Bridge Superstructure Section Properties for Model

Longitudinal Translation (U _x) (kip/in) x 10 ³	Transverse Translation (U _y) (kip/in) x 10 ³	Vertical Translation (U _z) (kip/in) x 10 ³	Transverse Rotation (R _x) (kip*in/rad) x 10 ⁹	Longitudinal Rotation (R _y) (kip*in/rad) x 10 ⁹	Torsional Rotation (R _z) (kip*in/rad) x 10 ⁹
57.64	57.64	50.21	1.18	1.18	2.22

Table 1-2: Foundation Spring Inputs



Graphic 1-1: Bridge Plan, Elevation, and Typical Pier Section

F1-2: Strength Limit State Load Combination Input

The following parameters are used to develop Strength Limit State Load combination demands on the structure. These values are provided for information. These demands are not developed further in this example; however, the column demands are summarized with moment magnification applied at the beginning of each design example.

Dead Loads

AASHTO (2014) 3.5.1

$\gamma_c := 0.155 \cdot \text{kcf}$ $f_c := 4 \cdot \text{ksi}$ concrete Class 4000 with reinforcement

$\gamma_{c_ps} := 0.165 \cdot \text{kcf}$ $f_{c_ps} := 9 \cdot \text{ksi}$ prestressed concrete girders

Wind Loads

AASHTO (2014) 3.8

Wind Pressure on Structure:

Assume wind exposure Category B and a gust factor of 1.00 as defined in AASHTO (2014) Table 3.8.1.2.1-1. The drag coefficient is as defined in AASHTO (2014) Table 3.8.1.2.1-2.

Wind Pressure on Vehicles:

$w_{WL} := 0.1 \text{klf}$ wind component on live load

Live Loads

AASHTO (2014) 3.6

Live load reaction at interior piers is controlled by 90 percent of the effect of two design trucks spaced a minimum of 50 feet apart, combined with 90 percent of the effect of the design lane load. Dynamic load allowance (IM) is assumed to be 33 percent. Pedestrian loading is assumed not to control.

Seismic Design Parameters

AASHTO (2104) 3.6

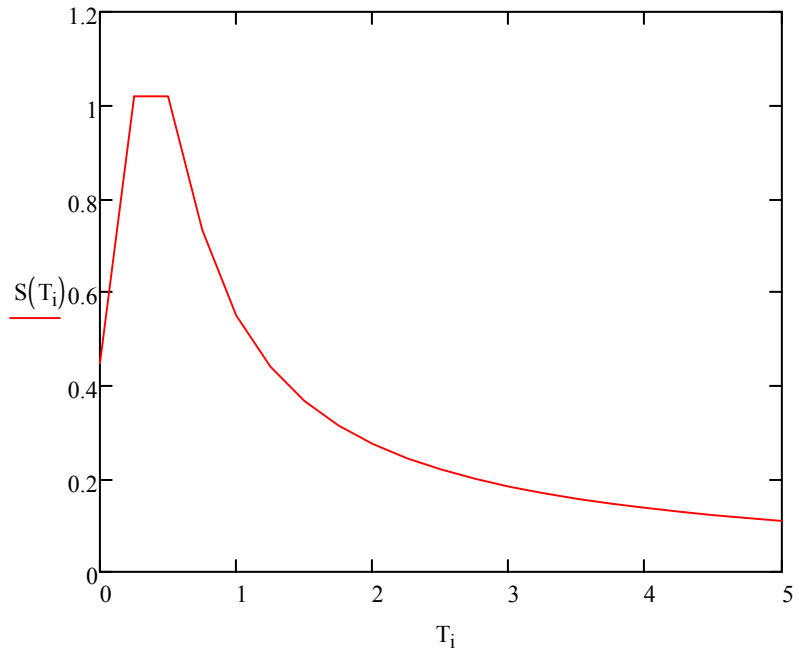
Site Response Spectrum Data with 5% Damping:

Note the damping used in the analysis may vary for the novel columns when compared to the conventional column process.

Peak ground acceleration	$PGA := 0.41$
Design short period acceleration	$S_{DS} := 1.02$
Design period 1.0 acceleration	$S_{D1} := 0.55$
Site coefficient of site peak ground acceleration	$F_{PGA} := 1.09$
Site coefficient for 0.2 sec	$F_a := 1.14$
Acceleration at short period	$S_s := 0.89$
Site coefficient for 1.0 sec	$F_v := 1.79$
Acceleration at 1.0 s period	$S_1 := 0.31$
Acceleration at zero period	$A_g := F_{PGA} \cdot PGA$

Function for period - acceleration

$$S(T) := \begin{cases} A_g & \text{if } T = 0 \\ T \cdot \frac{(S_{DS} - A_g)}{0.2 \cdot \frac{S_{D1}}{S_{DS}}} + A_g & \text{if } 0 < T \leq 0.2 \cdot \frac{S_{D1}}{S_{DS}} \\ S_{DS} & \text{if } 0.2 \cdot \frac{S_{D1}}{S_{DS}} < T \leq \frac{S_{D1}}{S_{DS}} \\ \frac{S_{D1}}{T} & \text{otherwise} \end{cases}$$



Plot 1-1: Response Spectrum Curve



NCHRP
Conventional Column Design



33301 Ninth Avenue South, Suite 300 Federal
Way, Washington 98003-2600

F2 - CONVENTIONAL REINFORCED CONCRETE COLUMN DESIGN

F2-1: Strength Design of Conventional Column

The following table shows the factored load for the Strength Limit State design of the conventional column. The moments in the transverse and longitudinal direction are magnified according to AASHTO (2014) Section 4.5.3.2.2b with simplifications identified previously.

Strength Factored Load	Units	Magnitude
Magnified Longitudinal Moment	kip-in	18,090
Magnified Transverse Moment	kip-in	45,950
Shear Longitudinal	kips	0
Shear Transverse	kips	166
Axial Load	kips	2,464

Table 2-1: Controlling Strength Load Combination Values

The column size is determined based on an iterative effort to optimize the size required to meet the strength design criteria. The following strength design calculations show the last iteration.

Axial-Moment Strength Check of Column

Section Properties:

The following design section properties are used for this example.

Diameter of column	$D := 5\text{ft}$	
Column height	$L := 28\text{ft}$	
Cover	$c := 2\text{in}$	
Diameter of longitudinal rebar	$d_{lr} := 1.41\text{in}$	Use 22 #11 bars
Area of longitudinal rebar	$a_{lr} := 1.56\text{in}^2$	
Number of longitudinal rebar	$n_{lr} := 22$	
Diameter of transverse reinforcement	$d_{tr} := 0.625\text{in}$	
Area of transverse reinforcement	$a_{tr} := 0.31\text{in}^2$	Use #5 @ 4 in.
Transverse rebar spacing	$s := 4\text{in}$	
Type of Transverse rebar	Type := "spiral"	
Concrete area	$A_g := \frac{\pi}{4} \cdot D^2 = 2.827 \times 10^3 \cdot \text{in}^2$	

Material Properties:

The following design material properties are used for this example.

Compression strength of concrete	$f'_c := -4\text{ksi}$	
Strain at peak compression	$\epsilon_{co} := -0.002$	AASHTO (2011) 8.4.4.1
Concrete crushing strain	$\epsilon_{cu} := 2 \cdot \epsilon_{co}$	AASHTO (2011) Fig. 8.4.4.1
Spalling strain	$\epsilon_{sp} := -0.005$	
Concrete density	$\gamma_c := 145\text{pcf}$	
Concrete module	$E_c := 33000 \cdot \left(\frac{\gamma_c \cdot \text{ft}^3}{\text{kip}} \right)^{1.5} \cdot \sqrt{ f'_c } \cdot \text{ksi} = 3.644 \times 10^3 \cdot \text{ksi}$	AASHTO (2014) 5.4.2.4-1
Yield strength of longitudinal rebar	$f_y := 60\text{ksi}$	A 706, Grade 60
Modulus of steel	$E_s := 29000\text{ksi}$	
Yield strength of spirals	$f_{yh} := 60\text{ksi}$	A 706, Grade 60
Strain at peak stress of spirals	$\epsilon_{suh} := 0.09$	AASHTO (2011) Table 8.4.2.1

Stress-Strain Calculations of Unconfined Concrete

Mander et al. 1988

Secant concrete modulus

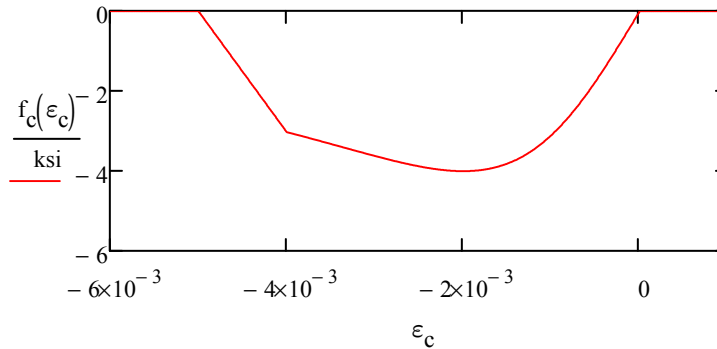
$$E_{\text{sec}} := \frac{f'_c}{\epsilon_{co}} = 2 \times 10^3 \cdot \text{ksi}$$

$$r := \frac{E_c}{E_c - E_{\text{sec}}} = 2.216$$

Stress-strain function of unconfined concrete

$$f_c(\epsilon_c) := \begin{cases} 0 & \text{if } \epsilon_c \geq 0 \\ \frac{f_c \cdot \frac{\epsilon_c}{\epsilon_{co}} \cdot r}{r - 1 + \left(\frac{\epsilon_c}{\epsilon_{co}}\right)^r} & \text{if } \epsilon_{cu} < \epsilon_c \leq 0 \\ \frac{-f_c \cdot \frac{\epsilon_{cu}}{\epsilon_{co}} \cdot r}{r - 1 + \left(\frac{\epsilon_{cu}}{\epsilon_{co}}\right)^r} \cdot \frac{\epsilon_{sp} - \epsilon_c}{\epsilon_{cu} - \epsilon_{sp}} & \text{if } \epsilon_{sp} < \epsilon_c \leq \epsilon_{cu} \\ 0 & \text{otherwise} \end{cases}$$

The following figure shows stress-strain curve for section analysis input.



Plot 2-1: Unconfined Concrete Stress-Strain Curve

Stress-Strain Calculations of Confined Concrete

Mander et al. 1988

Total area of longitudinal rebar

$$A_l := n_{lr} \cdot a_{lr}$$

$$A_l = 34.32 \cdot \text{in}^2$$

Core diameter of concrete

$$D' := D - d_{tr} - 2 \cdot c = 55.375 \cdot \text{in}$$

Core area

$$A_{cc} := \frac{\pi}{4} \cdot D'^2 - A_l$$

$$A_{cc} = 2.374 \times 10^3 \cdot \text{in}^2$$

Ratio longitudinal rebar/core $\rho_{cc} := \frac{A_l}{A_{cc}} \quad \rho_{cc} = 1.446\%$

Transverse rebar volumetric ratio $\rho_s := \frac{4 \cdot a_{tr}}{s \cdot D'} = 5.598 \times 10^{-3}$

Confinement effectiveness coefficient

$$K_e := \min \left[\begin{array}{l} \frac{1 - \frac{s - d_{tr}}{2 \cdot D'}}{1 - \rho_{cc}} \text{ if Type = "spiral"} \\ \frac{\left(1 - \frac{s - d_{tr}}{2 \cdot D'}\right)^2}{1 - \rho_{cc}} \text{ otherwise} \end{array} , 1 \right] = 0.984$$

Effective lateral confining pressure $f_l := \frac{1}{2} \cdot K_e \cdot \rho_s \cdot f_{yh}$

Confined concrete strength

$$f_{cc} := f_c \cdot \left(-1.254 + 2.254 \cdot \sqrt{1 + 7.94 \cdot \frac{f_l}{|f_c|}} - 2 \cdot \frac{f_l}{|f_c|} \right) = -5.043 \cdot \text{ksi}$$

Ultimate strain $\epsilon_{ccu} := - \left(0.004 + \frac{1.4 \cdot \rho_s \cdot f_{yh} \cdot \epsilon_{suh}}{|f_{cc}|} \right) = -0.012$

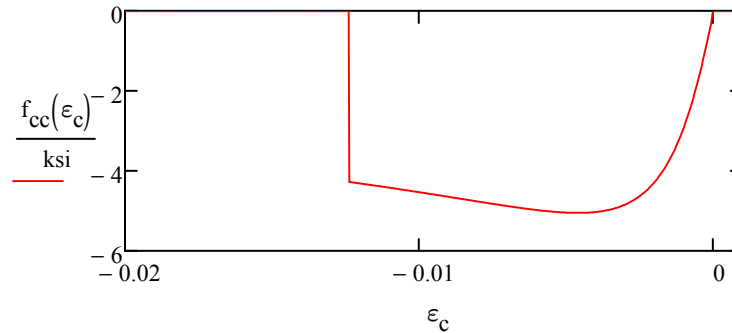
Strain at peak stress $\epsilon_{cc} := \epsilon_{co} \cdot \left[1 + 5 \cdot \left(\frac{f_{cc}}{f_c} - 1 \right) \right] = -4.608 \times 10^{-3}$

Secant concrete modulus

$$E_{sec} := \frac{f_{cc}}{\epsilon_{cc}} = 1.094 \times 10^3 \cdot \text{ksi} \quad r := \frac{E_c}{E_c - E_{sec}}$$

Stress-strain curve of confined concrete

$$f_{cc}(\epsilon_c) := \begin{cases} 0 & \text{if } \epsilon_c \geq 0 \\ \frac{f'_{cc} \cdot \frac{\epsilon_c}{\epsilon_{cc}} \cdot r}{r - 1 + \left(\frac{\epsilon_c}{\epsilon_{cc}}\right)^r} & \text{if } \epsilon_{ccu} \leq \epsilon_c \leq 0 \\ 0 & \text{otherwise} \end{cases}$$



Plot 2-2: Confined Concrete Stress-Strain Curve

Section Analysis software uses built-in stress-strain relations of conventional reinforced concrete columns to obtain Axial-Moment (P-M) interaction curves. Though this is standard for conventional columns, it is not standard for the novel column materials used in the following examples. Understanding what is being generated in conventional columns will help in understanding the differences in novel column analysis. The results generated in this example were based on the stress-strain relationships shown herein and not the standard Section Analysis software defaults.

Axial Capacity:

Capacity $\phi P_{on} := 0.75 \cdot [0.85 \cdot |(f'_c)| \cdot (A_g - A_l) + A_l \cdot f_y] = 8.667 \times 10^3 \cdot \text{kip}$ AASHTO (2014)

D/C Ratio $\frac{P_{u_ST1}}{\phi P_{on}} = 0.284$ < 1.0 **OK**

Axial-Moment (P-M) Interaction Capacity:

The column section is modeled in a Section Analysis Program to generate the nominal P-M Interaction Curve and associated strain in the steel and concrete. The steel strain values were used to identify the tension/compression-controlled region of the column.

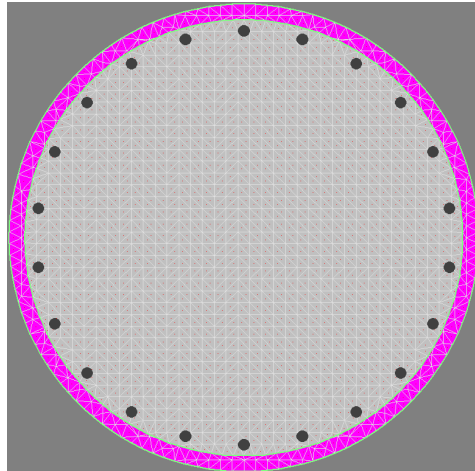


Image 2-1: Reinforced Concrete Column Cross Section

The following function was used to find the Resistance Factor for axial-moment capacity from nominal values according to AASHTO (2014) Figure C5.5.4.2.1-1.

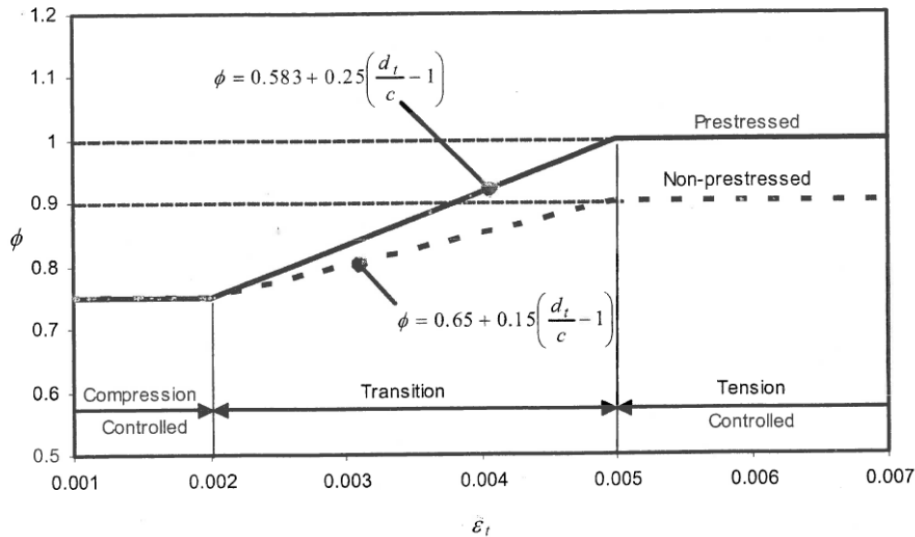
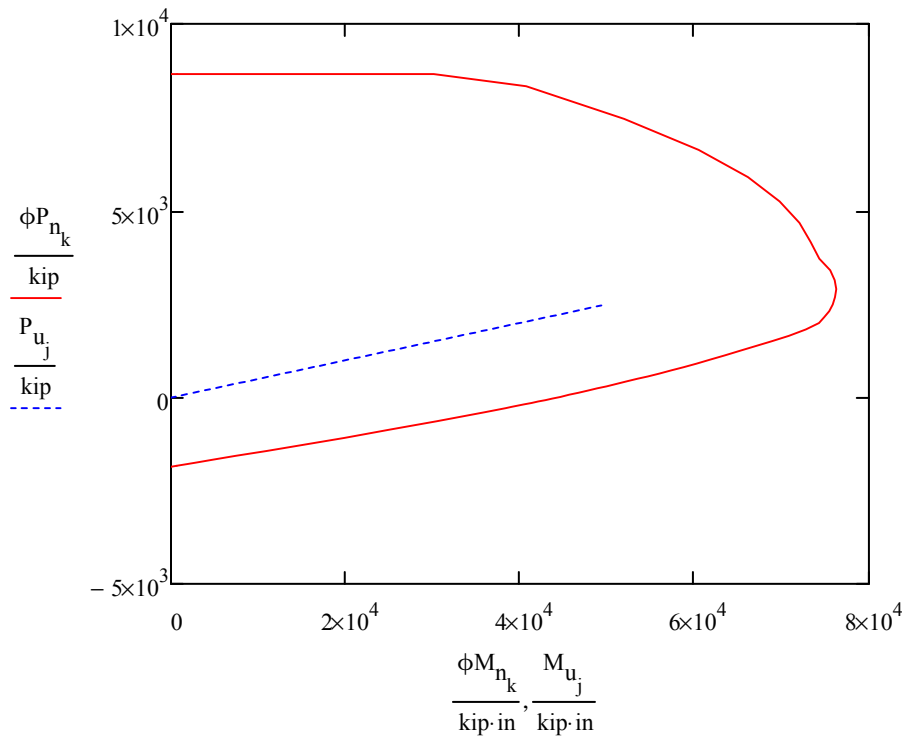


Image 2-2: Axial-Moment Resistance Factor for Columns

The following figure shows the P-M capacity curve of the conventional column, and compares it with the factored design loads. The demand was less than the capacity, and the section has sufficient strength for the factored loads.



Plot 2-3: Factored Axial-Moment (P-M) Capacity versus Demand for the Conventional Column

Demand	$M_{u_1} = 4.115 \times 10^3 \cdot \text{kip} \cdot \text{ft}$	$P_{u_1} = 2.464 \times 10^3 \cdot \text{kip}$
Capacity	$\phi M_{CAP} = 6.315 \times 10^3 \cdot \text{kip} \cdot \text{ft}$	$\phi = 0.843$
D/C Ratio	$DCR := \frac{M_{u_1}}{\phi M_{CAP}} = 0.652$	< 1.0 OK

F2-2: Seismic Design of Conventional Column

Material Properties:

AASHTO (2011)

The following design material properties were used for the seismic portion of the design example.

Concrete Properties (AASHTO (2011) Table 8.4.4):

Expected concrete strength	$f_{ce} := 1.3 \cdot f_c = -5.2 \cdot \text{ksi}$
Strain at peak compression	$\epsilon_{co} := -0.002$ 8.4.4.1 Guide Spec. (GS)
Concrete crushing strain	$\epsilon_{cu} := 2 \cdot \epsilon_{co}$ Fig.8.4.4.1 (GS)
Spalling strain	$\epsilon_{sp} := -0.005$
Concrete density	$\gamma_c := 145 \text{ pcf}$
Expected concrete modulus	$E_{ce} := 33000 \cdot \left(\frac{\gamma_c \cdot \text{ft}^3}{\text{kip}} \right)^{1.5} \cdot \sqrt{ f_{ce} \cdot \text{ksi}} = 4.155 \times 10^3 \cdot \text{ksi}$

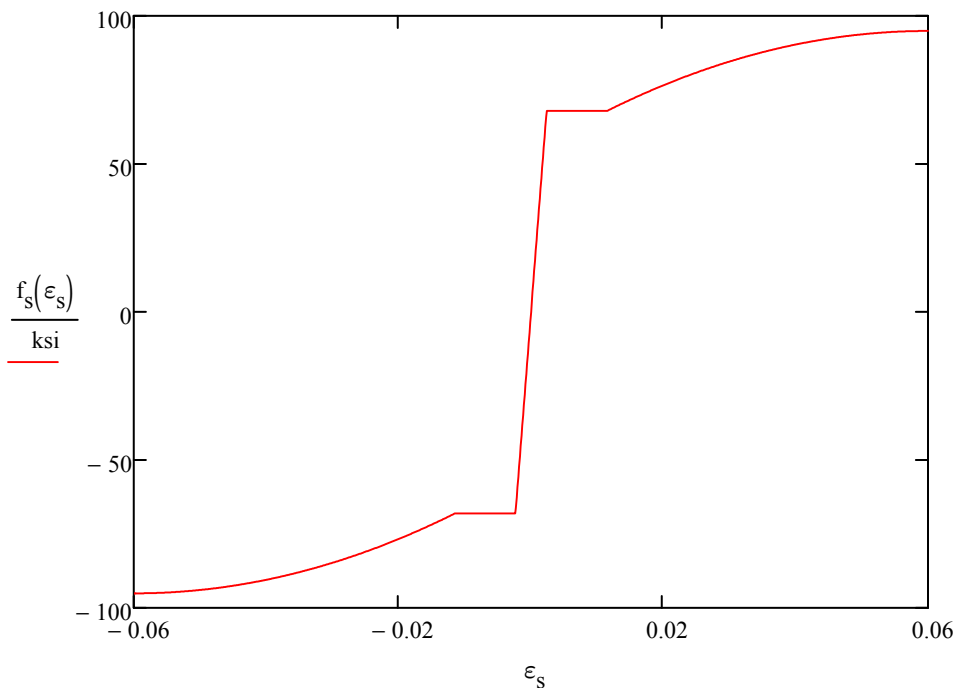
Longitudinal Reinforcement Properties (AASHTO (2011) Table 8.4.2.1):

Expected yield strain	$\epsilon_{ye} := 0.0023$
Number of rebar	$n := n_{lr}$
Expected longitudinal rebar yield strength	$f_{ye} := 68 \text{ ksi}$
Expected longitudinal rebar ultimate strength	$f_{ue} := 95 \text{ ksi}$
Reduced ultimate tensile strain	$\epsilon_{su} := 0.06$
Strain hardening	$\epsilon_{sh} := 0.0115$
Spacing of transverse rebar	$s := 4 \text{ in}$
Concrete core diameter	$D' := [D - (2c)] - d_{lr} = 54.59 \cdot \text{in}$
Overstrength factor	$\lambda := 1.2$ AASHTO (2011) 8.5

Stress-strain curves developed here for steel and confined and unconfined concrete were used in Section Analysis Program to obtain moment-curvature response.

Stress-strain relations of steel reinforcement

$$f_s(\epsilon_s) := \begin{cases} \left[-f_{ue} - (-f_{ue} + f_{ye}) \cdot \left(\frac{-\epsilon_{su} - \epsilon_s}{-\epsilon_{su} + \epsilon_{sh}} \right)^2 \right] & \text{if } \epsilon_s \leq -\epsilon_{sh} \\ -f_{ye} & \text{if } -\epsilon_{sh} < \epsilon_s \leq \frac{-f_{ye}}{E_s} \\ E_s \cdot \epsilon_s & \text{if } \frac{-f_{ye}}{E_s} < \epsilon_s \leq \frac{f_{ye}}{E_s} \\ f_{ye} & \text{if } \frac{f_{ye}}{E_s} < \epsilon_s \leq \epsilon_{sh} \\ \left[f_{ue} - (f_{ue} - f_{ye}) \cdot \left(\frac{\epsilon_{su} - \epsilon_s}{\epsilon_{su} - \epsilon_{sh}} \right)^2 \right] & \text{otherwise} \end{cases}$$



Plot 2-4: Stress-Strain Curve of A706 Reinforcement Steel

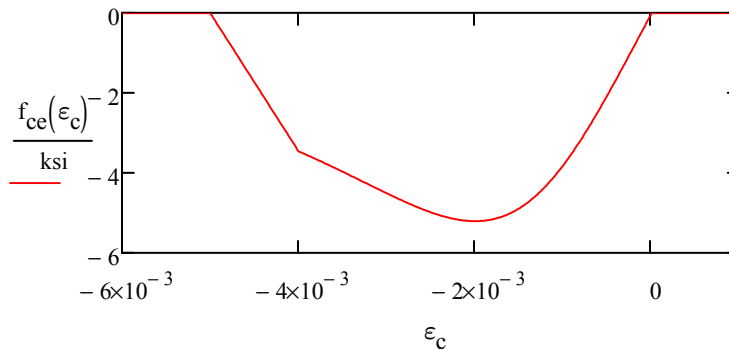
Stress-strain calculations of unconfined concrete (Mander Model)

Expected secant concrete modulus $E_{sec} := \frac{f_{ce}}{\epsilon_{co}} = 2.6 \times 10^3 \cdot \text{ksi}$

$$r := \frac{E_{ce}}{E_{ce} - E_{sec}} = 2.672$$

Stress-strain function of unconfined concrete (Mander Equations)

$$f_{ce}(\epsilon_c) := \begin{cases} 0 & \text{if } \epsilon_c \geq 0 \\ \frac{f_{ce} \cdot \frac{\epsilon_c}{\epsilon_{co}} \cdot r}{r - 1 + \left(\frac{\epsilon_c}{\epsilon_{co}}\right)^r} & \text{if } \epsilon_{cu} < \epsilon_c \leq 0 \\ \frac{-f_{ce} \cdot \frac{\epsilon_{cu}}{\epsilon_{co}} \cdot r}{r - 1 + \left(\frac{\epsilon_{cu}}{\epsilon_{co}}\right)^r} \cdot \frac{\epsilon_{sp} - \epsilon_c}{\epsilon_{cu} - \epsilon_{sp}} & \text{if } \epsilon_{sp} < \epsilon_c \leq \epsilon_{cu} \\ 0 & \text{otherwise} \end{cases}$$



Plot 2-5: Expected Unconfined Stress-Strain Curve

Stress-strain calculations of confined concrete (Mander Models)

Total area of longitudinal rebar	$A_l := n_{lr} \cdot a_{lr} = 34.32 \cdot \text{in}^2$
Core diameter of concrete	$D' := D - d_{tr} - 2 \cdot c = 55.375 \cdot \text{in}$
Core area	$A_{cc} := \frac{\pi}{4} \cdot D'^2 - A_l = 2.374 \times 10^3 \cdot \text{in}^2$
Ratio longitudinal rebar/core	$\rho_{cc} := \frac{A_l}{A_{cc}} = 1.446\%$
Stirrup volumetric ratio	$\rho_s := \frac{4 \cdot a_{tr}}{s \cdot D'} = 5.598 \times 10^{-3}$
Confinement effectiveness coefficient	$K_e := \min \left[\begin{array}{l} \frac{1 - \frac{s - d_{tr}}{2 \cdot D'}}{1 - \rho_{cc}} \text{ if Type = "spiral" } \\ \frac{\left(1 - \frac{s - d_{tr}}{2 \cdot D'}\right)^2}{1 - \rho_{cc}} \text{ otherwise} \end{array} \right] = 0.984$
Effective lateral confining pressure	$f_l := \frac{1}{2} \cdot K_e \cdot \rho_s \cdot f_{yh}$
Expected confined concrete strength	$f_{cce} := f_{ce} \cdot \left(-1.254 + 2.254 \cdot \sqrt{1 + 7.94 \cdot \frac{f_l}{ f_{ce} }} - 2 \cdot \frac{f_l}{ f_{ce} } \right) = -6.265 \cdot \text{ksi}$
Ultimate strain	$\epsilon_{ccu} := - \left(0.004 + \frac{1.4 \cdot \rho_s \cdot f_{yh} \cdot \epsilon_{suh}}{ f_{cce} } \right) = -0.011$

Expected ultimate strain of confined concrete is slightly less than nominal ultimate strain calculated in strength design (previous section) because the expected strength of concrete was higher than nominal strength.

Strain at peak stress $\epsilon_{cc} := \epsilon_{co} \cdot \left[1 + 5 \cdot \left(\frac{f_{cce}}{f_{ce}} - 1 \right) \right] = -4.048 \times 10^{-3}$

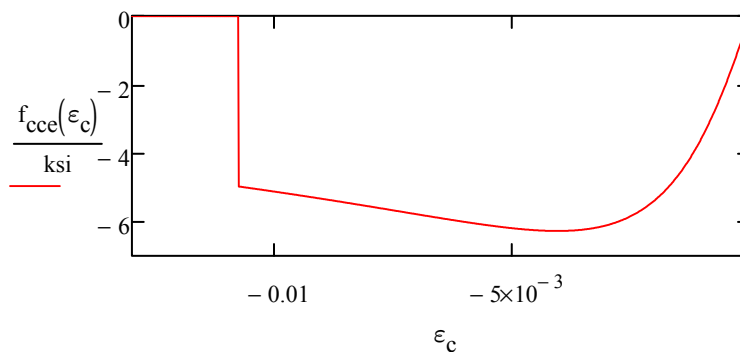
Expected secant concrete modulus $E_{sec} := \frac{f_{cce}}{\epsilon_{cc}} = 1.548 \times 10^3 \cdot \text{ksi}$

$$r := \frac{E_{ce}}{E_{ce} - E_{sec}}$$

Stress-strain curve of concrete

$$f_{cce}(\epsilon_c) := \begin{cases} 0 & \text{if } \epsilon_c \geq 0 \\ \frac{f_{cce} \cdot \frac{\epsilon_c}{\epsilon_{cc}} \cdot r}{r - 1 + \left(\frac{\epsilon_c}{\epsilon_{cc}} \right)^r} & \text{if } \epsilon_{ccu} \leq \epsilon_c \leq 0 \\ 0 & \text{otherwise} \end{cases}$$

:



Plot 2-6: Stress-Strain Curve of Confined Concrete

Plastic Hinge Length:

AASHTO (2011) 4.11.6

Longitudinal: double curvature

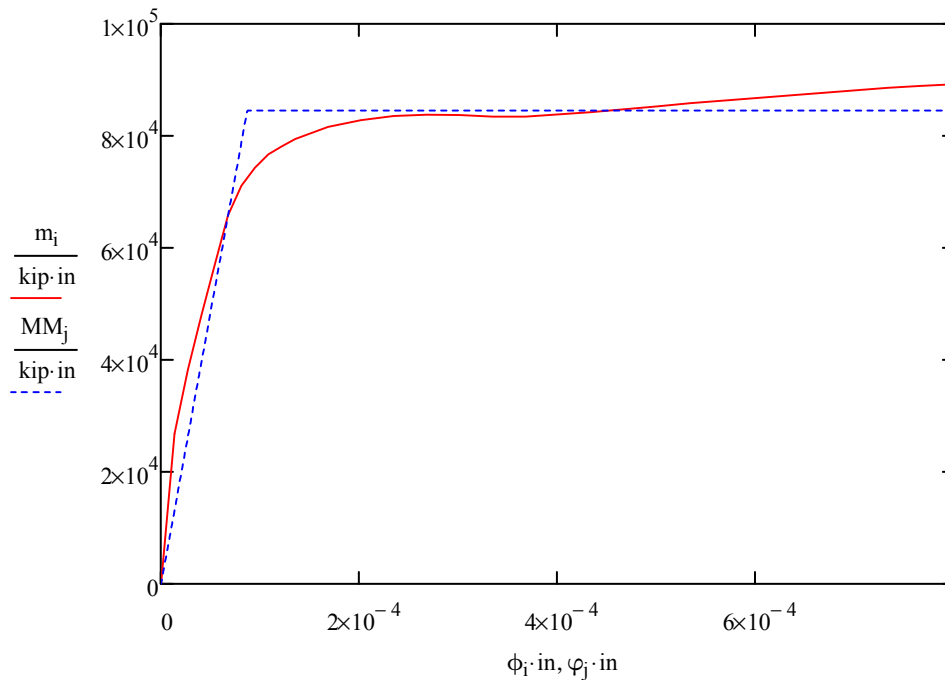
$$L_{P_X} := \max\left(0.08 \cdot \frac{L}{2} + 0.15 \cdot \frac{f_{ye}}{\text{ksi}} \cdot d_{lr}, 0.3 \cdot \frac{f_{ye}}{\text{ksi}} \cdot d_{lr}\right) = 28.764 \cdot \text{in}$$

Moment-Curvature Responses of the Column Section:

Moment-curvature response of column section is generated with a Section Analysis Program using expected material properties and the dead load axial loads acting on the column.

Axial load $P_f := -1500\text{kip}$

The following graph shows the moment-curvature response generated during the section analysis run and the idealized bilinear relationship to be used for the pushover analysis. The idealized curve is obtained according to AASHTO (2011) Section 8.5. The elastic portion of the curve, or initial stiffness, begins from the origin and passed through the first yield point of the reinforcing bar until it matches with the horizontal idealized line. The horizontal, or idealized moment capacity, is obtained by equating the upper and lower areas between the actual and the idealized curve beyond the first yielding of reinforcing bar. The second flat line should be iteratively shifted up and down to get the same area between bilinear and actual relationship after the first yield of reinforcement.



Plot 2-7: Conventional Column Moment-Curvature Response and Idealized Bilinear Curve

Idealized Bilinear Curve Parameters:

Capacity moment	$M_P = 8.455 \times 10^4 \cdot \text{kip} \cdot \text{in}$
Effective yield curvature	$\phi_{yi} = 8.672 \times 10^{-5} \cdot \frac{1}{\text{in}}$
Ultimate curvature	$\phi_u = 7.981 \times 10^{-4} \cdot \frac{1}{\text{in}}$
Effective initial stiffness	$EI_{\text{eff}} = 6.771 \times 10^6 \cdot \text{kip} \cdot \text{ft}^2$
Cracking stiffness reduction for demand analysis	$\alpha_{\text{crack}} := \frac{EI_{\text{eff}}}{E_{ce} \cdot \frac{\pi}{64} \cdot D^4} = 0.369$

Demand Analysis:

The response spectrum is defined in Section F1-2 with 5 percent damping.

Result of Demand Analysis:

The bridge was modeled using a Finite Element Program. The following figure shows the bridge model for demand and pushover analysis. For this design example, the seismic behavior of the bridge was investigated in longitudinal direction only. As the column is integrated with the superstructure, the column was designed for dual-hinge behavior with a hinge at both the base and the top of column. The abutments were unrestrained (roller bearing) in the longitudinal direction, parallel to the roadway. The transverse direction is single hinge at the base; however, the transverse design of the bridge is not investigated in this study.

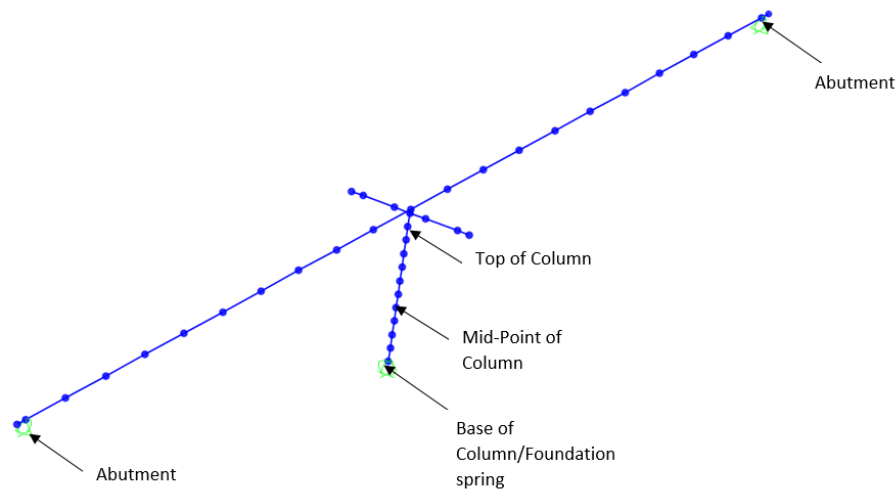
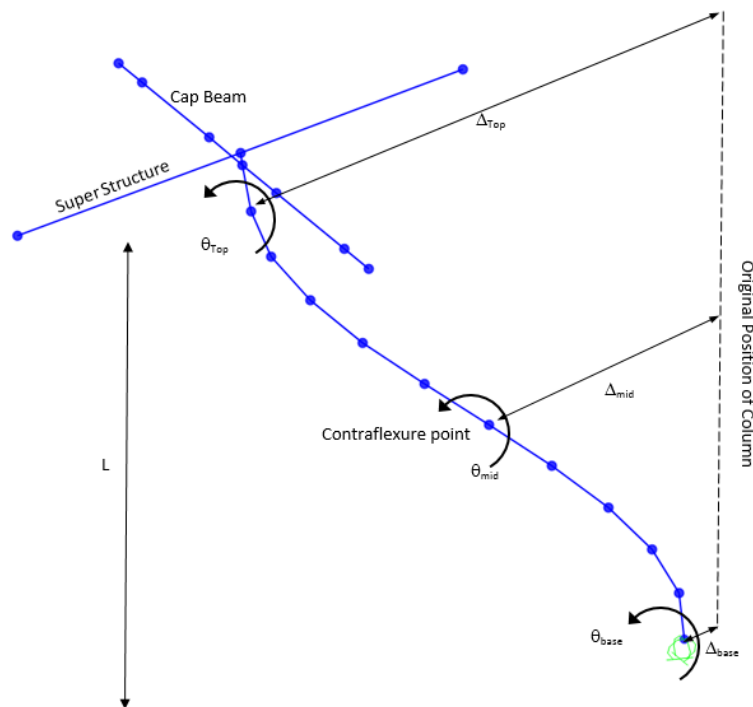


Image 2-3: Finite Element Bridge Model

The natural period of the bridge in longitudinal direction is 1.035 s. According to AASHTO 2011 Section 4.3.3, as the period of structure is longer than the 1.25Ts (Ts:short period, 0.54 s) then the displacement magnification factor would be 1.0.

Demand Displacement from Response Spectrum Analysis in Longitudinal Direction

The performance and ductility of each hinge were investigated separately. It was assumed that the moment capacity and the geometry of the column at both hinges are essentially identical; therefore, the contraflexure point for this column in the longitudinal direction was at the midheight of the column, and the performance of each hinge was evaluated for the lower and upper lengths of the column. The following figure shows the parameters needed to calculate the displacements of the column at each end. These displacements will be needed to find the performance and ductility of each hinge.



$$\Delta_{Bot_hinge} = \Delta_{mid} - \Delta_{base} - \theta_{base} \times L/2$$

$$\Delta_{Top_hinge} = \Delta_{mid} - \Delta_{top} - \theta_{top} \times L/2$$

Image 2-4: Bridge Model Column Curvature

Demand deflections in top and bottom hinges

$$\Delta_{D_{BOT}} := \left| \left| \text{Demand}_{SAP_{4,4}} \cdot \text{in} - \text{Demand}_{SAP_{3,4}} \cdot \text{in} \right| - \text{Demand}_{SAP_{3,8}} \cdot \frac{L}{2} \right| = 2.408 \cdot \text{in}$$

$$\Delta_{D_{TOP}} := \left| \left| \text{Demand}_{SAP_{4,4}} \cdot \text{in} - \text{Demand}_{SAP_{5,4}} \cdot \text{in} \right| - \text{Demand}_{SAP_{5,8}} \cdot \frac{L}{2} \right| = 1.99 \cdot \text{in}$$

Check P-Delta Effect:

AASHTO (2011) 4.11.5

Moment due to P-delta

$$|P_f| \cdot \max(\Delta_{D_{BOT}}, \Delta_{D_{TOP}}) = 3.612 \times 10^3 \cdot \text{kip} \cdot \text{in}$$

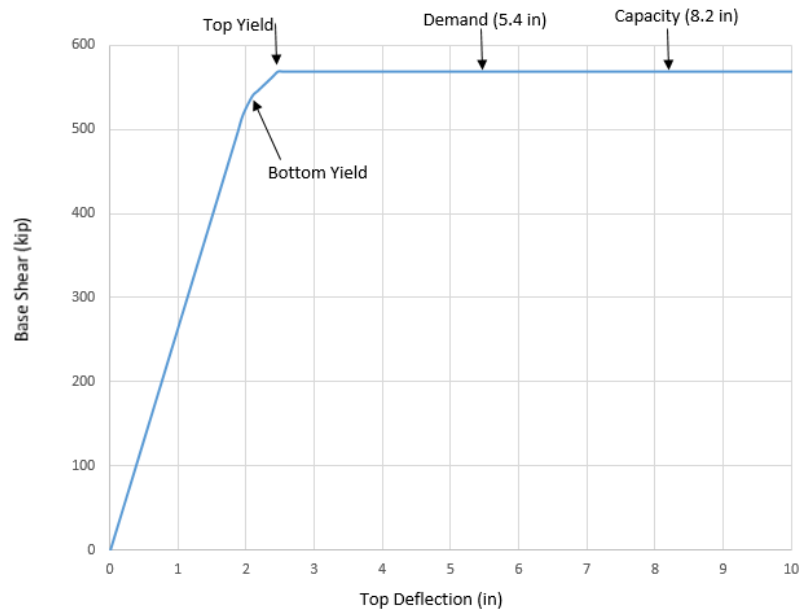
$$0.25 \cdot M_P = 2.114 \times 10^4 \cdot \text{kip} \cdot \text{in}$$

As the moment due to P-delta is much less than a quarter of M_P , then P-delta effect can be ignored.

Pushover Analysis

The two hinges at the top and bottom of the column were defined according to the idealized bilinear curve presented above. The bridge was pushed longitudinally to failure and the following results are obtained.

The following figure shows the Force-Top Displacement Response of the column in the longitudinal direction.



Plot 2-8: Force-Top Displacement Response of the Conventional Column

Yield Displacement of Column:

BOT hinge yield deflection $\Delta_{Y_{BOT}} = 0.973 \cdot \text{in}$

TOP hinge yield deflection $\Delta_{Y_{TOP}} = 0.917 \cdot \text{in}$

Yield displacement obtained from AASHTO (2011) using moment-curvature analysis

$$\Delta_{Y_Code} := \frac{\phi_{yi} \cdot (0.5L)^2}{3} = 0.816 \cdot \text{in} \quad \text{Close to FEA results above}$$

Capacity displacement obtained from Finite Element Analysis (FEA) program

$$\Delta_{C_{BOT}} = 4.065 \cdot \text{in}$$

$$\Delta_{C_{TOP}} = 4.071 \cdot \text{in}$$

Capacity displacement obtained from AASHTO (2011), top and bottom, as the point of counterflexure is in the middle of the column.

$$\Delta_{C_{BOT_Code}} := \frac{\phi_{yi} \cdot (0.5L)^2}{3} + (\phi_u - \phi_{yi}) \cdot L_{P_x} \cdot \left(\frac{L}{2} - \frac{L_{P_x}}{2} \right) = 3.959 \cdot \text{in}$$

$$\Delta_{C_{TOP_Code}} := \frac{\phi_{yi} \cdot (0.5L)^2}{3} + (\phi_u - \phi_{yi}) \cdot L_{P_x} \cdot \left(\frac{L}{2} - \frac{L_{P_x}}{2} \right) = 3.959 \cdot \text{in} \quad \text{Close to FEA results above}$$

Check demand/capacity ratio AASHTO (2011) 4.8

$$\frac{\Delta_{D_{BOT}}}{\Delta_{C_{BOT}}} = 0.592 \quad < 1.0 \quad \text{OK}$$

$$\frac{\Delta_{D_{TOP}}}{\Delta_{C_{TOP}}} = 0.489 \quad < 1.0 \quad \text{OK}$$

Check ductility of a single column bent AASHTO (2011) 4.9

$$\mu_{D_BOT} := \frac{\Delta_{D_{BOT}}}{\Delta_{Y_{BOT}}} = 2.475 \quad < 5.0 \quad \text{OK}$$

$$\mu_{D_TOP} := \frac{\Delta_{D_{TOP}}}{\Delta_{Y_{TOP}}} = 2.17 \quad < 5.0 \quad \text{OK}$$

$$\mu_{C_BOT} := \frac{\Delta_{C_BOT}}{\Delta_{Y_BOT}} = 4.178 \quad > 3.0 \quad \text{OK}$$

$$\mu_{C_TOP} := \frac{\Delta_{C_TOP}}{\Delta_{Y_TOP}} = 4.439 \quad > 3.0 \quad \text{OK}$$

For conventional columns, the checks required were in terms of displacement demand to capacity and column ductility. Drift ratio demand and capacity values below were for comparison purposes with novel column designs.

Demand drift ratio $\delta_{D_BOT} := \frac{\Delta_{D_BOT}}{\frac{L}{2}} = 1.433\%$

Demand drift ratio $\delta_{D_TOP} := \frac{\Delta_{D_TOP}}{\frac{L}{2}} = 1.184\%$

Capacity drift ratio $\delta_{C_BOT} := \frac{\Delta_{C_BOT}}{\frac{L}{2}} = 2.42\%$

Capacity drift ratio $\delta_{C_TOP} := \frac{\Delta_{C_TOP}}{\frac{L}{2}} = 2.423\%$

Maximum demand drift ratio $\delta_{D_max} := \frac{5 \cdot \min(\Delta_{Y_BOT}, \Delta_{Y_TOP})}{\frac{L}{2}} = 2.729\%$ AASHTO (2011) 4.9

Minimum capacity demand drift ratio $\delta_{C_min} := \frac{3 \cdot \max(\Delta_{Y_BOT}, \Delta_{Y_TOP})}{\frac{L}{2}} = 1.737\%$

Residual Drift Calculations:

REPORT 12-101 2.5.3-1

BOT hinge yield drift ratio $\delta_{Y_BOT} := \frac{\Delta_{Y_BOT}}{\frac{L}{2}} = 0.579\%$

TOP hinge yield drift ratio $\delta_{Y_TOP} := \frac{\Delta_{Y_TOP}}{\frac{L}{2}} = 0.546\%$

Residual drift factor (β)

REPORT 12-101 2.5.3-2

β factor for bottom hinge $\beta_{BOT} := \text{if}(\mu_{D_BOT} > 1.0, 0.04 \cdot \mu_{D_BOT}^2 + 0.14 \cdot \mu_{D_BOT}, 0) = 0.592$

β factor for top hinge $\beta_{TOP} := \text{if}(\mu_{D_TOP} > 1.0, 0.04 \cdot \mu_{D_TOP}^2 + 0.14 \cdot \mu_{D_TOP}, 0) = 0.492$

Residual drift ratio for bottom hinge $\delta_{r_BOT} := \beta_{BOT} \cdot \delta_{Y_BOT} = 0.343\%$

REPORT 12-101 2.5.3-1

Residual drift ratio for top hinge $\delta_{r_TOP} := \beta_{TOP} \cdot \delta_{Y_TOP} = 0.269\%$

Shear Design of Column:

The Strength Limit State shear design of the column was not included in this design example. The following example demonstrates the AASHTO (2011) shear design required to capacity protect against a brittle shear failure from the overstrength plastic forces.

Plastic shear developed in pier

Overstrength factor (λ) is equal to 1.2 for A706 reinforcing bars and because of the dual hinge behavior, the shear span was half the column length.

Overstrength plastic moment $M_{P0} := \lambda \cdot M_P = 8.455 \times 10^3 \cdot \text{kip} \cdot \text{ft}$

X direction $V_{P_x} := \frac{\lambda \cdot M_P}{\left(\frac{L - L_{P_x}}{2}\right)} = 660.473 \cdot \text{kip}$

Shear demand from elastic response spectrum analysis

X direction $V_{RSA_x} := 1349 \text{kip}$

Shear capacity design check

AASHTO (2011) 8.6

Cross section area

$$A_g := \frac{\pi}{4} \cdot D^2$$

Ductility factor for SDC D - AASHTO
Guide Spec 4.3.3

$$\mu_D := \max(\mu_{D_BOT}, \mu_{D_TOP}) = 2.475$$

Transverse reinforcement ratio at
bottom

$$\rho_s := \frac{4 \cdot a_{tr}}{D \cdot s} = 5.598 \times 10^{-3}$$

Ratio of longitudinal reinforcement

$$\rho_t := \frac{n \cdot a_{lr}}{A_g} = 0.012$$

Maximum allowable nominal stress in
rebar

$$f_s := \min(\rho_s \cdot f_{yh}, 0.35 \text{ ksi}) = 0.336 \text{ ksi}$$

Concrete shear stress adjustment

$$\alpha := \max\left(\frac{f_s}{0.15 \text{ ksi}} + 3.67 - \mu_D, 0\right) = 3.434$$

Concrete shear capacity

$$A := .032 \frac{\text{in}}{\sqrt{\text{kip}}} \alpha \cdot \left(1.0 \text{ ksi} + \frac{|P_f|}{2 \cdot A_g}\right) \cdot \sqrt{|f'_c|} \quad B := 0.11 \cdot \sqrt{|f'_c|} \cdot \frac{\text{kip}^{.5}}{\text{in}} \quad C := 0.047 \cdot \alpha \cdot \sqrt{|f'_c|} \cdot \frac{\text{kip}^{.5}}{\text{in}}$$

$$v_c := \begin{cases} 0 & \text{if } P_f \geq 0 \\ \min(A, B, C) & \text{otherwise} \end{cases} = 0.22 \cdot \text{ksi}$$

Concrete portion for shear capacity

$$V_c := 0.8 \cdot A_g \cdot v_c = 497.628 \cdot \text{kip}$$

Steel shear capacity

Nominal capacity of shear reinforcement

$$V_s := \frac{\pi}{2} \cdot f_{yh} \cdot a_{tr} \cdot \frac{D'}{s} = 404.47 \cdot \text{kip}$$

Factored shear capacity

$$V_{\text{Capacity}} := 0.9(V_c + V_s) = 811.889 \cdot \text{kip}$$

$$\frac{\min(V_{\text{RSA}_x}, V_{\text{P}_x})}{V_{\text{Capacity}}} = 0.814 < 1.0 \quad \mathbf{OK}$$

Overstrength plastic capacity for shear will also need to be designed in the transverse direction, but only the longitudinal direction was performed in this example. These forces would also be extended into the cross beam, superstructure, and foundations; though not shown herein.

Check the Minimum Lateral Capacity of Column:

AASHTO (2011) 8.7.1

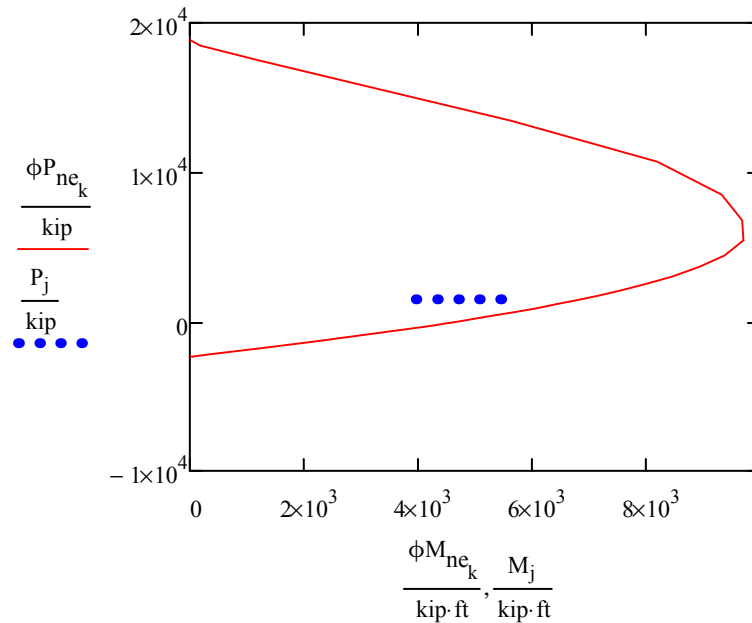
Transverse seismic (mass shared between column and abutment)

$$M_1 := 0.1 \cdot |P_f| \cdot (L + 8.5\text{ft}) \qquad P_1 := |P_f|$$

Longitudinal seismic (all mass on column-double curvature)

$$M_2 := 0.1 \cdot (2766\text{kip}) \cdot \frac{L}{2} = 3.872 \times 10^3 \cdot \text{kip} \cdot \text{ft} \qquad P_2 := |P_f|$$

Axial-moment (P-M) Interaction curve is generated for nominal expected material properties to check the minimum lateral strength of the section and to make sure that the demands are within the capacity curve.



Plot 2-9: Nominal Expected Axial-Moment (P-M) Capacity versus Demand for the Conventional Column

$$DCR_{\text{Trans}} := \frac{M_1}{\phi M_{\text{CAP}_1}} = 0.8 \qquad DCR_{\text{Long}} := \frac{M_2}{\phi M_{\text{CAP}_2}} = 0.566 \qquad < 1.0 \quad \text{OK}$$

This column design would meet the intent of the strength plus extreme code requirements for this bridge configuration. The design example output shown in Table 2-2 will be compared with each of the novel columns that follow to show similarities and differences to the conventional reinforced concrete column. In all cases, there were modifications required for material sizes, properties, and procedures for each of the novel column types.

Column Type	Conventional Column
Diameter (ft)	5.0
Longitudinal Reinforcement	22-#11
Spiral	#5@4"
Top Demand Drift Ratio (%)	1.18
Top Capacity Drift Ratio (%)	2.42
Bottom Demand Drift Ratio (%)	1.43
Bottom Capacity Drift Ratio (%)	2.42
Maximum Demand Drift Ratio (%)	2.73
Minimum Capacity Drift Ratio (%)	1.74
Shear Demand/Capacity Ratio	0.81
Bottom Residual Drift Ratio (%)	0.34
Top Residual Drift Ratio (%)	0.27
Overstrength Plastic Moment, M_{Po} (kip*ft)	8,455

Table 2-2: Summary Table for the Conventional Column (Longitudinal Direction Only)

Under the demand displacement for this structure, the plastic hinge rotation on the column section was around 0.011 rad. According to the intent of AASHTO (2011), this meets the life-safety criteria and has adequate displacement and ductility capacity. Detailing requirements need to be verified in the design process. The section analysis program shows that the design level rotation produces spalling of concrete cover (10 percent of the total cover around the section). The column uses about 60 percent of the rotational capacity. The section also has adequate shear capacity to exceed the demand from the displacement capacity and prevent a brittle failure. Not addressed in AASHTO (2011) is residual displacement that is expected when the bridge is in the vicinity of the earthquake fault. Conventional reinforced concrete bridge columns are susceptible to relatively large residual displacements that would render them unusable even when plastic hinge damage is moderate. Options for repairing plastic hinges in this column include, but are not limited to, removal and replacement of loose concrete cover, epoxy injection of cracks, and use of FRP wrap to improve concrete confinement. Feasibility of recovering residual displacements varies depending on the bridge and the residual drift ratio.



NCHRP
Conventional Column Design



33301 Ninth Avenue South, Suite 300 Federal Way,
Washington 98003-2600

This page is left blank intentionally.



NCHRP
SMA-ECC Column Design



33301 Ninth Avenue South, Suite 300 Federal
Way, Washington 98003-2600

F3 - SMA-ECC COLUMN DESIGN

F3-1: Strength Design of SMA-ECC Column

The following table shows the factored load for the Strength Limit State design of the SMA-ECC column. The moments in the transverse and longitudinal direction were magnified according to AASHTO (2014) Section 4.5.3.2.2b with simplifications identified previously.

Strength Factored Load	Units	Magnitude
Magnified Longitudinal Moment	kip-in	18,028
Magnified Transverse Moment	kip-in	45,620
Shear Longitudinal	kips	0
Shear Transverse	kips	178
Axial Load	kips	2,492

Table 3-1: Controlling Strength Load Combination Values

The 5- and 5.5-foot column diameters were initially considered in the design of the SMA-ECC column, but the required longitudinal reinforcement ratio to meet the Strength Limit load combination was above 2.5 percent, even with the 5.5-foot column. Therefore, the design was performed with a 6-foot-diameter column and a reinforcement ratio of 1.25 percent.

Axial-Moment Strength Check of Column

Section Properties:

The following design section properties were used for this example.

Diameter of column	$D := 6\text{ft}$	
Cover	$c := 2\text{in}$	
Column length	$L := 28\text{ft}$	
Longitudinal bar	$d_{\text{SMA}} := 1.41\text{in}$	
Area of longitudinal bar	$a_{\text{SMA}} := 1.56\text{in}^2$	Use 28 #11
Number of longitudinal bar	$n_{\text{SMA}} := 28$	
Diameter of transverse reinforcement	$d_{\text{tr}} := 0.875\text{in}$	
Area of transverse reinforcement	$a_{\text{tr}} := 0.6\text{in}^2$	Use #7 @ 3.5 in.
Transverse reinforcement spacing	$s := 3.5\text{in}$	
Type of transverse reinforcement	Type := "hoop"	

Concrete area $A_g := \frac{\pi}{4} \cdot D^2 = 4.072 \times 10^3 \cdot \text{in}^2$

Concrete core diameter $D' := [D - (2c)] - d_{tr} = 67.125 \cdot \text{in}$

Stress-strain curves are developed below for the SMA bar and both confined and unconfined ECC to use in a Section Analysis program in order to obtain the Axial-Moment (P-M) interaction and Moment-Curvature response.

Material Properties:

SMA Bar Nominal Properties: The nominal values were used here for strength design purpose. REPORT 12-101 3.1.3.1

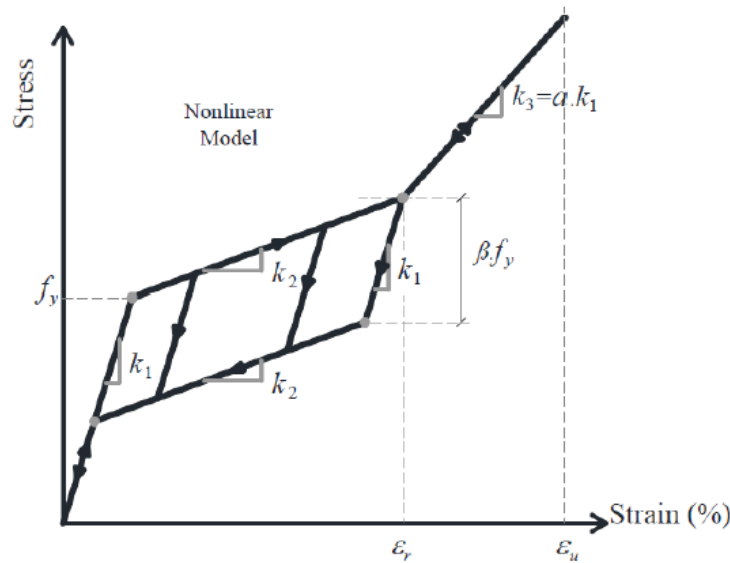


Image 3-1: SMA Stress-Strain Parameters

Austenite modulus $k_1 := 4500 \text{ksi}$

Post-yield stiffness $k_2 := 0 \text{ksi}$

Austenite yield strength $f_y := 45 \text{ksi}$

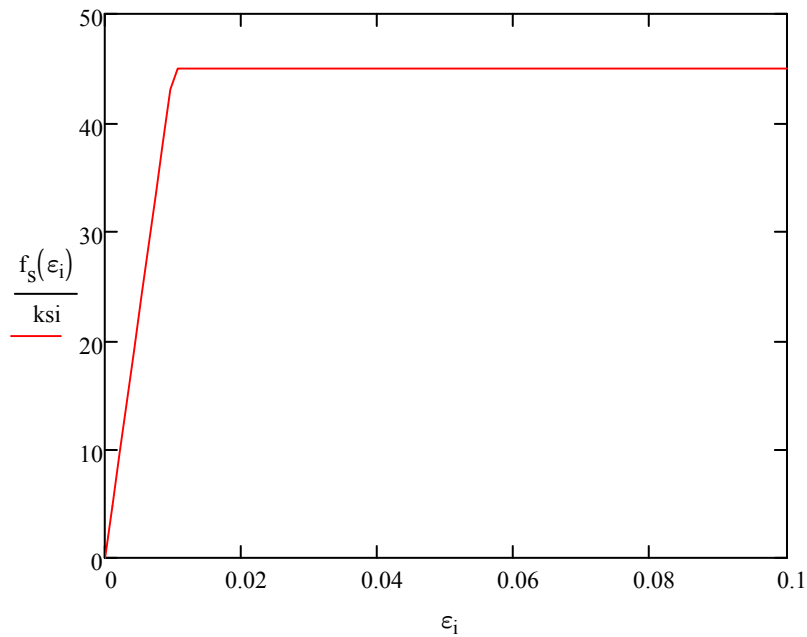
Recoverable superelastic strain $\epsilon_r := 0.06 \frac{\text{in}}{\text{in}}$

Secondary post-yield stiffness ratio $\alpha := 0$

Ultimate strain $\epsilon_u := 0.1 \frac{\text{in}}{\text{in}}$

Stress-Strain Calculations of SMA-ECC Bar:

$$f_s(\epsilon) := \begin{cases} k_1 \cdot \epsilon & \text{if } \epsilon \leq \frac{f_y}{k_1} \\ k_1 \cdot \frac{f_y}{k_1} + k_2 \cdot \left(\epsilon - \frac{f_y}{k_1} \right) & \text{if } \frac{f_y}{k_1} < \epsilon \leq \epsilon_r \\ k_1 \cdot \frac{f_y}{k_1} + k_2 \cdot \left(\epsilon_r - \frac{f_y}{k_1} \right) + \alpha \cdot k_1 \cdot (\epsilon - \epsilon_r) & \text{otherwise} \end{cases}$$



Plot 3-1: Nominal Stress-Strain Curve of SMA Bar

The third leg of the SMA stress-strain curve was not shown, as it was outside the limits of what was used in this example.

Stress-Strain Calculations of Unconfined ECC:

Report 12-101 3.1.3.2

- | | |
|----------------------------------|----------------------------------|
| Compression strength of concrete | $f_{ECC} := -4 \cdot \text{ksi}$ |
| Strain at peak compression | $\epsilon_{ECC0} := -0.002$ |
| Spalling strain | $\epsilon_{ECCsp} := -0.005$ |

Concrete module (modified secant
stiffness for seismic demand analysis)

$$E_{ECC} := \text{ksi} \cdot 1400 \cdot \left(\sqrt[3]{\left| \frac{f_{ECC}}{\text{ksi}} \right|} \right) = 2.222 \times 10^3 \cdot \text{ksi}$$

Report 12-101 3.1.3.2

Yield strength of longitudinal bar

$$f_{SMAy} := f_y = 45 \cdot \text{ksi}$$

Modulus of steel

$$E_{SMA} := k_1$$

Yield strength of stirrups

$$f_{yh} := 60 \text{ksi}$$

Strain at peak stress of stirrups

$$\varepsilon_{su} := 0.09$$

According to the Park model, the initial stiffness (r) of concrete was considered two times stiffer than the secant stiffness.

Secant concrete modulus

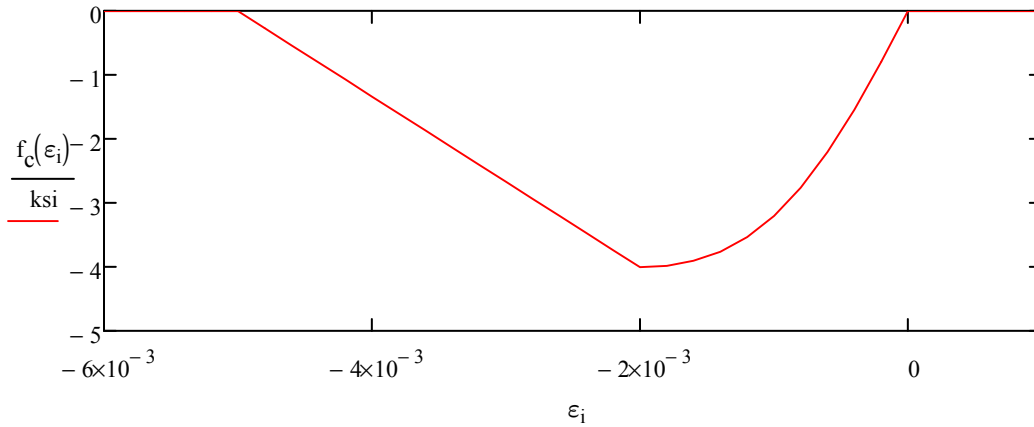
$$E_{sec} := \frac{f_{ECC}}{\varepsilon_{ECCo}} = 2 \times 10^3 \cdot \text{ksi}$$

Strain ratio

$$r := \frac{\frac{2 \cdot f_{ECC}}{\varepsilon_{ECCo}}}{\frac{2 \cdot f_{ECC}}{\varepsilon_{ECCo}} - E_{sec}} = 2$$

Stress-strain curve of unconfined concrete

$$f_c(\varepsilon) := \begin{cases} 0 & \text{if } \varepsilon \geq 0 \\ \frac{f_{ECC} \cdot \frac{\varepsilon}{\varepsilon_{ECCo}} \cdot r}{r - 1 + \left(\frac{\varepsilon}{\varepsilon_{ECCo}} \right)^r} & \text{if } \varepsilon_{ECCo} \leq \varepsilon < 0 \\ f_{ECC} \cdot \frac{\varepsilon - \varepsilon_{ECCsp}}{\varepsilon_{ECCo} - \varepsilon_{ECCsp}} & \text{if } \varepsilon_{ECCsp} \leq \varepsilon < \varepsilon_{ECCo} \\ 0 & \text{otherwise} \end{cases}$$



Plot 3-2: Nominal Unconfined ECC Stress-Strain Curve

Stress-Strain Calculations of Confined ECC:

		Report 12-101
Total area of longitudinal bar	$A_l := n_{SMA} \cdot a_{SMA}$	$A_l = 43.68 \cdot \text{in}^2$
Core area	$A_{cc} := \frac{\pi}{4} \cdot D'^2 - A_l$	$A_{cc} = 3.495 \times 10^3 \cdot \text{in}^2$
Ratio longitudinal bar/core	$\rho_{cc} := \frac{A_l}{A_{cc}}$	$\rho_{cc} = 1.25 \cdot \%$
Transverse reinforcement volumetric ratio	$\rho_s := \frac{4 \cdot a_{tr}}{s \cdot D'}$	
Effective lateral confining pressure	$f_l := \frac{2 \cdot a_{tr} \cdot f_{yh}}{s \cdot D'} = 0.306 \cdot \text{ksi}$	Report 12-101 3.1.3.2-2
Confined concrete strength		

$$f_{cc} := \begin{cases} f_{ECC} & \text{if } \frac{f_l}{|f_{ECC}|} \leq 0.035 \\ \left[f_{ECC} \cdot \left(-1.25 + 2 \cdot \sqrt{1 + 10.5 \cdot \frac{f_l}{|f_{ECC}|}} - 2 \cdot \frac{f_l}{|f_{ECC}|} \right) \right] & \text{otherwise} \end{cases}$$

= -5.134·ksi
Report 12-101 3.1.3.2-1

Residual strength (according to guideline)	$f_{ue} := 0.4 \cdot f_{cc} = -2.053 \cdot \text{ksi}$	Report 12-101 3.1.3.2-3
--	--	-------------------------

Strain at peak $\epsilon_{cc} := -0.0025 \cdot \left[1 + 2.7 \cdot \left(\frac{f_{cc}}{f_{ECC}} - 1 \right) \right] = -4.413 \times 10^{-3}$ Report 12-101 3.1.3.2-4

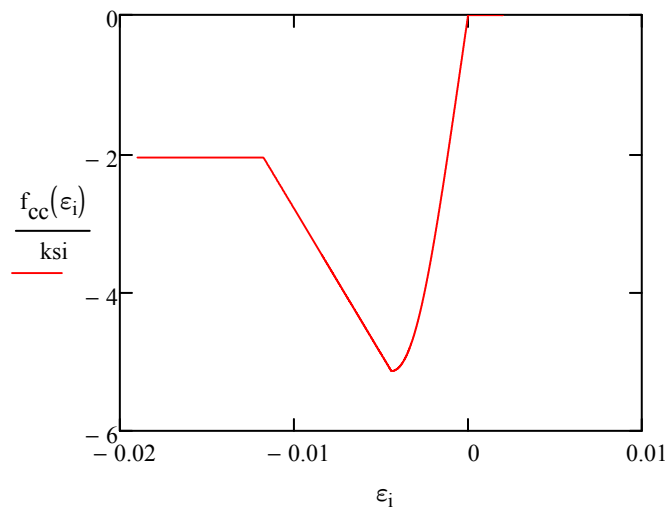
Ultimate strain $\epsilon_u := -0.004 + \frac{1.4 \cdot \rho_s \cdot f_{yh} \cdot \epsilon_{su}}{f_{cc}} = -0.019$ Report 12-101 3.1.3.2-5

Strain at descending branch $\epsilon_f := \epsilon_{cc} \cdot \left(9.5 - 0.8 \cdot \ln \left(1000 \cdot \frac{|f_{cc}|}{\text{ksi}} \right) \right) = -0.012$ Report 12-101 3.1.3.2-9

Stress-strain relationship $n := 0.2 \cdot \frac{|f_{cc}|}{\text{ksi}} + 2 = 3.027$ Report 12-101 3.1.3.2-8

$$f_{cc}(\epsilon) := \begin{cases} 0 & \text{if } \epsilon > 0 \\ \frac{f_{cc} \cdot n \cdot \frac{\epsilon}{\epsilon_{cc}}}{n - 1 + \left(\frac{\epsilon}{\epsilon_{cc}} \right)^n} & \text{if } \epsilon_{cc} < \epsilon \leq 0 \\ (f_{cc} - f_{ue}) \cdot \frac{\epsilon - \epsilon_f}{\epsilon_{cc} - \epsilon_f} + f_{ue} & \text{if } \epsilon_f \leq \epsilon < \epsilon_{cc} \\ f_{ue} & \text{if } \epsilon_u < \epsilon < \epsilon_f \\ 0 & \text{otherwise} \end{cases}$$

Report 12-101 3.1.3.2-6



Plot 3-3: Nominal Confined ECC Stress-Strain Curve

Axial Capacity:

$$z_1 := \min\left(1 - 0.02 \cdot \frac{|f_{ECC}|}{\text{ksi}}, 0.85\right) = 0.85$$

$$\phi P_{on} := 0.75 \cdot [z_1 \cdot |f_{ECC}| \cdot (A_g - A_l) + A_l \cdot f_y] = 1.175 \times 10^4 \cdot \text{kip}$$

$$\frac{P_{u_ST1}}{\phi P_{on}} = 0.212$$

Report 12-101 3.1.5.4

Report 12-101 3.1.5.4-2

Report 12-101 3.1.5.4-1

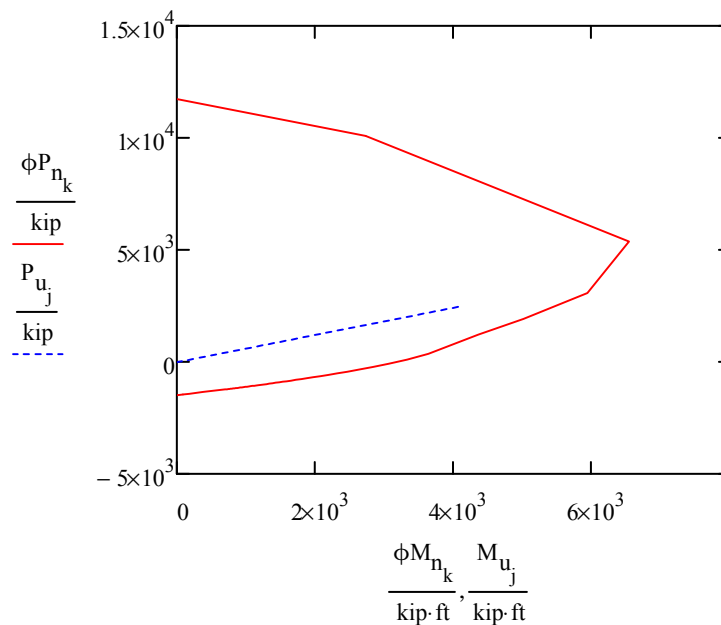
< 1.0 **OK**

Axial-Moment (P-M) Interaction Capacity:

The column section is modeled in a Section Analysis Program to generate the nominal P-M Interaction curve and associated strain in the steel and concrete. The steel strain values were used to identify the tension/compression-controlled region.

As the SMA bar has a large yielding strain in comparison to conventional steel, it was assumed the whole P-M curve has the lowest strength reduction factor of AASHTO (2014) of 0.75. This was just an assumption for the strength design of SMA-ECC columns. Additional research and investigation are required to more accurately apply reduction factors for the Strength Limit State design of this system.

The following figure shows the P-M capacity curve of the SMA-ECC column and compares it with the demand factored load. The demand was less than the capacity, and the section has sufficient strength for the factored loads.



Plot 3-4: Factored Axial-Moment (P-M) Capacity versus Demand for the SMA-ECC Column

Demand	$M_{u1} = 4.088 \times 10^3 \cdot \text{kip} \cdot \text{ft}$	$P_{u1} = 2.492 \times 10^3 \cdot \text{kip}$
Capacity	$\phi M_{CAP} = 5.449 \times 10^3 \cdot \text{kip} \cdot \text{ft}$	
D/C Ratio	$DCR := \frac{M_{u1}}{\phi M_{CAP}} = 0.75$	< 1.0 OK

F3-2: Seismic Design of SMA-ECC Novel Column

Material Properties:

The following design material properties were used for the seismic portion of the design example.

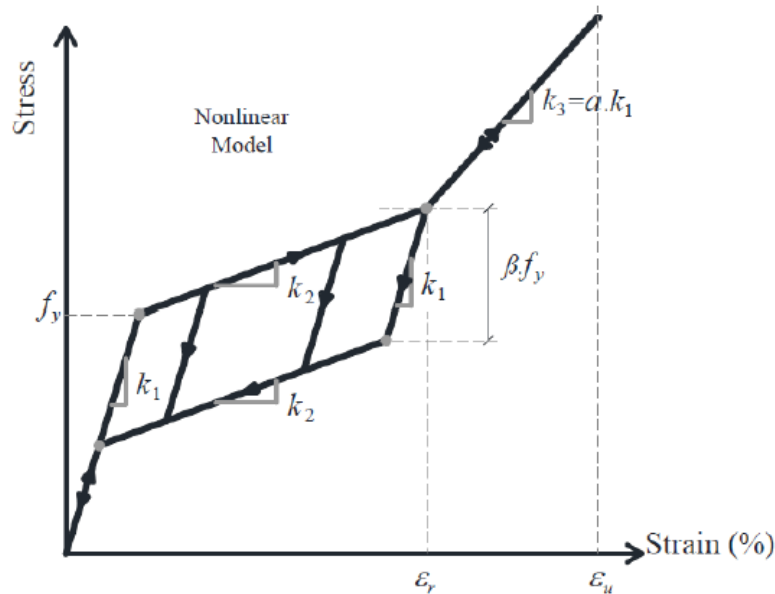
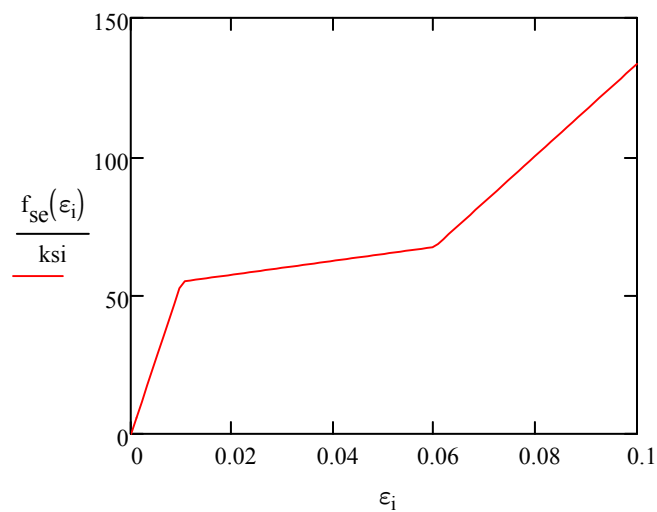


Image 3-2: SMA Stress-Strain Parameters

Austenite modulus	$k_1 := 5500 \text{ksi}$
Post-yield stiffness	$k_2 := 250 \text{ksi}$
Austenite expected yield strength	$f_{ye} := 55 \text{ksi}$
Recoverable superelastic strain	$\epsilon_r := 0.06 \frac{\text{in}}{\text{in}}$
Secondary post-yield stiffness ratio	$\alpha := 0.3$
Ultimate strain	$\epsilon_u := 0.1 \frac{\text{in}}{\text{in}}$

Stress-strain curve of SMA

$$f_{se}(\epsilon) := \begin{cases} k_1 \cdot \epsilon & \text{if } \epsilon \leq \frac{f_{ye}}{k_1} \\ k_1 \cdot \frac{f_{ye}}{k_1} + k_2 \cdot \left(\epsilon - \frac{f_{ye}}{k_1} \right) & \text{if } \frac{f_{ye}}{k_1} < \epsilon \leq \epsilon_r \\ k_1 \cdot \frac{f_{ye}}{k_1} + k_2 \cdot \left(\epsilon_r - \frac{f_{ye}}{k_1} \right) + \alpha \cdot k_1 \cdot (\epsilon - \epsilon_r) & \text{otherwise} \end{cases}$$



Plot 3-5: Expected Stress-Strain Curve of SMA Material

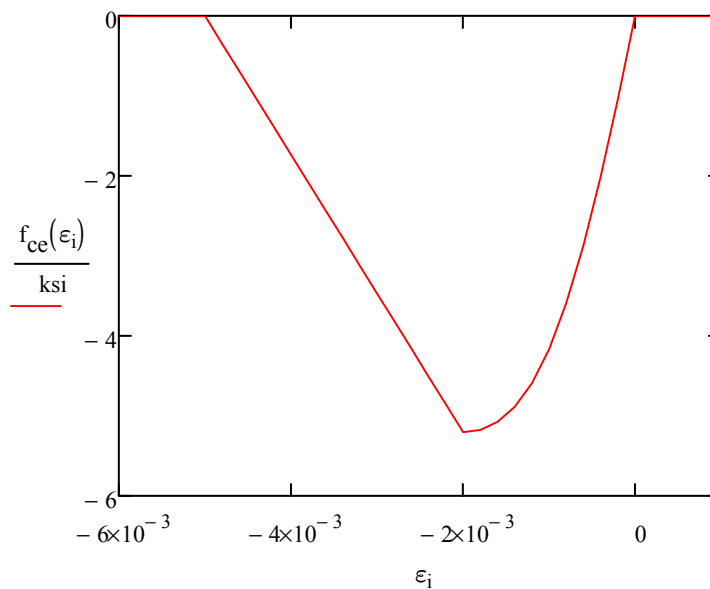
Expected Unconfined ECC:

Report 12-101

Expected compression strength of concrete	$f_{ECCe} := -4 \cdot \text{ksi} \cdot 1.3 = -5.2 \cdot \text{ksi}$
Strain at peak compression	$\epsilon_{ECCo} := -0.002$
Spalling strain	$\epsilon_{ECCsp} := -0.005$
Expected concrete module	$E_{ECCe} := \text{ksi} \cdot 1400 \cdot \left(\sqrt[3]{\frac{f_{ECCe}}{\text{ksi}}} \right) = 2.425 \times 10^3 \cdot \text{ksi}$
	Report 12-101 Fig. 3.1.3.2-1
Expected yield strength of longitudinal bar	$f_{SMAye} := 55 \text{ksi}$
Modulus of steel	$E_{SMA} := k_1$
Nominal yield strength of transverse reinforcement	$f_{yh} := 60 \text{ksi}$
Strain at peak stress of transverse reinforcement	$\epsilon_{su} := 0.09$
Overstrength factor for SMA bar	$\lambda := 1.2$
Secant concrete modulus	$E_{sec.e} := \frac{f_{ECCe}}{\epsilon_{ECCo}} = 2.6 \times 10^3 \cdot \text{ksi}$
Stress ratio	$r := \frac{\frac{2 \cdot f_{ECCe}}{\epsilon_{ECCo}}}{\frac{2 \cdot f_{ECCe}}{\epsilon_{ECCo}} - E_{sec.e}} = 2$

Expected stress-strain curve of unconfined concrete

$$f_{cc}(\epsilon) := \begin{cases} 0 & \text{if } \epsilon \geq 0 \\ \frac{f_{ECCe} \cdot \frac{\epsilon}{\epsilon_{ECCo}} \cdot r}{r - 1 + \left(\frac{\epsilon}{\epsilon_{ECCo}}\right)^r} & \text{if } \epsilon_{ECCo} \leq \epsilon < 0 \\ \frac{f_{ECCe} \cdot \frac{\epsilon - \epsilon_{ECCsp}}{\epsilon_{ECCo} - \epsilon_{ECCsp}}}{1} & \text{if } \epsilon_{ECCsp} \leq \epsilon < \epsilon_{ECCo} \\ 0 & \text{otherwise} \end{cases}$$



Plot 3-6: Expected Unconfined ECC Stress-Strain Curve

Expected Confined ECC:

Report 12-101

Total area of longitudinal bar

$$A_l := n_{SMA} \cdot a_{SMA}$$

$$A_l = 43.68 \cdot \text{in}^2$$

Core area

$$A_{cc} := \frac{\pi}{4} \cdot D^2 - A_l$$

$$A_{cc} = 3.495 \times 10^3 \cdot \text{in}^2$$

Ratio longitudinal bar/core

$$\rho_{cc} := \frac{A_l}{A_{cc}}$$

$$\rho_{cc} = 1.25\%$$

Transverse reinforcement volumetric ratio $\rho_s := \frac{4 \cdot a_{tr}}{s \cdot D'} \quad \rho_s = 1.022\%$

Effective lateral confining pressure $f_l := \frac{2 \cdot a_{tr} \cdot f_{yh}}{s \cdot D'} = 0.306 \text{ ksi} \quad \text{Report 12-101 3.1.3.2-2}$

Confined concrete strength

$$f_{cce} := \begin{cases} f_{ECCe} & \text{if } \frac{f_l}{|f_{ECCe}|} \leq 0.035 \\ \left[f_{ECCe} \cdot \left(-1.25 + 2 \cdot \sqrt{1 + 10.5 \cdot \frac{f_l}{|f_{ECCe}|}} - 2 \cdot \frac{f_l}{|f_{ECCe}|} \right) \right] & \text{otherwise} \end{cases} = -6.119 \text{ ksi}$$

Residual strength $f_{ue} := 0.4 \cdot f_{cce} = -2.448 \text{ ksi} \quad \text{Report 12-101 3.1.3.2-3}$

Strain at peak $\epsilon_{cc} := -0.0025 \cdot \left[1 + 2.7 \cdot \left(\frac{f_{cce}}{f_{ECCe}} - 1 \right) \right] = -3.693 \times 10^{-3} \quad \text{Report 12-101 3.1.3.2-4}$

Ultimate strain $\epsilon_u := -0.004 + \frac{1.4 \cdot \rho_s \cdot f_{yh} \cdot \epsilon_{su}}{f_{cce}} = -0.0166 \quad \text{Report 12-101 3.1.3.2-5}$

Expected ultimate strain of confined ECC was less than nominal ultimate strain calculated in the strength design section (previous section) because the expected strength of concrete was higher than nominal strength.

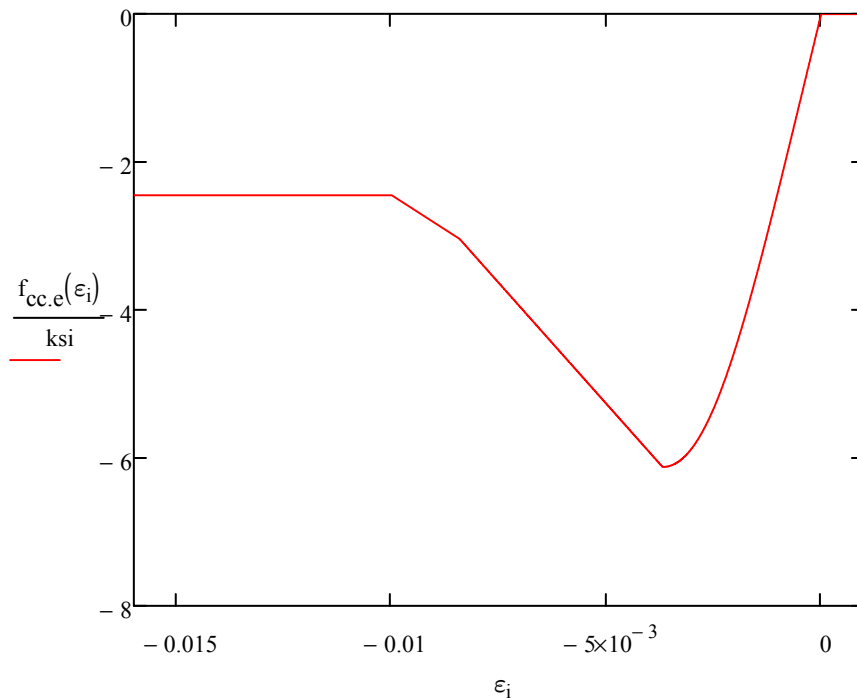
Strain at descending branch $\epsilon_f := \epsilon_{cc} \cdot \left(9.5 - 0.8 \cdot \ln \left(1000 \cdot \frac{|f_{cce}|}{\text{ksi}} \right) \right) = -9.324 \times 10^{-3} \quad \text{Report 12-101 3.1.3.2-9}$

Expected stress-strain relationship for confined ECC

$$n := 0.2 \cdot \frac{|f_{cce}|}{\text{ksi}} + 2 = 3.224$$

Report 12-101 3.1.3.2-8

$$f_{cc,e}(\epsilon) := \begin{cases} 0 & \text{if } \epsilon > 0 \\ \frac{f_{cce} \cdot n \cdot \frac{\epsilon}{\epsilon_{cc}}}{n - 1 + \left(\frac{\epsilon}{\epsilon_{cc}}\right)^n} & \text{if } \epsilon_{cc} < \epsilon \leq 0 \\ \left(f_{cce} - f_{ue}\right) \cdot \frac{\epsilon - \epsilon_f}{\epsilon_{cc} - \epsilon_f} + f_{ue} & \text{if } \epsilon_f \leq \epsilon < \epsilon_{cc} \\ f_{ue} & \text{if } \epsilon_u \leq \epsilon < \epsilon_f \\ 0 & \text{otherwise} \end{cases}$$



Plot 3-7: Expected Confined ECC Stress-Strain Curve

Plastic Hinge Length:

AASHTO (2011) 4.11.6

Longitudinal-double curvature

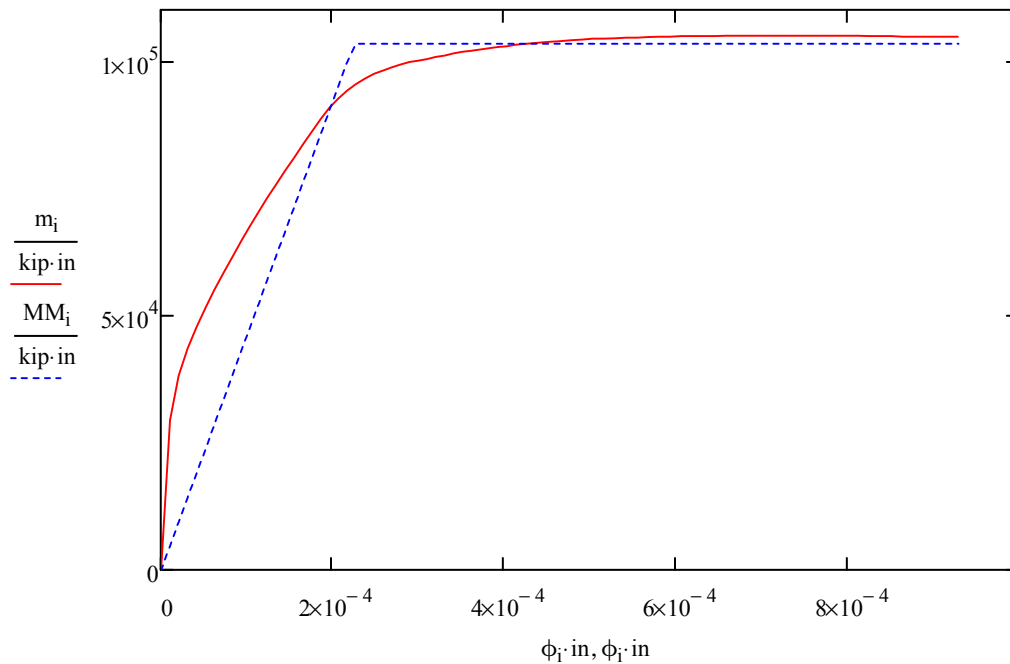
$$L_{P_X} := \max\left(0.08 \cdot \frac{L}{2} + 0.15 \cdot \frac{f_{ye}}{\text{ksi}} \cdot d_{SMA}, 0.3 \cdot \frac{f_{ye}}{\text{ksi}} \cdot d_{SMA}\right) = 25.073 \cdot \text{in}$$

Moment-Curvature Responses of the Section:

Moment-curvature response of the column section was generated using a Section Analysis software and applying the expected material properties and dead load axial loads on the column.

Axial load $P_f := -1565 \text{kip}$

The following graph shows the moment-curvature response generated during the section analysis run and the idealized bilinear relationship to be used for the pushover analysis. The idealized curve is obtained according to AASHTO (2011) Section 8.5. The elastic portion of the curve, or initial stiffness, begins from the origin and passed through the first yield point of the reinforcing bar until it matches with the horizontal idealized line. The horizontal, or idealized moment capacity, is obtained by equating the upper and lower areas between the actual and the idealized curve beyond the first yielding of reinforcing bar. The second flat line should be iteratively shifted up and down to get the same area between bilinear and actual relationship after the first yield of reinforcement.



Plot 3-8: SMA-ECC Column Moment-Curvature Response and Idealized Bilinear Curve

Idealized Bilinear Curve Parameters:

Ultimate moment from moment-curvature data points

$$M_u = 1.048 \times 10^5 \cdot \text{kip} \cdot \text{in}$$

Capacity moment

$$M_p = 1.034 \times 10^5 \cdot \text{kip} \cdot \text{in}$$

Effective yield curvature

$$\phi_{yi} = 2.246 \times 10^{-4} \cdot \frac{1}{\text{in}}$$

Ultimate curvature

$$\phi_u = 9.286 \times 10^{-4} \cdot \frac{1}{\text{in}}$$

Effective initial stiffness

$$EI_{\text{eff}} = 3.197 \times 10^6 \cdot \text{kip} \cdot \text{ft}^2$$

Cracking stiffness reduction (this ratio will be used for demand analysis)

$$\alpha_{\text{crack}} := \frac{EI_{\text{eff}}}{E_{\text{ECCe}} \cdot \frac{\pi}{64} \cdot D^4} = 0.144$$

Cracking stiffness from Report 12-101 3.1.4.2

Axial load ratio

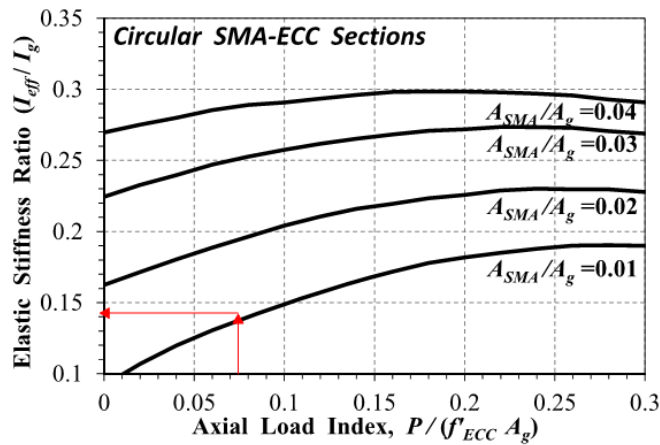
$$\frac{P_f}{f_{\text{ECCe}} \cdot A_g} = 0.074$$

Longitudinal bar ratio

$$\frac{n_{\text{SMA}} \cdot a_{\text{SMA}}}{A_g} = 0.011$$

$\alpha_{\text{crack_Guide_line}} := 0.142$

Very close to value obtained from moment-curvature analysis



(a) Circular Sections

Image 3-3: Effective Moment of Inertia for SMA-ECC Columns

Demand Analysis:

Site response spectrum is defined in Section F1-2. Because of the reduced hysteresis damping of SMA-ECC column in comparison to the conventional column, as is suggested in Report 12-101 Section 3.1.4.4, the 5 percent damping response spectrum is increased by 20 percent in the demand analysis to compensate for a lower damping ratio.

Result of Demand Analysis:

The bridge was modeled using a Finite Element Program. The following figure shows the bridge model for demand and pushover analysis. For this design example, the seismic behavior of the bridge was investigated in longitudinal direction only. As the column is integrated with the superstructure, the column was designed for dual-hinge behavior with a hinge at both the base and the top of column. The abutments were unrestrained (roller bearing) in the longitudinal direction, parallel to the roadway. The transverse direction is single hinge at the base; however, the transverse design of the bridge is not investigated in this study.

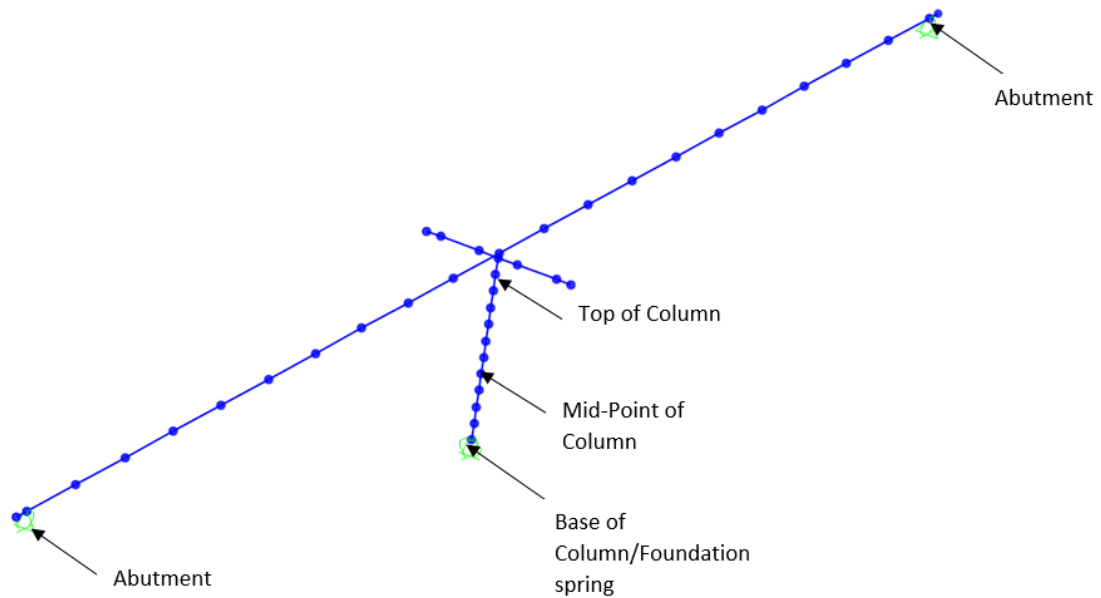
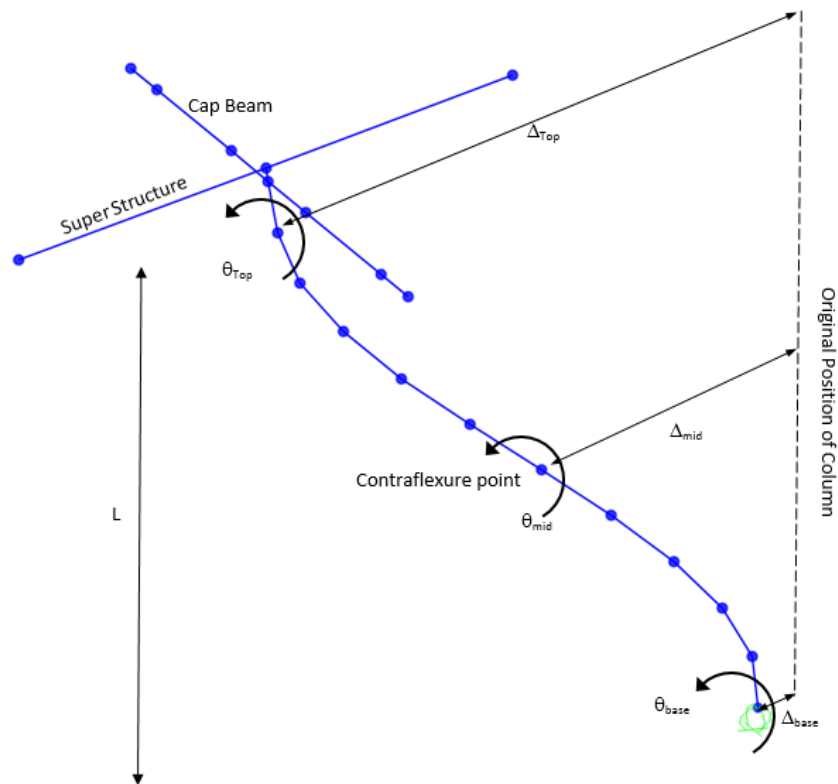


Image 3-4: Finite Element Bridge Model

The natural period of the bridge in longitudinal direction is 1.43 s. Elongation of the period was obvious due to softer behavior of SMA-ECC column compared to conventional column.

Demand Displacement from Response Spectrum Analysis in Longitudinal Direction:

The performance and ductility of each hinge were investigated separately. It was assumed that the moment capacity and the geometry of the column at both hinges are essentially identical; therefore, the contraflexure point for this column in the longitudinal direction was at the midheight of the column, and the performance of each hinge was evaluated for the lower and upper lengths of the column. The following figure shows the parameters needed to calculate the displacements of the column at each end. These displacements will be needed to find the performance and ductility of each hinge.



$$\Delta_{Bot_hinge} = \Delta_{mid} - \Delta_{base} - \theta_{base} \times L/2$$

$$\Delta_{Top_hinge} = \Delta_{mid} - \Delta_{Top} - \theta_{Top} \times L/2$$

Image 3-5: Bridge Model Column Curvature

Demand deflections in top and bottom hinges

$$\Delta_{\text{Demand}_{\text{BOT}}} := \left| \left| \text{Demand}_{\text{SAP}_{4,4}} \cdot \text{in} - \text{Demand}_{\text{SAP}_{3,4}} \cdot \text{in} \right| - \text{Demand}_{\text{SAP}_{3,8}} \cdot \frac{L}{2} \right| = 4.406 \cdot \text{in}$$

$$\Delta_{\text{Demand}_{\text{TOP}}} := \left| \left| \text{Demand}_{\text{SAP}_{4,4}} \cdot \text{in} - \text{Demand}_{\text{SAP}_{5,4}} \cdot \text{in} \right| - \text{Demand}_{\text{SAP}_{5,8}} \cdot \frac{L}{2} \right| = 4.032 \cdot \text{in}$$

Pushover Analysis:

The two hinges at the top and bottom of the column were defined according to the idealized bilinear curve presented above. The bridge was pushed longitudinally to failure and the following results are obtained.

Effect of P-Δ:

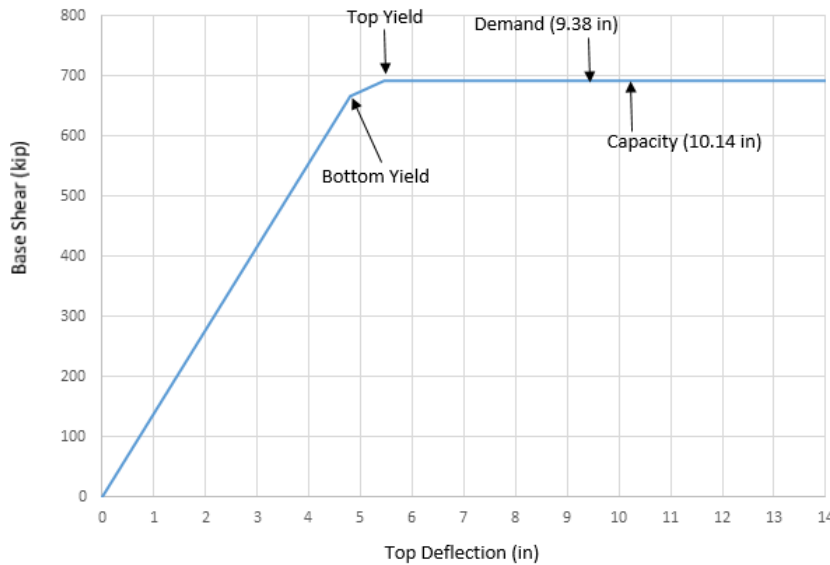
$$\frac{P_f}{f_{\text{ECCe}} \cdot A_g} = 0.074$$

< 0.15 **OK**

Report 12-101 3.1.6.5

As the ratio is less than 0.15, the effect of P-delta is neglected.

The following figure shows the Force-Top Displacement Response of the column in the longitudinal direction.



Plot 3-9: Force-Top Displacement Response of the SMA-ECC Column

Yield Displacement of Column:

BOT hinge yield deflection $\Delta_{Y_{BOT}} = 2.295 \cdot \text{in}$

TOP hinge yield deflection $\Delta_{Y_{TOP}} = 2.322 \cdot \text{in}$

Yield displacement obtained from AASHTO (2011) using moment-curvature analysis

$$\Delta_{Y_Code} := \frac{\phi_{yi} \cdot (0.5L)^2}{3} = 2.113 \cdot \text{in} \quad \text{Close to FEA results above}$$

Capacity displacement obtained from Finite Element Analysis (FEA) program

$$\Delta_{C_{BOT}} = 5.035 \cdot \text{in}$$

$$\Delta_{C_{TOP}} = 5.067 \cdot \text{in}$$

Capacity displacement obtained from AASHTO (2011), top and bottom, as the point of counterflexure was in the middle of the column.

$$\Delta_{C_{BOT_Code}} := \frac{\phi_{yi} \cdot (0.5L)^2}{3} + (\phi_u - \phi_{yi}) \cdot L_{P_x} \cdot \left(\frac{L}{2} - \frac{L_{P_x}}{2} \right) = 4.857 \cdot \text{in} \quad \text{Close to FEA results above}$$

$$\Delta_{C_{TOP_Code}} := \frac{\phi_{yi} \cdot (0.5L)^2}{3} + (\phi_u - \phi_{yi}) \cdot L_{P_x} \cdot \left(\frac{L}{2} - \frac{L_{P_x}}{2} \right) = 4.857 \cdot \text{in}$$

Check demand/capacity ratio

AASHTO (2011) 4.8

Capacity drift ratio $\delta_{C_{BOT}} := \frac{\Delta_{C_{BOT}}}{\frac{L}{2}} = 2.997\%.$

Capacity drift ratio $\delta_{C_{TOP}} := \frac{\Delta_{C_{TOP}}}{\frac{L}{2}} = 3.016\%.$

Demand drift ratio $\delta_{D_{BOT}} := \frac{\Delta_{Demand_{BOT}}}{\frac{L}{2}} = 2.623\%$

Demand drift ratio $\delta_{D_{TOP}} := \frac{\Delta_{Demand_{TOP}}}{\frac{L}{2}} = 2.4\%$

$$\frac{\delta_{D_{BOT}}}{\delta_{C_{BOT}}} = 0.875 < 1.0 \text{ OK}$$

$$\frac{\delta_{D_{TOP}}}{\delta_{C_{TOP}}} = 0.796 < 1.0 \text{ OK}$$

Minimum/Maximum Drift Requirements:

Report 12-101 3.1.4.6

Aspect ratio of column $(A_r) := \frac{L}{2 \cdot D} = 2.333$

Maximum Drift Demand Ratio:

Report 12-101 3.1.4.7

$$\mu_{D_{max}} := 5$$

AASHTO (2011) 4.9

$$\delta_{D_{max}} := 1.2 \cdot \left[\left[0.26 \cdot (A_r)^{0.81} \cdot \mu_{D_{max}} - 0.18 \cdot (A_r)^{0.57} \right] \% \right] = 2.749\%$$

Report 12-101 3.1.4.6-2

$$\frac{\delta_{D_{TOP}}}{\delta_{D_{max}}} = 0.873 < 1.0 \text{ OK}$$

$$\frac{\delta_{D_{BOT}}}{\delta_{D_{max}}} = 0.954 < 1.0 \text{ OK}$$

Minimum Drift Capacity Ratio:

Report 12-101 3.1.5.2

$$\mu_{C_min} := 3$$

Report 12-101 Table 3.1.5.2.1-1

$$\delta_{C_min} := \left[\left[0.26 \cdot (A_T)^{0.81} \cdot \mu_{C_min} - 0.18 \cdot (A_T)^{0.57} \right] \% \right] = 1.258 \%$$

$$\frac{\delta_{C_TOP}}{\delta_{C_min}} = 2.398 \quad > 1.0 \quad \text{OK}$$

$$\frac{\delta_{C_BOT}}{\delta_{C_min}} = 2.383 \quad > 1.0 \quad \text{OK}$$

The drift capacity ratio also needs to be modified according to Report 12-101 Section 3.1.6.3 if mechanical bar couplers are used. However, it was not considered for this design example.

Demand Ductility Calculations:

Report 12-101 3.1.4.6

Top demand ductility

$$\mu_{D_TOP} := \frac{\frac{\delta_{D_TOP}}{\%} + 0.18 \cdot (A_T)^{0.57}}{0.26 \cdot (A_T)^{0.81}} = 5.211$$

Bottom demand ductility

$$\mu_{D_BOT} := \frac{\frac{\delta_{D_BOT}}{\%} + 0.18 \cdot (A_T)^{0.57}}{0.26 \cdot (A_T)^{0.81}} = 5.643$$

Residual Drift Ratio:

Report 12-101 3.1.4.9

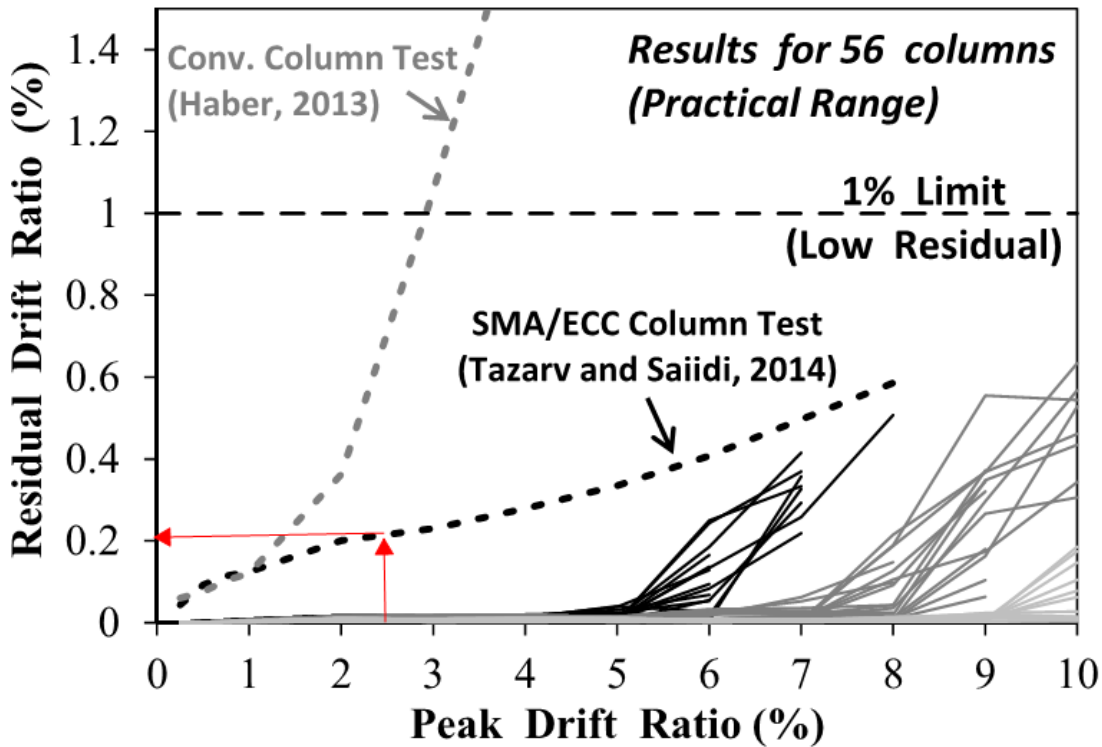


Image 3-6: Residual Drift Ratio for SMA-ECC

Bottom residual drift ratio from above Graph $\delta_{r_BOT} := 0.2\%$

Bottom residual drift ratio from above Graph $\delta_{r_TOP} := 0.2\%$

Developed Seismic Shear Demand:

Report 12-101 3.1.4.8

Plastic shear developed in column

If M_u (failure moment) is less than $1.2M_p$, then $1.2M_p$ is considered for design according to Report 12-101 Section 3.1.4.8.2. In the event that the failure moment occurs along the third leg of the expected stress-strain of the SMA bar material, then an overstrength factor of 1.4 is more appropriate. This needs to be verified in the analysis process as follows.

$$\frac{M_u}{\lambda \cdot M_P} = 0.845$$

Overstrength plastic moment

$$M_{P0} := \lambda \cdot M_P = 1.034 \times 10^4 \cdot \text{kip} \cdot \text{ft}$$

X direction

$$V_{P_x} := \frac{\lambda \cdot M_P}{\left(\frac{L - L_{P_x}}{2}\right)} = 798.041 \cdot \text{kip}$$

Shear demand from response spectrum analysis

X direction

$$V_{RSA_x} := 1233 \text{kip}$$

Shear Capacity Check:

Report 12-101 3.1.5.3

Cross section area

$$A_g := \frac{\pi}{4} \cdot D^2 = 4.072 \times 10^3 \cdot \text{in}^2$$

Ductility factor for SDC D

$$\mu_D := \max(\mu_{D_BOT}, \mu_{D_TOP}) = 5.643 \quad \text{AASHTO (2011) 4.3}$$

Transverse reinforcement ratio at bottom

$$\rho_s := \frac{4 \cdot a_{tr}}{D \cdot s} = 0.01$$

Ratio of longitudinal reinforcement

$$\rho_t := \frac{n \cdot a_{SMA}}{A_g} = 1.235 \times 10^{-3}$$

Maximum allowable nominal stress in bar

$$f_s := \min(\rho_s \cdot f_y, 0.35 \text{ksi}) = 0.35 \cdot \text{ksi}$$

Concrete shear stress adjustment

$$\alpha := \max\left(\frac{f_s}{0.15 \text{ksi}} + 3.67 - \mu_D, 0\right) = 0.36$$

Concrete shear capacity

$$A := .032 \frac{\text{in}}{\sqrt{\text{kip}}} \alpha \cdot \left(1.0 \text{ksi} + \frac{|P_f|}{2 \cdot A_g}\right) \cdot \sqrt{|f_{ECC}|}$$

$$B := 0.11 \cdot \sqrt{|f_{ECC}|} \cdot \frac{\text{kip}^5}{\text{in}}$$

$$C := 0.047 \cdot \alpha \cdot \sqrt{|f_{ECC}|} \cdot \frac{\text{kip}^5}{\text{in}}$$

$$v_c := \begin{cases} 0 & \text{if } P_f \geq 0 \\ \min(A, B, C) & \text{otherwise} \end{cases} = 0.027 \cdot \text{ksi}$$

Concrete portion for shear capacity

$$V_{c1} := 0.8 \cdot A_g \cdot v_c = 89.432 \cdot \text{kip}$$

ECC and fiber shear capacity

Report 12-101 3.1.5.3

$$f_{vcd} := \min \left(0.039 \cdot \text{ksi} \cdot \sqrt[3]{\frac{f_{ECC}}{\text{ksi}}}, 0.07 \text{ksi} \right) = 0.062 \cdot \text{ksi}$$

Distance from extreme compression fiber to the centroid of extreme longitudinal tension bar-from section analysis

$$d := 56.67 \text{in}$$

$$\beta_d := \min \left(2.5 \cdot \sqrt[4]{\frac{\text{in}}{d}}, 1.5 \right) = 0.911$$

$$b_w := 0.55 \cdot D$$

$$\rho_w := \frac{(n \cdot a_{SMA})}{A_g} = 1.235 \times 10^{-3}$$

$$\beta_p := \min \left(\sqrt[3]{100 \cdot \rho_w}, 1.5 \right) = 0.498$$

Necessary moment to cancel the compression stress due to axial $\sigma = P/A = M \cdot y / I_g$. This was determined by applying a moment in the opposite direction until only the axial load is present.

$$M_O := \frac{4 \cdot |P_f| \cdot D}{32}$$

$$\beta_n := 1 + 2 \cdot \frac{M_O}{\lambda \cdot M_P} = 1.227$$

$$\gamma_b := 1.3$$

Report 12-101 3.1.5.3.10

Tensile strength of ECC

$$V_{cd} := \beta_d \cdot \beta_p \cdot \beta_n \cdot f_{vcd} \cdot \frac{b_w \cdot d}{\gamma_b} = 59.507 \cdot \text{kip}$$

$$f_{vd} := 0.29 \text{ksi}$$

Distance between centroid compression and tension load-from section analysis

$$z := 4.34 \text{ft}$$

Assumed crack angle

$$\beta_u := 45 \text{deg}$$

$$V_{fd} := \frac{f_{vd} \cdot b_w \cdot z}{\gamma_b \cdot \tan(\beta_u)} = 460.067 \cdot \text{kip}$$

Report 12-101 3.1.5.3.12

$$V_{c2} := V_{cd} + V_{fd} = 519.574 \cdot \text{kip}$$

Concrete portion capacity

$$V_c := \min(V_{c1}, V_{c2}) = 89.432 \cdot \text{kip}$$

Steel shear capacity

Nominal capacity of shear reinforcement

$$V_s := \frac{\pi}{2} \cdot f_y \cdot a_{tr} \cdot \frac{D'}{s} = 813.392 \cdot \text{kip} \quad \text{Report 12-101 3.1.5.3.13}$$

Total shear capacity of section

$$V_{\text{Capacity}} := 0.9(V_c + V_s) = 812.542 \cdot \text{kip}$$

$$\frac{\min(V_{\text{RSA}_x}, V_{\text{P}_x})}{V_{\text{Capacity}}} = 0.982 < 1.0 \quad \text{OK}$$

The nominal shear capacity was at the limit permitted in the report. There was a built in factor of safety using the nominal properties for the shear calculations. A designer may want additional capacity and this can be accomplished by reducing the shear reinforcement spacing or increasing the shear reinforcement bar diameter. Note though, that #7 butt-welded hoops were used at 3.5-inch spacing on center. Adjustment to the confinement reinforcing steel will effect the Push-Over analysis and as defined above, the Demand Drift Ratio is already close to the maximum limit.

Overstrength plastic capacity for shear will also need to be designed in the transverse direction, but only the longitudinal direction is performed in this example. These forces would also be extended into the cross beam, superstructure, and foundations; though not shown herein.

Check the Minimum Lateral Capacity of Column:

AASHTO (2011) 8.7.1

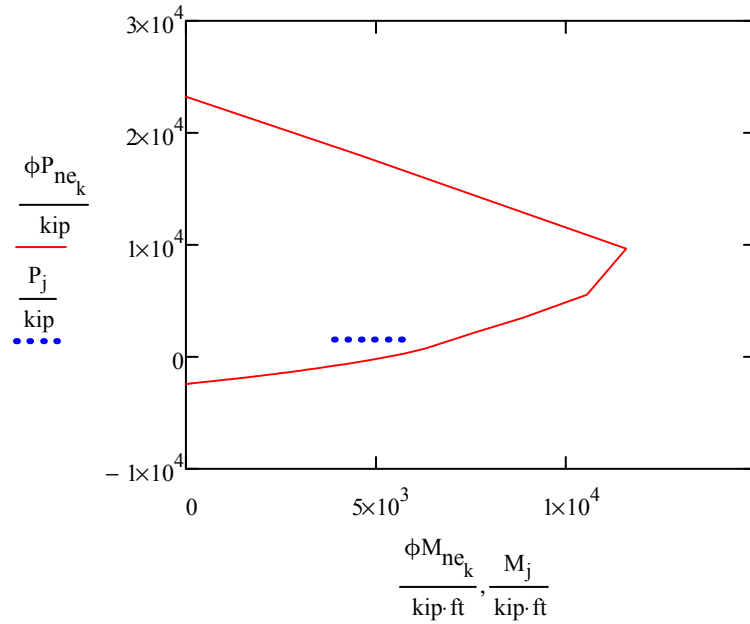
Transverse seismic (mass shared between column and abutment)

$$M_1 := 0.1 \cdot |P_f| \cdot (L + 8.5\text{ft}) \qquad P_1 := |P_f|$$

Longitudinal seismic (all mass on column-double curvature)

$$M_2 := 0.1 \cdot (2766\text{kip}) \cdot \frac{L}{2} = 3.872 \times 10^3 \cdot \text{kip} \cdot \text{ft} \qquad P_2 := |P_f|$$

Axial-moment (P-M) Interaction curve was generated for the nominal expected material to check the minimum lateral strength of section and to make sure that the demands were within the capacity curve.



Plot 3-10: Nominal Expected Axial-Moment (P-M) Capacity versus Demand

$$DCR_{Trans} := \frac{M_1}{\phi M_{CAP_1}} = 0.813 \qquad DCR_{Long} := \frac{M_2}{\phi M_{CAP_2}} = 0.551 < 1.0 \quad \text{OK}$$

Column Type	SMA-ECC Column	Conventional Column
Diameter (ft)	6.0	5.0
Longitudinal Reinforcement	28-#11	22-#11
Transverse Reinforcement	#7@3.5" (Hoop)	#5@4" (Spiral)
Top Demand Drift Ratio (%)	2.40	1.18
Top Capacity Drift Ratio (%)	3.02	2.42
Bottom Demand Drift Ratio (%)	2.62	1.43
Bottom Capacity Drift Ratio (%)	3.00	2.42
Maximum Demand Drift Ratio (%)	2.75	2.73
Minimum Capacity Drift Ratio (%)	1.26	1.74
Shear Demand/Capacity Ratio	0.98	0.81
Bottom Residual Drift Ratio (%)	0.2	0.34
Top Residual Drift Ratio (%)	0.2	0.27
Overstrength Plastic Moment, M_{Po} (kip*ft)	10,339	8,455

Table 3-2: Summary Table for the SMA-ECC Column (Longitudinal Direction Only)

Under the demand displacement of this structure, the plastic hinge rotation on the section was around 0.015 rad. The intent of these novel column procedures was to ensure life-safety criteria will be met and either keep the structure in service after the event or restored to service quickly because of the high damage tolerance of ECC. The Section Analysis Program shows that at this level of rotation there was spalling of ECC cover (above 25 percent of the total cover around the section), the column uses about 87 percent of the rotation capacity. Research on more than a dozen large-scale columns models has shown that the actual spalling of ECC takes place under drift ratios that substantially exceed the demand drift ratio of 2.62 percent. Because SMA bars are superelastic, they do not exhibit inelastic buckling, which can be the cause of major spalling of concrete in conventional reinforced concrete bridge columns. The section analysis also indicates that, although the shear demand was less than the capacity, almost 100 percent of shear capacity was used, and the gross section does not contribute to the shear resistance. The analytical methods for this material conservatively indicate additional damage will have occurred. Research has shown that at this level of drift demand, no repair of ECC will be necessary although some micocracks might be visible. Because crack widths were very small, epoxy injection of these cracks will not be feasible nor necessary.



NCHRP
SMA-FRP Confined Column



33301 Ninth Avenue South, Suite 300 Federal
Way, Washington 98003-2600

F4 - SMA-FRP CONFINED NOVEL COLUMN DESIGN

F4-1: Strength Design of SMA-FRP Confined Column

The following table shows the factored load for the Strength Limit State design of the conventional column. The moments in the transverse and longitudinal direction were magnified according to AASHTO (2014) Section 4.5.3.2.2b with simplifications identified previously.

Strength Factored Load	Units	Magnitude
Magnified Longitudinal Moment	kip-in	17,924
Magnified Transverse Moment	kip-in	45,071
Shear Longitudinal	kips	0
Shear Transverse	kips	176
Axial Load	kips	2,479

Table 4-1: Controlling Strength Load Combination Values

The column size was iteratively checked to optimize the design for strength load combinations. A 5-foot column exceeded the maximum drift demand in Report 12-101. The following calculation shows the last iteration for column size of 5.5 feet.

Axial-Moment Strength Check of Column

Section Properties:

The following design section properties were used for this example.

Transverse rebar strength	$f_{yh} := 60\text{ksi}$	
Diameter of column	$D := 5.5\text{ft}$	
Length of column	$L := 28\text{ft}$	
Concrete cover	$c := 2\text{in}$	
Area of longitudinal bar	$a_{SMA} := 1.56\text{in}^2$	
Diameter of longitudinal bar	$d_{SMA} := 1.41\text{in}$	
Number of bar	$n_{SMA} := 22$	Use 22 #11 bars
Transverse rebar #5	$a_{tr} := 0.31\text{in}^2$	Use #5 @ 4 in.
Diameter of transverse rebar #5	$d_{tr} := 0.625\text{in}$	
Spacing of transverse rebar	$s := 4\text{in}$	

Type of transverse rebar	Type := "spiral"
Concrete core diameter	$D' := [D - (2c)] - d_{tr} = 61.375 \cdot \text{in}$
Overstrength factor	$\lambda := 1.2$
Column cross section	$A_g := \frac{\pi}{4} \cdot D^2 = 3.421 \times 10^3 \cdot \text{in}^2$

Stress-strain curves were developed and shown below for SMA bar and both the confined and unconfined concrete to use in a Section Analysis program in order to obtain the Axial-Moment (P-M) interaction and Moment-Curvature response.

Material Properties:

SMA bar nominal properties used for strength design.

REPORT 12-101 (SMA-FRP)

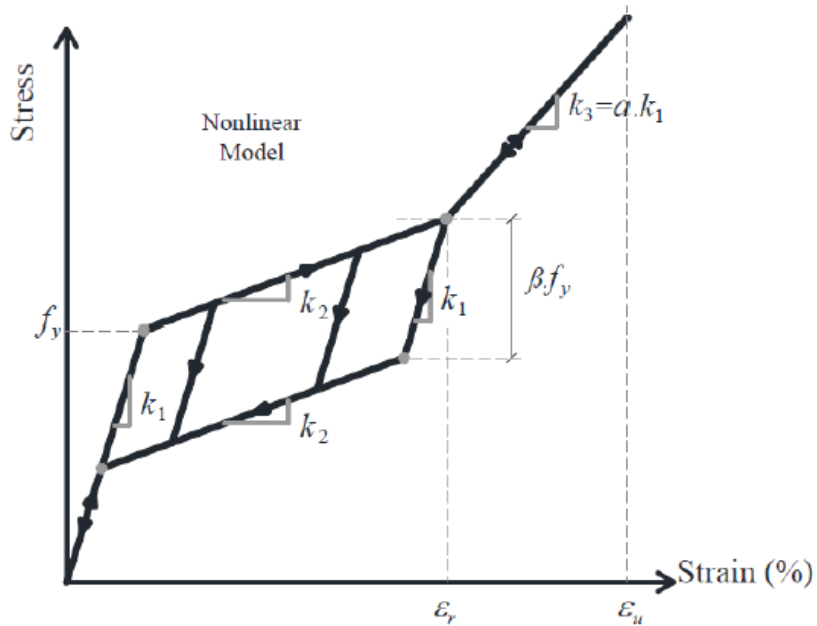


Image 4-1: SMA Stress-Strain Parameters

Austenite modulus	$k_1 := 4500 \text{ksi}$
Post-yield stiffness	$k_2 := 0 \text{ksi}$

Austenite yield strength $f_y := 45\text{ksi}$

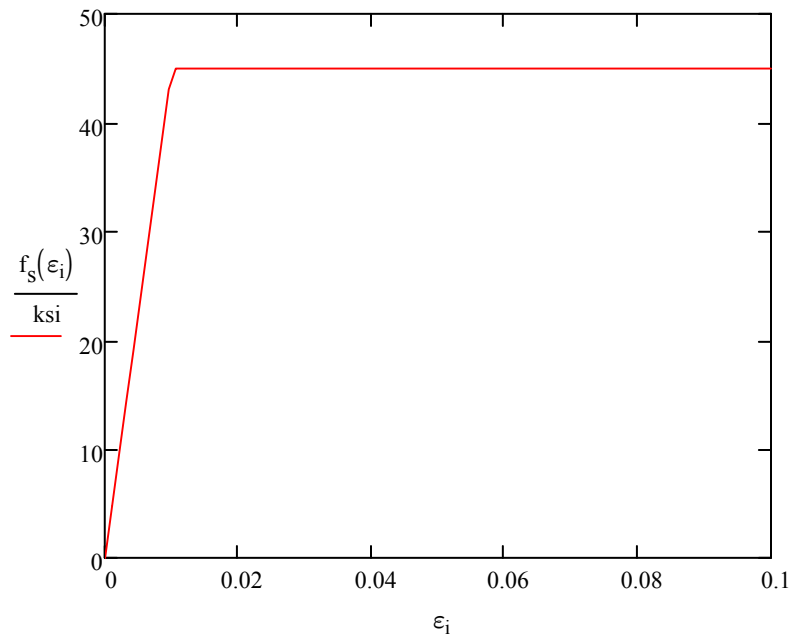
Recoverable superelastic strain $\epsilon_r := 0.06 \frac{\text{in}}{\text{in}}$

Secondary post-yield stiffness ratio $\alpha := 0$

Ultimate strain $\epsilon_u := 0.1 \frac{\text{in}}{\text{in}}$

Stress-strain curve of SMA

$$f_s(\epsilon) := \begin{cases} k_1 \cdot \epsilon & \text{if } \epsilon \leq \frac{f_y}{k_1} \\ k_1 \cdot \frac{f_y}{k_1} + k_2 \cdot \left(\epsilon - \frac{f_y}{k_1} \right) & \text{if } \frac{f_y}{k_1} < \epsilon \leq \epsilon_r \\ k_1 \cdot \frac{f_y}{k_1} + k_2 \cdot \left(\epsilon_r - \frac{f_y}{k_1} \right) + \alpha \cdot k_1 \cdot (\epsilon - \epsilon_r) & \text{otherwise} \end{cases}$$



Plot 4-1: Nominal Stress-Strain Curve of SMA Bar

The third leg of the SMA stress-strain curve was not shown, as it was outside the limits of what was used in this example.

Concrete Property:

The following design material properties concrete were used for this example.

Compression strength of concrete	$f'_c := -4 \cdot \text{ksi} = -4 \cdot \text{ksi}$
Strain at peak compression	$\epsilon_{co} := -0.002$
Concrete crushing strain	$\epsilon_{cu} := -0.004$
Spalling strain	$\epsilon_{sp} := -0.005$
Concrete density	$\gamma_c := 145 \text{pcf}$

Concrete modules of elasticity

$$E_c := 33000 \cdot \left(\frac{\gamma_c \cdot \text{ft}^3}{\text{kip}} \right)^{1.5} \cdot \sqrt{|f'_c| \cdot \text{ksi}} = 3.644 \times 10^3 \cdot \text{ksi} \quad \text{AASHTO (2014) 5.4.2.4-1}$$

Modulus of steel $E_s := k_1 = 4.5 \times 10^3 \cdot \text{ksi}$

Yield strength of stirrups $f_{yh} := 60 \text{ksi}$

Strain at peak stress of transverse reinforcement $\epsilon_{suh} := 0.09$

Stress-Strain of Unconfined Concrete:

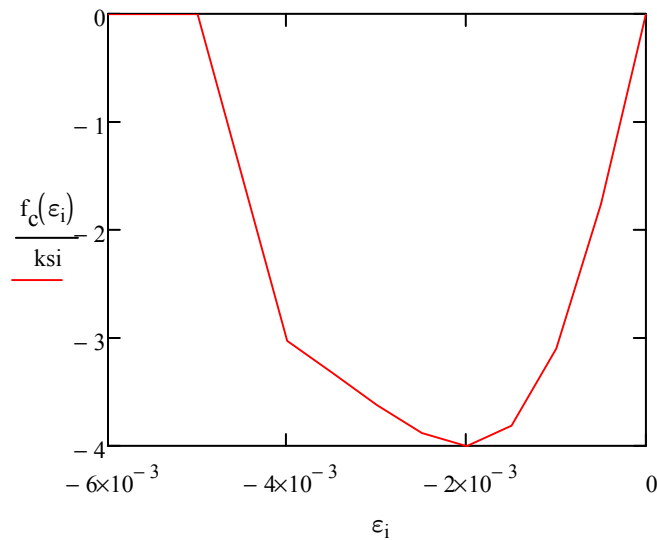
Mander et al., 1988

Secant concrete modulus $E_{sec} := \frac{f'_c}{\epsilon_{co}} = 2 \times 10^3 \cdot \text{ksi}$

$$r := \frac{E_c}{E_c - E_{sec}} = 2.216$$

Stress-strain curve of unconfined concrete

$$f_c(\epsilon) := \begin{cases} 0 & \text{if } \epsilon \geq 0 \\ \frac{f_c \cdot \frac{\epsilon}{\epsilon_{co}} \cdot r}{r - 1 + \left(\frac{\epsilon}{\epsilon_{co}}\right)^r} & \text{if } \epsilon_{cu} < \epsilon \leq 0 \\ \frac{-f_c \cdot \frac{\epsilon_{cu}}{\epsilon_{co}} \cdot r}{r - 1 + \left(\frac{\epsilon_{cu}}{\epsilon_{co}}\right)^r} \cdot \frac{\epsilon_{sp} - \epsilon}{\epsilon_{cu} - \epsilon_{sp}} & \text{if } \epsilon_{sp} < \epsilon \leq \epsilon_{cu} \\ 0 & \text{otherwise} \end{cases}$$



Plot 4-2: Unconfined Concrete Stress-Strain Curve

Confined Concrete due to Transverse Reinforcement:

Mander et al., 1988

Total area of longitudinal bar

$$A_l := n_{SMA} \cdot a_{SMA}$$

Core diameter of concrete

$$D' := D - d_{tr} - 2 \cdot c = 61.375 \cdot \text{in}$$

Core area $A_{cc} := \frac{\pi}{4} \cdot D'^2 - A_l$

Ratio longitudinal bar/core $\rho_{cc} := \frac{A_l}{A_{cc}}$

Transverse rebar volumetric ratio $\rho_s := \frac{4 \cdot a_{tr}}{s \cdot D'} = 5.051 \times 10^{-3}$

Confinement effectiveness coefficient

$$K_e := \min \left[\begin{array}{l} \frac{1 - \frac{s - d_{tr}}{2 \cdot D'}}{1 - \rho_{cc}} \text{ if Type = "spiral" } \\ \frac{\left[1 - \left(\frac{s - d_{tr}}{2 \cdot D'} \right) \right]^2}{1 - \rho_{cc}} \text{ otherwise} \end{array} \right] = 0.984$$

Effective lateral confining pressure $f_l := \frac{1}{2} \cdot K_e \cdot \rho_s \cdot f_{yh}$

Confined concrete strength $f_{cc} := f_c \cdot \left(-1.254 + 2.254 \cdot \sqrt{1 + 7.94 \cdot \frac{f_l}{|f_c|}} - 2 \cdot \frac{f_l}{|f_c|} \right) = -4.95 \cdot \text{ksi}$

Ultimate strain $\epsilon_{ccu} := - \left(0.004 + \frac{1.4 \cdot \rho_s \cdot f_{yh} \cdot \epsilon_{suh}}{|f_{cc}|} \right) = -0.012$

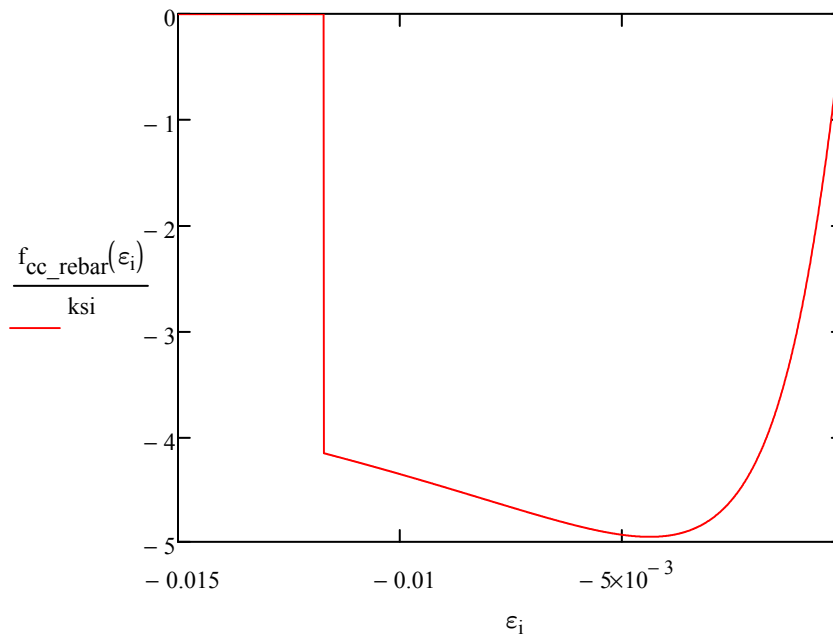
Strain at peak stress $\epsilon_{cc} := \epsilon_{co} \cdot \left[1 + 5 \cdot \left(\frac{f_{cc}}{f_c} - 1 \right) \right] = -4.374 \times 10^{-3}$

Secant concrete modulus $E_{sec} := \frac{f_{cc}}{\epsilon_{cc}} = 1.132 \times 10^3 \cdot \text{ksi}$

Stiffness ratio $r := \frac{E_c}{E_c - E_{sec}}$

Stress-strain curve of concrete due to transverse reinforcement

$$f_{cc_rebar}(\varepsilon) := \begin{cases} 0 & \text{if } \varepsilon \geq 0 \\ \frac{f_{cc} \cdot \frac{\varepsilon}{\varepsilon_{cc}} \cdot r}{r - 1 + \left(\frac{\varepsilon}{\varepsilon_{cc}}\right)^r} & \text{if } \varepsilon_{ccu} \leq \varepsilon \leq 0 \\ 0 & \text{otherwise} \end{cases}$$



Plot 4-3: Confined Concrete Stress-Strain Curve due to Transverse Reinforcement

Confined Concrete due to FRP Wrap:

REPORT 12-101 (SMA-FRP)

Material properties for FRP are determined from supplier-published product information. These material properties have to be selected early in the design process and should be bracketed if several products have to be specified in the construction contract.

Fiber type Carbon

Thickness of wrap $t_f := 0.04\text{in}$

Number of layer $n_f := 2.0$

FRP tensile strength $f_{fu} := 350\text{ksi}$

Environmental reduction factor $C_E := 0.85$

Modulus of FRP $E_f := 19000\text{ksi}$

$$\epsilon_{fe} := \frac{0.58 \cdot C_E \cdot f_{fu}}{E_f} = 9.082 \times 10^{-3} \quad \text{REPORT 12-101 3.2.3.2-3}$$

Section efficiency factor (circular column) $k_a := 1.0$ $k_b := 1.0$

Angle of fiber to longitudinal axis of pier $\alpha := \frac{\pi}{2}$

Confining pressure $f_l := \left(\frac{2 \cdot E_f \cdot n_f \cdot t_f \cdot \epsilon_{fe}}{D} \right) = 0.418 \cdot \text{ksi} \quad \text{REPORT 12-101 3.2.3.2-2}$

$$\frac{f_l}{|f_c|} = 0.105 \quad > 0.08 \quad \text{OK}$$

Maximum compressive strength REPORT 12-101 3.2.3.2-1

$$f_{cc} := -(|f_c| + 3.135 \cdot k_a \cdot f_l) = -5.311 \cdot \text{ksi}$$

Maximum compressive strain REPORT 12-101 3.2.3.2-4

$$\epsilon_{cu} := -\min \left[|\epsilon_{co}| \cdot \left[1.5 + 12 \cdot k_b \cdot \frac{f_l}{|f_c|} \cdot \left(\frac{|\epsilon_{fe}}{|\epsilon_{co}|} \right)^{0.45} \right], 0.01 \right] = -7.959 \times 10^{-3}$$

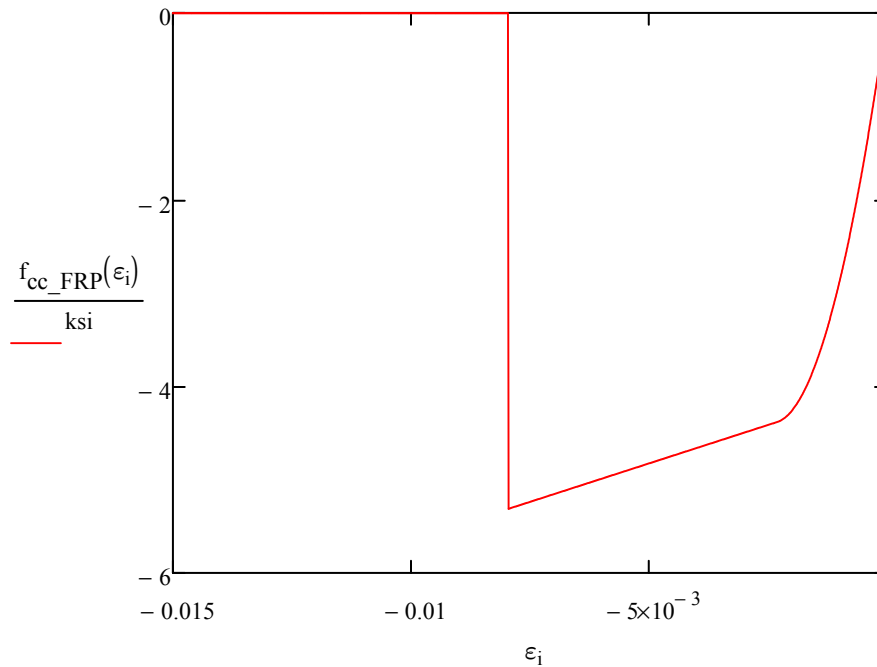
$$E_2 := \frac{f_{cc} - f_c}{\epsilon_{cu}} = 164.777 \cdot \text{ksi} \quad \text{REPORT 12-101 3.2.3.2-8}$$

$$\epsilon'_t := \frac{2 \cdot f_c}{E_c - E_2} = -2.299 \times 10^{-3}$$

Stress-strain curve of concrete

REPORT 12-101 3.2.3.2-6

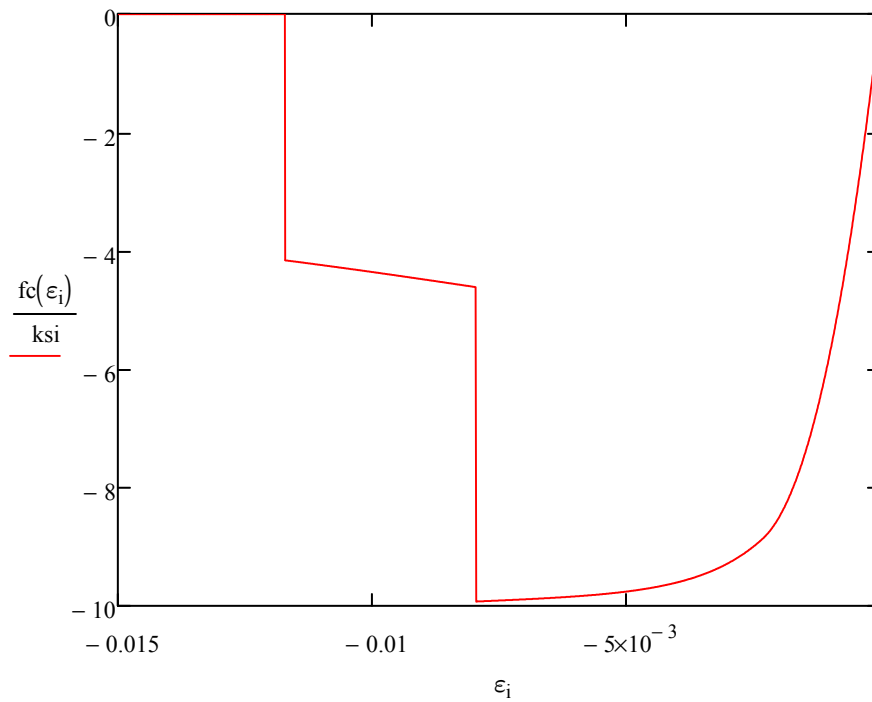
$$f_{cc_FRP}(\epsilon) := \begin{cases} \left[E_c \cdot \epsilon - \frac{(E_c - E_2)^2}{4 \cdot f_c} \cdot \epsilon^2 \right] & \text{if } \epsilon'_t \leq \epsilon \leq 0 \\ f_c + E_2 \cdot \epsilon & \text{if } \epsilon_{cu} \leq \epsilon < \epsilon'_t \\ 0 & \text{otherwise} \end{cases}$$



Plot 4-4: Confined Concrete Stress-Strain Curve due to FRP Wrap

Combined Confinements:

$$f_c(\varepsilon) := f_{cc_FRP}(\varepsilon) + f_{cc_rebar}(\varepsilon)$$



Plot 4-5: Combined Confined Concrete Stress-Strain Curve

Axial Capacity:

Capacity $\phi P_{on} := 0.75 \cdot [0.85 \cdot |F_{c_FRP}| \cdot (A_g - A_l) + A_l \cdot f_y] = 1.262 \times 10^4 \cdot \text{kip}$

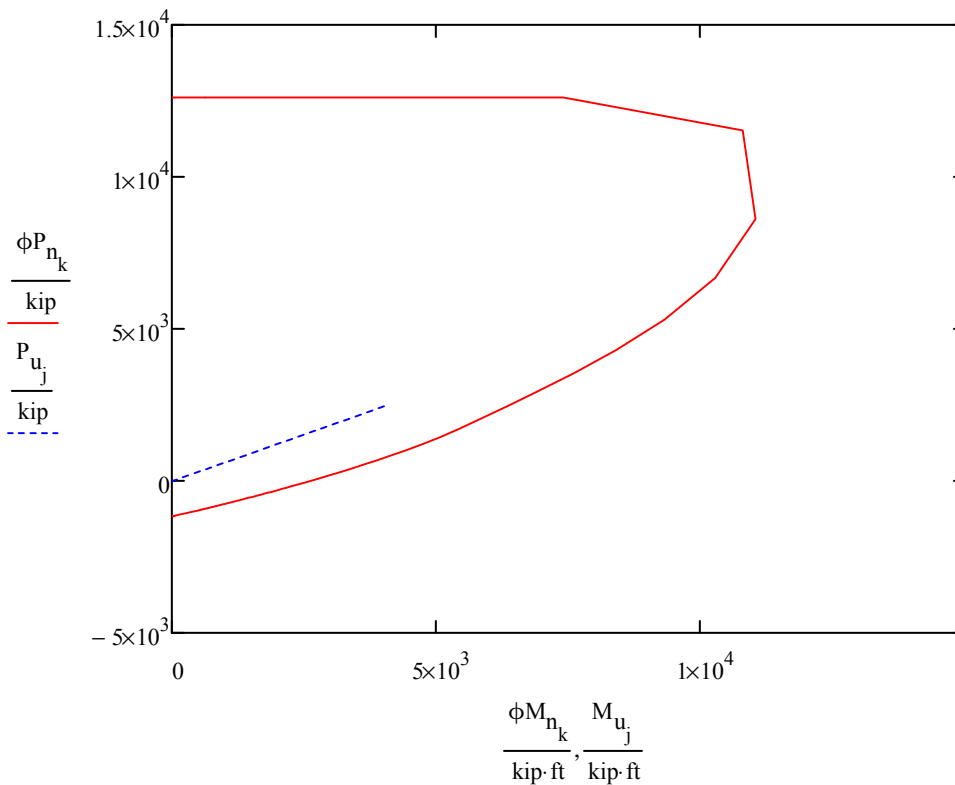
D/C ratio $\frac{P_{u_ST1}}{\phi P_{on}} = 0.196 < 1.0$ **OK**

Axial-Moment (P-M) Interaction Capacity:

The column section properties were modeled in a Section Analysis Program to generate the nominal P-M Interaction Curve and associated strain in the SMA and concrete. The SMA strain values were used to identify the tension/compression-controlled region.

As the SMA bar has a large yielding strain compared to conventional reinforcement, it was assumed the whole P-M curve has the lowest strength reduction factor of AASHTO (2014) of 0.75. This was just an assumption for the Strength Limit State design of SMA-FRP columns. Additional research and investigation will be required to more accurately apply reduction factors for the Strength Limit State design of this system.

The following figure shows the P-M capacity curve of the SMA-FRP column and compares it with the demand factored load. The demand was less than the capacity, and the section has sufficient strength for the factored loads.



Plot 4-6: Factored Axial-Moment (P-M) Capacity versus Demand for the SMA-FRP Column

Demand

$$M_{u_1} = 4.042 \times 10^3 \cdot \text{kip} \cdot \text{ft}$$

$$P_{u_1} = 2.479 \times 10^3 \cdot \text{kip}$$

Capacity $\phi M_{CAP} = 6.346 \times 10^3 \cdot \text{kip} \cdot \text{ft}$ $\phi := 0.75$

D/C ratio $DCR := \frac{M_{u1}}{\phi M_{CAP}} = 0.637$ < 1.0 **OK**

F4-2: Seismic Design of SMA-FRP Novel Column

Material Properties:

REPORT 12-101 (SMA-FRP)

The following design material properties were used for the seismic portion of the design example.

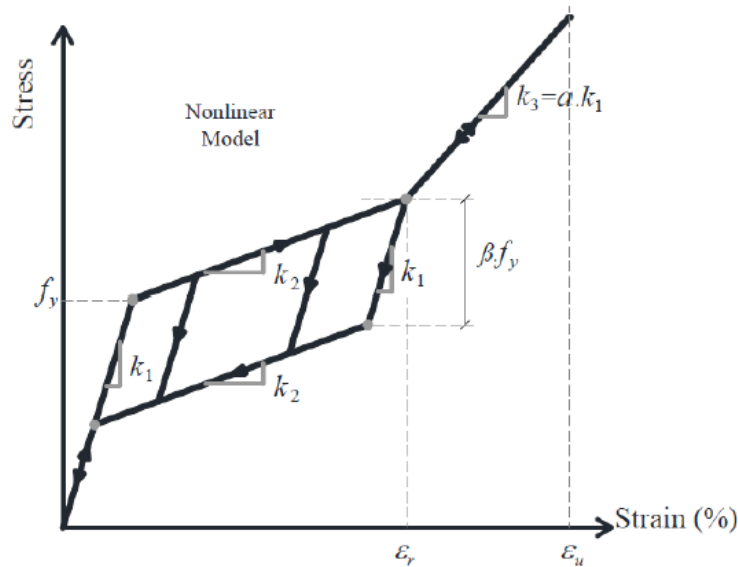


Image 4-2: SMA Stress-Strain Parameters

Austenite modulus $k_1 := 5500 \text{ksi}$

Post-yield stiffness $k_2 := 250 \text{ksi}$

Austenite expected yield strength $f_{ye} := 55 \text{ksi}$

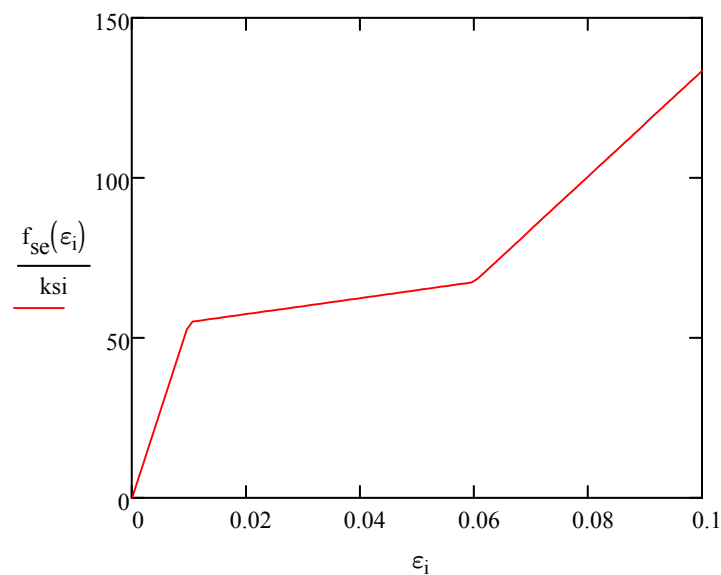
Recoverable superelastic strain $\epsilon_r := 0.06 \frac{\text{in}}{\text{in}}$

Secondary post-yield stiffness ratio $\alpha := 0.3$

Ultimate strain $\epsilon_u := 0.1 \frac{\text{in}}{\text{in}}$

Expected stress-strain curve of SMA

$$f_{se}(\epsilon) := \begin{cases} k_1 \cdot \epsilon & \text{if } \epsilon \leq \frac{f_{ye}}{k_1} \\ k_1 \cdot \frac{f_{ye}}{k_1} + k_2 \cdot \left(\epsilon - \frac{f_{ye}}{k_1} \right) & \text{if } \frac{f_{ye}}{k_1} < \epsilon \leq \epsilon_r \\ k_1 \cdot \frac{f_{ye}}{k_1} + k_2 \cdot \left(\epsilon_r - \frac{f_{ye}}{k_1} \right) + \alpha \cdot k_1 \cdot (\epsilon - \epsilon_r) & \text{otherwise} \end{cases}$$



Plot 4-7: Expected Stress-Strain Curve of SMA Material

Expected Unconfined Concrete:

Mander et al., 1988

Expected compression strength of concrete $f_{ce} := -4 \cdot 1.3 \text{ksi} = -5.2 \cdot \text{ksi}$

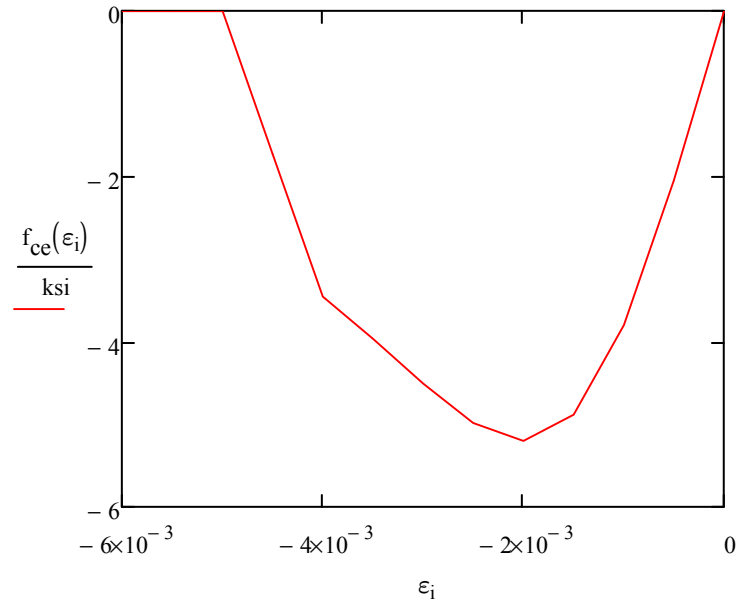
Strain at peak compression $\epsilon_{co} := -0.002$

Concrete crushing strain $\epsilon_{cu} := -0.004$

Spalling strain	$\epsilon_{sp} := -0.005$
Concrete density	$\gamma_c := 145 \text{ pcf}$
Expected concrete modulus	$E_{ce} := 33000 \cdot \left(\frac{\gamma_c \cdot \text{ft}^3}{\text{kip}} \right)^{1.5} \cdot \sqrt{ f_{ce} \cdot \text{ksi}} = 4.155 \times 10^3 \cdot \text{ksi}$
Modulus of steel	$E_s := k_1 = 5.5 \times 10^3 \cdot \text{ksi}$
Nominal yield strength of transverse rebar	$f_{yh} := 60 \text{ ksi}$
Strain at peak stress of transverse rebar	$\epsilon_{suh} := 0.09$
Secant concrete modulus	$E_{sec.e} := \frac{f_{ce}}{\epsilon_{co}} = 2.6 \times 10^3 \cdot \text{ksi}$
Stiffness ratio	$r := \frac{E_{ce}}{E_{ce} - E_{sec.e}} = 2.672$

Expected stress-strain curve of unconfined concrete

$$f_{ce}(\epsilon) := \begin{cases} 0 & \text{if } \epsilon \geq 0 \\ \frac{f_{ce} \cdot \frac{\epsilon}{\epsilon_{co}} \cdot r}{r - 1 + \left(\frac{\epsilon}{\epsilon_{co}} \right)^r} & \text{if } \epsilon_{cu} < \epsilon \leq 0 \\ \frac{-f_{ce} \cdot \frac{\epsilon_{cu}}{\epsilon_{co}} \cdot r}{r - 1 + \left(\frac{\epsilon_{cu}}{\epsilon_{co}} \right)^r} \cdot \frac{\epsilon_{sp} - \epsilon}{\epsilon_{cu} - \epsilon_{sp}} & \text{if } \epsilon_{sp} < \epsilon \leq \epsilon_{cu} \\ 0 & \text{otherwise} \end{cases}$$



Plot 4-8: Expected Stress-Strain Curve of Unconfined Concrete

Expected Confined Concrete due to Transverse Reinforcement:

Mander et al., 1988

Total area of longitudinal bar

$$A_l := n_{SMA} \cdot a_{SMA}$$

$$A_l = 34.32 \cdot \text{in}^2$$

Core diameter of concrete

$$D' := D - d_{tr} - 2 \cdot c = 61.375 \cdot \text{in}$$

$$D' = 61.375 \cdot \text{in}$$

Core area

$$A_{cc} := \frac{\pi}{4} \cdot D'^2 - A_l$$

$$A_{cc} = 2.924 \times 10^3 \cdot \text{in}^2$$

Ratio longitudinal bar/core

$$\rho_{cc} := \frac{A_l}{A_{cc}}$$

$$\rho_{cc} = 1.174\%$$

Transverse rebar volumetric ratio

$$\rho_s := \frac{4 \cdot a_{tr}}{s \cdot D'} = 5.051 \times 10^{-3}$$

Confinement effectiveness coefficient

$$K_e := \min \left[\begin{array}{l} \frac{1 - \frac{s - d_{tr}}{2 \cdot D'}}{1 - \rho_{cc}} \text{ if Type = "spiral"} \\ \frac{\left(1 - \frac{s - d_{tr}}{2 \cdot D'}\right)^2}{1 - \rho_{cc}} \text{ otherwise} \end{array} \right] = 0.984$$

Effective lateral confining pressure

$$f_l := \frac{1}{2} \cdot K_e \cdot \rho_s \cdot f_{yh}$$

Expected confined concrete strength

$$f_{cce} := f_{ce} \cdot \left(-1.254 + 2.254 \cdot \sqrt{1 + 7.94 \cdot \frac{f_l}{|f_{ce}|}} - 2 \cdot \frac{f_l}{|f_{ce}|} \right) = -6.168 \cdot k$$

Ultimate strain

$$\epsilon_{ccu} := - \left(0.004 + \frac{1.4 \cdot \rho_s \cdot f_{yh} \cdot \epsilon_{suh}}{|f_{cce}|} \right) = -0.01$$

Expected ultimate strain of confined concrete due to transverse reinforcement was slightly less than that of calculated for nominal property of concrete (strength design section); because the expected strength of concrete was higher than nominal strength.

Strain at peak stress

$$\epsilon_{cc} := \epsilon_{co} \cdot \left[1 + 5 \cdot \left(\frac{f_{cce}}{f_{ce}} - 1 \right) \right] = -3.861 \times 10^{-3}$$

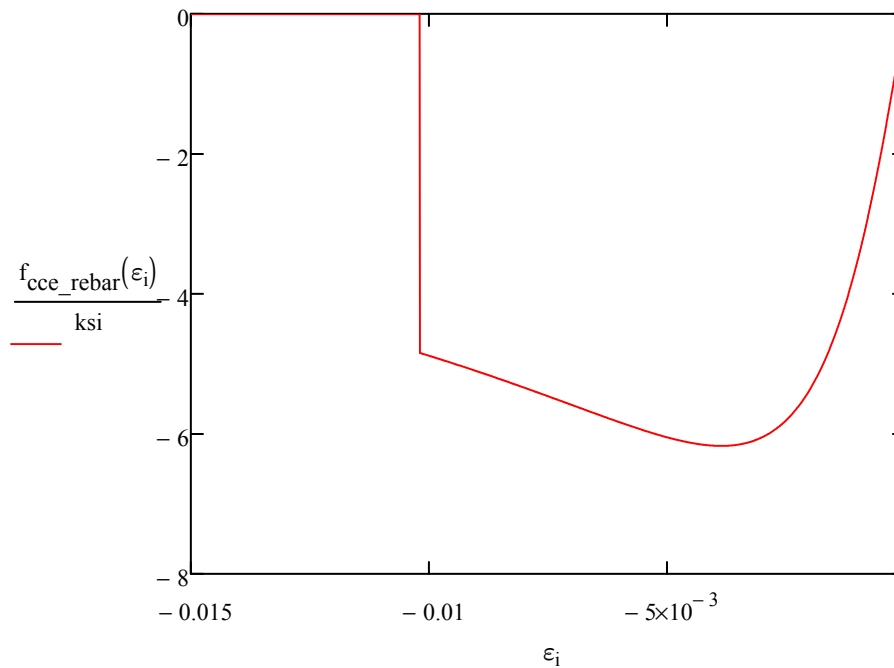
Secant concrete modulus

$$E_{sec.e} := \frac{f_{cce}}{\epsilon_{cc}} = 1.597 \times 10^3 \cdot \text{ksi}$$

$$r := \frac{E_{ce}}{E_{ce} - E_{sec.e}} = 1.625$$

Expected stress-strain curve of confined concrete from reinforcement

$$f_{cce_rebar}(\epsilon) := \begin{cases} 0 & \text{if } \epsilon \geq 0 \\ \frac{f_{cce} \cdot \frac{\epsilon}{\epsilon_{cc}} \cdot r}{r - 1 + \left(\frac{\epsilon}{\epsilon_{cc}}\right)^r} & \text{if } \epsilon_{ccu} \leq \epsilon \leq 0 \\ 0 & \text{otherwise} \end{cases}$$



Plot 4-9: Expected Confined Stress-Strain Curve of Confined Concrete due to Transverse Reinforcement

Confined Concrete due to FRP Wrap:

REPORT 12-101 (SMA-FRP)

Fiber type	Carbon
FRP tensile strength	$f_{fu} := 350\text{ksi}$
Environmental reduction factor	$C_E := 0.85$
Modulus of FRP	$E_f := 19000\text{ksi}$

$$\epsilon_{fe} := \frac{0.58 \cdot C_E \cdot f_{fu}}{E_f} = 9.082 \times 10^{-3} \quad \text{REPORT 12-101 3.2.3.2-3}$$

Section efficiency factor-circular

$$k_a := 1.0$$

Angle of fiber to longitudinal axis of pier

$$\alpha := \frac{\pi}{2}$$

Confining pressure

$$f_1 := \left(\frac{2 \cdot E_f \cdot n_f \cdot t_f \cdot \epsilon_{fe}}{D} \right) = 0.418 \cdot \text{ksi} \quad \text{REPORT 12-101 3.2.3.2-2}$$

$$\frac{f_1}{|f_{ce}|} = 0.0804 \quad > 0.08 \quad \text{OK}$$

Maximum compressive strength

$$f_{cce} := -(|f_{ce}| + 3.135 \cdot k_a \cdot f_1) = -6.511 \cdot \text{ksi}$$

REPORT 12-101 3.2.3.2-1

Maximum compressive strain

REPORT 12-101 3.2.3.2-4

$$\epsilon_{cu} := -\min \left[|\epsilon_{co}| \cdot \left[1.5 + 12 \cdot k_b \cdot \frac{f_1}{|f_{ce}|} \cdot \left(\left| \frac{\epsilon_{fe}}{\epsilon_{co}} \right| \right)^{0.45} \right], 0.01 \right] = -6.814 \times 10^{-3}$$

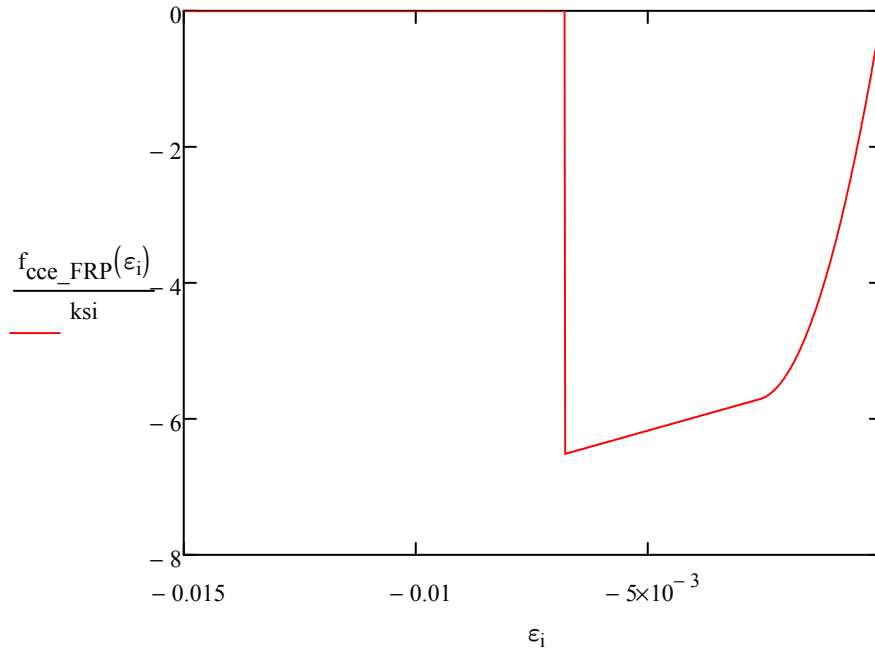
$$E_2 := \frac{f_{cce} - f_{ce}}{\epsilon_{cu}} = 192.447 \cdot \text{ksi} \quad \text{REPORT 12-101 3.2.3.2-8}$$

$$E_{ce} = 4.155 \times 10^3 \cdot \text{ksi} \quad \text{REPORT 12-101 3.2.3.2-7}$$

$$\epsilon'_t := \frac{2 \cdot f_{ce}}{E_{ce} - E_2} = -2.625 \times 10^{-3}$$

Stress-strain curve of confined concrete from FRP wrap

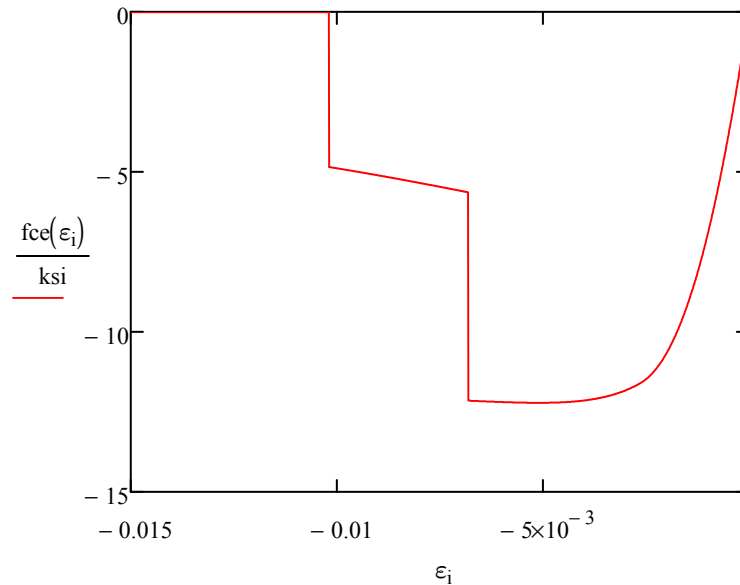
$$f_{cce_FRP}(\epsilon) := \begin{cases} \left[E_{ce} \cdot \epsilon - \frac{(E_{ce} - E_2)^2}{4 \cdot f_{ce}} \cdot \epsilon^2 \right] & \text{if } \epsilon'_t \leq \epsilon \leq 0 \\ f_{ce} + E_2 \cdot \epsilon & \text{if } \epsilon_{cu} \leq \epsilon < \epsilon'_t \\ 0 & \text{otherwise} \end{cases}$$



Plot 4-10: Expected Stress-Strain Curve of Confined Concrete due to FRP Wrap

Combined Confinements:

$$f_{ce}(\epsilon) := f_{cce_FRP}(\epsilon) + f_{cce_rebar}(\epsilon)$$



Plot 4-11: Combined Expected Stress-Strain Curve of Confined Concrete

Plastic Hinge Length

REPORT 12-101 3.2.5.1-1

Longitudinal-double curvature

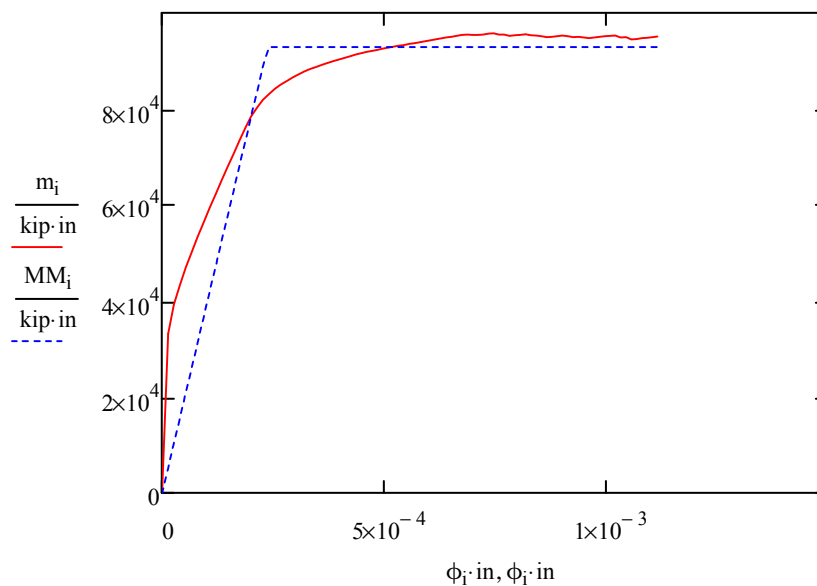
$$L_{P_X} := \max\left(0.08 \cdot \frac{L}{2} + 0.15 \cdot \frac{f_{ye}}{\text{ksi}} \cdot d_{SMA}, 0.3 \cdot \frac{f_{ye}}{\text{ksi}} \cdot d_{SMA}\right) = 25.073 \cdot \text{in}$$

Moment-Curvature Responses of the Section

The Moment-Curvature response of the column section was generated using a Section Analysis Program with the expected material properties and the axial dead load applied to the column.

Axial load $P_f := -1534 \text{kip}$

The following graph shows the moment-curvature response generated during the section analysis run and the idealized bilinear relationship to be used for the pushover analysis. The idealized curve is obtained according to AASHTO (2011) Section 8.5. The elastic portion of the curve, or initial stiffness, begins from the origin and passed through the first yield point of the reinforcing bar until it matches with the horizontal idealized line. The horizontal, or idealized moment capacity, is obtained by equating the upper and lower areas between the actual and the idealized curve beyond the first yielding of reinforcing bar. The second flat line should be iteratively shifted up and down to get the same area between bilinear and actual relationship after the first yield of reinforcement.



Plot 4-12: SMA-FRP Column Moment-Curvature Response and Idealized Bilinear Curve

Idealized Bilinear Curve Parameters:

Ultimate moment from moment-curvature data points $M_u = 9.511 \times 10^4 \cdot \text{kip} \cdot \text{in}$

Plastic moment $M_p = 9.296 \times 10^4 \cdot \text{kip} \cdot \text{in}$

Effective yield curvature $\phi_{yi} = 2.376 \times 10^{-4} \cdot \frac{1}{\text{in}}$

Ultimate curvature $\phi_u = 1.116 \times 10^{-3} \cdot \frac{1}{\text{in}}$

Effective initial stiffness $EI_{\text{eff}} = 3.912 \times 10^8 \cdot \text{kip} \cdot \text{in}^2$

Cracking stiffness reduction $\alpha_{\text{crack}} := \frac{EI_{\text{eff}}}{E_{\text{ce}} \cdot \frac{\pi}{64} \cdot D^4} = 0.101$

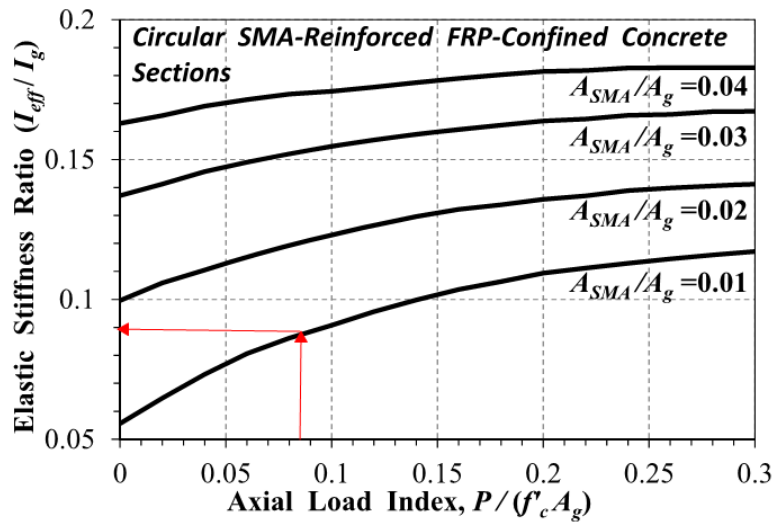
Check cracking stiffness $\frac{n_{\text{SMA}} \cdot a_{\text{SMA}}}{A_g} = 0.01$

REPORT 12-101 3.2.4.3

$$\frac{P_f}{f'_{\text{ce}} \cdot A_g} = 0.086$$

$$\alpha_{\text{crack_Guide_line}} := 0.09$$

Very close to value obtained from moment-curvature analysis



(a) Circular Sections

Image 4-3: Effective Moment of Inertia for SMA-Reinforced FRP-Confined Columns

Demand Analysis

The site Response Spectrum Analysis curve was defined in Section F1-2. As SMA-FRP columns have less hysteresis damping, in comparison to conventional columns, it was suggested in Report 12-101 Section 3.2.4.5, that the 5 percent damping be increased by 20 percent in the demand analysis to compensate for a lower damping ratio.

Result of Demand Analysis

The bridge was modeled using a Finite Element Program. The following figure shows the bridge model for demand and pushover analysis. For this design example, the seismic behavior of the bridge was investigated in longitudinal direction only. As the column is integrated with the superstructure, the column was designed for dual-hinge behavior with a hinge at both the base and the top of column. The abutments were unrestrained (roller bearing) in the longitudinal direction, parallel to the roadway. The transverse direction is single hinge at the base; however, the transverse design of the bridge is not investigated in this study.

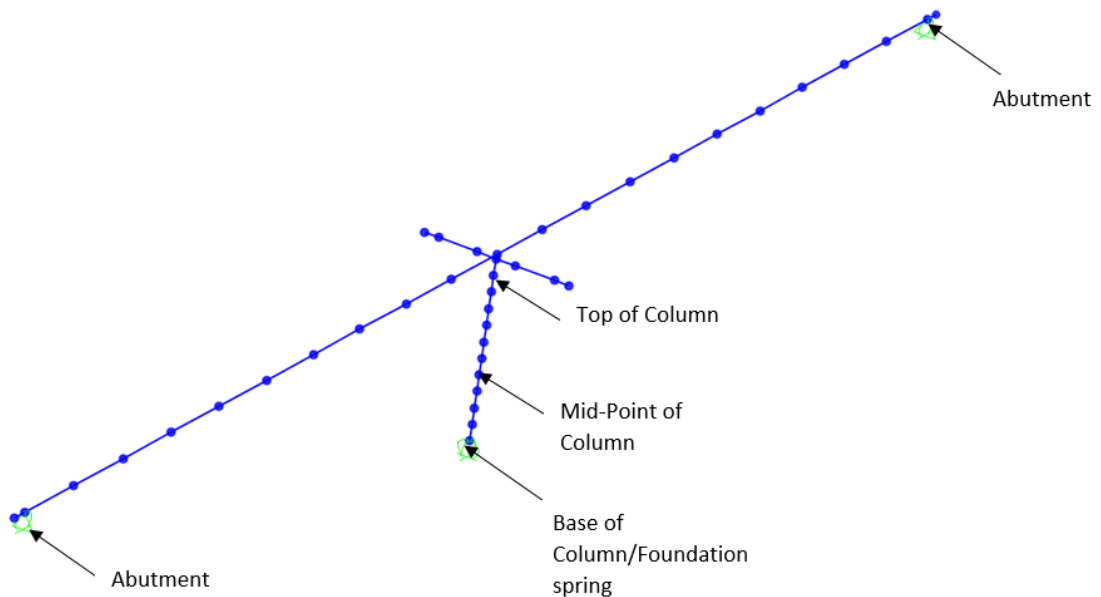
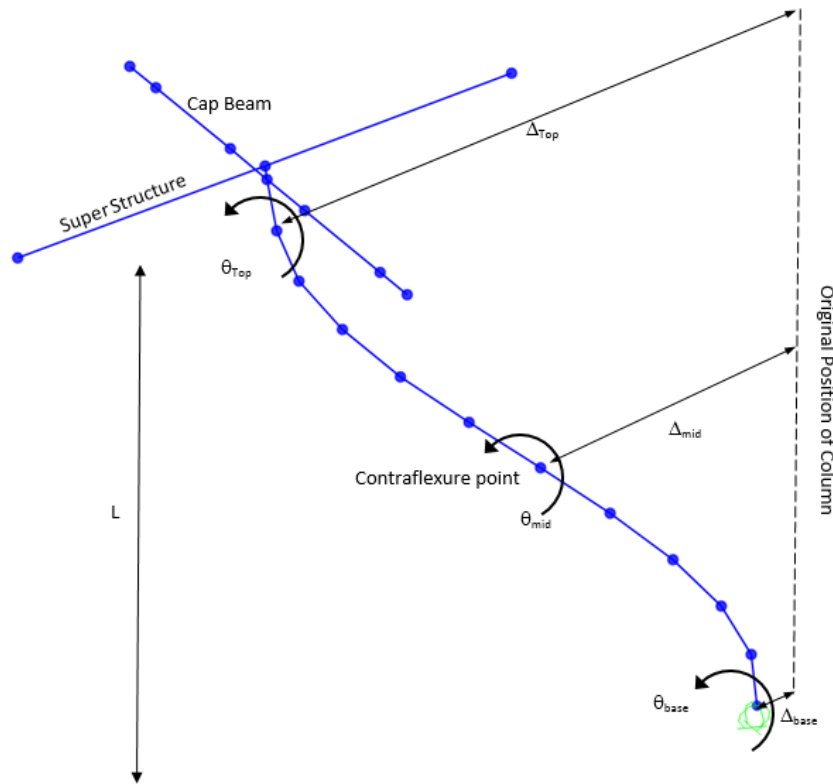


Image 4-4: Finite Element Bridge Model

The natural period of the bridge in the longitudinal direction was 1.53 s. Elongation of the period was consistent with the softer behavior of the SMA-FRP column in comparison to the conventional column.

Demand Displacement from Response Spectrum Analysis in Longitudinal Direction

The performance and ductility of each hinge were investigated separately. It was assumed that the moment capacity and the geometry of the column at both hinges are essentially identical; therefore, the contraflexure point for this column in the longitudinal direction was at the midheight of the column, and the performance of each hinge was evaluated for the lower and upper lengths of the column. The following figure shows the parameters needed to calculate the displacements of the column at each end. These displacements will be needed to find the performance and ductility of each hinge.



$$\Delta_{\text{Bot_hinge}} = \Delta_{\text{mid}} - \Delta_{\text{base}} - \theta_{\text{base}} \times L/2$$

$$\Delta_{\text{Top_hinge}} = \Delta_{\text{mid}} - \Delta_{\text{Top}} - \theta_{\text{Top}} \times L/2$$

Image 4-5: Bridge Model Column Curvature

Demand deflections in top and bottom hinges

$$\Delta_{\text{Demand}_{\text{BOT}}} := \left| \left| \text{Demand}_{\text{SAP}_{4,4}} \cdot \text{in} - \text{Demand}_{\text{SAP}_{3,4}} \cdot \text{in} \right| - \text{Demand}_{\text{SAP}_{3,8}} \cdot \frac{L}{2} \right| = 4.699 \cdot \text{in}$$

$$\Delta_{\text{Demand}_{\text{TOP}}} := \left| \left| \text{Demand}_{\text{SAP}_{4,4}} \cdot \text{in} - \text{Demand}_{\text{SAP}_{5,4}} \cdot \text{in} \right| - \text{Demand}_{\text{SAP}_{5,8}} \cdot \frac{L}{2} \right| = 4.355 \cdot \text{in}$$

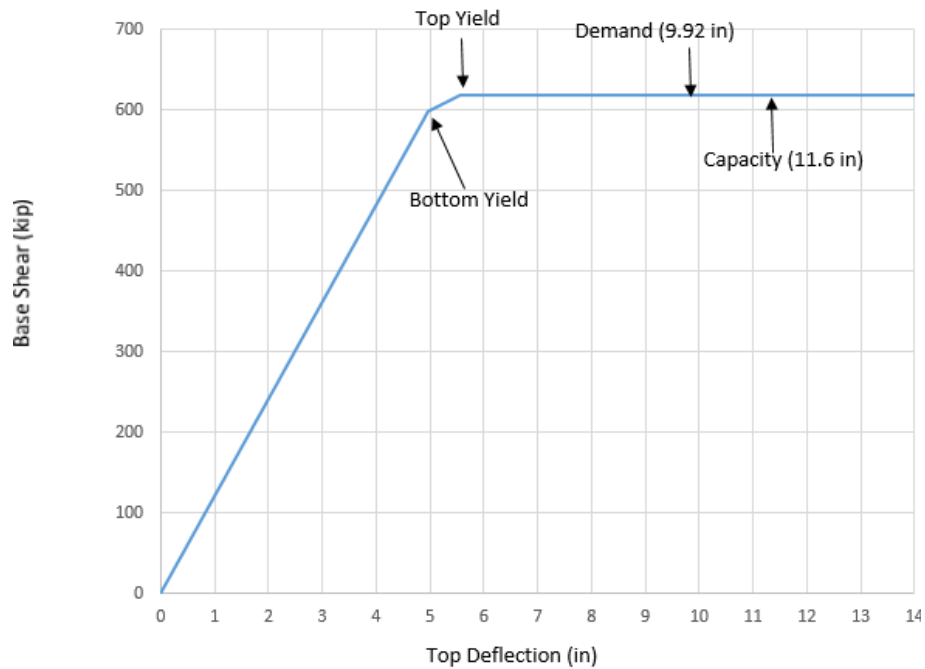
Pushover Analysis

The two hinges at the top and bottom of the column were defined according to the idealized bilinear curve presented above. The bridge was pushed longitudinally to failure and the following results were obtained.

Effect of P-Δ $\frac{P_f}{f_{ce} \cdot A_g} = 0.086 < 0.15$ **OK** REPORT 12-101 3.1.6.5

As the ratio is less than 0.15, the effect of P-delta was neglected.

The following figure shows the Force-Top Displacement Response of the column in the longitudinal direction.



Plot 4-13: Force-Top Displacement Response of the SMA-FRP Column

Yield Displacement of Column

BOT hinge yield deflection $\Delta_{Y_{BOT}} = 2.405 \cdot \text{in}$

TOP hinge yield deflection $\Delta_{Y_{TOP}} = 2.419 \cdot \text{in}$

Yield displacement obtained from AASHTO (2011) using moment-curvature analysis

$$\Delta_{Y_Code} := \frac{\phi_{yi} \cdot (0.5L)^2}{3} = 2.235 \cdot \text{in} \quad \text{Close to FEA results above}$$

Capacity displacement obtained from Finite Element Analysis (FEA) program

$$\Delta_{C_{BOT}} = 5.81 \cdot \text{in}$$

$$\Delta_{C_{TOP}} = 5.844 \cdot \text{in}$$

Capacity displacement obtained from AASHTO (2011), top and bottom, as the point of counterflexure was in the middle of the column.

$$\Delta_{C_{BOT_Code}} := \frac{\phi_{yi} \cdot (0.5L)^2}{3} + (\phi_u - \phi_{yi}) \cdot L_{P_x} \cdot \left(\frac{L}{2} - \frac{L_{P_x}}{2} \right) = 5.659 \cdot \text{in} \quad \text{Close to FEA results above}$$

$$\Delta_{C_{TOP_Code}} := \frac{\phi_{yi} \cdot (0.5L)^2}{3} + (\phi_u - \phi_{yi}) \cdot L_{P_x} \cdot \left(\frac{L}{2} - \frac{L_{P_x}}{2} \right) = 5.659 \cdot \text{in}$$

AASHTO (2011) 4.6

Check Demand/Capacity Drift Ratio

Capacity drift ratio $\delta_{C_{BOT}} := \frac{\Delta_{C_{BOT}}}{\frac{L}{2}} = 3.459 \cdot \%$

Capacity drift ratio $\delta_{C_{TOP}} := \frac{\Delta_{C_{TOP}}}{\frac{L}{2}} = 3.479 \cdot \%$

Demand drift ratio $\delta_{D_{BOT}} := \frac{\Delta_{Demand_{BOT}}}{\frac{L}{2}} = 2.797 \cdot \%$

Demand drift ratio $\delta_{D_{TOP}} := \frac{\Delta_{Demand_{TOP}}}{\frac{L}{2}} = 2.592 \cdot \%$

Bottom of column $\frac{\delta_{D_{BOT}}}{\delta_{C_{BOT}}} = 0.809$ < 1.0 **OK**

Top of column $\frac{\delta_{D_{TOP}}}{\delta_{C_{TOP}}} = 0.745$ < 1.0 **OK**

Minimum/Maximum Drift Requirements:

REPORT 12-101 3.2.4.6

Aspect ratio of column $(A_r) := \frac{L}{2 \cdot D} = 2.545$

Maximum Drift Demand Ratio:

REPORT 12-101 3.2.4.7

$\mu_{D_{max}} := 5$

AASHTO (2011) 4.9

$\delta_{D_{max}} := 1.2 \cdot \left[\left[0.26 \cdot (A_r)^{0.81} \cdot \mu_{D_{max}} - 0.18 \cdot (A_r)^{0.57} \right] \% \right] = 2.957\%$

REPORT 12-101 3.2.4.6-2

$\frac{\delta_{D_{TOP}}}{\delta_{D_{max}}} = 0.877$ < 1.0 **OK**

$\frac{\delta_{D_{BOT}}}{\delta_{D_{max}}} = 0.946$ < 1.0 **OK**

Minimum Drift Capacity Ratio:

REPORT 12-101 3.2.5.2

$\mu_{C_{min}} := 3$

REPORT 12-101
Table 3.2.5.2.1-1

$\delta_{C_{min}} := \left[\left[0.26 \cdot (A_r)^{0.81} \cdot \mu_{C_{min}} - 0.18 \cdot (A_r)^{0.57} \right] \% \right] = 1.356\%$

REPORT 12-101 3.2.4.6-2

$\frac{\delta_{C_{TOP}}}{\delta_{C_{min}}} = 2.565$ > 1.0 **OK**

$\frac{\delta_{C_{BOT}}}{\delta_{C_{min}}} = 2.551$ > 1.0 **OK**

Demand Ductility Calculations:

REPORT 12-101 3.2.4.6

Top demand ductility

$$\mu_{D_TOP} := \frac{\frac{\delta_{D_TOP}}{\%} + 0.18 \cdot (A_r)^{0.57}}{0.26 \cdot (A_r)^{0.81}} = 5.231$$

Bottom demand ductility

$$\mu_{D_BOT} := \frac{\frac{\delta_{D_BOT}}{\%} + 0.18 \cdot (A_r)^{0.57}}{0.26 \cdot (A_r)^{0.81}} = 5.601$$

Residual Drift Ratio:

Report 12-101 3.2.4.9

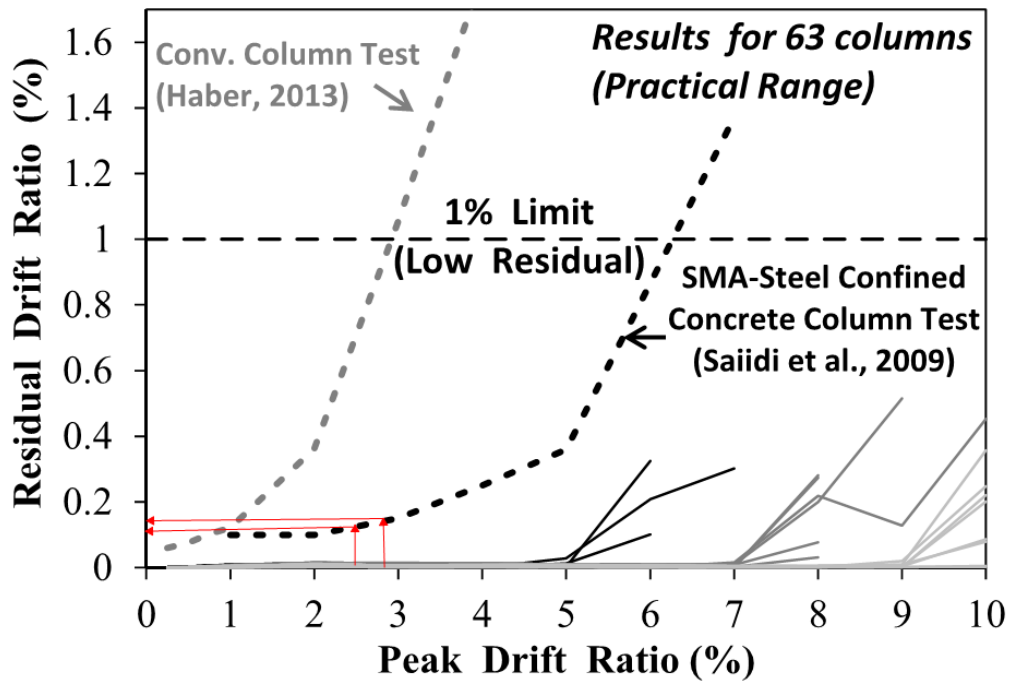


Image 4-6: Residual Drift Ratio for SMA-FRP Confined

Bottom residual drift ratio from above Graph $\delta_{r_BOT} := 0.15\%$

Bottom residual drift ratio from above Graph $\delta_{r_TOP} := 0.12\%$

Developed Seismic Shear Demand:

REPORT 12-101 3.2.4.8.2

If M_u (failure moment) is less than $1.2M_p$, then $1.2M_p$ is considered for design according to Report 12-101 Section 3.1.4.8.2. In the event that the failure moment occurs along the third leg of the expected stress-strain of the SMA bar material, then an overstrength factor of 1.4 will be more appropriate. This needs to be verified in the analysis process as follows.

$$\frac{M_u}{\lambda \cdot M_p} = 0.853$$

Overstrength plastic moment

$$M_{p0} := \lambda \cdot M_p = 9.296 \times 10^3 \cdot \text{kip} \cdot \text{ft}$$

Plastic Shear Developed in Column

X direction
$$V_{p_x} := \frac{\lambda \cdot M_p}{\left(\frac{L - L_{p_x}}{2}\right)} = 717.506 \cdot \text{kip}$$

Shear Demand from Response Spectrum Analysis

X direction
$$V_{RSA_x} := 1134 \text{kip}$$

Shear Capacity Check:

REPORT 12-101 3.2.5.3

Cross section area

$$A_g := \frac{\pi}{4} \cdot D^2$$

Ductility factor for SDC D

$$\mu_D := \max(\mu_{D_BOT}, \mu_{D_TOP}) = 5.601 \quad \text{AASHTO (2011) 4.3.3}$$

Transverse reinforcement ratio at bottom

$$\rho_s := \frac{4 \cdot a_{tr}}{D \cdot s} = 5.051 \times 10^{-3} \quad \text{REPORT 12-101 3.2.5.3-7}$$

Ratio of longitudinal reinforcement

$$\rho_t := \frac{n_{SMA} \cdot a_{SMA}}{A_g} = 0.01$$

AASHTO (2011) Figure C8.6.3-1 identifies a maximum spacing of 8 inches for flexural reinforcement. This condition was not met in this example, due to the additional confinement of the FRP wrap.

Maximum allowable nominal stress in rebar

REPORT 12-101 3.2.5.3-6

$$f_s := \min(\rho_s \cdot f_{yh}, 0.35 \text{ksi}) = 0.303 \cdot \text{ksi}$$

Concrete shear stress adjustment

REPORT 12-101 3.2.5.3-5

$$\alpha := \max\left(\frac{f_s}{0.15\text{ksi}} + 3.67 - \mu_D, 0\right) = 0.09$$

Concrete Shear Capacity

$$A := .032 \frac{\text{in}}{\sqrt{\text{kip}}} \alpha \cdot \left(1.0\text{ksi} + \frac{|P_f|}{2 \cdot A_g}\right) \cdot \sqrt{|f'_c|} \quad B := 0.11 \cdot \sqrt{|f'_c|} \cdot \frac{\text{kip}^{.5}}{\text{in}} \quad C := 0.047 \cdot \alpha \cdot \sqrt{|f'_c|} \cdot \frac{\text{kip}^{.5}}{\text{in}}$$

$$v_c := \begin{cases} 0 & \text{if } P_f \geq 0 \\ \min(A, B, C) & \text{otherwise} \end{cases} = 7.031 \times 10^{-3} \cdot \text{ksi} \quad \text{REPORT 12-101 3.2.5.3-4}$$

Concrete portion for shear capacity

$$V_c := 0.8 \cdot A_g \cdot v_c = 19.244 \cdot \text{kip} \quad \text{REPORT 12-101 3.2.5.3-3}$$

FRP Shear Capacity

$$\epsilon_{fe} := \min\left(0.004, 0.75 \cdot \frac{f_{fu}}{E_f}\right) = 4 \times 10^{-3} \quad \text{REPORT 12-101 3.2.5.3-11}$$

$$f_{fe} := \epsilon_{fe} \cdot E_f = 76 \cdot \text{ksi} \quad \text{REPORT 12-101 3.2.5.3-10}$$

$$V_f := 2 \cdot n_f \cdot t_f \cdot f_{fe} \cdot (\sin(\alpha) + \cos(\alpha)) \cdot D = 802.56 \cdot \text{kip} \quad \text{REPORT 12-101 3.2.5.3-9}$$

Steel Portion

$$\text{Nominal capacity of shear reinforcement} \quad V_s := \frac{\pi}{2} \cdot f_{yh} \cdot a_{tr} \cdot \frac{D'}{s} = 448.295 \cdot \text{kip} \quad \text{REPORT 12-101 3.2.5.3-8}$$

$$\frac{V_s + V_f}{0.25 \cdot \sqrt{\text{ksi}} \cdot |f'_c| \cdot (0.8 \cdot A_g)} = 0.914 < 1.0 \quad \text{OK} \quad \text{REPORT 12-101 3.2.5.3-12}$$

Total shear capacity of section

REPORT 12-101 3.2.5.3-2

$$V_{\text{Capacity}} := 0.9(V_c + V_s + 0.95V_f) = 1.107 \times 10^3 \cdot \text{kip}$$

$$\frac{\min(V_{\text{RSA}_x}, V_{\text{P}_x})}{V_{\text{Capacity}}} = 0.648 < 1.0 \quad \text{OK}$$

Overstrength plastic capacity for shear will also need to be designed in the transverse direction, but only the longitudinal direction was performed in this example. These forces would also be extended into the cross beam, superstructure, and foundations; though not shown herein.

Check the Minimum Lateral Capacity of Column

AASHTO (2011) 8.7.1

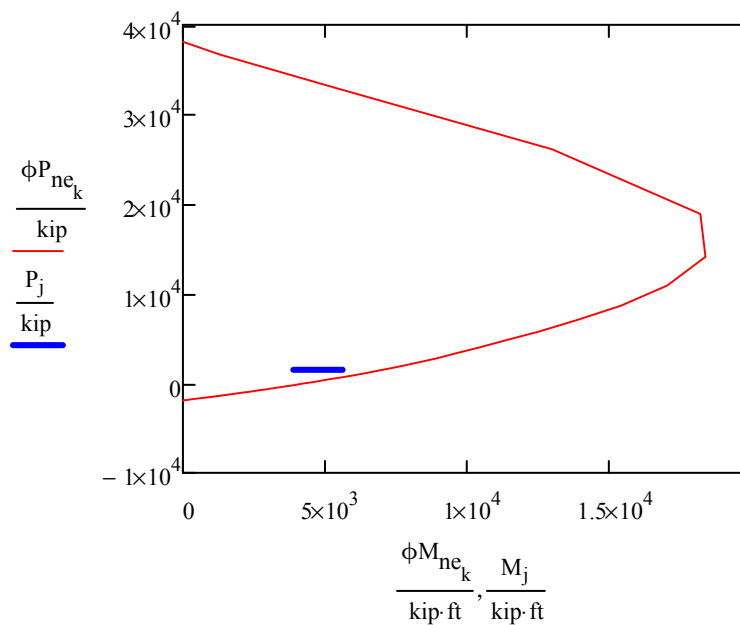
Transverse seismic (mass shared between column and abutment)

$$M_1 := 0.1 \cdot |P_f| \cdot (L + 8.5\text{ft}) = 5.599 \times 10^3 \cdot \text{kip} \cdot \text{ft} \quad P_1 := |P_f|$$

Longitudinal seismic (all mass on column-double curvature)

$$M_2 := 0.1 \cdot (2766\text{kip}) \cdot \frac{L}{2} = 3.872 \times 10^3 \cdot \text{kip} \cdot \text{ft} \quad P_2 := |P_f|$$

Axial-moment (P-M) Interaction curve was generated for nominal expected material properties to check the minimum lateral strength of the section and to make sure that the demands are within the capacity curve.



Plot 4-14: Nominal Expected Axial-Moment (P-M) Capacity versus Demand

$$DCR_{\text{Trans}} := \frac{M_1}{\phi M_{\text{CAP}_1}} = 0.798 \quad DCR_{\text{Long}} := \frac{M_2}{\phi M_{\text{CAP}_2}} = 0.552 \quad < 1.0 \quad \text{OK}$$

Column Type	SMA-FRP Column	Conventional Column
Diameter (ft)	5.5	5.0
Longitudinal Reinforcement	22-#11	22-#11
Spiral	#5@4" (Spiral)	#5@4" (Spiral)
Top Demand Drift Ratio (%)	2.59	1.18
Top Capacity Drift Ratio (%)	3.48	2.42
Bottom Demand Drift Ratio (%)	2.80	1.43
Bottom Capacity Drift Ratio (%)	3.46	2.42
Maximum Demand Drift Ratio (%)	2.96	2.73
Minimum Capacity Drift Ratio (%)	1.36	1.74
Shear Demand/Capacity Ratio	0.65	0.81
Bottom Residual Drift Ratio (%)	0.15	0.34
Top Residual Drift Ratio (%)	0.12	0.27
Overstrength Plastic Moment, M_{Po} (kip*ft)	9296	8,455

Table 4-2: Summary Table for the SMA-FRP Column (Longitudinal Direction Only)

Under the demand displacement of this structure, the plastic hinge rotation on the section was around 0.016 rad. The intent of these novel column procedures was to ensure life-safety criteria will be met and either keep the structure in service after the event or restore to service quickly. The Section Analysis Program showed that at this level of rotation there was crushing of concrete cover (less than 15 percent of the total cover around the section), the column used about 80 percent of the rotation capacity, and the section has a shear capacity reserve of about 35 percent. Seismic testing of large-scale FRP-wrapped columns has indicated that concrete failure does not occur until fracture of the FRP wrap, which usually takes place at drift ratios substantially higher than the drift ratio demand of 2.8 percent for this column. It is unlikely that any repair would be necessary at this drift level.



NCHRP
Hybrid Rocking Column



33301 Ninth Avenue South, Suite 300 Federal
Way, Washington 98003-2600

F5 - FRP CONFINED HYBRID ROCKING COLUMN DESIGN

F5-1: Strength Design of FRP Confined Hybrid Rocking Column

The following table shows the factored load for the Strength Limit State design of the FRP Confined Hybrid Rocking Column. The moments in the transverse and longitudinal direction were magnified according to AASHTO (2014) Section 4.5.3.2.2b with simplifications identified previously.

Strength Factored Load	Units	Magnitude
Magnified Longitudinal Moment	kip-in	18,896
Magnified Transverse Moment	kip-in	50,485
Shear Longitudinal	kips	0
Shear Transverse	kips	175
Axial Load	kips	2,464

Table 5-1: Controlling Strength Load Combination Values

The column size was iteratively checked to optimize the design for strength load combinations. The column size was also selected to make sure it would be allowed to neglect the P-delta effect according to Report 12-101 Section 3.1.6.5.

Axial-Moment Strength Check of Column

Section Properties:

Diameter of column	$D := 5\text{ft}$	
Length of column	$L := 28\text{ft}$	
Concrete cover	$c := 2\text{in}$	
Longitudinal rebar #11	$a_{lr} := 1.56\text{in}^2$	Use 19 #11
Diameter of longitudinal rebar #11	$d_{lr} := 1.41\text{in}$	
Number of rebar	$n_{lr} := 19$	
Transverse rebar #5	$a_{tr} := 0.31\text{in}^2$	
Diameter of transverse rebar #5	$d_{tr} := 0.625\text{in}$	Use #5 @ 4 in.
Spacing of transverse rebar	$s := 4\text{in}$	
Type of transverse rebar	Type := "spiral"	
Concrete core diameter	$D' := [D - (2c)] - d_{lr} = 54.59\text{in}$	
Column cross section	$A_g := \frac{\pi}{4} \cdot D^2 = 2.827 \times 10^3 \cdot \text{in}^2$	

Material Properties:

Transverse rebar strength	$f_{yh} := 60\text{ksi}$	
Longitudinal rebar yield strength	$f_y := 60\text{ksi}$	A 706, Gr 60
Area of each strand	$A_{str} := 0.217\text{in}^2$	
Number of strand	$n := 56$	
Ultimate yield	$f_{pu} := 270\text{ksi}$	Steel Tendon Gr 270
Final stress after loss	$f_{pi} := 0.2 \cdot f_{pu} = 54 \cdot \text{ksi}$	
Minimum strands ratio	$\frac{A_{str} \cdot n}{A_g} = 4.298 \times 10^{-3}$	>0.004 OK Report 12-101 3.3.6.2.3-1
Total force in PT after loss	$F_{pi} := f_{pi} \cdot A_{str} \cdot n = 656.208 \cdot \text{kip}$	
Yielding of tendon	$f_{py} := 245\text{ksi}$	
Modulus of tendon	$E_p := 28500\text{ksi}$	Report 12-101 3.3.3.1-1
Yield strain of tendon	$\epsilon_{py} := \frac{f_{py}}{E_p} = 8.596 \times 10^{-3}$	

Stress-Strain Calculations of Unconfined Concrete

Mander et al. 1988

Compression strength of concrete	$f'_c := -4 \cdot \text{ksi}$	
Strain at peak compression	$\epsilon_{co} := -0.002$	
Concrete crushing strain	$\epsilon_{cu} := -0.004$	
Spalling strain	$\epsilon_{sp} := -0.005$	
Concrete density	$\gamma_c := 145\text{pcf}$	
Concrete module	$E_c := 33000 \cdot \left(\frac{\gamma_c \cdot \text{ft}^3}{\text{kip}} \right)^{1.5} \cdot \sqrt{ f'_c } \cdot \text{ksi} = 3.644 \times 10^3 \cdot \text{ksi}$	AASHTO (2014) 4.2.4-1
Modulus of steel	$E_s := 29000\text{ksi}$	

Yield strength of transverse rebar

$$f_{yh} := 60 \text{ ksi}$$

Strain at peak stress of transverse rebar

$$\epsilon_{suh} := 0.09$$

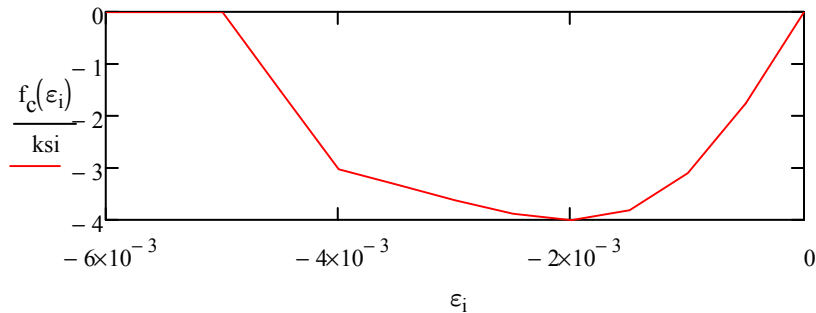
Secant concrete modulus

$$E_{sec} := \frac{f_c}{\epsilon_{co}} = 2 \times 10^3 \cdot \text{ksi}$$

$$r := \frac{E_c}{E_c - E_{sec}} = 2.216$$

Stress-strain curve of unconfined concrete

$$f_c(\epsilon) := \begin{cases} 0 & \text{if } \epsilon \geq 0 \\ \frac{f_c \cdot \frac{\epsilon}{\epsilon_{co}} \cdot r}{r - 1 + \left(\frac{\epsilon}{\epsilon_{co}}\right)^r} & \text{if } \epsilon_{cu} < \epsilon \leq 0 \\ \frac{-f_c \cdot \frac{\epsilon_{cu}}{\epsilon_{co}} \cdot r}{r - 1 + \left(\frac{\epsilon_{cu}}{\epsilon_{co}}\right)^r} \cdot \frac{\epsilon_{sp} - \epsilon}{\epsilon_{cu} - \epsilon_{sp}} & \text{if } \epsilon_{sp} < \epsilon \leq \epsilon_{cu} \\ 0 & \text{otherwise} \end{cases}$$



Plot 5-1: Unconfined Concrete Stress-Strain Curve

Stress-Strain Calculations of Confined Concrete

Mander et al. 1988

Confinement due to Transverse Reinforcement

Total area of longitudinal rebar

$$A_{lR} := n_{lR} \cdot a_{lR} \quad A_{lR} = 29.64 \cdot \text{in}^2$$

Core diameter of concrete

$$D' := D - d_{tr} - 2 \cdot c = 55.375 \cdot \text{in} \quad D' = 55.375 \cdot \text{in}$$

Core area

$$A_{cc} := \frac{\pi}{4} \cdot D'^2 - A_{lR} \quad A_{cc} = 2.379 \times 10^3 \cdot \text{in}^2$$

Ratio longitudinal rebar/core

$$\rho_{cc} := \frac{A_{lR}}{A_{cc}} \quad \rho_{cc} = 1.246 \cdot \%$$

Transverse rebar volumetric ratio

$$\rho_s := \frac{4 \cdot a_{tr}}{s \cdot D'} = 5.598 \times 10^{-3}$$

Confinement effectiveness coefficient

$$K_e := \min \left[\begin{array}{l} \left[\frac{1 - \frac{s - d_{tr}}{2 \cdot D'}}{1 - \rho_{cc}} \text{ if Type} = \text{"spiral"} \right], 1 \\ \left[\frac{\left[1 - \left(\frac{s - d_{tr}}{2 \cdot D'} \right) \right]^2}{1 - \rho_{cc}} \text{ otherwise} \right] \end{array} \right] = 0.982$$

Effective lateral confining pressure

$$f'_l := \frac{1}{2} \cdot K_e \cdot \rho_s \cdot f_{yh}$$

Confined concrete strength

$$f'_{cc} := f'_c \cdot \left(-1.254 + 2.254 \cdot \sqrt{1 + 7.94 \cdot \frac{f'_l}{|f'_c|}} - 2 \cdot \frac{f'_l}{|f'_c|} \right) = -5.041 \cdot \text{ksi}$$

Ultimate strain

$$\epsilon_{ccu} := - \left(0.004 + \frac{1.4 \cdot \rho_s \cdot f_{yh} \cdot \epsilon_{suh}}{|f'_{cc}|} \right) = -0.012$$

Strain at peak stress

$$\epsilon_{cc} := \epsilon_{co} \cdot \left[1 + 5 \cdot \left(\frac{f'_{cc}}{f'_c} - 1 \right) \right] = -4.604 \times 10^{-3}$$

Secant concrete modulus

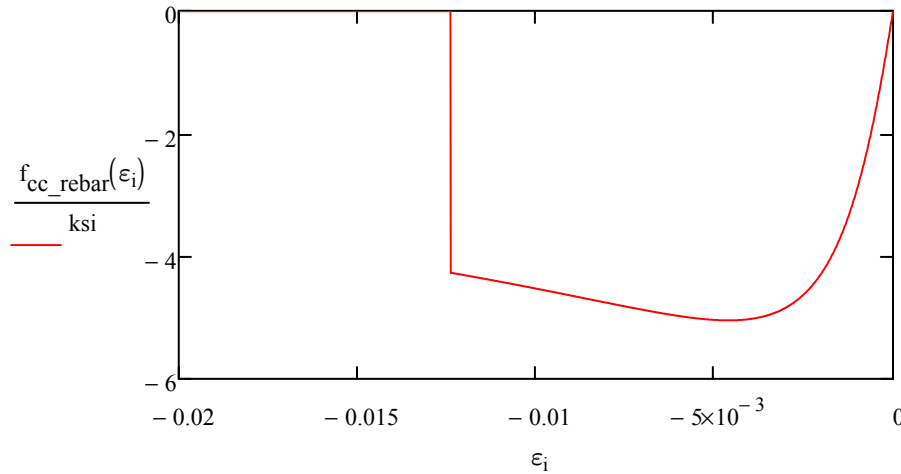
$$E_{sec} := \frac{f'_{cc}}{\epsilon_{cc}} = 1.095 \times 10^3 \cdot \text{ksi}$$

Stiffness ratio

$$r := \frac{E_c}{E_c - E_{sec}}$$

Stress-strain curve of confined concrete due to transverse reinforcement

$$f_{cc_rebar}(\epsilon) := \begin{cases} 0 & \text{if } \epsilon \geq 0 \\ \frac{f_{cc} \cdot \frac{\epsilon}{\epsilon_{cc}} \cdot r}{r - 1 + \left(\frac{\epsilon}{\epsilon_{cc}}\right)^r} & \text{if } \epsilon_{ccu} \leq \epsilon \leq 0 \\ 0 & \text{otherwise} \end{cases}$$



Plot 5-2: Confined Concrete Stress-Strain Curve due to Transverse Reinforcement

Confinement due to FRP Wrap

Report 12-101 3.3.3.2

Fiber type	Carbon
Thickness of wrap	$t_f := 0.04\text{in}$
Number of layer	$n_f := 2.0$
FRP tensile strength	$f_{fu} := 350\text{ksi}$
Environmental reduction factor	$C_E := 0.85$
Modulus of FRP	$E_f := 19000\text{ksi}$

$$\epsilon_{fe} := \frac{0.58 \cdot C_E \cdot f_{fu}}{E_f} = 9.082 \times 10^{-3} \quad \text{Report 12-101 3.3.3.2-3}$$

Section efficiency factor $k_a := 1.0 \quad k_b := 1.0$

Angle of fiber to longitudinal axis of pier $\alpha := \frac{\pi}{2}$

Confining pressure $f_1 := \max\left(\frac{2 \cdot E_f \cdot n_f \cdot t_f \cdot \epsilon_{fe}}{D}\right) = 0.46 \cdot \text{ksi} \quad \text{Report 12-101 3.3.3.2-2}$

$$\frac{f_1}{|f_c|} = 0.115 > 0.08 \quad \text{OK}$$

Maximum compressive strength $f_{cc} := -(|f_c| + 3.135 \cdot k_a \cdot f_1) = -5.443 \cdot \text{ksi}$

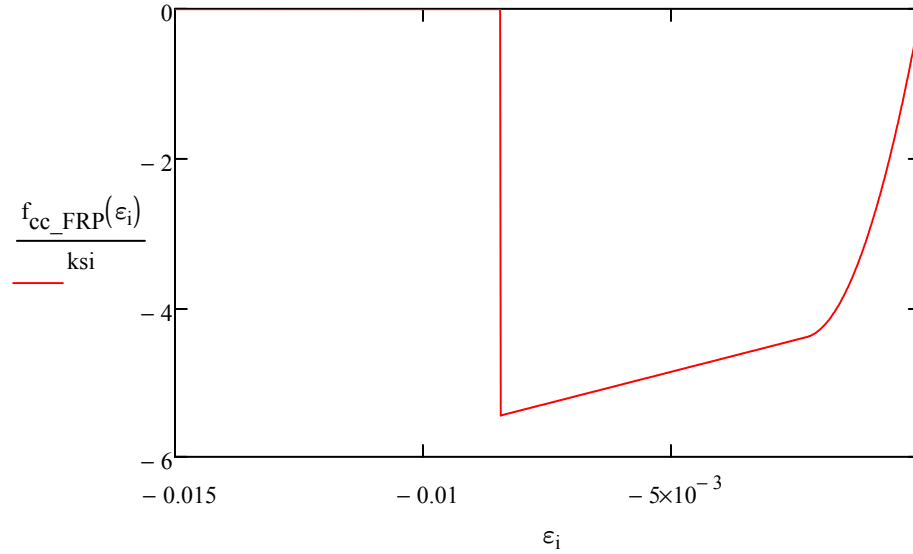
Maximum compressive strain $\epsilon_{cu} := -\min\left[|\epsilon_{co}| \cdot \left[1.5 + 12 \cdot k_b \cdot \frac{f_1}{|f_c|} \cdot \left(\left|\frac{\epsilon_{fe}}{\epsilon_{co}}\right|\right)^{0.45}\right], 0.01\right] = -8.454 \times 10^{-3}$

$$E_2 := \frac{f_{cc} - f_c}{\epsilon_{cu}} = 170.624 \cdot \text{ksi} \quad \text{Report 12-101 3.3.3.2-8}$$

$$\epsilon'_t := \frac{2 \cdot f_c}{E_c - E_2} = -2.303 \times 10^{-3}$$

Stress-strain curve of confined concrete due to FRP wrap

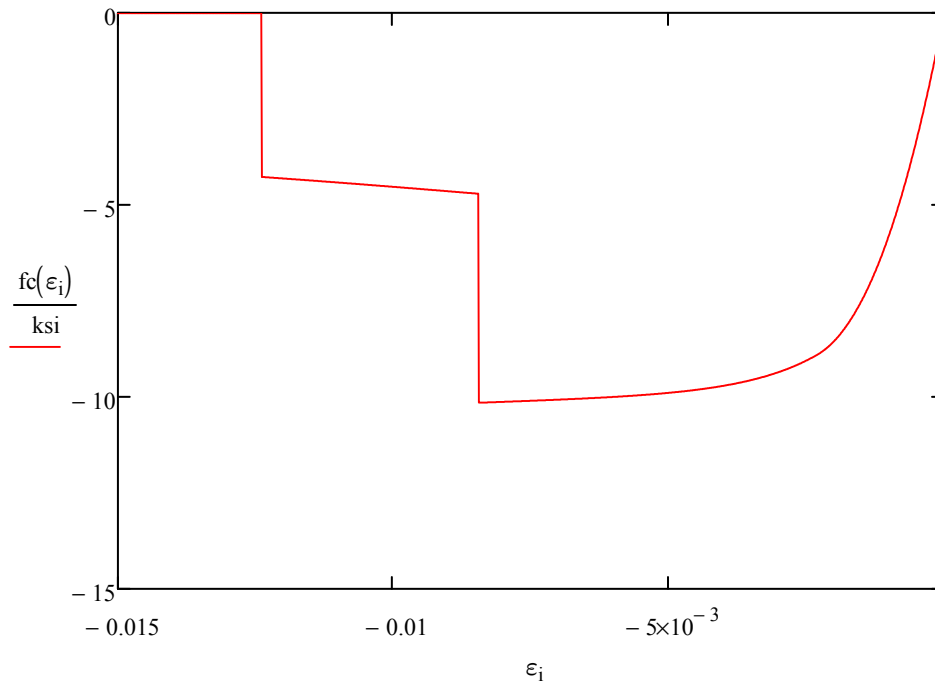
$$f_{cc_FRP}(\epsilon) := \begin{cases} \left[E_c \cdot \epsilon - \frac{(E_c - E_2)^2}{4 \cdot f_c} \cdot \epsilon^2 \right] & \text{if } \epsilon'_t \leq \epsilon \leq 0 \\ f_c + E_2 \cdot \epsilon & \text{if } \epsilon_{cu} \leq \epsilon < \epsilon'_t \\ 0 & \text{otherwise} \end{cases} \quad \text{Report 12-101 3.3.3.2-6}$$



Plot 5-3: Confined Concrete Stress-Strain Curve due to FRP Wrap

Combined Confinements:

$$f_c(\epsilon) := f_{cc_FRP}(\epsilon) + f_{cc_rebar}(\epsilon)$$



Plot 5-4: Combined Confined Concrete Stress-Strain Curve

Axial Capacity:

Capacity $\phi P_{on} := 0.75 \cdot [0.85 \cdot |F_{c_FRP}| \cdot (A_g - A_l) + A_l \cdot f_y] = 1.104 \times 10^4 \cdot \text{kip}$

D/C ratio $\frac{P_{u_ST1} + F_{pi}}{\phi P_{on}} = 0.283 < 1.0$ **OK**

Axial-Moment (P-M) Interaction Capacity

The column section was modeled in a Section Analysis Program to generate the nominal P-M Interaction curve and associated strain in the steel and concrete. The steel strain values were used to identify the tension/compression-controlled region.

The following function was used to find the factored axial-moment resistance from nominal values according to AASHTO (2014) Figure C5.5.4.2.1-1.

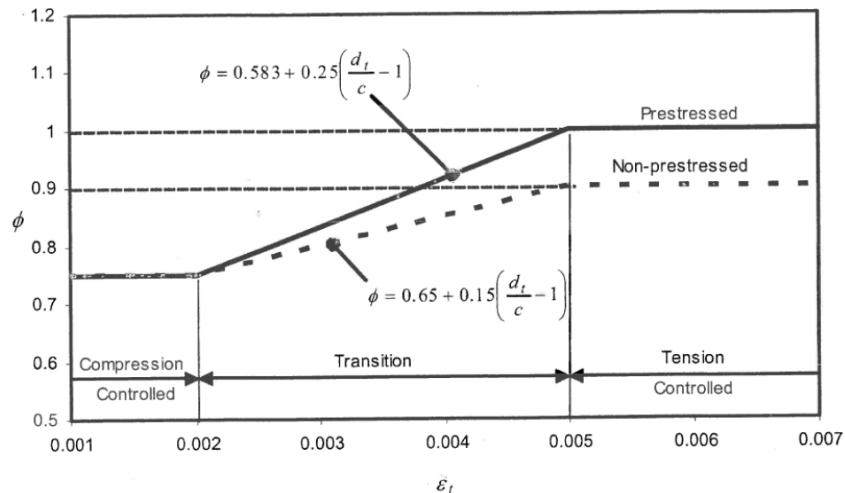
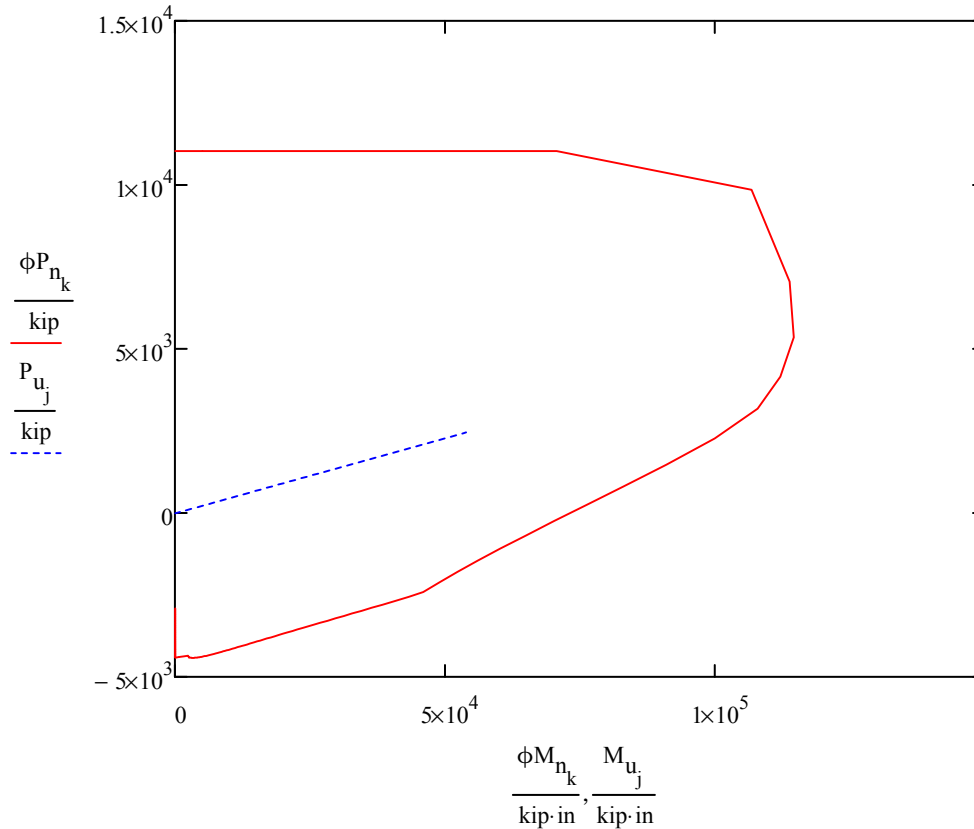


Image 5-1: Axial-Moment Resistance Factor for Columns

The following figure shows the P-M capacity curve of the Hybrid Rocking column, and compares it with the demand factored loads. The demand was less than the capacity, and the section has sufficient strength for the factored loads.



Plot 5-5: Factored Axial-Moment (P-M) Capacity versus Demand for the Hybrid Rocking Column

Demand	$M_{u_1} = 4.492 \times 10^3 \cdot \text{kip} \cdot \text{ft}$	$P_{u_1} = 2.464 \times 10^3 \cdot \text{kip}$
Capacity	$\phi M_{CAP} = 8.463 \times 10^3 \cdot \text{kip} \cdot \text{ft}$	$\phi = 0.9$
D/C ratio	$DCR := \frac{M_{u_1}}{\phi M_{CAP}} = 0.531$	< 1.0 OK

F5-2: Seismic Design of FRP Confined Hybrid Rocking Novel Column

Material Properties

The following design material properties are used for the seismic portion of the design example.

Expected yield strength	$f_{ye} := 68 \text{ksi}$	A 706, Gr 60 AASHTO (2011) 8.4.2-1
-------------------------	---------------------------	---------------------------------------

Expected ultimate strength	$f_{ue} := 95\text{ksi}$
Expected yield strain	$\epsilon_{ye} := 0.0023$
Hardening strain	$\epsilon_{sh} := 0.0115$
Ultimate tensile strain	$\epsilon_u := 0.06$
Strain at peak stress of spirals	$\epsilon_{suh} := 0.09$
Overstrength factor	$\lambda := 1.2$

Plastic hinge length AASHTO (2011) 4.11.6

Longitudinal-double curvature $L_{P_X} := \max\left(0.08 \cdot \frac{L}{2} + 0.15 \cdot \frac{f_{ye}}{\text{ksi}} \cdot d_{lr}, 0.3 \cdot \frac{f_{ye}}{\text{ksi}} \cdot d_{lr}\right) = 28.764 \cdot \text{in}$

Stress-Strain Calculations of Expected Unconfined Concrete

Mander et al. 1988

Compression strength of concrete	$f_{ce} := -4 \cdot 1.3 \cdot \text{ksi} = -5.2 \cdot \text{ksi}$
Strain at peak compression	$\epsilon_{co} := -0.002$
Concrete crushing strain	$\epsilon_{cu} := -0.004$
Spalling strain	$\epsilon_{sp} := -0.005$
Concrete density	$\gamma_c := 145\text{pcf}$

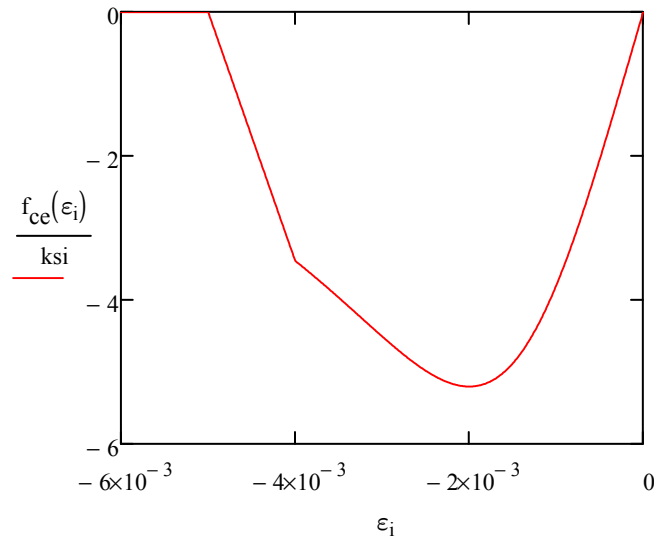
Concrete module $E_{ce} := 33000 \cdot \left(\frac{\gamma_c \cdot \text{ft}^3}{\text{kip}}\right)^{1.5} \cdot \sqrt{|f_{ce}| \cdot \text{ksi}} = 4.155 \times 10^3 \cdot \text{ksi}$ AASHTO (2014) 5.4.2.4-1

Secant concrete modulus $E_{\text{sec.e}} := \frac{f_{ce}}{\epsilon_{co}} = 2.6 \times 10^3 \cdot \text{ksi}$

Stiffness ratio $r := \frac{E_{ce}}{E_{ce} - E_{\text{sec.e}}} = 2.672$

Stress-strain curve of unconfined concrete

$$f_{ce}(\varepsilon) := \begin{cases} 0 & \text{if } \varepsilon \geq 0 \\ \frac{f_{ce} \cdot \frac{\varepsilon}{\varepsilon_{co}} \cdot r}{r - 1 + \left(\frac{\varepsilon}{\varepsilon_{co}}\right)^r} & \text{if } \varepsilon_{cu} < \varepsilon \leq 0 \\ \frac{-f_{ce} \cdot \frac{\varepsilon_{cu}}{\varepsilon_{co}} \cdot r}{r - 1 + \left(\frac{\varepsilon_{cu}}{\varepsilon_{co}}\right)^r} \cdot \frac{\varepsilon_{sp} - \varepsilon}{\varepsilon_{cu} - \varepsilon_{sp}} & \text{if } \varepsilon_{sp} < \varepsilon \leq \varepsilon_{cu} \\ 0 & \text{otherwise} \end{cases}$$



Plot 5-6: Expected Unconfined Concrete Stress-Strain Curve

Expected Confined Concrete due to Transverse Reinforcement:

Mander et al. 1988

Total area of longitudinal rebar

$$A_l := n_{lr} \cdot a_{lr}$$

$$A_l = 29.64 \cdot \text{in}^2$$

Core diameter of concrete

$$D' := D - d_{tr} - 2 \cdot c = 55.375 \cdot \text{in}$$

$$D' = 55.375 \cdot \text{in}$$

Core area

$$A_{cc} := \frac{\pi}{4} \cdot D'^2 - A_l$$

$$A_{cc} = 2.379 \times 10^3 \cdot \text{in}^2$$

Ratio longitudinal rebar/core

$$\rho_{cc} := \frac{A_l}{A_{cc}}$$

$$\rho_{cc} = 1.246 \cdot \%$$

Transverse rebar volumetric ratio

$$\rho_s := \frac{4 \cdot a_{tr}}{s \cdot D'} = 5.598 \times 10^{-3}$$

Confinement effectiveness coefficient

$$K_e := \min \left[\begin{array}{l} \frac{1 - \frac{s - d_{tr}}{2 \cdot D'}}{1 - \rho_{cc}} \text{ if Type = "spiral"} \\ \frac{\left[1 - \left(\frac{s - d_{tr}}{2 \cdot D'} \right) \right]^2}{1 - \rho_{cc}} \text{ otherwise} \end{array} , 1 \right] = 0.982$$

Effective lateral confining pressure

$$f_l := \frac{1}{2} \cdot K_e \cdot \rho_s \cdot f_{yh}$$

Confined concrete strength

$$f_{cce} := f_{ce} \cdot \left(-1.254 + 2.254 \cdot \sqrt{1 + 7.94 \cdot \frac{f_l}{|f_{ce}|}} - 2 \cdot \frac{f_l}{|f_{ce}|} \right)$$

$$f_{cce} = -6.263 \cdot \text{ksi}$$

Ultimate strain

$$\epsilon_{ccu} := - \left(0.004 + \frac{1.4 \cdot \rho_s \cdot f_{yh} \cdot \epsilon_{suh}}{|f_{cce}|} \right) = -0.011$$

Expected ultimate strain of confined ECC was less than nominal ultimate strain calculated in the strength design section (previous section) because the expected strength of concrete was higher than nominal strength.

Strain at peak stress

$$\epsilon_{cc} := \epsilon_{co} \cdot \left[1 + 5 \cdot \left(\frac{f_{cce}}{f_{ce}} - 1 \right) \right] = -4.044 \times 10^{-3}$$

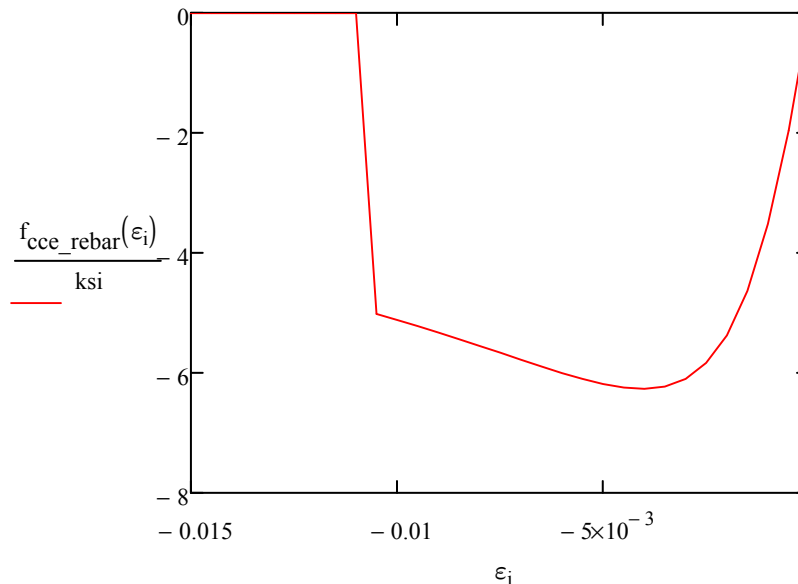
Secant concrete modulus

$$E_{\text{sec.e}} := \frac{f_{cce}}{\epsilon_{cc}} = 1.549 \times 10^3 \cdot \text{ksi}$$

Stiffness ratio $r := \frac{E_{ce}}{E_{ce} - E_{sec.e}} = 1.594$

Stress-strain curve of confined concrete due to transverse reinforcement

$$f_{cce_rebar}(\epsilon) := \begin{cases} 0 & \text{if } \epsilon \geq 0 \\ \frac{f_{cce} \cdot \frac{\epsilon}{\epsilon_{cc}} \cdot r}{r - 1 + \left(\frac{\epsilon}{\epsilon_{cc}}\right)^r} & \text{if } \epsilon_{ccu} \leq \epsilon \leq 0 \\ 0 & \text{otherwise} \end{cases}$$



Plot 5-7: Expected Confined Concrete Stress-Strain Curve due to Transverse Reinforcement

Expected Confined Concrete due to FRP Wrap:

Report 12-101 3.3.3.2-2

Confining pressure $f_1 := \max\left(\frac{2 \cdot E_f \cdot n_f \cdot t_f \cdot \epsilon_{fe}}{D}\right) = 0.46 \cdot \text{ksi}$

Report 12-101 3.3.3.2-2

$$\frac{f_1}{|f_{ce}|} = 0.088 > 0.08 \quad \text{OK}$$

Maximum compressive strength

$f_{cce} := -(|f_{ce}| + 3.135 \cdot k_a \cdot f_1) = -6.643 \cdot \text{ksi}$ Report 12-101 3.3.3.2-1

Maximum compressive strain

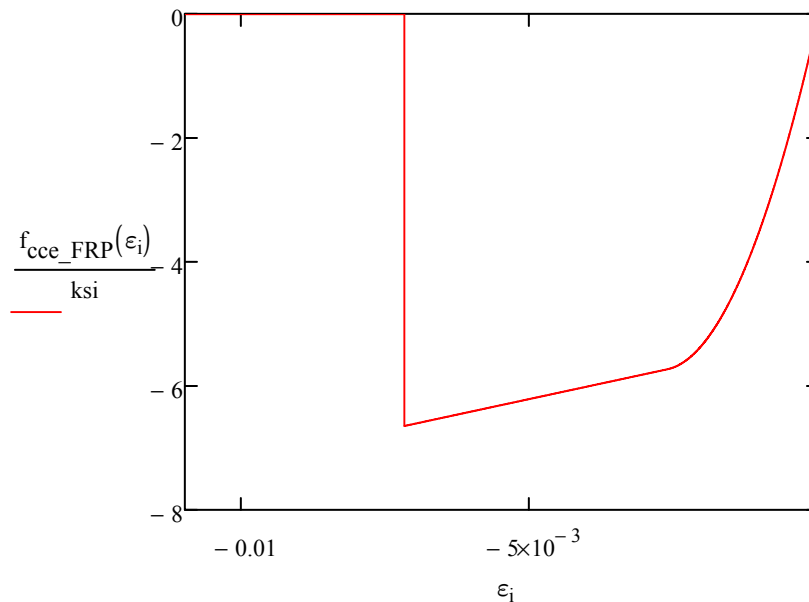
$$\epsilon_{cu} := -\min\left[|\epsilon_{co}| \cdot \left[1.5 + 12 \cdot k_b \cdot \frac{f_1}{|f_{ce}|} \cdot \left(\left|\frac{\epsilon_{fe}}{\epsilon_{co}}\right|\right)^{0.45}\right], 0.01\right] = -7.196 \times 10^{-3} \quad \text{Report 12-101 3.3.3.2-4}$$

$$E_2 := \frac{f_{cce} - f_{ce}}{\epsilon_{cu}} = 200.47 \cdot \text{ksi} \quad \text{Report 12-101 3.3.3.2-8}$$

$$\epsilon'_t := \frac{2 \cdot f_{ce}}{E_{ce} - E_2} = -2.63 \times 10^{-3}$$

Stress-strain relationship

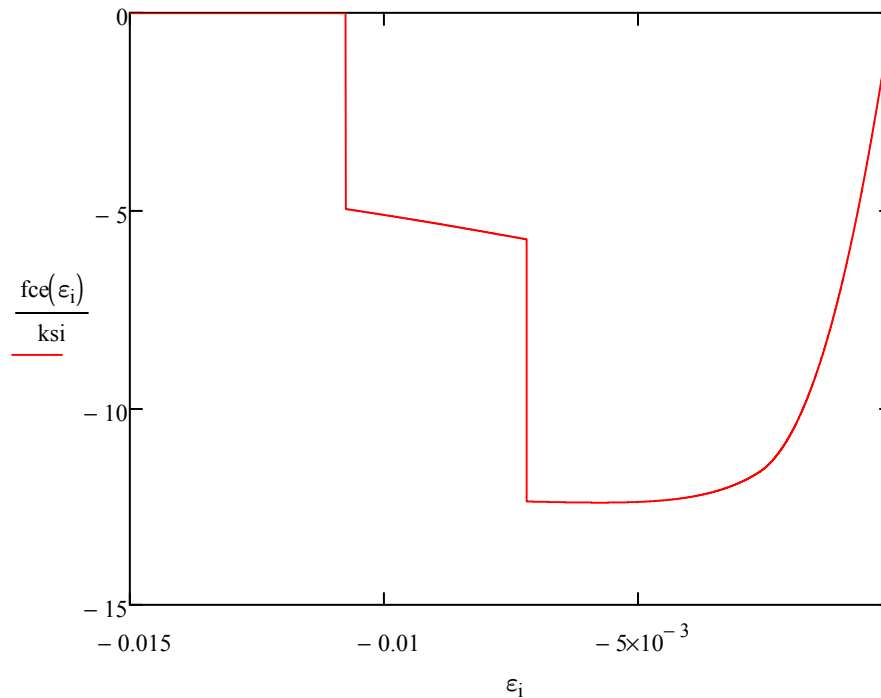
$$f_{cce_FRP}(\epsilon) := \begin{cases} \left[E_{ce} \cdot \epsilon - \frac{(E_{ce} - E_2)^2}{4 \cdot f_{ce}} \cdot \epsilon^2 \right] & \text{if } \epsilon'_t \leq \epsilon \leq 0 \\ f_{ce} + E_2 \cdot \epsilon & \text{if } \epsilon_{cu} \leq \epsilon < \epsilon'_t \\ 0 & \text{otherwise} \end{cases} \quad \text{Report 12-101 3.3.3.2-6}$$



Plot 5-8: Expected Confined Concrete Stress-Strain Curve due to FRP Wrap

Combined Confinements:

$$f_{ce}(\varepsilon) := f_{cce_FRP}(\varepsilon) + f_{cce_rebar}(\varepsilon)$$



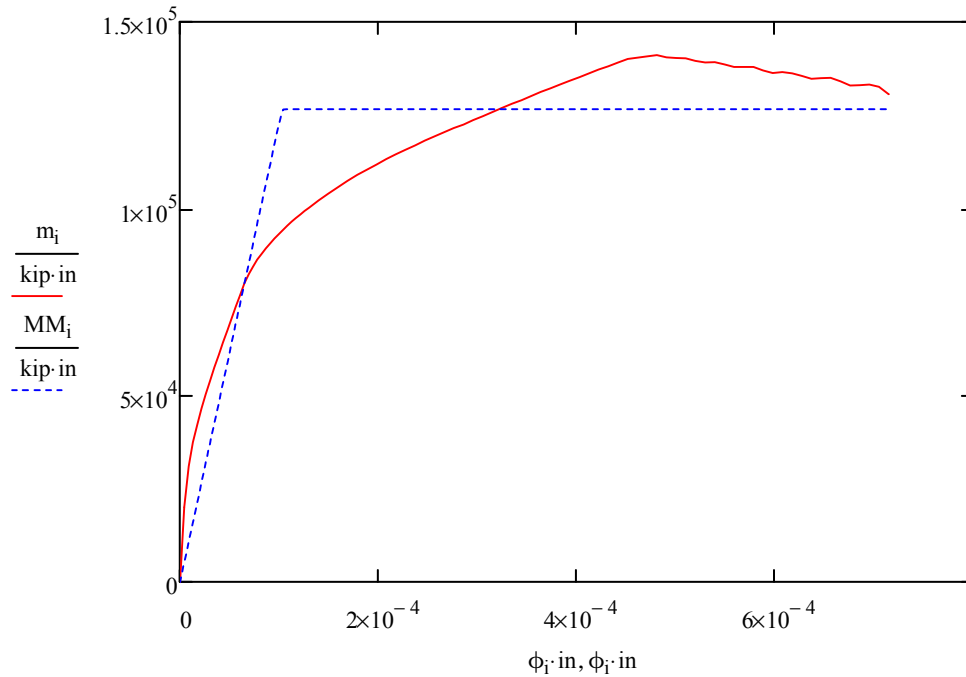
Plot 5-9: Combined Expected Stress-Strain Curve of Confined Concrete

Moment-Curvature Responses of the Section

The Moment-Curvature response of column section was generated by using a Section Analysis Program with the expected material properties and the applied axial dead load on the column.

Axial load $P_f := -1502\text{kip}$

The following graph shows the moment-curvature response generated during the section analysis run and the idealized bilinear relationship to be used for the pushover analysis. The idealized curve is obtained according to AASHTO (2011) Section 8.5. The elastic portion of the curve, or initial stiffness, begins from the origin and passed through the first yield point of the reinforcing bar until it matches with the horizontal idealized line. The horizontal, or idealized moment capacity, is obtained by equating the upper and lower areas between the actual and the idealized curve beyond the first yielding of reinforcing bar. The second flat line should be iteratively shifted up and down to get the same area between bilinear and actual relationship after the first yield of reinforcement.



Plot 5-10: Hybrid Rocking Column Moment-Curvature Response and Idealized Bilinear Curve

Idealized Bilinear Curve Parameters:

The Moment-Curvature plot above shows that the moment starts to decay after reaching the column peak value. The descending branch was due to the strength drop of the confined concrete (shown in Plot 5-9) and has some residual strength from the transverse rebar. At the failure point (crushing of the concrete core), the strength drop in the section was less than 20 percent of the largest moment. The ultimate moment defined in Report 12-101 Section 3.3.4.8, was considered here as the largest moment read from the curve in Plot 5-10. The shear design was based on the maximum of largest developed moment or the overstrength plastic moment, in this case the overstrength moment controls, as follows.

Largest developed moment	$M_u = 1.412 \times 10^5 \cdot \text{kip} \cdot \text{in}$
Plastic moment	$M_p = 1.267 \times 10^5 \cdot \text{kip} \cdot \text{in}$
Effective yield curvature	$\phi_{yi} = 1.027 \times 10^{-4} \cdot \frac{1}{\text{in}}$
Ultimate curvature	$\phi_u = 7.142 \times 10^{-4} \cdot \frac{1}{\text{in}}$
Effective initial stiffness	$EI_{\text{eff}} = 1.234 \times 10^9 \cdot \text{kip} \cdot \text{in}^2$

Cracking stiffness reduction

$$\alpha_{\text{crack}} := \frac{EI_{\text{eff}}}{E_{\text{ce}} \cdot \frac{\pi}{64} \cdot D^4} = 0.467$$

Demand Analysis

Like the conventional column, 5 percent damping site response spectrum data was used in the demand analysis Report 12-101 Section 3.3.4.3.

Result of Demand Analysis

The bridge was modeled using a Finite Element Program. The following figure shows the bridge model for demand and pushover analysis. For this design example, the seismic behavior of the bridge was investigated in longitudinal direction only. As the column is integrated with the superstructure, the column was designed for dual-hinge behavior with a hinge at both the base and the top of column. The abutments were unrestrained (roller bearing) in the longitudinal direction, parallel to the roadway. The transverse direction is single hinge at the base; however, the transverse design of the bridge is not investigated in this study.

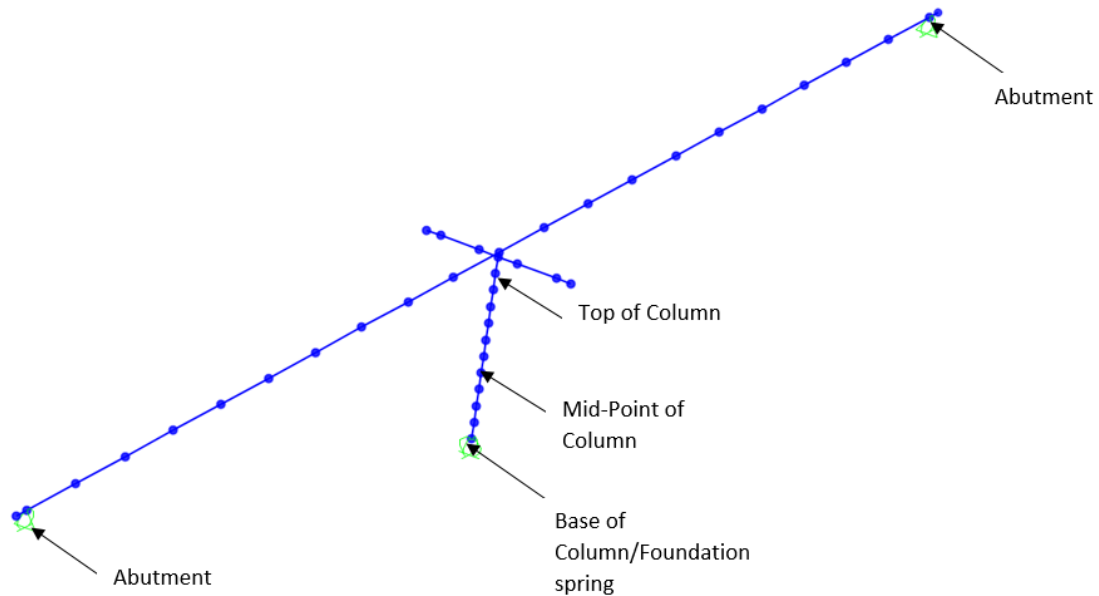
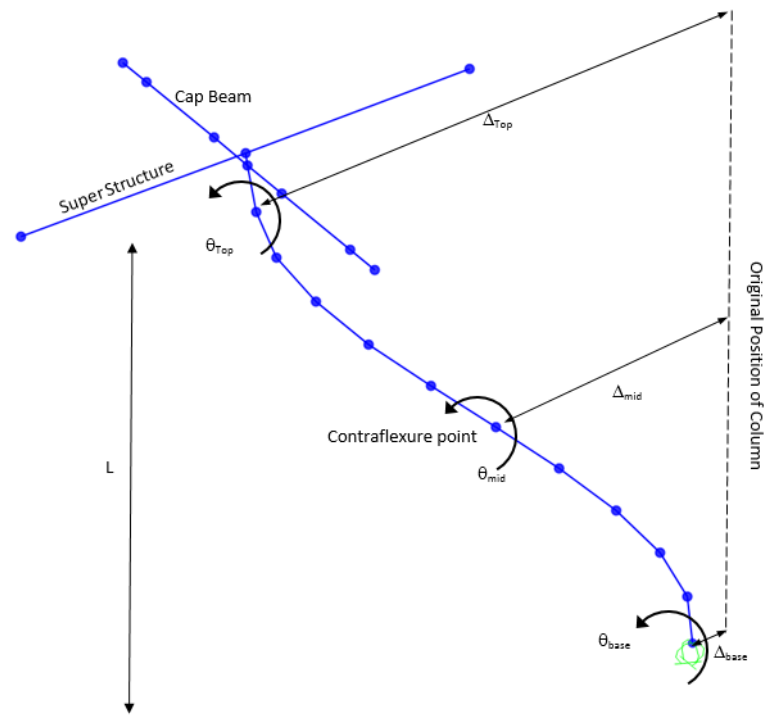


Image 5-2: Finite Element Bridge Model

The natural period of the bridge in longitudinal direction was 0.95 s. A reduction in the period from the conventional column was consistent with the increased axial force generated with post-tensioned strands.

Demand Displacement from Response Spectrum Analysis in Longitudinal Direction

The performance and ductility of each hinge were investigated separately. It was assumed that the moment capacity and the geometry of the column at both hinges are essentially identical; therefore, the contraflexure point for this column in the longitudinal direction was at the midheight of the column, and the performance of each hinge was evaluated for the lower and upper lengths of the column. The following figure shows the parameters needed to calculate the displacements of the column at each end. These displacements will be needed to find the performance and ductility of each hinge.



$$\Delta_{Bot_hinge} = \Delta_{mid} - \Delta_{base} - \theta_{base} \times L/2$$

$$\Delta_{Top_hinge} = \Delta_{mid} - \Delta_{Top} - \theta_{Top} \times L/2$$

Plot 5-3: Bridge Model Column Curvature

Check the Elastic Response of Tendons under the Demand Seismic Loads

The total strain in tendon was read from Moment-Curvature calculation in the Section Analysis Program under the demand curvature to make sure the tendons were in the elastic range.

Tendon strain at bottom hinge under demand curvature $\epsilon_{str_BOT} = 0.006842$

Tendon strain at top hinge under demand curvature $\epsilon_{str_TOP} = 0.005409$

Tendons := if($\max(\epsilon_{str_TOP}, \epsilon_{str_BOT}) \leq \epsilon_{py}$, "Elastic", "Non Elastic") = "Elastic"

Tendons = "Elastic"

Tendons are elastic - **OK**

Demand deflections in top and bottom hinges

$$\Delta_{Demand_BOT} := \left| \left| Demand_{SAP_{4,4}} \cdot in - Demand_{SAP_{3,4}} \cdot in \right| - Demand_{SAP_{3,8}} \cdot \frac{L}{2} \right| = 2.124 \cdot in$$

$$\Delta_{Demand_TOP} := \left| \left| Demand_{SAP_{4,4}} \cdot in - Demand_{SAP_{5,4}} \cdot in \right| - Demand_{SAP_{5,8}} \cdot \frac{L}{2} \right| = 1.663 \cdot in$$

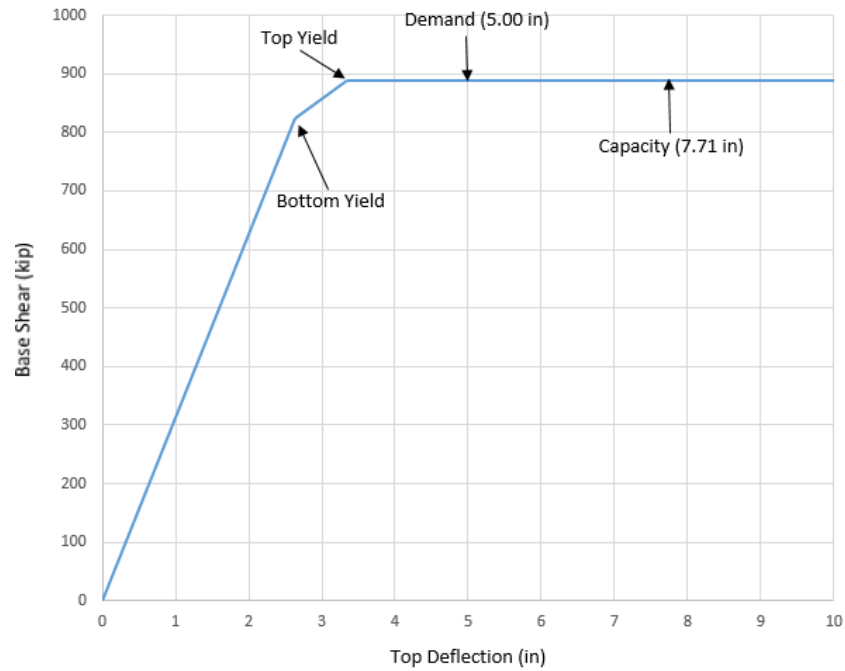
Pushover Analysis

The two hinges at the top and bottom of the column were defined according to the idealized bilinear curve presented above. The bridge was pushed longitudinally to failure and the following results were obtained.

Effect of P- Δ $\frac{P_f}{f'_{ce} \cdot A_g} = 0.102$ Report 12-101 3.1.6.5

As the ratio is less than 0.15, the effect of P-delta is neglected.

The following figure shows the Force-Top Displacement Response of the column in the longitudinal direction.



Plot 5-11: Force-Top Displacement Response of the Hybrid Rocking Column

Yield Displacement of Column:

BOT hinge yield deflection $\Delta_{Y_{BOT}} = 1.096 \text{ in}$

TOP hinge yield deflection $\Delta_{Y_{TOP}} = 1.086 \text{ in}$

Yield displacement obtained from AASHTO (2011) using moment-curvature analysis

$$\Delta_{Y_Code} := \frac{\phi_{yi} \cdot (0.5L)^2}{3} = 0.966 \text{ in} \quad \text{Close to FEA results above}$$

Capacity displacement obtained from Finite Element Analysis (FEA) program

$$\Delta_{C_{BOT}} = 3.771 \text{ in}$$

$$\Delta_{C_{TOP}} = 3.798 \text{ in}$$

Capacity displacement obtained from AASHTO (2011), top and bottom, as the point of counterflexure is in the middle of the column.

$$\Delta_{C_{BOT_Code}} := \frac{\phi_{yi} \cdot (0.5L)^2}{3} + (\phi_u - \phi_{yi}) \cdot L_{P_x} \cdot \left(\frac{L}{2} - \frac{L_{P_x}}{2} \right) = 3.668 \cdot \text{in}$$

Close to FEA results above

$$\Delta_{C_{TOP_Code}} := \frac{\phi_{yi} \cdot (0.5L)^2}{3} + (\phi_u - \phi_{yi}) \cdot L_{P_x} \cdot \left(\frac{L}{2} - \frac{L_{P_x}}{2} \right) = 3.668 \cdot \text{in}$$

Check demand/capacity ratio

AASHTO (2011) 4-8

Capacity drift ratio

$$\delta_{C_{BOT}} := \frac{\Delta_{C_{BOT}}}{\frac{L}{2}} = 2.244\%$$

Capacity drift ratio

$$\delta_{C_{TOP}} := \frac{\Delta_{C_{TOP}}}{\frac{L}{2}} = 2.261\%$$

Demand drift ratio

$$\delta_{D_{BOT}} := \frac{\Delta_{Demand_{BOT}}}{\frac{L}{2}} = 1.264\%$$

Demand drift ratio

$$\delta_{D_{TOP}} := \frac{\Delta_{Demand_{TOP}}}{\frac{L}{2}} = 0.99\%$$

$$\frac{\delta_{D_{BOT}}}{\delta_{C_{BOT}}} = 0.563 < 1.0 \text{ OK}$$

$$\frac{\delta_{D_{TOP}}}{\delta_{C_{TOP}}} = 0.438 < 1.0 \text{ OK}$$

Minimum/Maximum Drift Requirements:

Report 12-101 3.3.4.6

Aspect ratio of column

$$(A_r) := \frac{L}{2 \cdot D} = 2.8$$

Maximum Drift Demand Ratio:

Report 12-101 3.3.4.7

$$\mu_{D_max} := 5$$

AASHTO (2011) 4.9

$$\delta_{D_max} := 1.2 \cdot \left[0.26 \cdot (A_r)^{0.81} \cdot \mu_{D_max} - 0.18 \cdot (A_r)^{0.57} \right] \% = 3.203\%$$

Report 12-101 3.3.4.6-2

$$\frac{\delta_{-D_{TOP}}}{\delta_{-D_{max}}} = 0.309 < 1.0 \text{ OK}$$

$$\frac{\delta_{-D_{BOT}}}{\delta_{-D_{max}}} = 0.395 < 1.0 \text{ OK}$$

Minimum Drift Capacity Ratio:

Report 12-101 3.3.5.2

$$\mu_{C_min} := 3$$

Report 12-101
Table 6.3.5.2.1-1

$$\delta_{-C_{min}} := \left[\left[0.26 \cdot (A_r)^{0.81} \cdot \mu_{C_min} - 0.18 \cdot (A_r)^{0.57} \right] \% \right] = 1.472\%$$

$$\frac{\delta_{-C_{TOP}}}{\delta_{-C_{min}}} = 1.536 > 1.0 \text{ OK}$$

$$\frac{\delta_{-C_{BOT}}}{\delta_{-C_{min}}} = 1.524 > 1.0 \text{ OK}$$

Residual Drift

Report 12-101 3.3.4.9

$$\frac{A_l}{A_g} = 0.01$$

$$a := 0.026 \cdot \left(\frac{f_{pi}}{f_{py}} \right) + 0.047 = 0.053$$

$$b := -0.55 \cdot \left(\frac{f_{pi}}{f_{py}} \right) + 0.32 = 0.199$$

$$c := 0.36 \cdot \left(\frac{f_{pi}}{f_{py}} \right) - 0.27 = -0.191$$

Residual displacement at upper half $\delta_{r_TOP} := a \cdot \left(\frac{\delta_{-D_{TOP}}}{\%} \right)^2 + b \cdot \frac{\delta_{-D_{TOP}}}{\%} + c = 0.058 < 1\% \text{ Low residual drift column-OK}$

Residual displacement at lower half $\delta_{r_BOT} := a \cdot \left(\frac{\delta_{-D_{BOT}}}{\%} \right)^2 + b \cdot \frac{\delta_{-D_{BOT}}}{\%} + c = 0.145 < 1\% \text{ Low residual drift column-OK}$

Demand Ductility Calculations:

Report 12-101 3.3.4.6

$$\text{Top demand ductility } \mu_{D_TOP} := \frac{\frac{\delta_{D_TOP}}{\%} + 0.18 \cdot (A_T)^{0.57}}{0.26 \cdot (A_T)^{0.81}} = 2.194$$

$$\text{Bottom demand ductility } \mu_{D_BOT} := \frac{\frac{\delta_{D_BOT}}{\%} + 0.18 \cdot (A_T)^{0.57}}{0.26 \cdot (A_T)^{0.81}} = 2.653$$

Developed Seismic Shear Demand:

Report 12-101 3.3.4.8

Plastic shear developed in column

$$\frac{M_u}{\lambda \cdot M_P} = 0.929$$

If M_u (largest moment) was less than $1.2M_P$, then $1.2M_P$ was considered for design according to Report 12-101 Section 3.3.4.8.2.

$$\text{Overstrength plastic moment } M_{P0} := \lambda \cdot M_P = 1.267 \times 10^4 \cdot \text{kip} \cdot \text{ft}$$

$$\text{X direction } V_{P_X} := \frac{\lambda \cdot M_P}{\left(\frac{L - L_{P_X}}{2}\right)} = 989.887 \cdot \text{kip}$$

Shear demand from response spectrum analysis

$$\text{X direction } V_{RSA_X} := 1437 \text{kip}$$

Shear Capacity Check:

Report 12-101 3.3.5.3

Shear Capacity Design Check

AASHTO (2011) 8.6

Cross section

$$A_g := \frac{\pi}{4} \cdot D^2$$

Ductility factor for SDC D

$$\mu_D := \max(\mu_{D_BOT}, \mu_{D_TOP}) \quad \text{AASHTO (2011) 4.3.3}$$

$$\mu_D = 2.653$$

Transverse reinforcement ratio at bottom

$$\rho_s := \frac{4 \cdot a_{tr}}{D' \cdot s} = 5.598 \times 10^{-3}$$

Ratio of longitudinal reinforcement $\rho_t := \frac{n_{lr} \cdot a_{lr}}{A_g} = 0.01$

AASHTO (2011) Figure C8.6.3-1 identifies a maximum spacing of 8 inches for flexural reinforcement. This condition was not met in this example, due to the additional confinement of the FRP wrap.

Maximum allowable nominal stress in rebar $f_s := \min(\rho_s \cdot f_{yh}, 0.35 \text{ksi}) = 0.336 \cdot \text{ksi}$

$\alpha := \max\left(\frac{f_s}{0.15 \text{ksi}} + 3.67 - \mu_D, 0\right) = 3.256$

Concrete shear stress adjustment

Concrete Shear Capacity

$$A := .032 \frac{\text{in}}{\sqrt{\text{kip}}} \alpha \left(1.0 \text{ksi} + \frac{|P_f|}{2 \cdot A_g} \right) \cdot \sqrt{|f_c|} \quad B := 0.11 \cdot \sqrt{|f_c|} \cdot \frac{\text{kip}^{\cdot 5}}{\text{in}} \quad C := 0.047 \cdot \alpha \cdot \sqrt{|f_c|} \cdot \frac{\text{kip}^{\cdot 5}}{\text{in}}$$

$$v_c := \begin{cases} 0 & \text{if } P_f \geq 0 \\ \min(A, B, C) & \text{otherwise} \end{cases} = 0.22 \cdot \text{ksi}$$

Concrete portion for shear capacity $V_c := 0.8 \cdot A_g \cdot v_c = 497.628 \cdot \text{kip}$

FRP Shear Capacity $\epsilon_{fe} := \min\left(0.004, 0.75 \cdot \frac{f_{fu}}{E_f}\right) = 4 \times 10^{-3}$ Report 12-101 3.3.5.3-11

$f_{fe} := \epsilon_{fe} \cdot E_f = 76 \cdot \text{ksi}$ Report 12-101 3.3.5.3-10

$V_f := 2 \cdot n_f \cdot t_f \cdot f_{fe} \cdot (\sin(\alpha) + \cos(\alpha)) \cdot D = 729.6 \cdot \text{kip}$ Report 12-101 3.3.5.3-9

Steel Portion

Nominal capacity of shear reinforcement $V_s := \frac{\pi}{2} \cdot f_{yh} \cdot a_{tr} \cdot \frac{D'}{s} = 404.47 \cdot \text{kip}$ Report 12-101 3.3.5.3-8

$\frac{V_s + V_f}{0.25 \cdot \sqrt{\text{ksi}} \cdot |f_c| \cdot (0.8 \cdot A_g)} = 1.003 < 1.0$ **NO** Report 12-101 3.2.5.3.12

Then $V_f := 0.25 \cdot \sqrt{\text{ksi}} \cdot |f_c| \cdot (0.8 \cdot A_g) - V_s$

Total shear capacity of section $V_{\text{Capacity}} := 0.9(V_c + V_s + 0.95V_f) = 1.433 \times 10^3 \cdot \text{kip}$

$$\frac{\min(V_{RSA_x}, V_{P_x})}{V_{Capacity}} = 0.691 < 1.0 \text{ OK}$$

Overstrength plastic capacity for shear will also need to be designed in the transverse direction, but only the longitudinal direction was performed in this example. These forces would also be extended into the cross beam, superstructure, and foundations; though not shown herein.

Check the Minimum Lateral Capacity of Column:

AASHTO (2011) 8.7.1

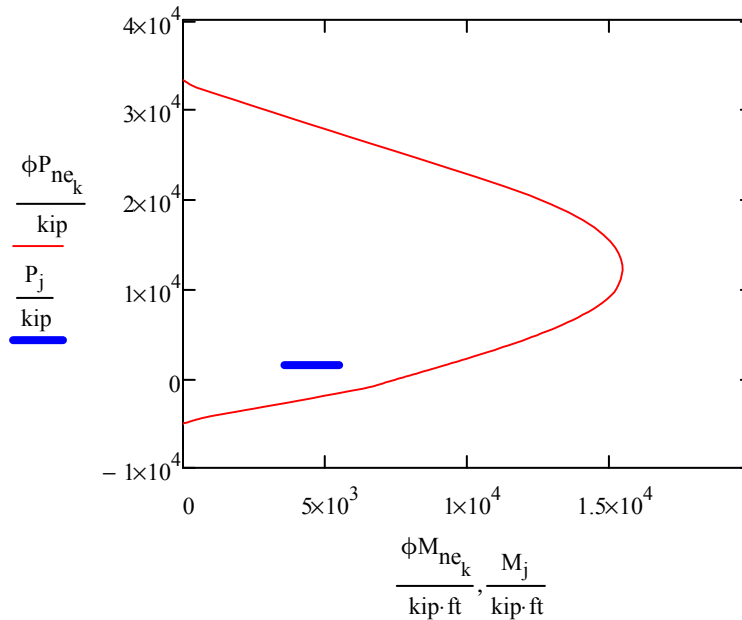
Transverse seismic (mass shared between column and abutment)

$$M_1 := 0.1 \cdot |P_f| \cdot (L + 8.5\text{ft}) \qquad P_1 := |P_f|$$

Longitudinal seismic (all mass on column-double curvature)

$$M_2 := 0.1 \cdot (2540\text{kip}) \cdot \frac{(L)}{2} = 3.556 \times 10^3 \cdot \text{kip} \cdot \text{ft} \qquad P_2 := |P_f|$$

Axial-Moment (P-M) Interaction curve was generated for the nominal expected material properties to check the minimum lateral strength of the section and to make sure that the demands were within the capacity curve.



Plot 5-12: Nominal Expected Axial-Moment (P-M) Capacity versus Demand

$$DCR_{Trans} := \frac{M_1}{\phi M_{CAP_1}} = 0.596 \quad DCR_{Long} := \frac{M_2}{\phi M_{CAP_2}} = 0.386 < 1.0 \quad \text{OK}$$

Column Type	Hybrid Rocking Column	Conventional Column
Diameter (ft)	5.0	5.0
Longitudinal Reinforcement	19-#11	22-#11
Spiral	#5@4" (Spiral)	#5@4" (Spiral)
Top Demand Drift Ratio (%)	0.99	1.18
Top Capacity Drift Ratio (%)	2.26	2.42
Bottom Demand Drift Ratio (%)	1.26	1.43
Bottom Capacity Drift Ratio (%)	2.24	2.42
Maximum Demand Drift Ratio (%)	3.20	2.73
Minimum Capacity Drift Ratio (%)	1.47	1.74
Shear Demand/Capacity Ratio	0.69	0.81
Bottom Residual Drift Ratio (%)	0.15	0.34
Top Residual Drift Ratio (%)	0.06	0.27
Overstrength Plastic Moment, M_{Po} (kip*ft)	12672	8,455

Table 5-2: Summary Table for the Hybrid Rocking Column (Longitudinal Direction Only)

Under the demand displacement of this structure, the plastic hinge rotation on the section was around 0.008 rad. The intent of these novel column was to ensure life-safety criteria will be met and either keep the structure in service after the event or restore to service quickly. The Section Analysis Program showed that at this level of rotation there was no spalling of concrete cover, the column uses about 55 percent of the rotation capacity, and the section has about 30 percent of the shear capacity left. The column is in good condition and the residual drift is low (less than 1 percent); therefore, just minor cracks might be observed on the surface of concrete cover. Columns with a residual drift ratio of 1 percent or less are categorized as "low residual displacement" according to the evaluation guidelines. Seismic testing of large-scale FRP-wrapped columns has indicated that concrete failure does not occur until fracture of the FRP wrap, which usually takes place at drift ratios substantially higher than the drift ratio demand of 1.26 percent for this column. It is unlikely that any repair would be necessary at this drift level.



NCHRP
Hybrid Rocking Column



33301 Ninth Avenue South, Suite 300 Federal
Way, Washington 98003-2600

This page is left blank intentionally.

F6 - REFERENCES

F6-1: References

AASHTO. (2014). "AASHTO LRFD Bridge Design Specifications," Washington, DC, American Association of State Highway and Transportation Officials. Seventh Edition, as amended by interim Bridge Specifications 2015 and 2016.

AASHTO. (2011). "AASHTO Guide Specifications for LRFD Seismic Bridge Design," Washington, DC, American Association of State Highway and Transportation Officials. Second Edition, as amended by interim Bridge Specifications 2012 through 2015.

REPORT 12-101. Final Report on Seismic Design of Bridge Columns with Improved Energy Dissipating Mechanisms, Infrastructure Innovation, LLC, December 2016.

Mander, J.B., M.J.N. Priestley, and R. Park. 1988. Theoretical Stress-Strain Model for Confined Concrete. Journal of Structural Engineering, v. 114. no. 22686, p. 1804-1825.

APPENDICES

NCHRP 12-101

App. A – Literature Review

App. B – Survey of State Departments of Transportation

App. C – Synthesis of Literature

App. D – Novel Column and Construction Concepts

App. E – Demonstration of Evaluation Guidelines

App. F – Detailed Design Examples for Three Novel Columns

App. G – Benefits and Economic Impact of Novel Columns

App. H – Relationship between Drift Ratio and Displacement Ductility

App. I – Modeling Methods and Validation for Novel Columns

TABLE OF CONTENTS

APPENDICES	I
TABLE OF CONTENTS.....	II
APPENDIX G.....	G-1
G.1 Introduction.....	G-2
G.2 Estimation of Cost Impact	G-2
G.2.1 Reference Reinforced Concrete Bridge	G-3
G.2.2 SMA-Reinforced ECC Bridge.....	G-4
G.2.3 Analysis Procedures	G-4
G.2.4 Analysis Results for Reinforced Concrete Bridge.....	G-6
G.2.5 Analysis Results for SMA-Reinforced ECC Bridge	G-9
G.2.6 Initial and Repair Costs for Conventional Reinforced Concrete Bridge	G-10
G.2.7 Initial and Repair Cost for SMA-Reinforced ECC Bridge.....	G-11
G.3 Qualitative Estimate of Economic Impact	G-12
G.4 References.....	G-13

APPENDIX G

Benefits and Economic Impact of Novel Columns

Qualitatively identify the benefits and potential economic impact of the proposed guidelines.

G.1 Introduction

A qualitative estimate of the benefits of new concepts can be expressed only in general terms. The common feature of novel columns is that they make possible to keep bridges in service even under strong earthquakes that could put conventional RC bridges out of commission. This feature has numerous ramifications as listed below. Placing a dollar value on benefits from each aspect require substantially detailed information, effort, budget, and time, which are beyond the scope of the current project.

The direct benefits from keeping bridges in service are:

- 1- Keeping the highway network operational after earthquakes, when the network is needed the most for emergency response traffic such as ambulances, fire trucks, damage assessment staff, etc.,
- 2- Avoiding massive traffic jams due to bridge closure,
- 3- Avoiding interruption to commerce that could have local, regional, national, and even international consequences depending on the location of the bridge,
- 4- Eliminating or substantially reducing the repair cost, and
- 5- Eliminating the need for bridge replacement.

Furthermore, keeping bridges in service through the utilization of novel materials could yield the following indirect benefits:

- 1- Instilling confidence in the general public and taxpayers in proper use of their tax dollars,
- 2- Instilling confidence in new technologies, and
- 3- Motivating bridge engineers and bridge owner in adopting new and advanced materials and structural details that deviate significantly from the normal practice.

G.2 Estimation of Cost Impact

To obtain an estimate of the cost impact, the research team decided to perform a somewhat detailed cost impact analysis focusing on one of the novel column concepts selected by the NCHRP panel to obtain an approximate benchmark. It is possible to use this result and qualitatively estimate the cost impact of using novel columns.

A representative existing reinforced concrete bridge was selected as reference and analyzed in the transverse direction to determine the possible damage expected after the earthquake and estimate the repair cost. The initial cost was calculated using available unit prices and the existing design. Another bridge, in which the concrete columns of the reference bridge would be replaced by SMA-reinforced ECC columns, was subsequently designed for the same seismic hazard and following the guidelines proposed in this study, and the initial and repair costs were also assessed. The federally mandated routine inspection cost is expected to be the same for conventional reinforced concrete and this novel column. Another component of the economic impact evaluation is the maintenance cost. However, since SMA-reinforced ECC columns are yet to be deployed in the field, there is no information on maintenance of these columns. Since SMA is not susceptible to corrosion, it is believed that the maintenance cost of SMA-reinforced ECC members would be less than or, at most, comparable to that of reinforced concrete columns. Application of SMA-steel splice in marine environment with extensive chloride exposure is not recommended since steel bar may corrode faster compared to steel-reinforced columns.

The two bridges were analyzed in the transverse direction assuming a seat-type abutment with sacrificial shear keys that act as a fuse to protect the abutment piles. The damage to the shear keys would not result in any repair cost difference between the two versions of the bridge. Longitudinal motions were not considered in the qualitative economic analysis presented in this document. Sacrificial elements under longitudinal motions are the abutment back walls that damage in the backfill soil due to movement of the superstructure. Because novel columns are generally more flexible than conventional reinforced concrete columns, they expect to impose larger displacements into the backfill, thus leading to higher backfill repair

ratio and the axial load index. The analyses were conducted along the transverse direction of the bridge only, deeming it as being the more critical direction. To obtain conservative estimates of the drift ratio demand in each bent, the column bases were assumed to be fixed and the bridge superstructure was assumed to be on rollers at abutments.

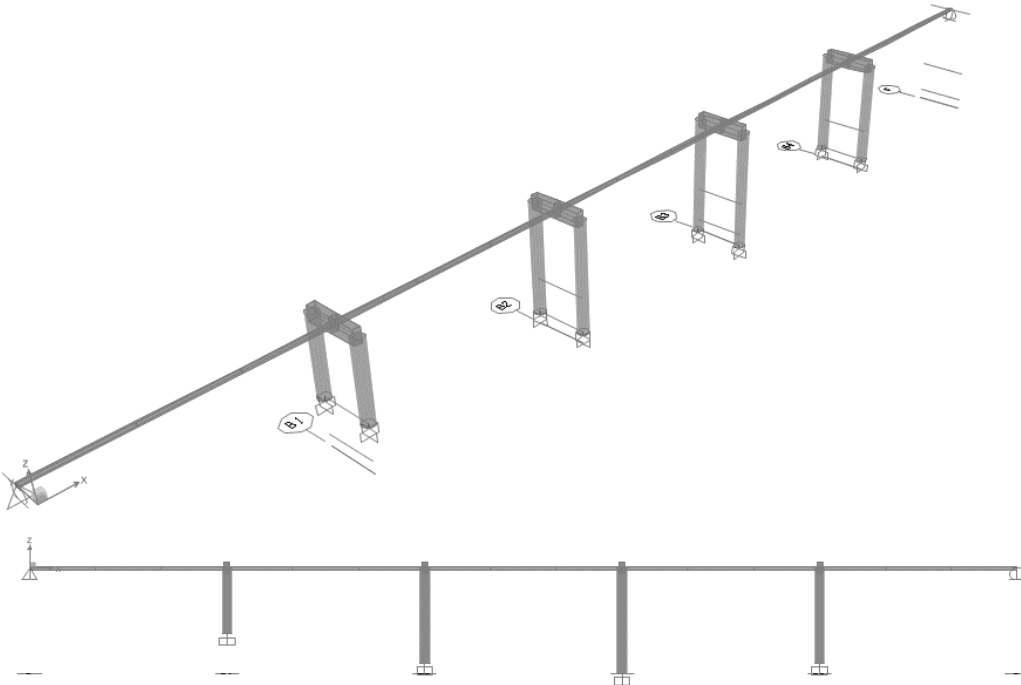


Figure G.2.3.1-1. Three-dimensional bridge model in SAP2000

The uniformly distributed dead load assigned to the superstructure was 13 kip/ft, which consisted of 11.7 kip/ft from the dead load of components (box girder self-weight plus barriers) and 1.3 kip/ft from the dead load of wearing surfaces (asphalt concrete pavement plus a utility line). Modal spectral analysis was performed to determine the seismic displacement demand on each of the bents of the reference RC bridge and the SMA-ECC bridge. This analysis was based on the design acceleration spectrum for the bridge given by the AASHTO SGS and shown in Fig. G.2.3.1-2. Twelve vibration modes were included in the analysis to guarantee a modal participating mass of 99% in total. The response was obtained using the complete quadratic modal combination method (CQC). For the SMA-reinforced ECC bridge, the response spectrum ordinates were multiplied by a factor of 1.2 to account for the lower damping ratio of SMA-ECC columns, as set forth in section 3.1.4.4 of the proposed guidelines in Chapter 3.

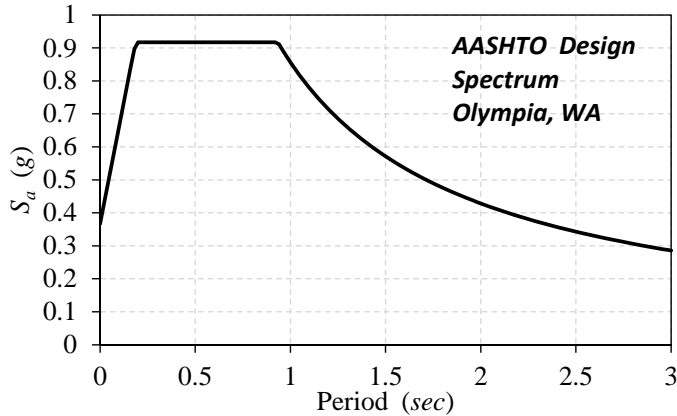


Figure G.2.3.1-2. Design response spectrum

G.2.3.2 Nonlinear Models for Each Bent

Two-dimensional nonlinear models were developed in a finite-element software, OpenSees (2016), to assess the displacement capacity of each bent accounting for both material and geometric nonlinearities. The columns were modelled as force-based distributed plasticity frame elements with fiber sections connected by a rigid link element representing the cap-beam. The fiber sections were built using appropriate constitutive stress-strain relationships for each material according to either AASHTO SGS (2014) or the proposed guidelines. The axial reactions in each column from the dead load analysis in SAP 2000 were assigned as gravity point loads at the top of each column. Each bent was subjected to an increasing lateral displacement until failure.

G.2.4 Analysis Results for Reinforced Concrete Bridge

The base shear-drift ratio pushover curves for each bent of the RC bridge are shown in Fig. G.2.4-1. Each plot shows a dotted line representing a bilinear elastic-plastic idealization of the pushover curve calculated using equivalent energy principles (AASHTO SGS). The plots also include the point where the first yield in the reinforcement takes place and the point corresponding to the drift demand calculated in the SAP 2000 model. The drift ratio demand (δ_D), the effective yield drift ratio (δ_{yi}), the residual drift ratio (δ_r), the displacement ductility capacity (μ_c), the displacement ductility demand (μ_d), the damage index (DI), and the expected damage state (DS) for each bent are listed in Table G.2.4-1. The damage index is a parameter developed by Vosooghi and Saiidi (2010) for RC columns, and in the present study measures how far into the ‘inelastic’ range each bent responds. The damage index is calculated as:

$$DI = \frac{\mu_d - 1}{\mu_c - 1} \quad (G.2.4-1)$$

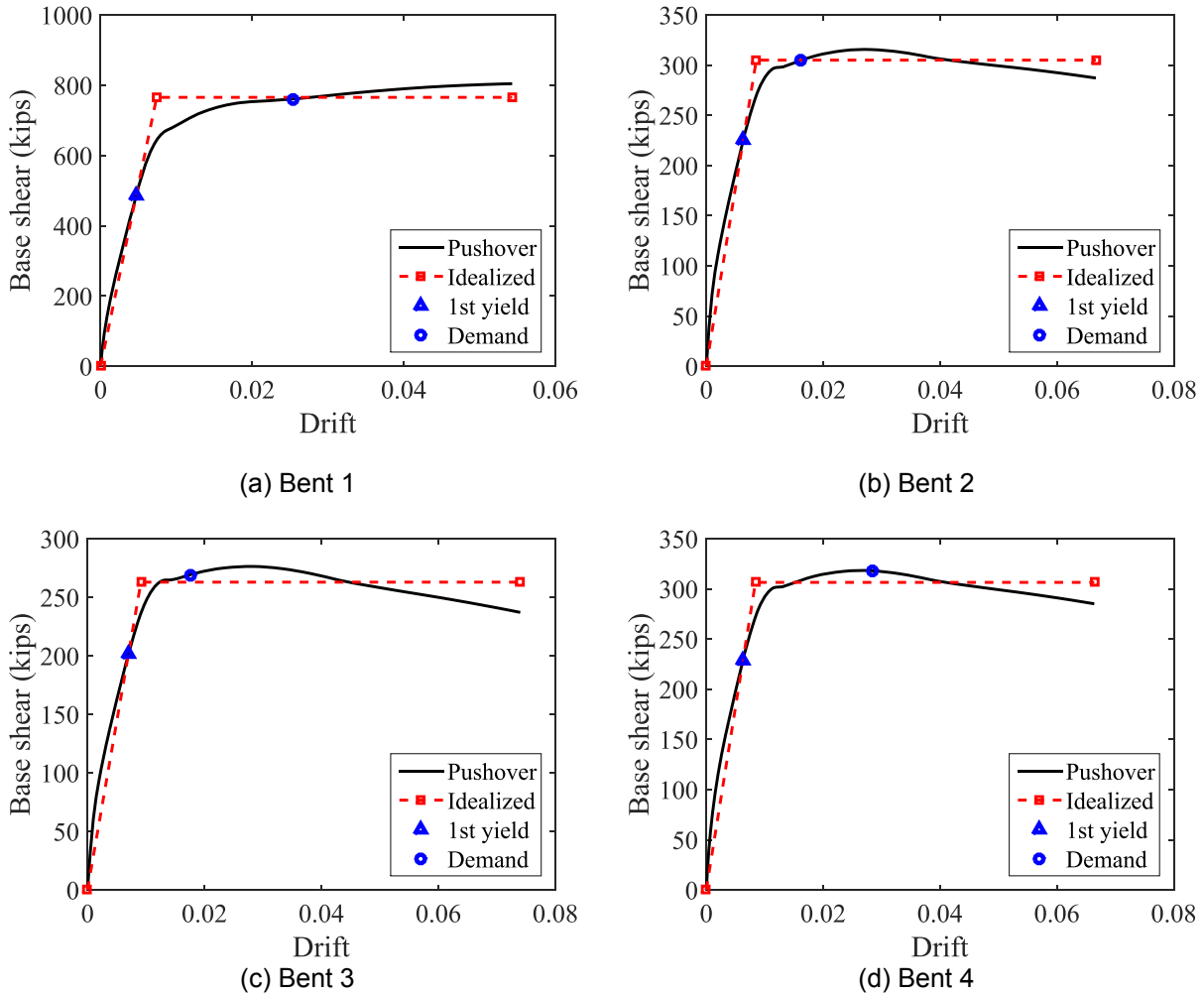


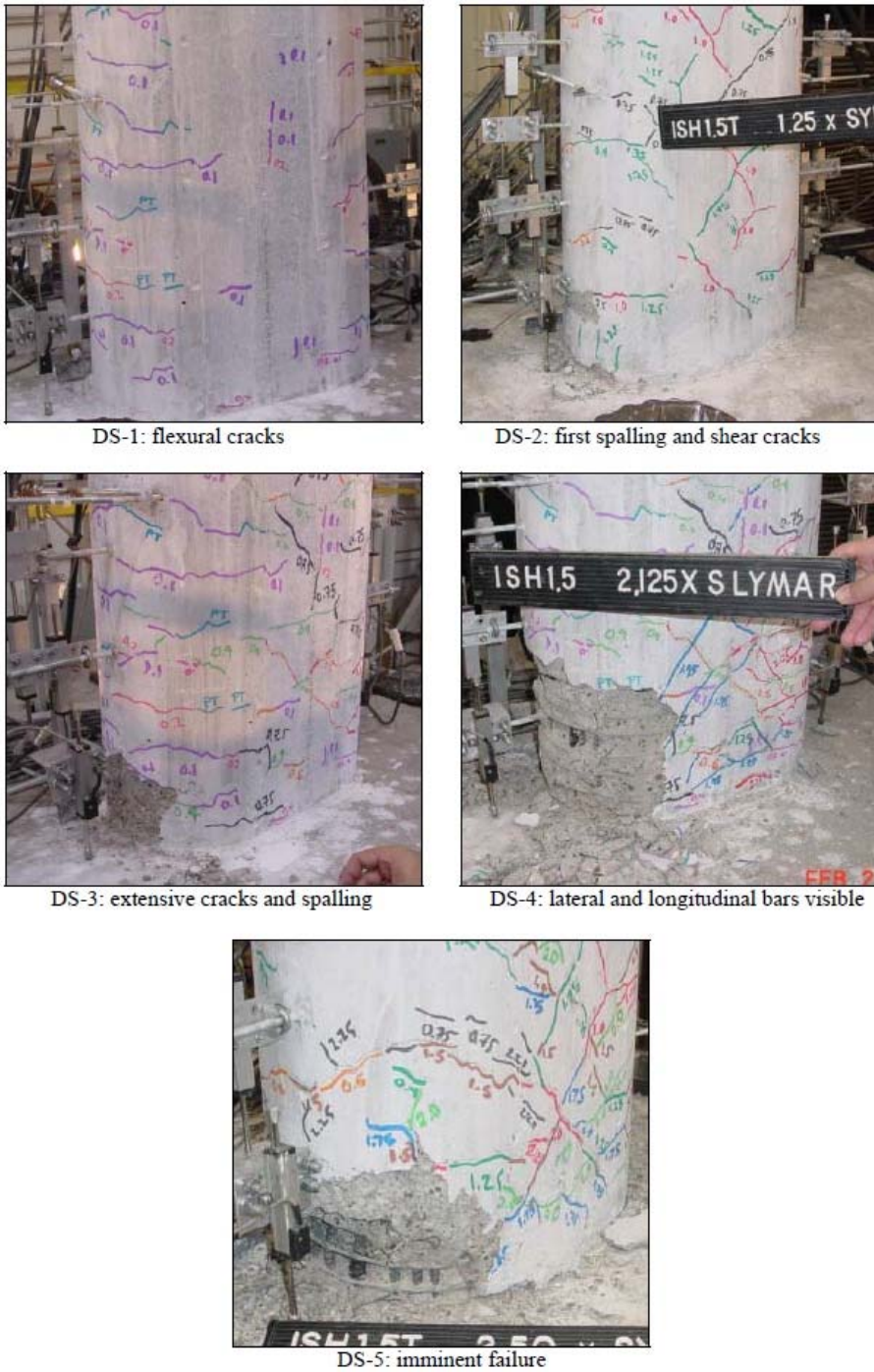
Figure G.2.4-1. Pushover curves for each bent of RC bridge

Table G.2.4-1. RC bridge analysis results and damage state for each bent

Parameter	Notation	Bent			
		1	2	3	4
Drift Ratio Demand	δ_D (%)	2.54	1.61	1.75	2.84
Effective Yield Drift Ratio	δ_{yi} (%)	0.74	0.85	0.91	0.84
Residual Drift Ratio	δ_r (%)	0.70	0.35	0.38	0.78
Displacement Ductility Capacity	μ_c	7.3	7.8	8.1	7.9
Displacement Ductility Demand	μ_d	3.4	1.9	1.9	3.4
Damage Index	DI	0.38	0.13	0.13	0.35
Damage State	DS	3	2	2	3

The maximum damage index is one, which corresponds to failure. A zero damage index indicates that the bent drift and base shear are at the effective yield point. When the index is negative, the bent is in the

elastic range. Vosooghi and Saiidi (2010) correlated different damage indexes with the expected damage states of RC bridge columns, DS-1 to DS-5, as shown in Fig. G.2.4-2. Damage states DS-2, DS-3, DS-4, and DS-5 correspond according to Vosooghi and Saiidi (2010), approximately to damage indexes of 0.15, 0.35, 0.55, and 0.80, respectively. The damage states in Table G.2.4-1 were defined for each bent according to these reference values.



Source: Vosooghi and Saiidi (2010)

Figure G.2.4-2. Damage states for RC bridge columns

The residual drifts reported in Table G.2.4-1 were calculated using the formula developed by Ardakani and Saiidi (2013), equation 2.5.3-1 from Chapter 2. Since the residual drift in all bents is less than 1%, there is no loss of functionality under the design earthquake because the permanent tilting of the column is relatively small. However, as shown in Fig. G.2.4-2, the damage at the plastic hinges would require repair consisting of epoxy injection in the cracks, patching the spalled zones with repair mortar, and wrapping the plastic hinge with FRP fabrics.

G.2.5 Analysis Results for SMA-Reinforced ECC Bridge

The base shear-drift ratio pushover curves for each bent of the SMA-reinforced ECC bridge are shown in Fig. G.2.5-1. The drift ratio demand (δ_D), the drift ratio capacity (δ_c), and the effective yield drift ratio ($\delta_{y,i}$) for each bent are listed in Table G.2.5-1. Since the damage index concept and damage states utilized for the RC bridge are not applicable to the SMA-reinforced ECC bridge, the assessment of the extent of damage was done by examining the calculated ECC cover and confined core strains for each bent at the demand drift level and exercising judgment. It is known that ECC, unlike concrete, does not spall, which means that there is no patching or FRP wrapping required to repair damaged ECC plastic hinges. It was found that epoxy injection will be needed in all of the plastic hinges in bents 1 and 4 and two of the hinges in bent 2 and bent 3.

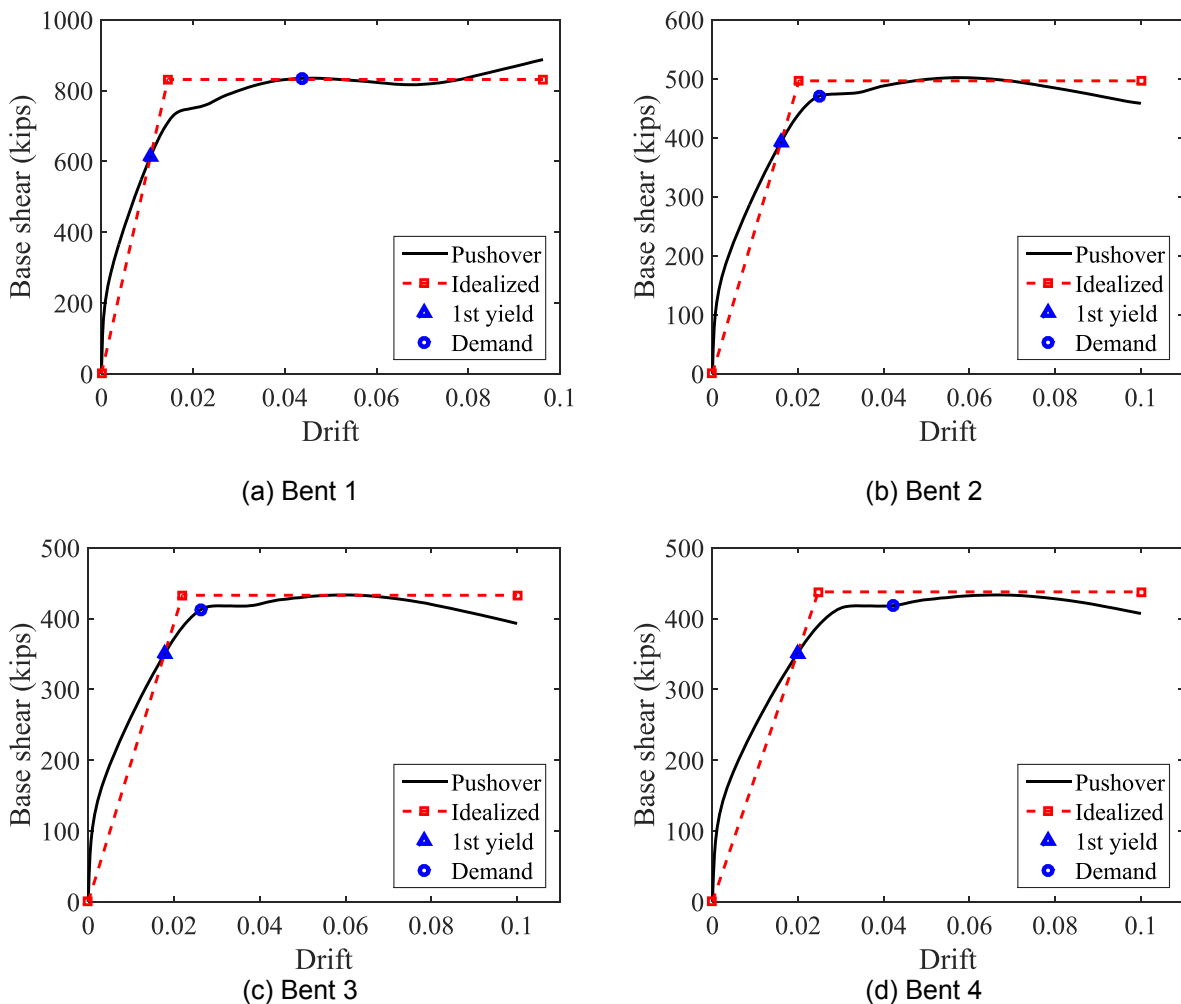


Figure G.2.5-1. Pushover curves for each bent of the SMA-reinforced ECC bridge

Table G.2.5-1. SMA reinforced ECC bridge analysis results

Parameter	Notation	Bent			
		1	2	3	4
Drift Ratio Demand	δ_D (%)	4.38	2.49	2.62	4.21
Effective Yield Drift Ratio	δ_{yi} (%)	1.45	2.02	2.22	2.47
Drift Ratio Capacity	δ_c (%)	9.63	10	10	10

G.2.6 Initial and Repair Costs for Conventional Reinforced Concrete Bridge

The initial cost of the bridge was calculated based on the upper bound unit costs reported in Chapter 12 “Quantities, Costs and Specifications” of the Bridge Design Manual LRFD M 23-50 of the Washington Department of Transportation (2016). The cost breakdown is shown in Table G.2.6-1 for a total initial cost of approximately 7.6 million dollars, not including labor, equipment, and design and consulting fees.

Table G.2.6-1. Initial cost of RC bridge

Initial cost of RC Bridge

1. Substructure

LOCATION	ITEM	UNIT	UNIT COST	QTY	MEASUREMENT EA	COST
Abutment	Excavation Class A Incl Haul - Earth	CY	\$30	2	681.48	\$40,889
Abutment	Pile tip (CIP concrete with steel casing - short tip)	EACH	\$250	24	1	\$6,000
Abutment	Soil excavation for shaft including haul	CY	\$600	24	5.82	\$83,776
Abutment	Placing permanent casing for shaft	EACH	\$3,000	24	1	\$72,000
Abutment	Concrete class 4000P (CIP piling)	CY	\$250	24	5.82	\$34,907
Abutment	Concrete class 4000 (footings)	CY	\$600	2	186.67	\$224,000
Pier foundation	Excavation Class A Incl Haul - Earth	CY	\$30	4	355.56	\$42,667
Pier foundation	Cofferdam	SF	\$30	4	1184	\$142,080
Pier foundation	Pile tip (CIP concrete with steel casing - short tip)	EACH	\$250	72	1	\$18,000
Pier foundation	Soil excavation for shaft including haul	CY	\$600	72	5.82	\$251,327
Pier foundation	Placing permanent casing for shaft	EACH	\$3,000	72	1	\$216,000
Pier foundation	Concrete class 4000P (CIP piling)	CY	\$250	72	5.82	\$104,720
Pier foundation	Concrete class 4000 (footings)	CY	\$600	4	195.56	\$469,333
Bent 1 columns	Concrete class 4000	CY	\$400	2	13.96	\$11,170
Bent 1 columns	Longitudinal reinforcement - #11 Gr. 60	LBS	\$1.30	56	212.52	\$15,471
Bent 1 columns	Transverse reinforcement - #5@2.125" (assumed)	LBS	\$1.30	2	1945.2	\$5,057
Bent 2 columns	Concrete class 4000	CY	\$400	2	20.94	\$16,755
Bent 2 columns	Longitudinal reinforcement - #10 Gr. 60	LBS	\$1.30	40	236.665	\$12,307
Bent 2 columns	Transverse reinforcement - #5@3" (assumed)	LBS	\$1.30	2	2132.2	\$5,544
Bent 3 columns	Concrete class 4000	CY	\$400	2	23.27	\$18,617
Bent 3 columns	Longitudinal reinforcement - #10 Gr. 60	LBS	\$1.30	40	258.18	\$13,425
Bent 3 columns	Transverse reinforcement - #5@3" (assumed)	LBS	\$1.30	2	2369.1	\$6,160
Bent 4 columns	Concrete class 4000	CY	\$400	2	20.94	\$16,755
Bent 4 columns	Longitudinal reinforcement - #10 Gr. 60	LBS	\$1.30	40	236.665	\$12,307
Bent 4 columns	Transverse reinforcement - #5@3" (assumed)	LBS	\$1.30	2	2132.2	\$5,544

2. Superstructure

LOCATION	ITEM	UNIT	UNIT COST	QTY	MEASUREMENT EA	COST
Superstructure	RC box girder (water crossing w/piling)	SF	\$250.00	1	21500	\$5,375,000.00
Superstructure ends	Bridge approach slab	SF	\$250.00	2	860	\$430,000.00

TOTAL COST = \$7,649,809

An accurate estimation of the repair cost of the structure would require a detailed assessment of the damage, the site and structure conditions, and other factors such as traffic control, environmental impact and stream protection, construction of cofferdams, special inspection, and the need for specialized labor such as divers for the repair of underwater plastic hinges and equipment such as under bridge inspection trucks, among others. Such an analysis is beyond of the scope of this study. Nonetheless, an expert contractor with extensive experience in repair of bridges and building structures who is also closely familiar

with ECC was consulted to provide an approximate estimate for the repair cost of the damaged plastic hinges in this study. The expert estimated that each RC plastic hinge would require four work days for the cracks to be injected with epoxy and the spalled zones to be repaired with mortar, assuming a three-man crew with a daily cost of \$3,000 including supplies and consumables and \$1,000 of direct material cost. It was also the expert’s opinion that the FRP wrapping would require one day of work with the same crew at \$3,000 daily rate plus \$2,000 of material cost. This would result in a total cost of \$13,000 for the epoxy injection and mortar repair, and \$5,000 for FRP wrapping per plastic hinge. Utilizing these unit costs the repair cost of the RC bridge was estimated at \$248,000, as shown in Table G.2.6-2. For expedited repair that require 24/7 work, the cost could increase by 40%, changing the repair cost to approximately \$350,000, which is 4.6% of the initial cost of the RC bridge. The total initial and repair cost for the RC bridge is approximately \$8M.

Table G.2.6-2. Repair cost of RC bridge

Repair cost of RC Bridge

LOCATION	ITEM	UNIT	UNIT COST	QTY	MEASUREMENT EA	COST
Bent 1 plastic hinges	Epoxy injection in the cracks and mortar repair for spalled concrete	EACH	\$13,000	4	1	\$52,000
Bent 1 plastic hinges	FRP wrapping	EACH	\$5,000	4	1	\$20,000
Bent 2 plastic hinges	Epoxy injection in the cracks and mortar repair for spalled concrete	EACH	\$13,000	4	1	\$52,000
Bent 3 plastic hinges	Epoxy injection in the cracks and mortar repair for spalled concrete	EACH	\$13,000	4	1	\$52,000
Bent 4 plastic hinges	Epoxy injection in the cracks and mortar repair for spalled concrete	EACH	\$13,000	4	1	\$52,000
Bent 4 plastic hinges	FRP wrapping	EACH	\$5,000	4	1	\$20,000

TOTAL REPAIR COST = \$248,000

G.2.7 Initial and Repair Cost for SMA-Reinforced ECC Bridge

The initial cost of the bridge was calculated based on the same unit prices as the RC bridge, but including the updated quantities for the materials and the unit costs for ECC and SMA reported in Appendix C. As shown in Table G.2.7-1, the total initial cost for the SMA-reinforced ECC bridge was estimated at approximately 8.5 million dollars, not including labor, equipment, and design and consulting fees. This initial cost represents an 11.5% increase over the initial cost of the RC bridge. The repair expert consulted was of the opinion that since there is no FRP wrapping or grout patching needed for ECC plastic hinges, and considering the multiple fine cracks that tend to form in ECC, the repair cost per plastic hinge would be approximately \$4,000 per column, which is one-third of the repair cost for the RC plastic hinges. As shown in Table G.2.7-2, the total repair cost for the SMA-reinforced ECC bridge was estimated at \$48,000, which is 80% lower than the repair cost of the RC bridge. With a surcharge of 40% for expedited repair, the repair cost changes to \$67,000, which is less than 1% of the initial cost of the SMA/ECC bridge. The total initial and repair cost for the SMA/ECC bridge is approximately \$8.6M, or a 7.4% increase over the corresponding cost of the RC bridge.

Considering the high performance and resiliency of SMA and ECC compared to reinforced concrete, the 7.4% difference between the initial plus repair cost of the RC bridge relative to the initial cost of the novel bridge does not seem to be as significant. This is further discussed in the next section.

Table G.2.7-1. Initial cost of SMA-reinforced ECC bridge

Initial cost of SMA-ECC Bridge

1. Substructure

LOCATION	ITEM	UNIT	UNIT COST	QTY	MEASUREMENT EA	COST
Abutment	Excavation Class A Incl Haul - Earth	CY	\$30	2	681.48	\$40,889
Abutment	Pile tip (CIP concrete with steel casing - short tip)	EACH	\$250	24	1	\$6,000
Abutment	Soil excavation for shaft including haul	CY	\$600	24	5.82	\$83,776
Abutment	Placing permanent casing for shaft	EACH	\$3,000	24	1	\$72,000
Abutment	Concrete class 4000P (CIP piling)	CY	\$250	24	5.82	\$34,907
Abutment	Concrete class 4000 (footings)	CY	\$600	2	186.67	\$224,000
Pier foundation	Excavation Class A Incl Haul - Earth	CY	\$30	4	355.56	\$42,667
Pier foundation	Cofferdam	SF	\$30	4	1184	\$142,080
Pier foundation	Pile tip (CIP concrete with steel casing - short tip)	EACH	\$250	72	1	\$18,000
Pier foundation	Soil excavation for shaft including haul	CY	\$600	72	5.82	\$251,327
Pier foundation	Placing permanent casing for shaft	EACH	\$3,000	72	1	\$216,000
Pier foundation	Concrete class 4000P (CIP piling)	CY	\$250	72	5.82	\$104,720
Pier foundation	Concrete class 4000 (footings)	CY	\$600	4	195.56	\$469,333
Bent 1 columns	Concrete class 4000	CY	\$400	2	10.91	\$8,727
Bent 1 columns	Longitudinal reinforcement - #14 Gr. 60	LBS	\$1.30	56	248.625	\$18,100
Bent 1 columns	Transverse reinforcement - #6@3"	LBS	\$1.30	2	2589.6	\$6,733
Bent 1 plastic hinges	4000 psi ECC	CY	\$250	4	10.91	\$10,908
Bent 1 plastic hinges	Longitudinal reinforcement - #11 SMA	LBS	\$105	56	32.7	\$192,354
Bent 2 columns	Concrete class 4000	CY	\$400	2	21.82	\$17,453
Bent 2 columns	Longitudinal reinforcement - #14 Gr. 60	LBS	\$1.30	56	363.375	\$26,454
Bent 2 columns	Transverse reinforcement - #6@3"	LBS	\$1.30	2	3884.4	\$10,099
Bent 2 plastic hinges	4000 psi ECC	CY	\$250	4	10.91	\$10,908
Bent 2 plastic hinges	Longitudinal reinforcement - #11 SMA	LBS	\$105	56	32.7	\$192,354
Bent 3 columns	Concrete class 4000	CY	\$400	2	25.45	\$20,362
Bent 3 columns	Longitudinal reinforcement - #14 Gr. 60	LBS	\$1.30	56	401.625	\$29,238
Bent 3 columns	Transverse reinforcement - #6@3"	LBS	\$1.30	2	4316.0	\$11,221
Bent 3 plastic hinges	4000 psi ECC	CY	\$250	4	10.91	\$10,908
Bent 3 plastic hinges	Longitudinal reinforcement - #11 SMA	LBS	\$105	56	32.7	\$192,354
Bent 4 columns	Concrete class 4000	CY	\$400	2	21.82	\$17,453
Bent 4 columns	Longitudinal reinforcement - #14 Gr. 60	LBS	\$1.30	56	363.375	\$26,454
Bent 4 columns	Transverse reinforcement - #6@3"	LBS	\$1.30	2	3884.4	\$10,099
Bent 4 plastic hinges	4000 psi ECC	CY	\$250	4	10.91	\$10,908
Bent 4 plastic hinges	Longitudinal reinforcement - #11 SMA	LBS	\$105	56	32.7	\$192,354

2. Superstructure

LOCATION	ITEM	UNIT	UNIT COST	QTY	MEASUREMENT EA	COST
Superstructure	RC box girder (water crossing w/piling)	SF	\$250.00	1	21500	\$5,375,000.00
Superstructure ends	Bridge approach slab	SF	\$250.00	2	860	\$430,000.00

TOTAL COST = \$8,526,139

Table G.2.7-2. Repair cost of SMA-reinforced ECC bridge

Repair cost of SMA-ECC bridge

LOCATION	ITEM	UNIT	UNIT COST	QTY	MEASUREMENT EA	COST
Bent 1 plastic hinges	Epoxy injection in the cracks	EACH	\$4,000	4	1	\$16,000
Bent 2 plastic hinges	Epoxy injection in the cracks	EACH	\$4,000	2	1	\$8,000
Bent 3 plastic hinges	Epoxy injection in the cracks	EACH	\$4,000	2	1	\$8,000
Bent 4 plastic hinges	Epoxy injection in the cracks	EACH	\$4,000	4	1	\$16,000

TOTAL COST = \$48,000

G.3 Qualitative Estimate of Economic Impact

The aforementioned analysis was based on the design earthquake loading. Had a stronger earthquake level been considered, the damage states in the RC bridge would change from DS-3 to DS-5 thus approximately doubling the repair cost for the RC bridge, whereas the incremental repair cost for the SMA-reinforced bridge would be perhaps 50% more. This would further reduce the 7.4% cost difference to approximately 3.3%. The cost increase may be eliminated or even turn into cost reduction when considering that the RC bridge has to be closed to traffic for a potentially long period, thus increasing the user cost due to the traffic congestion and detours significantly. A comprehensive evaluation of the user cost impact is

beyond the scope of the current project. However, it is useful to estimate the user cost impact of bridge closure assuming that the bridge discussed in the previous section is in an urban area with a moderate average daily traffic (ADT) of 15,000 with a peak hour ADT of 3,000. It is further assumed that taking the detour due to bridge closure adds 30 minutes and 15 minutes to travel time during the peak and non-peak hours, respectively. The added traffic on the detour route is likely to increase travel time for the traffic that normally takes that route. However, this increase in user cost is ignored to simplify the cost impact analysis. Cost models are available to estimate the value of user time for cost impact analysis in pavement and transportation engineering. A model presented in Caltrans (2013) puts the time value of automobile and truck drivers at \$13/hour and \$29.60/hour, respectively. Assuming that 80% of the traffic in the example bridge is due to automobiles, the average user cost is approximately \$16/hour. Using a user cost of \$16/hour and assuming a single driver per vehicle, the daily increase in the user cost associated with the bridge closure is estimated at \$24,000 and \$48,000 for the peak and non-peak hour traffic, respectively, for a total of \$72,000 per day. This figure could be substantially higher in large urban areas with higher ADT and longer detours. Assuming that bridge closure duration to repair the RC and SMA/ECC is 30 days, and 7 days, respectively, the total initial, repair, and user cost for the RC bridge is \$10.6M and that for the SMA/ECC bridge \$9.13M, or a 13% reduction.

The use of novel columns is likely to eliminate the need for bridge replacement should a very strong earthquake occur that brings the RC bridge near collapse. In such a case, substantial saving is realized by eliminating the cost of a new bridge.

The cost difference for SMA-reinforced FRP jacketed columns is expected to be comparable to that for SMA-reinforced ECC columns. However, the different for the hybrid rocking columns might be lower when steel tendons are used. Considering the concern for corrosion of unbonded steel tendons, one might choose the CFRP (carbon fiber reinforced polymer) tendon alternative for post-tensioning. Research data on columns with these tendons is scarce, but is promising. The cost of CFRP tendons for column application is yet to be established, but it is known that the combined cost of CFRP tendons and anchorage exceeds that for steel tendons.

In the absence of a more detailed analysis of the initial and repair cost impact of using novel concepts in bridge plastic hinges and based on the above discussion, it appears that a qualitative estimate of the economic impact based on the initial and repair cost is in the range of 5 to 10%.

An economic impact analysis based on the initial and repair cost does not capture other potentially substantial savings associated with no or shorter bridge closure. The primary beneficiary of the faster recovery from the earthquake is the travelling public. The national trend in extensive deployment of accelerated bridge construction (ABC) methods is driven primarily by the desire to better serve the public by faster project delivery. In that respect, the resilience of novel bridge columns has much in common with ABC. The primary direct benefit from using novel columns is the speed by which the bridge service can be resorted. This is expected to reduce substantially user costs, traffic control, and construction zone safety risk. The quantification of these benefits is subject to many factors that vary depending on the bridge location, average daily traffic, right of way, among others. Should the cost of saving in traffic control, user costs, and impact on other aspects of prolonged repair of conventional RC bridges be included, the 5 to 10% increase in the initial and repair cost could be overshadowed by these savings resulting in saving in the overall cost.

In summary, the use of SMA/ECC could increase the initial cost by 5 to 10%. However, when the user cost due to bridge closure after an earthquake is considered, there can be more than 10% saving in the overall cost.

G.4 References

1. AASHTO (2014). "AASHTO Guide Specifications for LRFD Seismic Bridge Design," Washington, DC: American Association of State Highway and Transportation Officials.

2. Ardakani, S.M.S. and Saiidi, M.S. (2013). "Design of Reinforced Concrete Bridge Columns for Near-Fault Earthquakes," Center for Civil Engineering Earthquake Research, Department of Civil and Environmental Engineering, University of Nevada, Reno, Nevada, Report No. CCEER-13-13, 393 pp.
3. Caltrans (2013). <http://www.dot.ca.gov/hq/maint/Pavement/Offices/Pavement_Engineering/LCCA_index.html>, Life-Cycle Cost Analysis.
4. Computers and Structures, Inc. (2011). "SAP2000 Nonlinear Version 15.1.0", Berkeley, CA.
5. MCEER/ATC (2003). "Recommended LRFD Guidelines for the Seismic Design of Highway Bridges," MCEER/ATC-49, MCEER/ATC Joint Venture, NCHRP 12-49 Project Team.
6. OpenSees (2016). <<http://opensees.berkeley.edu/index.php>>, OpenSees 2.5.0.
7. Vosooghi, A. and Saiidi, M.S. (2010). "Post-Earthquake Evaluation and Emergency Repair of Damaged RC Bridge Columns Using CFRP Materials," Center for Civil Engineering Earthquake Research, Department of Civil and Environmental Engineering, University of Nevada, Reno, Nevada, Report No. CCEER-10-05, 679 pp.
8. Washington Department of Transportation. (2016). "Bridge Design Manual LRFD M 23-50.16," Olympia, Washington

APPENDICES

NCHRP 12-101

App. A – Literature Review

App. B – Survey of State Departments of Transportation

App. C – Synthesis of Literature

App. D – Novel Column and Construction Concepts

App. E – Demonstration of Evaluation Guidelines

App. F – Detailed Design Examples for Three Novel Columns

App. G – Benefits and Economic Impact of Novel Columns

App. H – Relationship between Drift Ratio and Displacement Ductility

App. I – Modeling Methods and Validation for Novel Columns

TABLE OF CONTENTS

APPENDICES	I
TABLE OF CONTENTS.....	II
APPENDIX H.....	H-1
H.1 Introduction.....	H-2
H.2 Methodology	H-2
H.3 Model Verification.....	H-3
H.4 Parametric Study.....	H-4
H.4.1 Parameters	H-4
H.4.2 Results	H-6
H.5 Proposed Drift-Ductility Equations	H-8
H.6 References.....	H-9

APPENDIX H

Relationship between Drift Ratio and Displacement Ductility

H.1 Introduction

Displacement ductility is not necessarily a suitable criterion to evaluate the deformation capacity of novel bridge columns since the effective “yield” displacement in novel columns may exceed that of conventional columns, which could lead to a smaller displacement ductility capacity, whereas the novel column may have a displacement capacity that exceeds that of conventional columns. This could be misleading and, unless closely examined, leads to a false conclusion about the seismic performance of novel columns. For example, displacement capacity of a SMA-reinforced column may be twice a conventional reinforced concrete (RC) column displacement capacity, but, because yield strain of SMA is greater than steel yield strain, the idealized yield displacement of an SMA-reinforced column is relatively large and its displacement ductility (the ratio of the ultimate displacement to the idealized yield displacement) may be lower than that of a conventional RC member. One solution is to use drift ratio (the ratio of the column lateral displacement to the column height) to fairly compare the seismic performance of novel columns with conventional columns. Because current bridge seismic design codes for conventional RC columns mostly utilize displacement ductility, simple equations to convert displacement ductilities to drift ratios were developed for RC columns in the current study. The equations provide an option to engineers who are more comfortable to utilize displacement ductility in design. This section describes the process to develop the equations.

H.2 Methodology

The AASHTO Guide Specifications for LRFD Seismic Bridge Design (AASHTO SGS) (2014) allow design of reinforced concrete (RC) columns based on moment-curvature analysis (Fig. H-1). Concrete and steel material models are presented in the code with the specified and expected material properties. Fiber section models are usually used to perform moment-curvature analysis. Then the curvature is converted to the column tip displacement. Subsequently, the ductility is calculated as the ratio of the column ultimate displacement to the idealized yield displacement. The ultimate point is usually defined as a point where the concrete core fails in compression (when the extreme core concrete fiber strain is 1.5 times the calculated strain capacity), the reinforcing bars fracture, or the resisting moment or the lateral load capacity drops by 15% with respect to its peak. The displacement ductility capacity (μ_c) of a column can be calculated as:

$$\mu_c = 1 + 3\left(\frac{\phi_u}{\phi_{yi}} - 1\right) \frac{L_p}{L} \left(1 - 0.5 \frac{L_p}{L}\right) \quad (\text{H-1})$$

where L is the length of column from point of maximum moment to the point of contraflexure. The idealized yield curvature (ϕ_{yi}) is calculated by equating the area under the actual moment-curvature curve to the area under the idealized curve from yield point to the ultimate point (Fig. H-1). L_p is the plastic hinge length:

$$L_p = 0.08L + 0.15f_{ye}d_{bt} \geq 0.3f_{ye}d_{bt} \quad (\text{H-2})$$

where f_{ye} (ksi) is the expected yield strength of the longitudinal column reinforcing steel bars and d_{bt} (in.) is the nominal diameter of longitudinal column reinforcing steel bars.

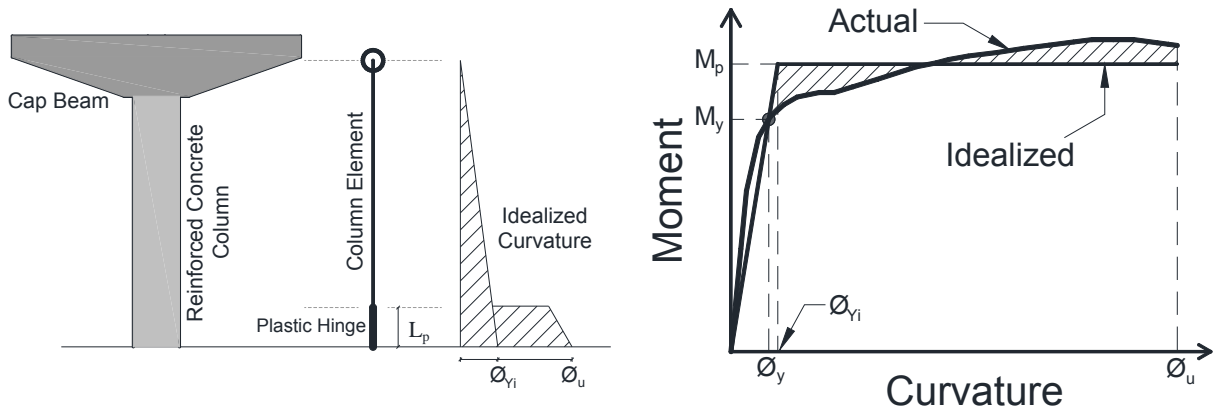


Figure H-1. AASHTO displacement-based design method

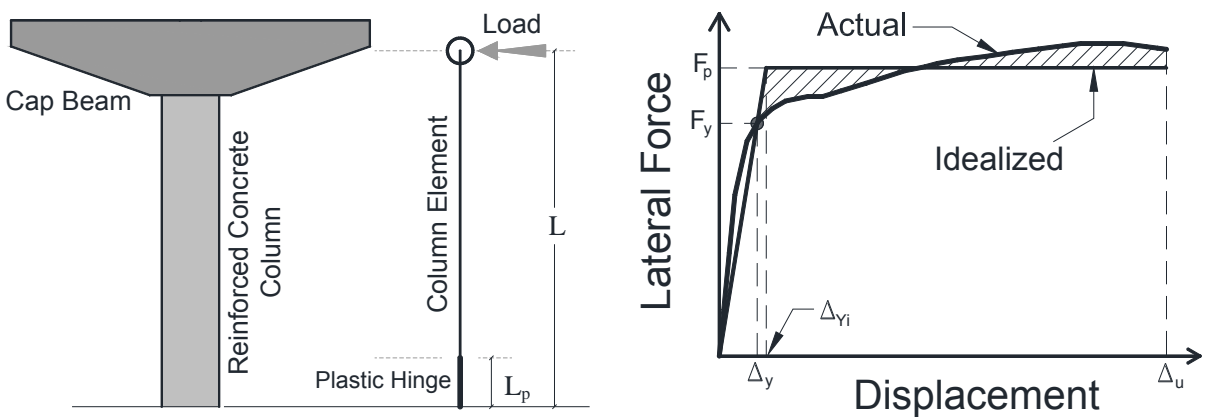


Figure H-2. Pushover analysis for design of RC columns

Pushover analysis is also allowed by the code for design of RC columns, which is more reliable than the moment-curvature analysis since displacements are directly calculated usually including $P - \Delta$ effects and system effects in general cases. The pushover analysis (Fig. H-2) was used in the present study to establish relationship between the displacement ductility capacity (μ_c) and the drift ratio capacity (δ_c), which is the ratio of the column lateral ultimate displacement to the column height.

$$\mu_c = \frac{\Delta_u}{\Delta_{yi}} \quad (H-3)$$

and

$$\delta_c = \frac{\Delta_u}{L} \quad (H-4)$$

H.3 Model Verification

A half-scale RC bridge column was tested by Haber et al. (2013) in which the column diameter was 2 ft and the column height was 9 ft. The column was longitudinally reinforced with 11-#8 steel bars and transversely with #3 spiral at 2 in. pitch. The applied axial load was 200 kips resulting in an approximately 10% axial load index (the ratio of the applied axial load to the product of the specified compressive concrete strength and the column gross-section area). OpenSees (2013), an open source finite element software, was utilized for simulations. A fiber-section model was used with a distributed plasticity element with five

integration points. Fig. H-3 shows the measured and calculated force-drift hysteresis and pushover response. It can be seen that the model was able to successfully reproduce the column behavior. Detailed information regarding the column and modeling method can be found in Tazarv and Saiidi (2014).

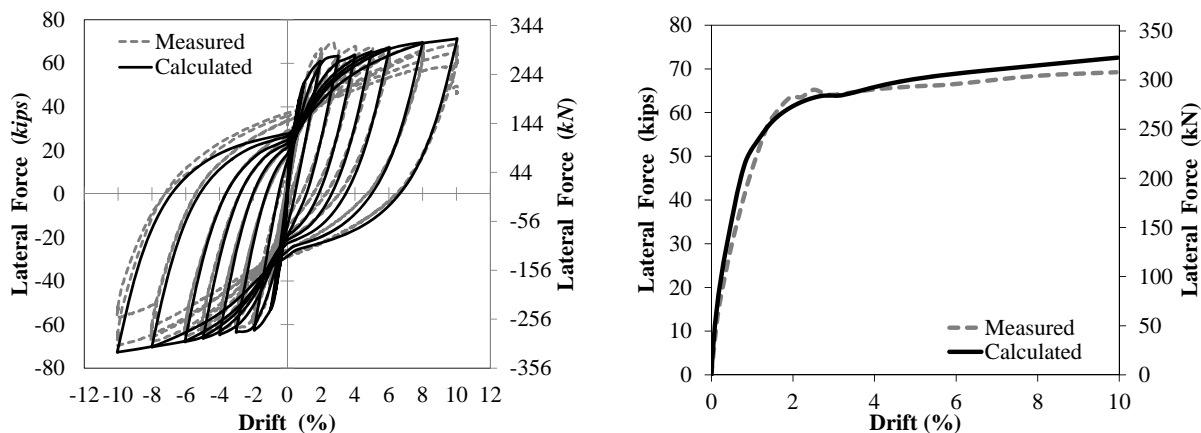


Figure H-3. Model verification for a half-scale bridge column

This analytical model was used as the base model for further analyses but excluding the bond-slip effect since this effect is usually ignored in practice. Furthermore, the material properties were adjusted based on the AASHTO SGS (2014).

H.4 Parametric Study

H.4.1 Parameters

An extensive parametric study was performed to determine the relationship between the displacement ductility and drift ratio of conventional RC columns. The variables were eight longitudinal steel ratios (1, 1.25, 1.5, 1.75, 2, 2.25, 2.5, and 2.75%), 11 volumetric transverse steel ratios (0.08, 0.25, 0.5, 0.75, 1, 1.25, 1.5, 1.75, 2, 2.25 and 2.5%), three axial load indices (5, 10, and 15%), three aspect ratios (4, 6, 8), and three compressive strengths for concrete (4, 5, and 6 *ksi*). ASTM A706 Grade 60 steel bars were assumed in all columns. Two column diameters, 4 *ft* and 5 *ft*, were assumed then the column height were adjusted based on the aspect ratio. Standard bar sizes were used to achieve steel ratios that were close to the target ratios.

Totally, 696 RC columns were designed. One sample result is shown in Fig. H-4 for a column with 4-*ft* diameter, 24-*ft* height, 1% longitudinal steel ratio (18-#9), 1% volumetric transverse steel ratio (#6 hoops at 4-*in.* pitch), and 10% axial load index (905-*kip* axial load). The compressive strength of the concrete was 5 *ksi* and the expected steel properties were based on the AASHTO SGS (2014).

To further validate the results, the displacement ductility was calculated utilizing moment-curvature analysis according to the code. Fig. H-5 shows the moment-curvature relationship and Table H-1 presents a summary of the calculations. It can be seen that both methods (pushover and moment-curvature) resulted in close estimation of the displacement ductility capacity with 8% difference (7.19 vs. 7.77). The differences in the drift ratios are attributed to the approximation in the plastic hinge length.

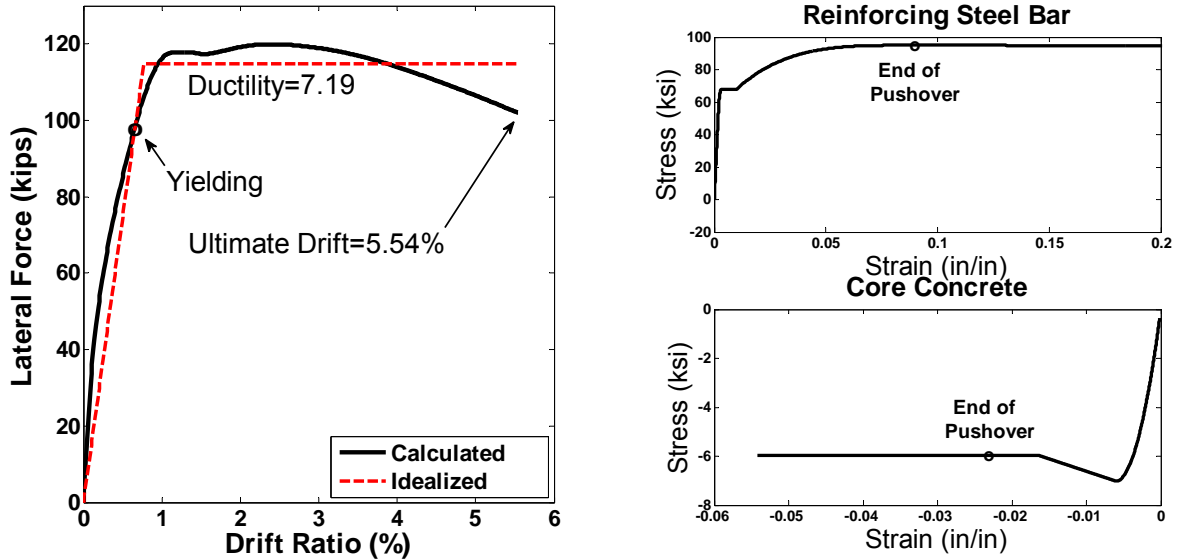


Figure H-4. Sample of column design using pushover analysis

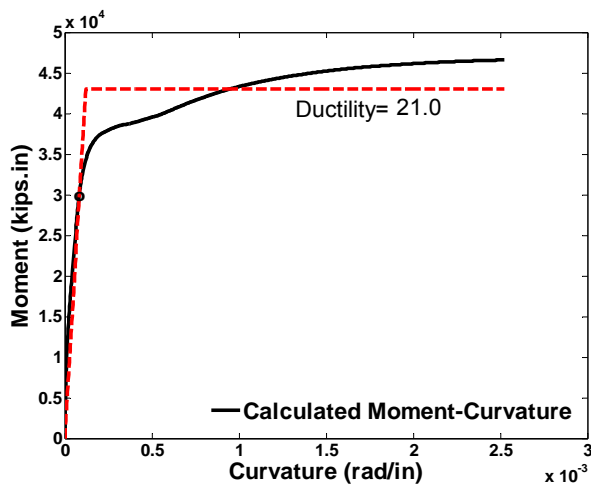


Figure H-5. Sample of column design using moment-curvature analysis

Table H-1. Displacement ductility capacity based on moment-curvature relationship

Parameters	Value
Column Length (in.)	288
Plastic Hinge Length (in.)	34.5
Idealized yield Curvature (rad/in.)	1.2e-04
Ultimate Curvature (rad/in.)	0.0025
Curvature Ductility	21.0
Idealized yield Drift (%)	1.15
Ultimate Drift (%)	8.96
Displacement Ductility Capacity	7.77

H.4.2 Results

Figure H-6 shows drift ratios for different displacement ductilities at the ultimate point for 118 columns, all with 4-ft diameter, an aspect ratio of 6, and a concrete compressive strength of 5-ksi. All the other parameters were varied according to the ranges described in previous sections. A linear relationship was observed between the drift ratio capacity and the displacement ductility capacity with $R^2=0.89$. Figure H-6 also includes the upper and lower bound lines, which were calculated based on 15% deviation from the regression line. The method to obtain 15% bounds is discussed in subsequent sections. The bottom cluster of the data shown in the figure is for columns with minimum confinements. Both drift and ductility were increased when the transverse steel ratio was increased, as expected. A ductility in the range of three to five was considered to be of most interest and is highlighted in the figure.

Similar analyses were carried out on 394 other columns, all with 4-ft diameter and an aspect ratio of 6 but different concrete compressive strengths (Fig. H-7). It can be seen that the effect of concrete compressive strength is not significant on drift-ductility relationship especially in the ductility range of three to five (labeled as “practical range”) and may be excluded from final equations, which is presented subsequently.

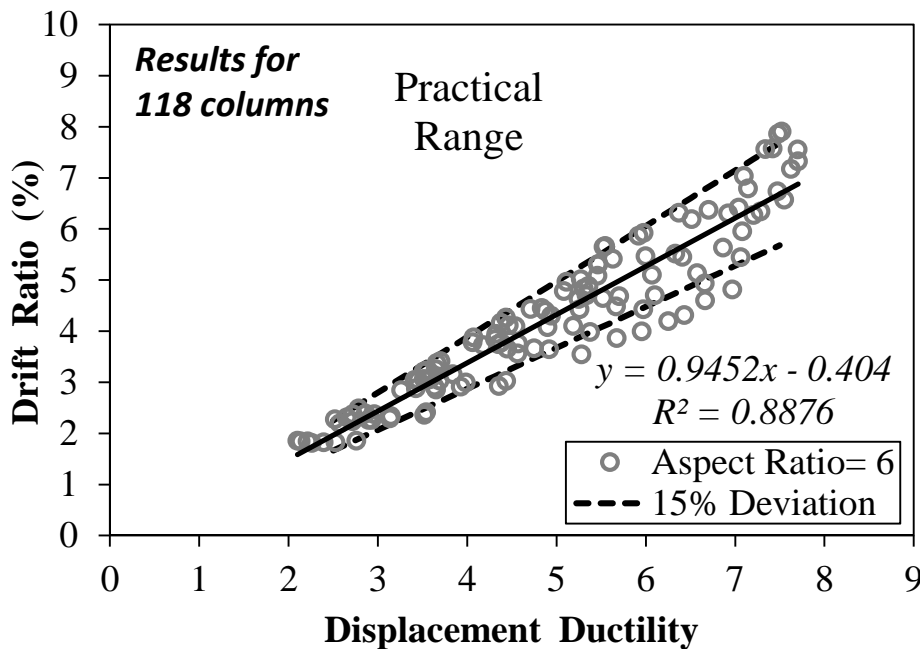


Figure H-6. Drift-ductility relationship for 4-ft, 5-ksi columns with aspect ratio of 6

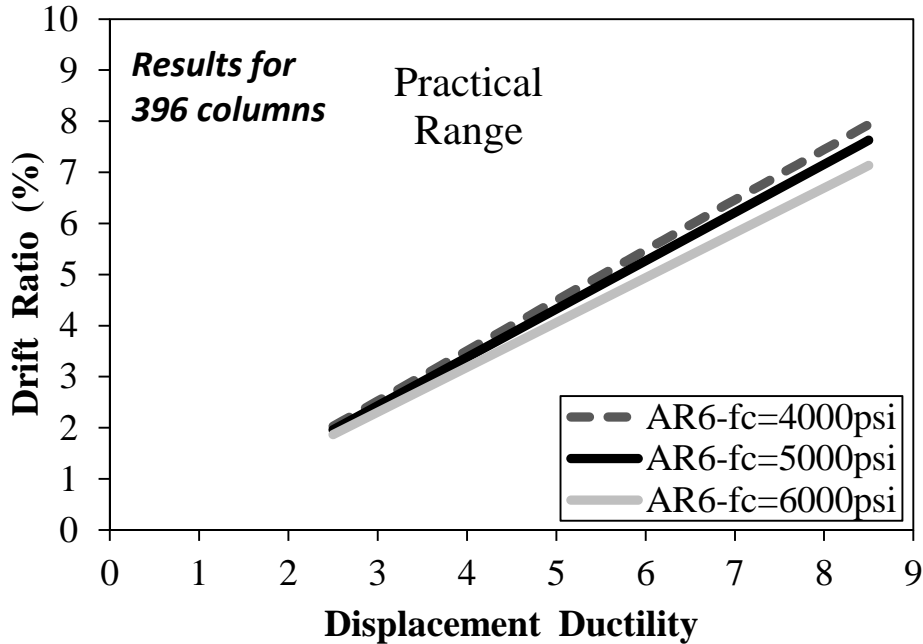


Figure H-7. Drift-ductility relationship for 4-ft columns with aspect ratio of 6

The effect of column diameter on the drift-ductility relationship was also investigated (Fig. H-8). It was observed that the column diameter has insignificant effects on the drift-ductility relationship.

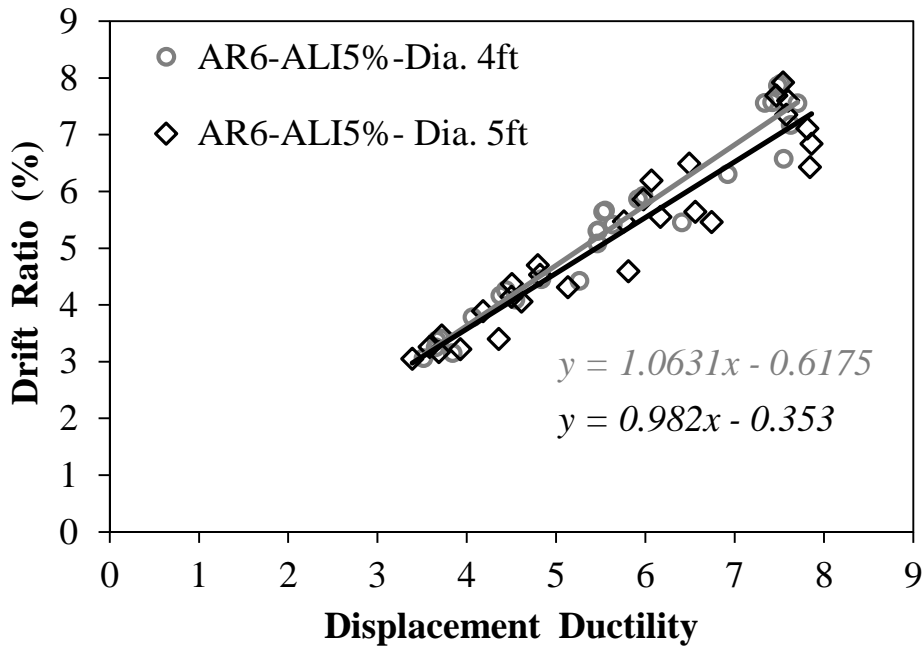


Figure H-8. Drift-ductility relationship for 5-ksi columns with aspect ratio 6

The effect of the aspect ratio on drift-ductility relationship was also studied (Fig. H-9). It was found that different aspect ratios significantly change the drift-ductility relationship but the relationship is linear for each aspect ratio.

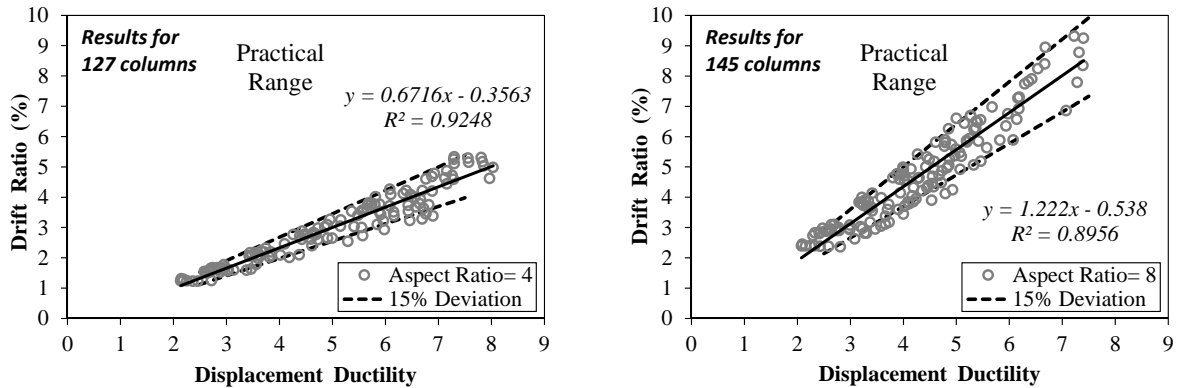


Figure H-9. Drift-ductility relationship for 4-ft, 5-ksi columns with different aspect ratios

The upper and lower bound of regression lines were plotted in the above figures. The upper bound was selected for the design since it is more conservative in terms of converting ductility to drift ratio. A probability analysis was performed (Fig. H-10) to select the upper bound. The vertical axis is the probability of exceedance calculated based on the number of columns that exceed the upper bound at a certain deviation from the regression line. Only 6% of 390 columns exceed the upper bound when the upper bound was 15% higher than the regression line (15% deviation). In other words, the estimated drift ratio capacity for 94% of the columns will always be equal to or higher (from 1 to 30%) than the RC column drift ratio capacity.

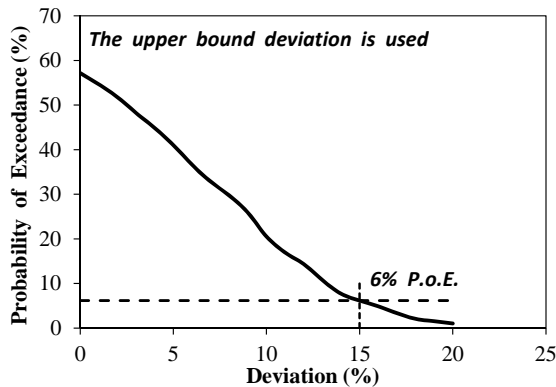


Figure H-10. Selection of upper bound limit

H.5 Proposed Drift-Ductility Equations

It was found that the column aspect ratio is a critical parameter to establish drift-ductility relationships. As stated before, a linear relationship exists between drift and ductility for each aspect ratio. The upper bound of regression analysis was proposed for design of novel columns. Fig. H-11 shows the proposed relationships and Table H-2 presents the proposed drift-ductility equations for different aspect ratios. Linear interpolation can be used for intermediate aspect ratios. These equations are conservative to ensure that the drift capacity of a novel column will exceed the drift capacity of its reference conventional RC column with a probability of 94%. The equations were solely developed to determine drift capacity of RC columns for a given displacement ductility with the intention of comparing the drift capacity of novel columns with that of RC columns. For example, the equations show that a conventional RC column with

an aspect ratio of six designed for a ductility of four would have an upper bound drift ratio of 3.95. Therefore, a novel column should have a drift capacity of at least 3.95 to be as deformable as an RC column.

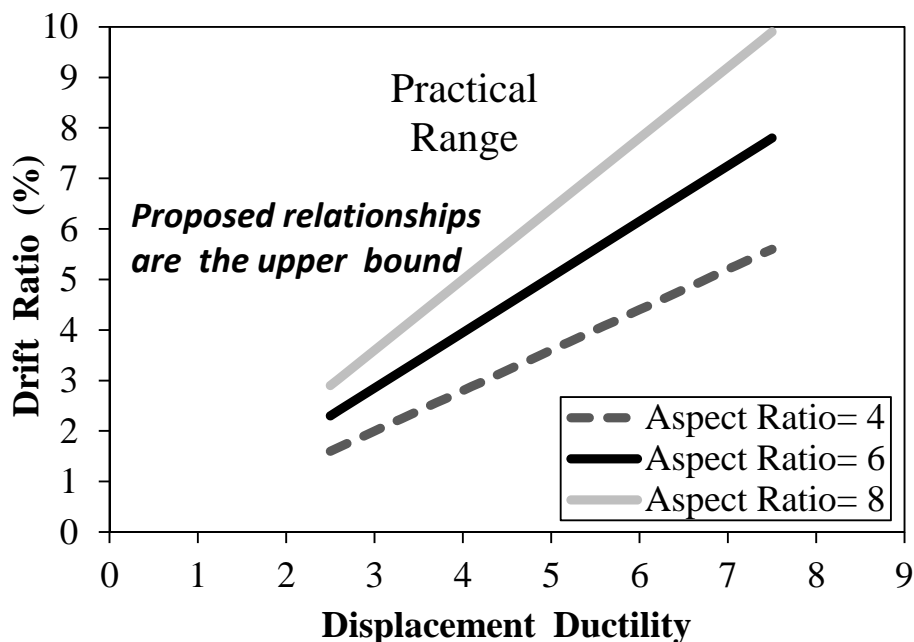


Figure H-11. Proposed drift-ductility relationships

Table H-2. Proposed drift-ductility equations

Parameters	Proposed Equation
Column Aspect Ratio 4	$\delta = 0.8\mu - 0.40$
Column Aspect Ratio 6	$\delta = 1.1\mu - 0.45$
Column Aspect Ratio 8	$\delta = 1.4\mu - 0.60$

Note: " δ " is the drift ratio (%) and " μ " is the displacement ductility

Use linear interpolation for intermediate aspect ratios

H.6 References

1. AASHTO. (2014). "AASHTO Guide Specifications for LRFD Seismic Bridge Design," Washington, DC: American Association of State Highway and Transportation Officials.
2. Haber, Z.B., Saiidi, M.S. and Sanders, D.H. (2013). "Precast Column-Footing Connections for Accelerated Bridge Construction in Seismic Zones," Center for Civil Engineering Earthquake Research, Department of Civil and Environmental Engineering, University of Nevada, Reno, Nevada, *Report No. CCEER-13-08*, 612 pp.
3. OpenSees. (2013). "Open System for Earthquake Engineering Simulations," Version 2.4.1, Berkeley, CA. Available online: <http://opensees.berkeley.edu>.
4. Tazarv, M. and Saiidi, M.S. (2014). "Next Generation of Bridge Columns for Accelerated Bridge Construction in High Seismic Zones," Center For Civil Engineering Earthquake Research, Department of Civil and Environmental Engineering, University of Nevada, Reno, Nevada, *Report No. CCEER-14-06*, 400 pp.

APPENDICES

NCHRP 12-101

App. A – Literature Review

App. B – Survey of State Departments of Transportation

App. C – Synthesis of Literature

App. D – Novel Column and Construction Concepts

App. E – Demonstration of Evaluation Guidelines

App. F – Detailed Design Examples for Three Novel Columns

App. G – Benefits and Economic Impact of Novel Columns

App. H – Relationship between Drift Ratio and Displacement Ductility

App. I – Modeling Methods and Validation for Novel Columns

TABLE OF CONTENTS

APPENDICES	I
TABLE OF CONTENTS.....	II
APPENDIX I	I-1
I.1 Introduction	I-2
I.2 Columns with SMA-Reinforced ECC Plastic Hinges	I-2
I.2.1 Cracked Stiffness for SMA-Reinforced ECC Sections.....	I-2
I.2.1.1 Tazarv and Saiidi (2014).....	I-3
I.2.1.2 Nakashoji and Saiidi (2014)	I-4
I.2.1.3 Saiidi et al. (2009).....	I-5
I.2.2 Nonlinear Dynamic Analysis of SMA-Reinforced ECC Columns.....	I-6
I.2.3 Residual Displacements of SMA-Reinforced ECC Columns	I-9
I.3 Columns with SMA-Reinforced FRP Confined Concrete	I-10
I.3.1 Modeling Method.....	I-10
I.3.2 Residual Displacements of SMA-Reinforced FRP Confined Concrete columns	I-10
I.4 Columns with Hybrid Rocking Connections.....	I-12
I.4.1 Modeling Method.....	I-12
I.4.2 Parametric Study	I-14
I.4.2.1 Cracked Stiffness of Hybrid Rocking Columns	I-14
I.4.2.2 Minimum Steel Tendon Area for Hybrid Rocking Columns	I-15
I.4.2.3 Residual Drifts for Hybrid Rocking Columns	I-17
I.5 References	I-20

APPENDIX I

Modeling Methods and Validation for Novel Columns

I.1 Introduction

An extensive nonlinear analysis of various novel columns was carried out in this project. The important findings and conclusions were presented in the main body of the document but modeling methods and validation are presented herein. This appendix presents the background analyses that led to the recommendations about modeling of three columns with novel plastic hinges. The columns are: (1) SMA-reinforced ECC, (2) SMA-reinforced FRP confined concrete, and (3) hybrid rocking.

I.2 Columns with SMA-Reinforced ECC Plastic Hinges

I.2.1 Cracked Stiffness for SMA-Reinforced ECC Sections

Simple graphs were developed to facilitate calculation of the cracked stiffness of SMA-reinforced ECC columns based on the section properties and axial load (Fig. I-1).

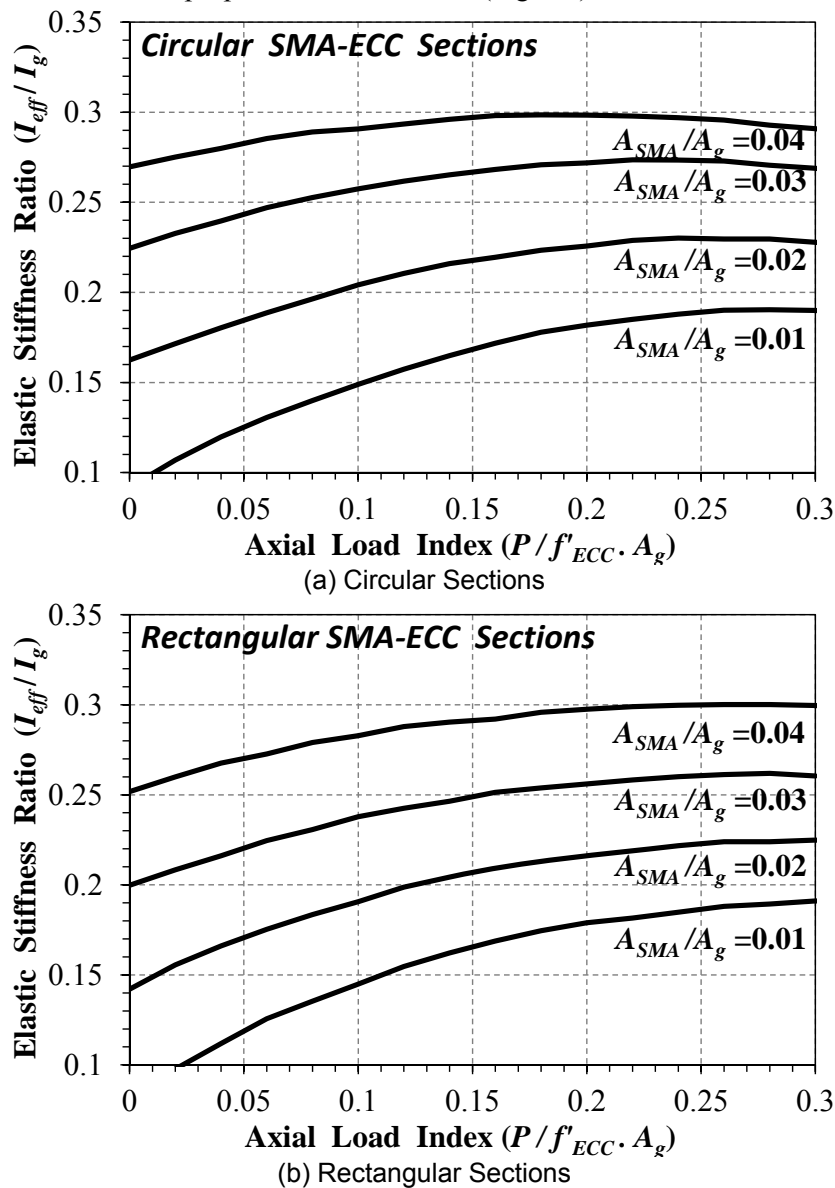


Figure I-1. Effective moment of inertia for SMA-reinforced ECC columns

The available test data for three column models was utilized in this section to verify the graphs by comparing the calculated and measured initial stiffness ratios of the columns.

1.2.1.1 Tazarv and Saiidi (2014)

Figure I-2 shows the column geometry and reinforcement and Table I-1 presents the initial stiffness calculations. The ratio of cracked to uncracked initial stiffness was 0.24 based on Fig. I-1. The measured initial stiffness ratio from the column test was 0.28, which is in close agreement with the calculated stiffness. The slight difference is because the material properties in the development of the graphs were based on recommended design values, which were different from the measured properties of the column. For example, the SMA austenite modulus that was used in developing the graphs was 5500 ksi based on the SMA material model presented in the guideline, while the measured SMA austenite modulus for this column model was 7288 ksi.

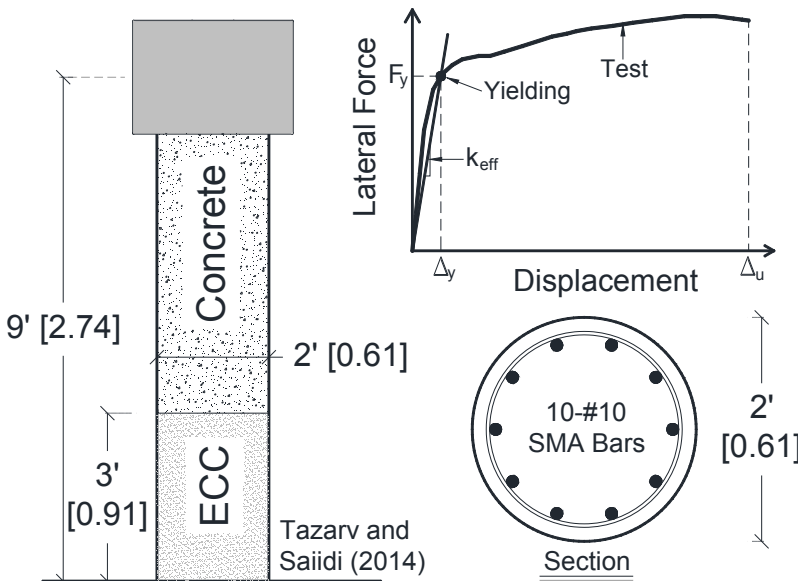


Figure I-2. SMA-reinforced ECC column model tested by Tazarv and Saiidi (2014)

Table I-1. Calculated and measured initial stiffness for SMA-reinforced ECC column

Calculated Stiffness	Measured Stiffness
<p>Column Axial Load (P)= 215.6 kips Column Diameter (D)= 24 in. Column Length (L)= 108 in. f'_{ECC}=6.39 ksi</p> <p>$A_g = \pi r^2 = \pi \times 12^2 = 452.4 \text{ in}^2$ Axial Load Index=$P/(f'_{ECC}A_g)$=0.075 $A_{SMA}/A_g=10 \times 1.27/452.4=0.028$</p> <p>From graph I-1a: $I_{eff}/I_g=0.24$ or $k_{eff}/k_g=0.24$</p>	<p>Test Data: Yield Force (F_y)= 44.6 kips Yield Disp. (Δ_y)= 1.56 in.</p> <p>$k_{eff} = F_y / \Delta_y = 28.6 \text{ kip/in}$</p> <p>$I_g = \frac{\pi}{4} r^4 = \frac{\pi}{4} 12^4 = 16286 \text{ in}^4$ $E_{ECC}=1400(f'_{ECC})^{1/3}=2598 \text{ ksi}$ $k_g=3E_{ECC}I_g/L^3= 100.76 \text{ kip/in}$</p> <p>$k_{eff}/k_g=0.28$</p>

1.2.1.2 Nakashoji and Saiidi (2014)

Two column models were tested by Nakashoji and Saiidi, one with 14.5-in. long SMA bars and the other with 18-in. SMA bars in the plastic hinge. The latter was analyzed herein because the SMA bar length is more representative of SMA-reinforced columns. Figure I-3 shows the column geometry and reinforcement, and Table I-2 presents the initial stiffness calculations. Even though the column section is square, Fig. I.1a was used because the column core and the pattern of the SMA bars was circular. The ratio of cracked to uncracked initial stiffness was 0.14 using the graph. The measured initial stiffness ratio from the column test was 0.18, which is in good agreement with the calculated stiffness.

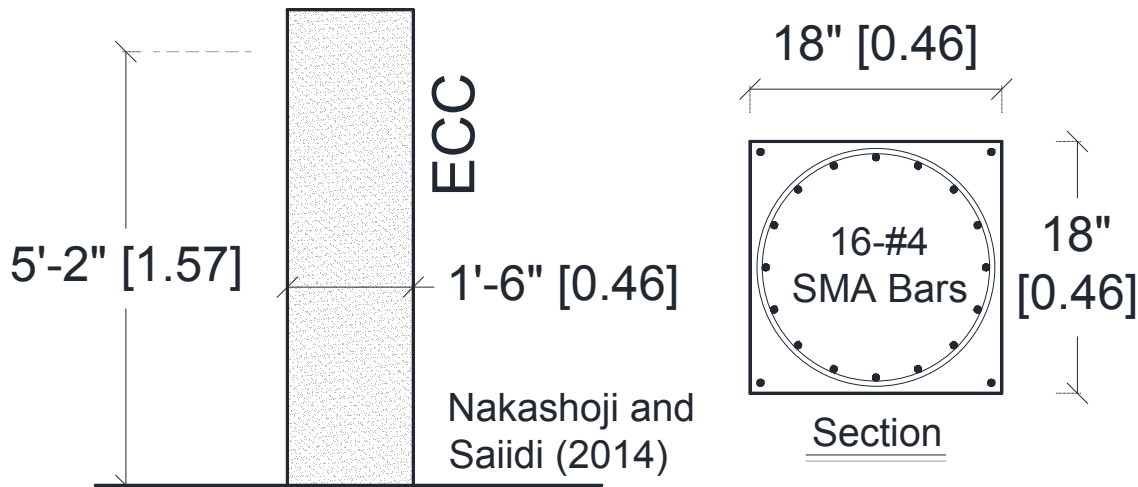


Figure I-3. SMA-reinforced ECC column model tested by Nakashoji and Saiidi (2014)

Table I-2. Calculated and measured initial stiffness for SMA-reinforced ECC column

Calculated Stiffness	Measured Stiffness
Column Axial Load (P)= 140 kips Column Side Dimension (D)= 18 in. Column Length (L)= 62 in. f'_{ECC} =6.89 ksi $A_g = D^2 = 18^2 = 324 \text{ in}^2$ Axial Load Index= $P/(f'_{ECC}A_g)$ =0.063 $A_{SMA}/A_g=16*0.2/324=0.01$ From graph (I-1a): $I_{eff}/I_g=0.14$ or $k_{eff}/k_g=0.14$ From graph (I-1b): $I_{eff}/I_g=0.13$ or $k_{eff}/k_g=0.13$	Test Data: Yield Force (F_y)= 31.6 kips Yield Disp. (Δ_y)= 0.59 in. $k_{eff} = F_y / \Delta_y = 53 \text{ kip/in}$ $I_g = \frac{1}{12} D^4 = \frac{1}{12} 18^4 = 8748 \text{ in}^4$ $E_{ECC}=1400(f'_{ECC})^{1/3}=2664 \text{ ksi}$ $k_g=3E_{ECC}I_g/L^3= 293.5 \text{ kip/in}$ $k_{eff}/k_g=0.18$

I.2.1.3 Saiidi et al. (2009)

Figure I-4 shows the column geometry and reinforcement and Table I-3 presents the initial stiffness calculations. The calculated ratio of cracked to uncracked stiffness was 0.20 using the graph. The measured initial stiffness ratio from the column test was 0.24, which is in good agreement with the calculated stiffness ratio.

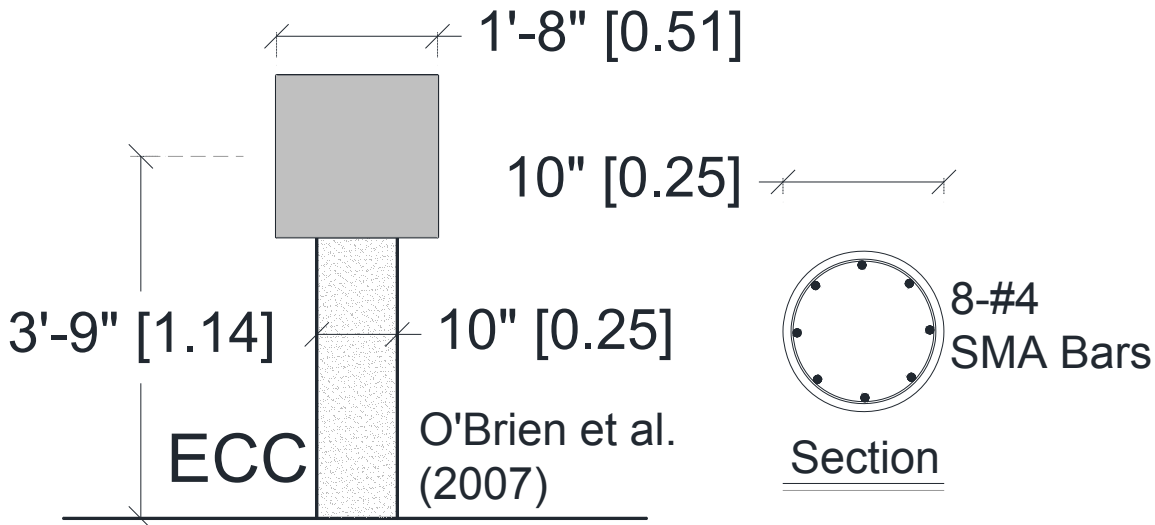


Figure I-4. SMA-reinforced ECC column model tested by Saiidi et al. (2009)

Table I-3. Calculated and measured initial stiffness for SMA-reinforced ECC column

Calculated Stiffness	Measured Stiffness
<p>Column Axial Load (P)= 35 kips Column Diameter (D)= 10 in. Column Length (L)= 45 in. f'_{ECC}=5.19 ksi</p> <p>$A_g = \pi r^2 = \pi \times 5^2 = 78.5 \text{ in}^2$ Axial Load Index=$P/(f'_{ECC}A_g)$=0.087 $A_{SMA}/A_g=8*0.2/78.5=0.02$</p> <p>From graph I-1a: $I_{eff}/I_g=0.20$ or $k_{eff}/k_g=0.20$</p>	<p>Test Data: Yield Force (F_y)= 8.69 kips Yield Disp. (Δ_y)= 0.91 in.</p> <p>$k_{eff} = F_y / \Delta_y = 9.55 \text{ kip/in}$</p> <p>$I_g = \frac{\pi}{4} r^4 = \frac{\pi}{4} 5^4 = 490.8 \text{ in}^4$ $E_{ECC}=1400(f'_{ECC})^{1/3}=2423.9 \text{ ksi}$ $k_g=3E_{ECC}I_g/L^3= 39.17 \text{ kip/in}$</p> <p>$k_{eff}/k_g=0.24$</p>

I.2.2 Nonlinear Dynamic Analysis of SMA-Reinforced ECC Columns

Nonlinear dynamic analyses were carried out to investigate various response trends and to specify different parameters for SMA-reinforced ECC columns such as damping ratio and displacement demand amplification factor. In the SMA-reinforced ECC column design guideline, the damping ratio was specified as 3.2% for these columns based on more than 180 nonlinear dynamic analyses. In this section, the modeling method and the details of the properties of the columns and the input motions along with sample aggregate results are presented. Detailed discussion of the results of these analysis were presented in Ch. 3 in sections 3.1.4.3 and 3.1.4.4).

Modeling method for dynamic analyses were based on a robust analytical model developed by Tazarv and Saïdi (2013), which closely reproduced a full-scale RC bridge column test responses. The column was tested on a shake table at the University of California, San Diego (UCSD) with the test data being available online (Concrete Column Blind Prediction Contest, 2010). The column height from the footing surface to the center of inertial mass was 27 ft (8.23 m). The column diameter was 4 ft (1.22 m). More details regarding the column geometry and the modeling method for RC and SMA-reinforced columns are presented in the paper. The model developed for the SMA-reinforced column were adopted in this study as base model then column geometry and ECC material properties were varied to accomplish the parametric study.

The input motions were a series of artificial earthquakes generated based on AASHTO design spectrum for downtown of Los Angeles, which falls in SDC D. Fig. I-5 shows the AASHTO design spectra for SDC A, B, and C that were obtained for downtowns New York City (NY), Las Vegas (NV), and Portland (OR) in addition to the spectrum for Los Angeles.

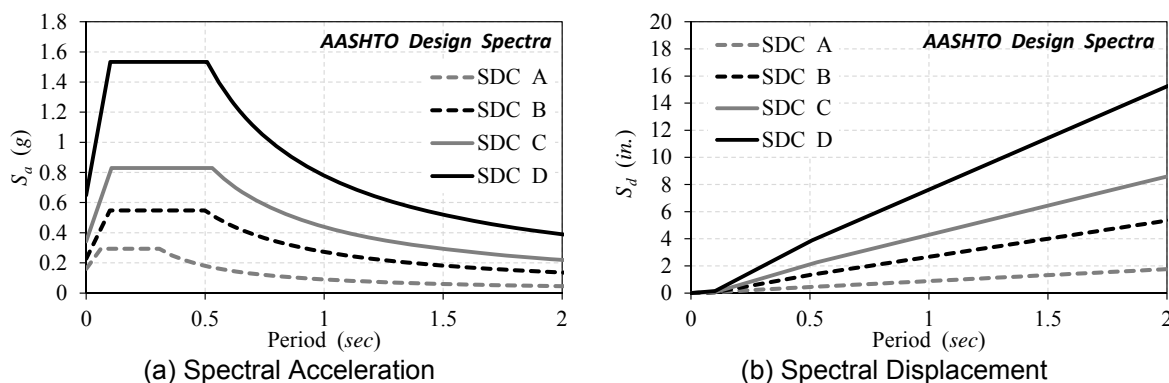


Figure I-5. AASHTO design spectrum for Los Angeles

SeismoArtif (2013) was utilized to generate artificial ground motions. Figure I-6a shows spectral acceleration for three artificial motions, and Fig. I-6b and I-6c show acceleration history for EQ1 and EQ3. It can be seen that the spectral acceleration of the artificial ground motions were in close agreement with the target design spectrum.

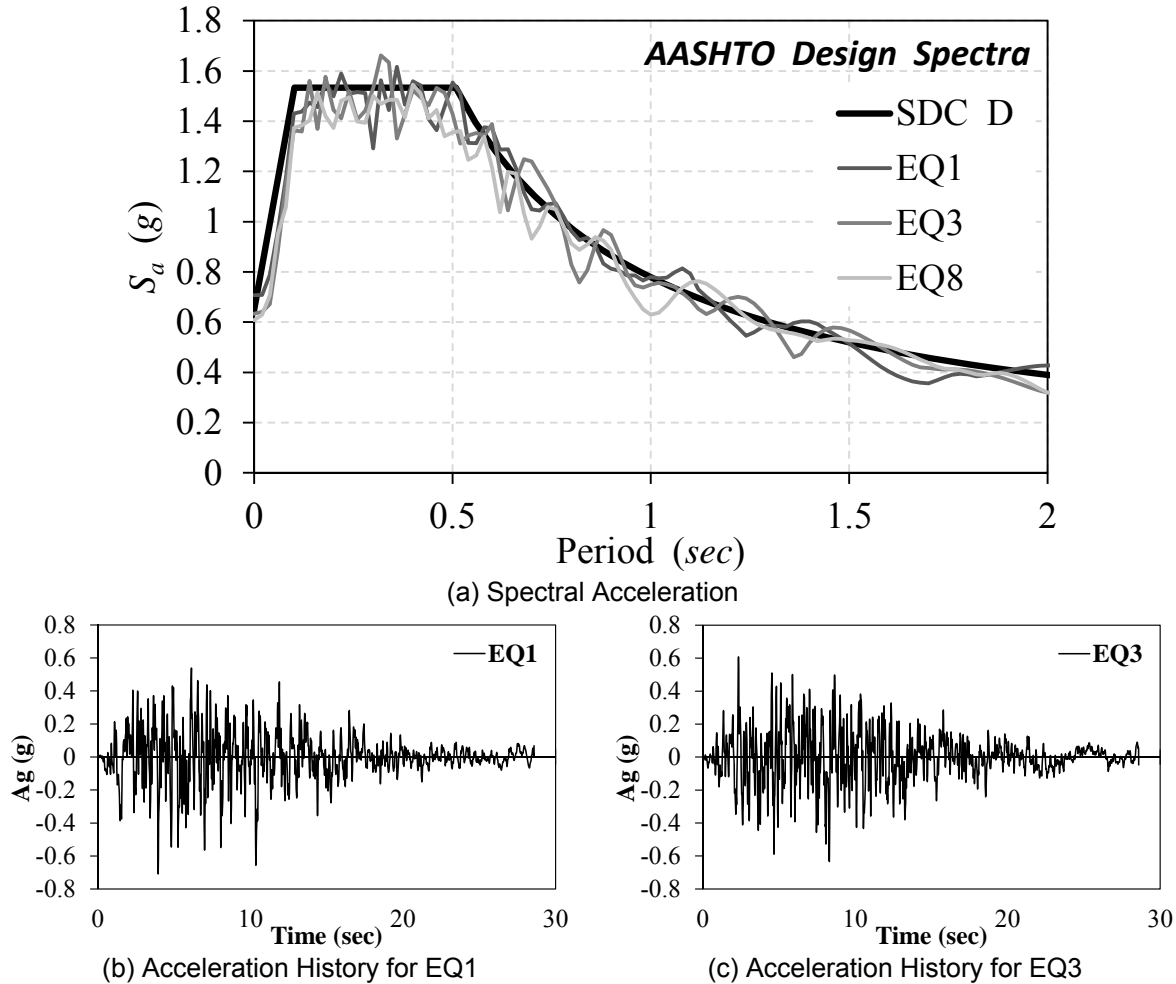


Figure I-6. Artificial ground motions based on AASHTO design spectrum for Los Angeles

Two aspect ratios, 4 and 6, were selected for the columns. The diameter was assumed to be 5 ft (1.52 m). Four longitudinal reinforcement ratios (1, 2, 3, and 4%) with one transverse steel ratio (1.07%) were selected for columns. To be able to cover a wide range of structural periods, the axial load index was varied from 0.0 to 20% at 2% intervals. The axial load was subsequently converted to mass. More than 90 columns were analyzed under each ground motion to establish a relationship between the nonlinear dynamic displacement demands and spectral displacements. It is worth mentioning that columns that failed due to SMA bar fracture or core ECC failure were excluded from the spectral versus the nonlinear displacement graphs presented in the guideline.

Table I-4 presents the material modeling methods and Fig. I-7 shows one example of analysis results for a column with aspect ratio of 4, axial load index of 14%, longitudinal SMA ratio of 2%, and an effective period of 1.67 sec. The displacement demand was 13.95 in. (354 mm or 5.8% drift ratio) and the SDC-D spectral displacement for this column was 12.7 in. (323 mm).

Table I-4. Fiber material model used in SMA-reinforced ECC column nonlinear analysis

ECC Fibers	
<p>Application: unconfined ECC</p> <p>Type: Concrete02 $f'_{cc} = -5000 \text{ psi } (-34.8 \text{ MPa})$ $\epsilon_{cc} = -0.002 \text{ in./in.}$ $f'_{cu} = 0.0 \text{ psi } (0.0 \text{ MPa})$ $\epsilon_{cu} = -0.005 \text{ in./in.}$ $f_{ct} = 0.0$ $E_t = 0.0$</p> <p>Note: 1- No tensile strength for ECC resulted in a better match in terms of initial stiffness and unloading path for test models.</p>	<p>Application: confined ECC (based on Motaref's model)</p> <p>Type: Concrete02 $f'_{cc} = -6300 \text{ psi } (-43.4 \text{ MPa})$ $\epsilon_{cc} = -0.00425 \text{ in./in.}$ $f'_{cu} = 0.4 f'_{cc}$ $\epsilon_{cu} = -0.0182 \text{ in./in.}$ $f_{ct} = 0.0$ $E_t = 0.0$</p>
SMA Fibers	
<p>Application: in plastic hinge area</p> <p>Type: SelfCentering $k_1 = 5500 \text{ ksi } (37920 \text{ MPa})$ $k_2 = 250 \text{ ksi } (1725 \text{ MPa})$ $f_y = 55 \text{ ksi } (379 \text{ MPa})$ $\beta = 0.60$ $\epsilon_r = 0.06 \text{ in./in.}$ $\alpha = 0.30$ $\epsilon_u = 0.10 \text{ in./in.}$</p>	

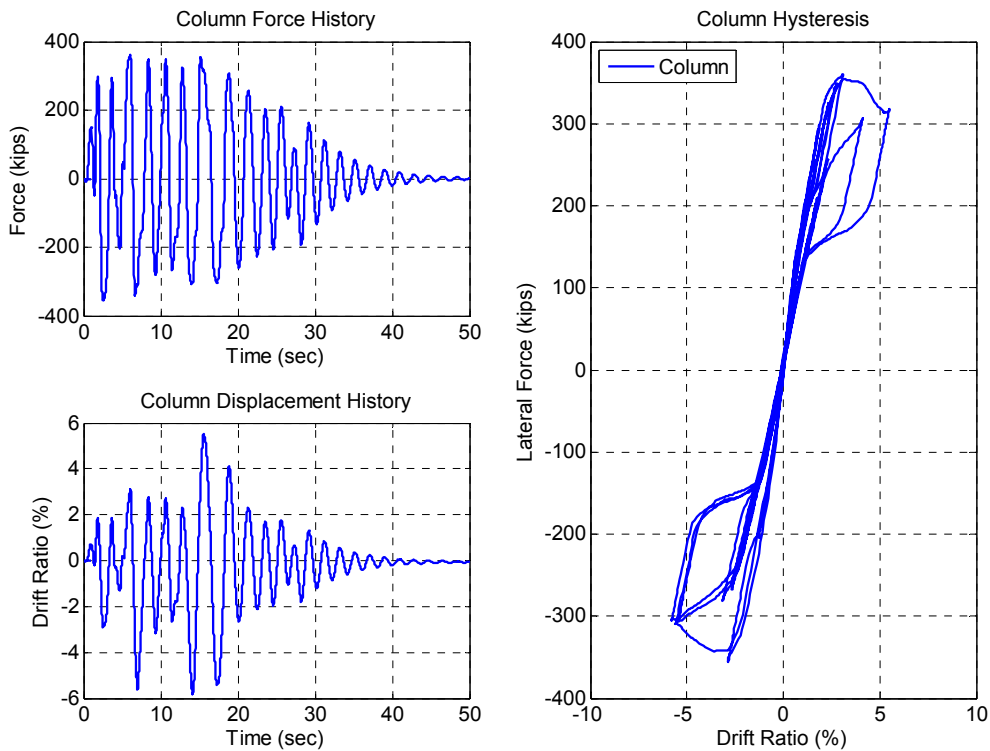


Figure I-7. Sample of nonlinear dynamic analysis

I.2.3 Residual Displacements of SMA-Reinforced ECC Columns

Residual horizontal displacements are defined as displacements that cannot be recovered after a severe event (e.g. earthquakes) due to primarily significant yielding of the member longitudinal reinforcement. The residual displacement of a column under earthquake loading is the displacement at the end of displacement history. In column models subjected to displacement-controlled cyclic loading, the displacement at zero-force in the column force-displacement hysteresis curves may be used as a measure of residual displacement. Large residual displacements affect the functionality of bridges after the event and may result in bridge closure or total replacement.

A parametric study was carried out to investigate the performance of SMA-reinforced ECC bridge columns in terms of residual displacements. Three aspect ratios, 4, 6, and 8, were selected for the columns. The diameter was assumed to be 5 ft (1.52 m) for all columns. Seven longitudinal reinforcement ratios (1, 1.5, 2, 2.5, 3, 3.5, and 4%) with one transverse steel ratio (1.07%, No 6 spirals at 3 in. pitch) were selected for columns. The column concrete compressive strength was 5000 psi. Three axial load indexes, 5, 10, and 15%, were selected. Sixty-three cyclic load analyses were carried out to establish a relationship between the residual and peak drift ratios. The residual drift is defined as the ratio of the residual horizontal displacement to the column height.

Figure I-8a shows a sample of cyclic analysis results for a column with an aspect ratio of 6, a longitudinal reinforcement ratio of 2%, and an axial load index of 5%. Subsequently, the residual drift ratios of each analysis (drift ratio at zero-force) was plotted against the corresponding peak drift ratios (the maximum drift ratio for each cycle) as shown in Fig. I-8c.

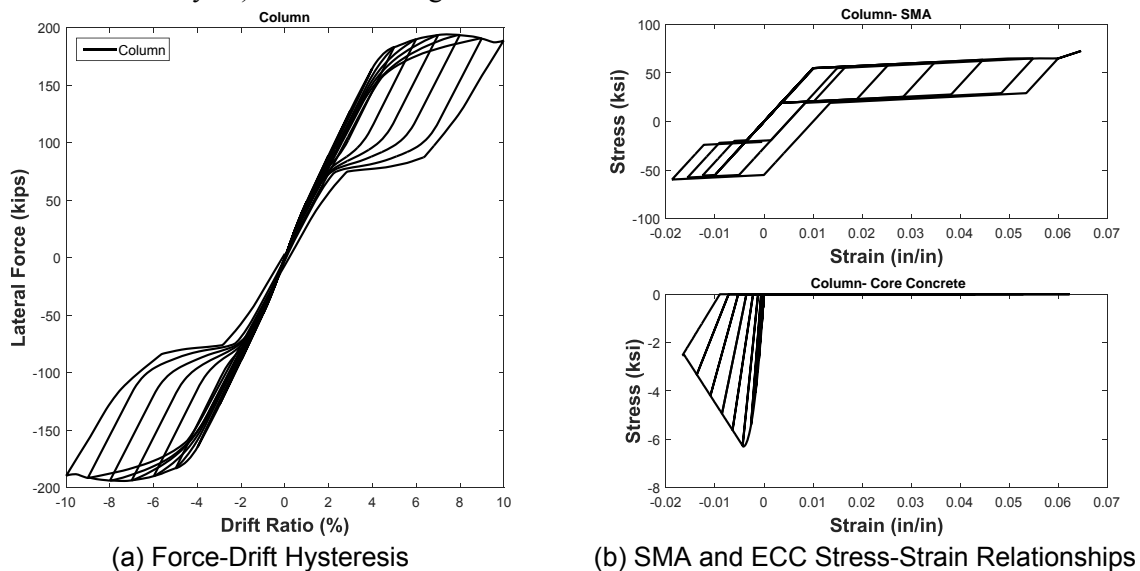


Figure I-8. Sample of cyclic analysis for SMA-reinforced ECC columns

The aforementioned procedure was repeated for all columns and the results were compiled in Fig. I-9 (the curves in the lower part of the figure). The measured residual-peak drift relationship for a conventional bridge column (aspect ratio = 4.5) as well as an SMA-reinforced ECC column was included in the figure to compare the measured and calculated residual drifts. It can be seen that the measured and calculated residual drifts for SMA-reinforced ECC columns are substantially lower than 1% drift ratio for a wide range of peak drift ratios (from 0 to 10% drift ratio) while the conventional column residual drift ratio exceeded the 1% drift limit at a peak drift ratio of 3% and more. The analytical results underestimated the residual displacements compared to the measured results because very small residual displacements are sensitive to simplifying assumptions typically made in analytical models.

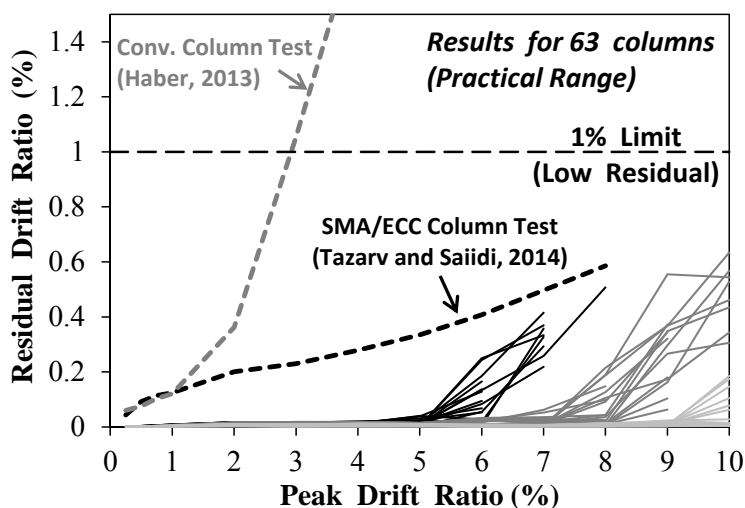


Figure I-9. Residual drifts of SMA-reinforced ECC columns

I.3 Columns with SMA-Reinforced FRP Confined Concrete

I.3.1 Modeling Method

There is no available test data on the seismic performance of SMA-reinforced FRP-confined concrete columns. The analytical model for this column type was based on the SMA-reinforced ECC columns as presented in the previous sections. However, steel-confined ECC was replaced with FRP-confined concrete.

I.3.2 Residual Displacements of SMA-Reinforced FRP Confined Concrete columns

A parametric study was carried out to investigate the performance of SMA-reinforced FRP-confined bridge columns in terms of residual displacements. Three aspect ratios, 4, 6, and 8, were selected for the columns. The diameter was assumed to be 5 ft (1.52 m) for all columns. Seven longitudinal reinforcement ratios (1, 1.5, 2, 2.5, 3, 3.5, and 4%) with one FRP tube ($t_f=0.3$ in., $f_{fu}=150$ ksi, and $E_f=11900$ ksi) were selected for columns. The column concrete compressive strength was 5000 psi. Three axial load indexes, 5, 10, and 15%, were assumed. No transverse steel reinforcement was included in this parametric study. The displacement capacity of and the residual displacements of SMA/FRP columns were investigated. Sixty-three cyclic load analyses were carried out to establish a relationship between the residual and peak drift ratios.

Figure I-10 shows a sample of cyclic analysis results for a column with an aspect ratio of 6, a longitudinal reinforcement ratio of 2%, and an axial load index of 5%. The ultimate displacement (SMA fracture or core concrete failure) was marked by a circle. Subsequently, the residual drift ratios of each analysis (drift

ratio at zero-force) were plotted against the corresponding peak drift ratios (the maximum drift ratio for each cycle) up to the ultimate drift ratio (Fig. I-10c).

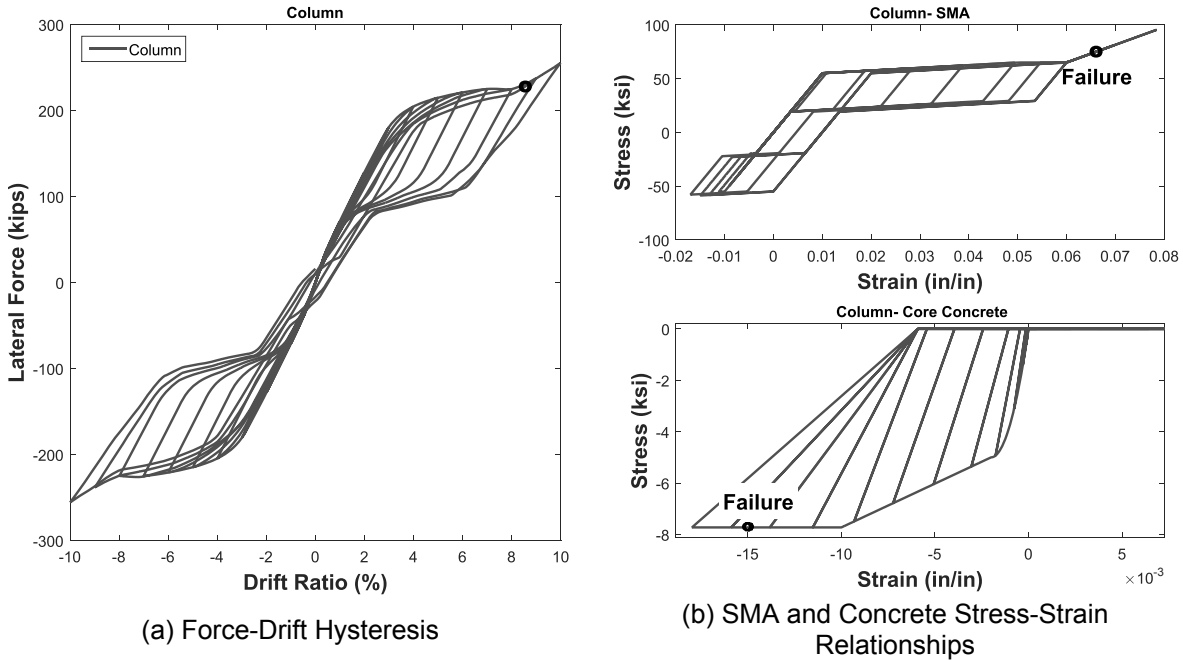


Figure I-10. Sample of cyclic analysis for SMA-reinforced FRP-confined concrete columns

The procedure described above was repeated for all columns and the results were compiled in Fig. I-11. The measured residual-peak drift relationship for a conventional bridge column (aspect ratio = 4.5) as well as an SMA-reinforced steel-confined column was included in the figure for comparison. It can be seen that the calculated residual drifts for SMA-reinforced FRP-confined concrete columns are substantially lower than 1% drift ratio for a wide range of peak drift ratios (from 0 to 10% drift ratio) while the conventional column residual drift ratio exceeded the 1% drift limit at a peak drift ratio of 3% and more.

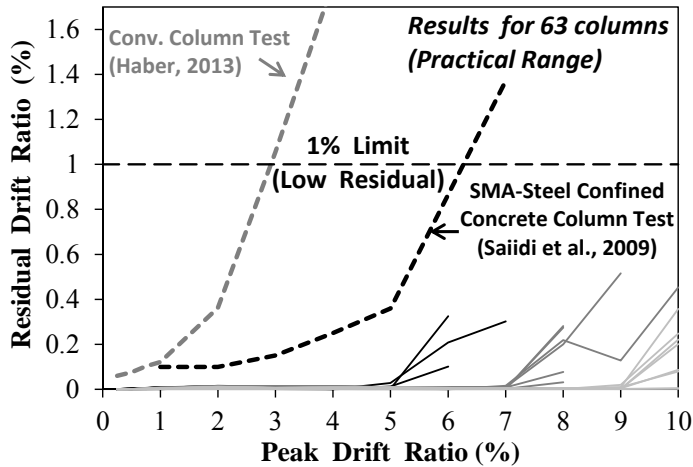


Figure I-11. Residual drifts of SMA-reinforced FRP-confined concrete columns

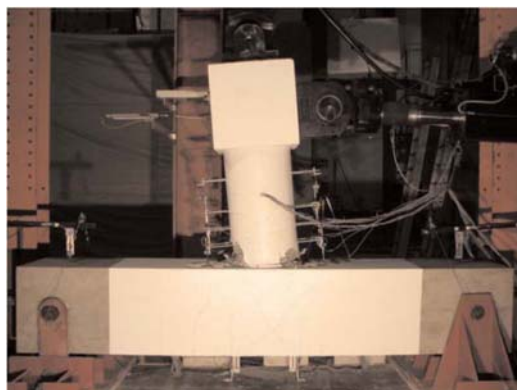
I.4 Columns with Hybrid Rocking Connections

I.4.1 Modeling Method

A rocking column is a column that is post-tensioned in the axial direction. Two types of rocking columns exist: (1) simple and (2) hybrid. No longitudinal reinforcing bar crosses the rocking surface in the former, but the latter includes longitudinal reinforcement at the interface. The post tensioning material in this document is steel because the available column seismic test data are for steel tendons. Limited data on seismic performance of columns with FRP tendons are emerging, but the available information is not sufficient for development of analysis and design guidelines. Seismic test data are available for several simple rocking column models, but data for hybrid rocking columns is scarce. A literature review was conducted to determine which of the available hybrid rocking test data can be utilized for modeling. Jeong et al. (2008) tested four single column models and a two-column bent on shake tables (Fig. I-12a), all with hybrid rocking connections. Restrepo et al. (2011) tested a hybrid rocking column connected to a cap beam in an inverted T-shape setup (Fig. I-12b). Larkin et al. (2012) tested two half-scale hybrid rocking columns with two different column longitudinal reinforcement ratios (Fig. I-12c). Among these models, a column (PT-HL) by Larkin et al. (2012) was selected for further study due to the availability of all the necessary modeling parameters (e.g. the measured strength of materials, loading protocol, column geometry, etc.) as well as the large scale factor of the model.



(a) Jeong et al. (2008)



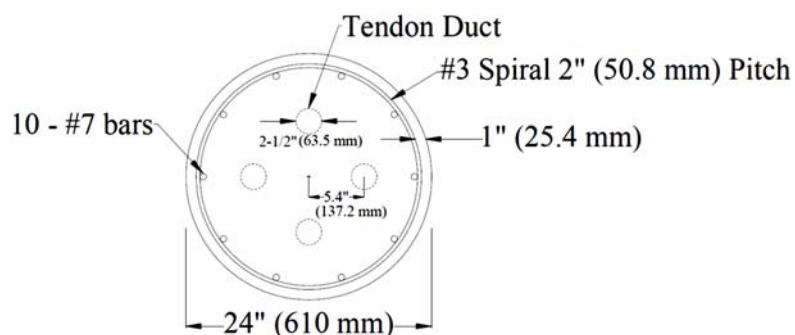
(b) Restrepo et al. (2011)



(c) Larkin et al. (2012)

Figure I-12. Hybrid rocking column tests

The height and the diameter of PT-HL were 108 in. and 24 in. respectively. This column was longitudinally reinforced with 10 No. 7 reinforcing steel bars and transversely with No. 3 spirals at 2 in. pitch. The column was post-tensioned with four 0.6-in.-diameter strands per duct as shown in Fig. I-13.



(a) Column Section



(b) Tendon Anchorage at Column Top

Figure I-13. Hybrid rocking column test by Larkin et al. (2012)

A two-node three-dimensional OpenSees model was developed to analyze this column. The column element was a force-based element, “forceBeamColumn”, with five integration points. Table I-5 presents material model parameters used in the PT-HL model. The test day compressive strength of column concrete was used for the unconfined concrete fibers, which were modeled using “Concrete01”. The Mander’s model was used to determine the confined concrete model parameters, which was also “Concrete01”. The core concrete was divided into 30 circumferential by 10 radial fibers, and the cover concrete was divided into 10 circumferential by 10 radial fibers. At the first integration point located at the column base, steel fibers were modeled using “ReinforcingSteel” with a modified stress-strain behavior accounting for the bond-slip effect (according to a method presented in Tazarv and Saiidi, 2014). From the second to the fifth integration points, the original steel model was used. All 16 tendons were lumped at the center of the section and were modeled using a “corotTruss” element, which allows the change of axial load in the local direction of the element. This column was post-tensioned with a total force of 194 kips, with each tendon stressed to $0.2f_{py}$. The tendon fiber was “Steel02” material model post-tensioned with an “InitStressMaterial” material model. The four ducts were replaced with an equivalent-area duct in the center of the section, which was modeled as a hollow section. The column axial load, 122 kips, was applied to the model, and the $P - \Delta$ effect was included.

Figure I-14 shows the measured and calculated force-drift relationships. The correlation between the measured and calculated results was close. This figure also shows the measured and calculated residual-peak drift ratio relationships for PT-HL. The calculated residual drifts were on average 35% higher than the measured drifts. However, the error between the measured and calculated residual drifts was minimal under higher peak drift ratios, and the trend was captured well.

Table I-5. Fiber material model used in PT-HL hybrid rocking column analysis

Concrete Fibers	
Application: unconfined concrete Type: Concrete01 $f'_{cc} = -4570 \text{ psi } (-31.5 \text{ MPa})$ $\epsilon_{cc} = -0.002 \text{ in./in.}$ $f'_{cu} = 0.0 \text{ psi } (0.0 \text{ MPa})$ $\epsilon_{cu} = -0.005 \text{ in./in.}$ $f_{ct} = 0.0$ $E_t = 0.0$	Application: confined concrete (based on Mander's model) Type: Concrete01 $f'_{cc} = -6650 \text{ psi } (-45.8 \text{ MPa})$ $\epsilon_{cc} = -0.00656 \text{ in./in.}$ $f'_{cu} = 0.76 f'_{cc}$ $\epsilon_{cu} = -0.0285 \text{ in./in.}$ $f_{ct} = 0.0$ $E_t = 0.0$
Steel Fibers	
Application: first integration point at column base accounting for bond-slip effect Type: ReinforcingSteel $f_y = 69.8 \text{ ksi } (481.2 \text{ MPa})$ $f_{su} = 111.2 \text{ ksi } (766.7 \text{ MPa})$ $E_s = 18212 \text{ ksi } (165567 \text{ MPa})$ $E_{sh} = 0.093E_s$ $\epsilon_{sh} = 0.005 \text{ in./in.}$ (use smaller value to converge*) $\epsilon_{su} = 0.1715 \text{ in./in.}$	Application: second to fifth integration points Type: ReinforcingSteel $f_y = 69.8 \text{ ksi } (481.2 \text{ MPa})$ $f_{su} = 111.2 \text{ ksi } (766.7 \text{ MPa})$ $E_s = 29000 \text{ ksi } (200000 \text{ MPa})$ $E_{sh} = 0.043E_s$ $\epsilon_{sh} = 0.0125 \text{ in./in.}$ $\epsilon_{su} = 0.17 \text{ in./in.}$
Tendon Fibers	
Type: Steel02 $f_{y-ps} = 247 \text{ ksi } (1703 \text{ MPa})$ $E_{s-ps} = 28500 \text{ ksi } (196500 \text{ MPa})$ $E_{sh-ps} = 0.0197E_s$	

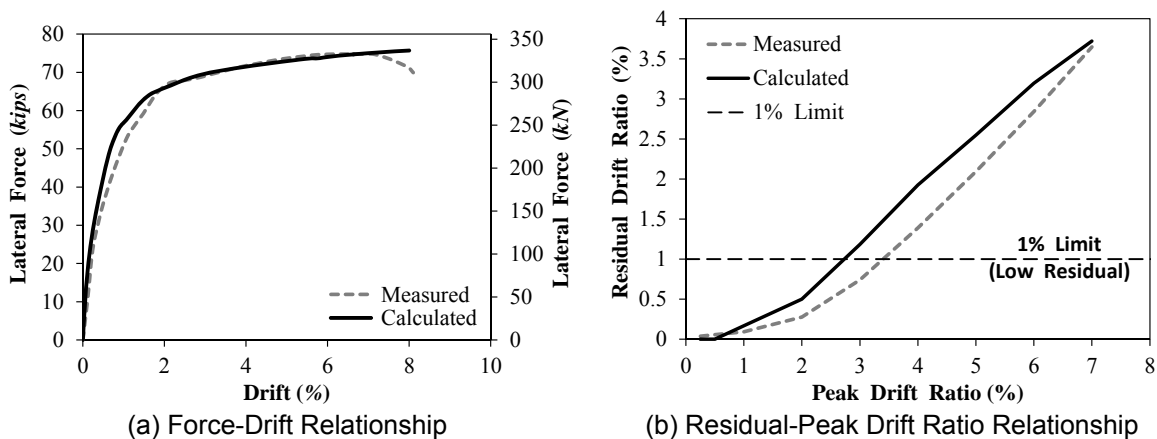


Figure I-14. PT-HL hybrid rocking column analytical model results

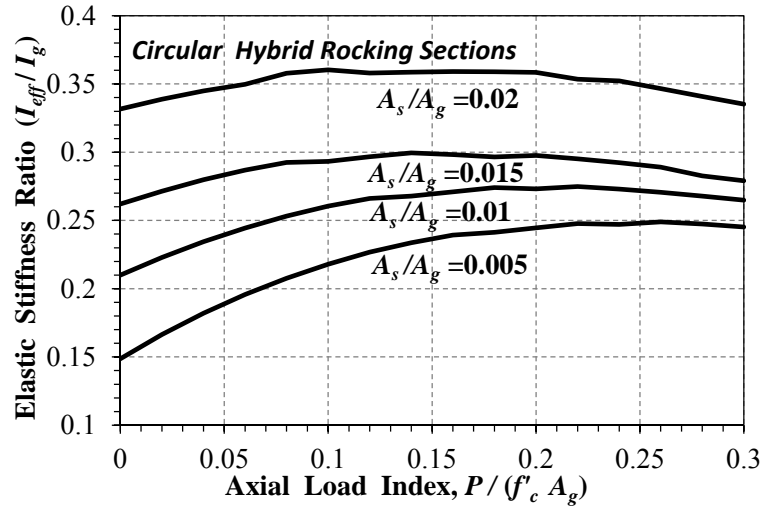
I.4.2 Parametric Study

Extensive parametric studies were conducted to determine the effect of practical ranges for different design parameters on the seismic response of hybrid rocking columns. The cracked stiffness, the minimum tendon area, and residual drifts are discussed herein.

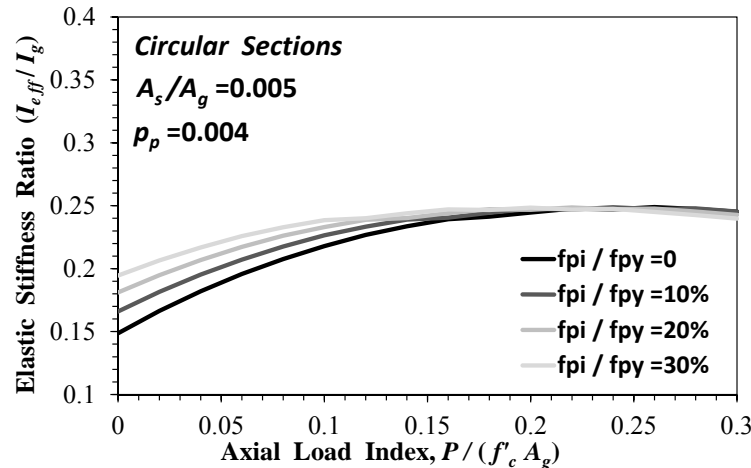
I.4.2.1 Cracked Stiffness of Hybrid Rocking Columns

Simple graphs were developed in previous sections for different novel columns to facilitate calculation of the cracked stiffness based on the section properties and axial load. Figure I-15a shows one example of

such graph for circular hybrid rocking columns. Since the proposed design guideline allows a wide range of design parameters (e.g. $0.0025A_g \leq A_s \leq 0.025A_g, f_{pi}/f_{py} \leq 0.3$), the influence of all these variables cannot be presented in a single graph. For example, Fig. I-15b shows the effective stiffness ratio of a circular hybrid rocking column with different initial tendon stresses. It can be seen that for low axial loads, there is approximately 30% difference in the cracked stiffness when the initial tendon stress ratio (f_{pi}/f_{py}) increases from 0 to 0.3. Therefore, one graph cannot represent all the practical cases. The proposed guideline requires a moment-curvature analysis to calculate the cracked stiffness of hybrid rocking columns.



(a) $A_p/A_g = 0.004, f_{pi}/f_{py} = 0$



(b) $A_p/A_g = 0.004, A_s/A_g = 0.005$

Figure I-15. Effective moment of inertia for hybrid rocking columns

I.4.2.2 Minimum Steel Tendon Area for Hybrid Rocking Columns

Tendons in hybrid rocking columns should remain elastic during earthquakes to maximize the self-centering tendency and to avoid post-earthquake re-tensioning or replacement of the tendons. Pushover analysis was conducted for over 650 hybrid rocking columns to identify the important parameters that affect tendon stresses. Three aspect ratios, 4, 6, and 8, were selected for the columns. The diameter was assumed to be 5 ft (1.52 m) for all columns. The column concrete compressive strength was 5000 psi. Seven longitudinal reinforcing steel bar ratios ($A_s/A_g = 0.25, 0.5, 0.75, 1.0, 1.5, 2.0,$ and 2.5%) with one transverse steel ratio (1.07%, No 6 spirals at 3 in. pitch) were selected for columns. Eleven steel tendon ratios (A_p/A_g

= 0 to 1% with a 0.1% increment) were selected. Three axial load indexes, 5, 10, and 15%, were assumed. Seven tendon initial stress ratios ($f_{pi}/f_{py} = 0, 5, 10, 15, 20, 25, 30\%$) were selected. The $P - \Delta$ effect was included in all analyses.

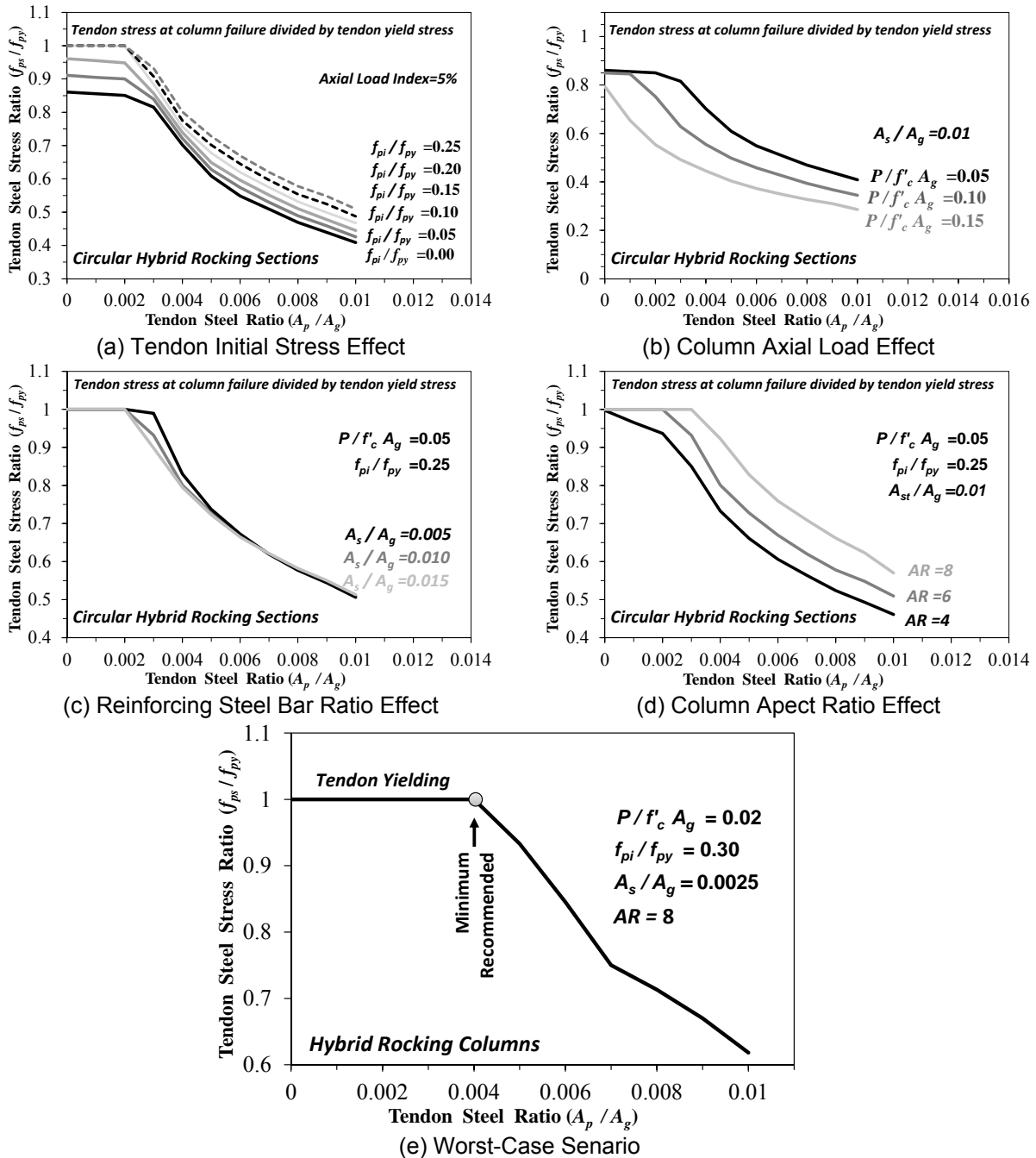


Figure I-16. Results of parametric study to determine minimum tendon area

Figure I-16 shows sample results for the parametric study. The vertical axis presents the tendon stress at the column failure normalized to the tendon yield strength. Therefore, a tendon stress ratio of 1.0 indicates that tendons yielded before the reinforcing steel bar fractures or the confined concrete fails. It can be seen in Fig. I-16a that more steel tendon is needed to avoid tendon yielding when the tendon initial stress is

minimal. Figure I-16b shows that columns with relatively small axial loads need more tendons to keep the tendons elastic at the column failure. Figure I-16c shows that columns with relatively small longitudinal steel ratio need more tendons to prevent tendon yielding. It can be seen from Fig. I-16d that taller columns also require more tendons. Therefore, an extreme condition to determine the minimal tendon area is when a tall column (e.g. aspect ratio of 8) with low axial load (e.g. axial load index of 2%) is lightly reinforced with steel bars (e.g. $A_s/A_g=0.0025$) (Fig. I-16e). A minimum steel tendon ratio (A_p/A_g) of 0.004 was found to be suitable for all cases to ensure the linear-elastic behavior of steel tendons in hybrid rocking columns.

1.4.2.3 Residual Drifts for Hybrid Rocking Columns

The main advantage of hybrid rocking columns over conventional columns is their lower lateral residual displacements. There is currently no design equation for residual displacement estimation of this type of columns. More than 250 cyclic load analyses (similar to those discussed in I.2.3) were carried out to develop a design equation for the estimation of hybrid rocking column residual displacements. Three aspect ratios, 4, 6, and 8, were selected for the columns. The diameter was assumed to be 5 ft (1.52 m) for all columns. The column concrete compressive strength was 5000 *psi*. Seven longitudinal reinforcing steel bar ratios ($A_s/A_g = 0.25, 0.5, 0.75, 1.0, 1.5, 2.0, \text{ and } 2.5\%$) with one transverse steel ratio (1.07%, No 6 spirals at 3 in. pitch) were selected for the columns. Three axial load indexes, 5, 10, and 15%, were assumed. Four tendon initial stress ratios ($f_{pi}/f_{py} = 0, 10, 20, \text{ and } 30\%$) were selected. The recommended tendon steel ratio (A_p/A_g) of 0.004 was used in all analyses. The $P - \Delta$ effect was included in all analyses.

Figure I-17 shows the results of all analyses. The residual drift ratio (the ratio of column lateral residual displacement to the column height) was plotted against the peak drift ratio (the ratio of column lateral ultimate displacement to the column height). It was found that the tendon initial stress ratio (f_{pi}/f_{py}) and the column longitudinal reinforcing steel bar ratio (A_s/A_g) are the most important parameters that control the hybrid rocking column residual drifts. It can be seen that increasing the tendon initial stress ratio results in lower residual drifts, and hybrid rocking columns with a longitudinal reinforcing steel bar ratio of 0.005 or less showed insignificant residual drifts (curves under the 1% drift ratio limit).

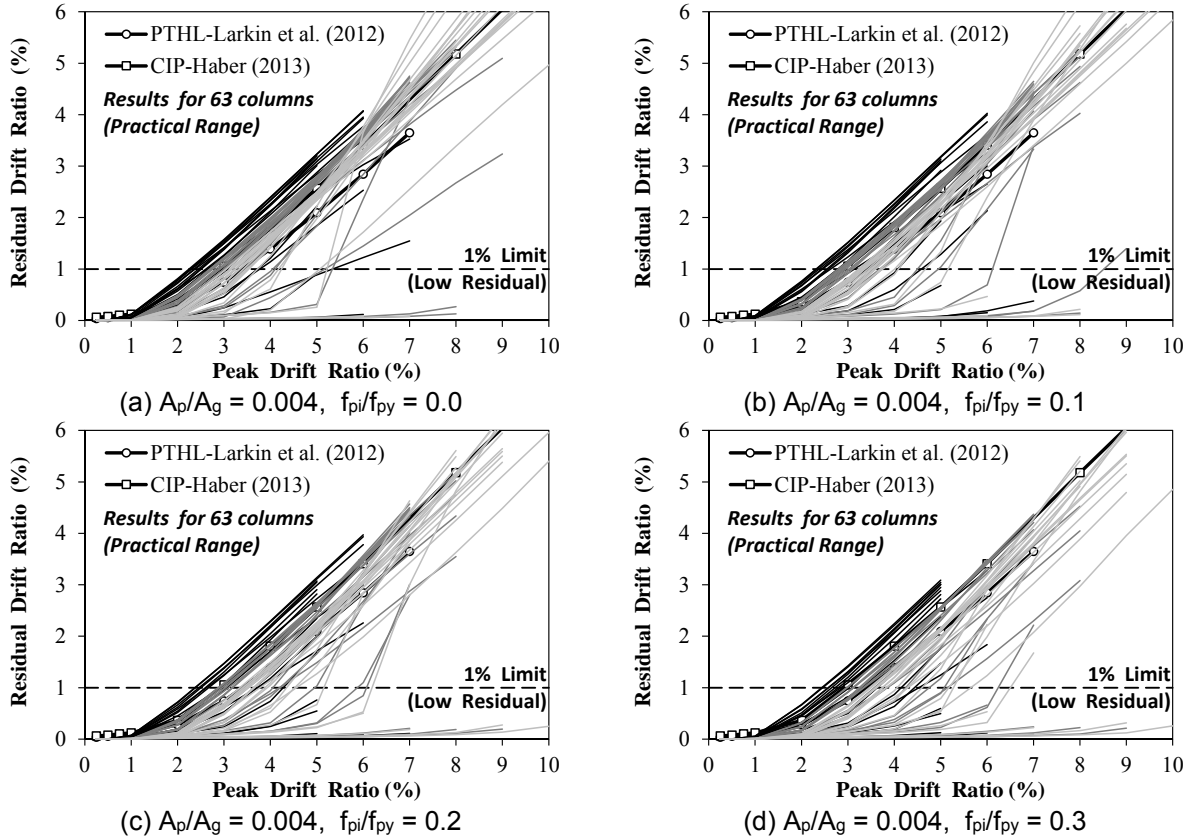


Figure I-17. Results of parametric study to develop residual-peak drift relationship

Based on these observation, the curves pertaining to columns with a longitudinal reinforcing steel bar ratio of 0.005 or smaller were excluded from further analyses then a statistical analysis (Fig. I-18) was carried out to fit a polynomial of the second order to each subfigure of Fig. I-17. Another curve-fitting on the coefficients of the polynomials was conducted to develop a single-equation for the residual drift estimation of hybrid rocking columns as:

$$\delta_r = a\delta^2 + b\delta + c \quad (I-1)$$

where δ_r is the residual drift ratio (%) and δ is the peak drift ratio (%), and

$$\begin{aligned} a &= 0.026(f_{pi}/f_{py}) + 0.047 \\ b &= -0.55(f_{pi}/f_{py}) + 0.32 \\ c &= 0.36(f_{pi}/f_{py}) - 0.27 \end{aligned} \quad (I-2)$$

where f_{pi} is the tendon initial stress after all losses and f_{py} is the yield strength of the tendon.

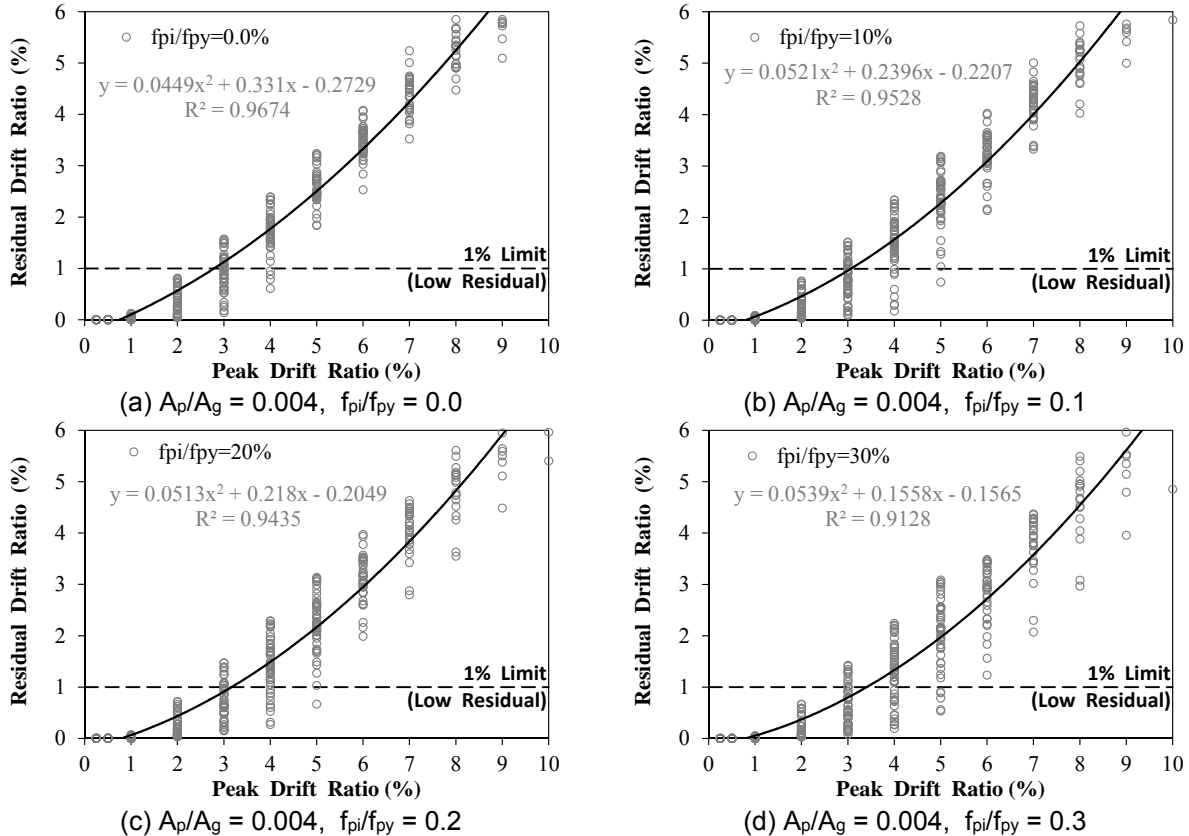


Figure I-18. Results of statistical analysis to develop residual-peak drift relationship

To validate the accuracy of the proposed equation, the PT-HL column model tested by Larkin et al. (2012) (for more information refer to section I.4) was analyzed. Figure I-19a shows the measured and calculated (using Eq. I-1) residual-peak drift ratio relationships. It can be seen that the equation resulted in a good correlation with the test data. Furthermore, it was found that a scaled version of this equation can be used for hybrid rocking columns with a reinforcing steel bar ratio (A_s / A_g) between 0.5% and 1.0%. A scale factor of 0.8 resulted in a good correlation between residual drifts estimated by the equation and those measured in the PT-LL column tested by Larkin et al. (2012). Table I-6 presents a summary of the equations developed for hybrid rocking columns.

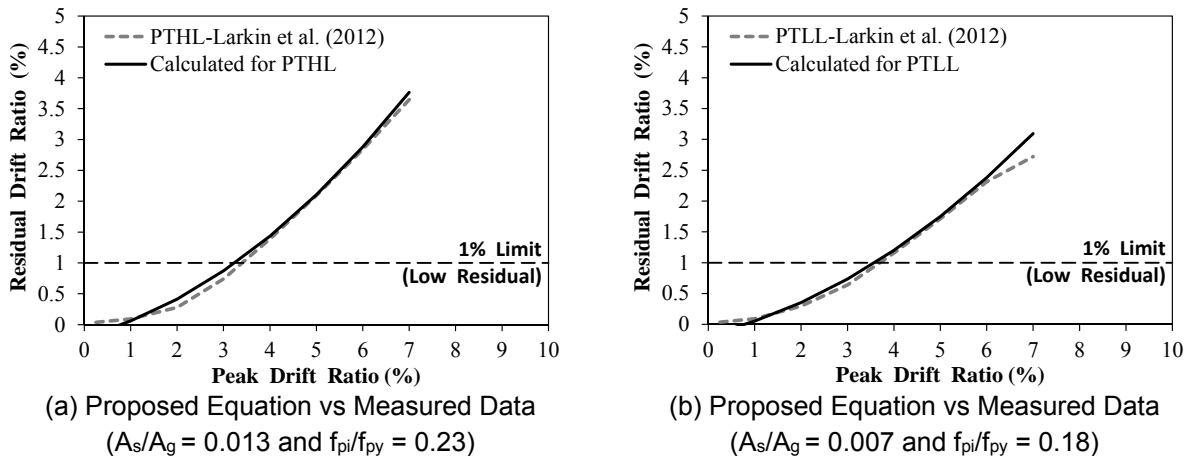


Figure I-19. Residual drift equation validation for hybrid rocking columns

Table I-6. Residual drift ratio for hybrid rocking columns

Longitudinal Reinforcing Steel Bar Ratio (A_s/A_g)	Residual Drift Ratio (%)
$A_s/A_g \leq 0.005$	$\delta_r \leq 1.0\%$
$0.005 < A_s/A_g < 0.01$	$\delta_r = 0.8(a\delta^2 + b\delta + c)$
$A_s/A_g \geq 0.01$	$\delta_r = a\delta^2 + b\delta + c$

Note: “ δ ” is the peak drift ratio (%) and “ δ_r ” is the residual drift ratio (%).

I.5 References

1. AASHTO. (2013). “AASHTO LRFD Bridge Design Specifications,” Washington, DC, American Association of State Highway and Transportation Officials.
2. AASHTO. (2014). “AASHTO Guide Specifications for LRFD Seismic Bridge Design,” Washington, DC: American Association of State Highway and Transportation Officials.
3. Concrete Column Blind Prediction Contest. (2010). http://nisee2.berkeley.edu/peer/prediction_contest/.
4. Jeong, H.I.L., Sakai, J., Mahin, S.A. (2008). Shaking Table Tests and Numerical Investigation of Self-Centering Reinforced Concrete Bridge Columns. PEER-2008/06, Pacific Earthq. Engrg. Res. Center, Univ. of California at Berkeley, California, 399 pp.
5. Larkin, A.S., Sanders, D., and Saiidi, M. (2012). “Unbonded Prestressed Columns for Earthquake Resistance,” Center for Civil Engineering Earthquake Research, Department of Civil and Environmental Engineering, University of Nevada, Reno, Nevada, *Report No. CCEER-12-02*, 256 pp.
6. Mander, J.B., Priestley, M.J.N., and Park, R. (1988). “Theoretical Stress-Strain Model for Confined Concrete.” *Journal of Structural Engineering*, ASCE, Vol. 114, No. 8, pp. 1804-1826.
7. Nakashoji, B. and Saiidi, M.S. (2014). “Seismic Performance of Square Nickel-Titanium Reinforced ECC Columns with Headed Couplers,” Center For Civil Engineering Earthquake Research, Department Of Civil and Environmental Engineering, University of Nevada, Reno, Nevada, *Report No. CCEER-14-05*, 252 pp.
8. O’Brien, M., Saiidi, M.S., and Sadrossadat-Zadeh, M. (2006). “A Study of Concrete Bridge Columns Using Innovative Materials Subjected to Cyclic Loading,” Center for Civil Engineering Earthquake Research, Department of Civil Engineering, University of Nevada, Reno, Nevada, Report No. CCEER-06-04, 246 pp.
9. OpenSees. (2013). “Open System for Earthquake Engineering Simulations,” Version 2.4.1, Berkeley, CA. Available online: <http://opensees.berkeley.edu>.
10. Restrepo, J.I., Tobolski, M.J. and Matsumoto, E.E. (2011). “Development of a Precast Bent Cap System for Seismic Regions,” National Cooperative Highway Research Program, NCHRP Report 681, Washington, D.C., NCHRP Report 681, 116 pp.
11. Saiidi, M.S., O’Brien, M. and Sadrossadat-Zadeh, M. (2009). “Cyclic Response of Concrete Bridge Columns Using Superelastic Nitinol and Bendable Concrete,” *ACI Structural Journal*, Vol. 106, No. 1, pp. 69-77.
12. Seissoft. (2013). SeismoArtif v2.1-A Computer Program for Generating Artificial Earthquake Accelerograms Matched to a Specific Target Response Spectrum. Available from <http://www.seissoft.com>.

13. Tazarv, M. and Saiidi, M.S. (2013) “Analytical Studies of the Seismic Performance of a Full-Scale SMA-Reinforced Bridge Column,” (Invited Paper), *International Journal of Bridge Engineering*, Vol. 1, No. 1, pp. 37-50.
14. Tazarv, M. and Saiidi, M.S. (2014). “Next Generation of Bridge Columns for Accelerated Bridge Construction in High Seismic Zones,” Center For Civil Engineering Earthquake Research, Department of Civil and Environmental Engineering, University of Nevada, Reno, Nevada, *Report No. CCEER-14-06*, 400 pp.